

Joint Network-Channel Coding Schemes for Relay Networks

Joint Network-Channel Coding Schemes for Relay Networks

by

Mikel Hernaez Arrazola



Dissertation Submitted for the Degree of Doctor of Philosophy

Under the supervision of:

Professor Pedro M. Crespo
Dr. Javier Del Ser

University of Navarra–TECNUN
Faculty of Telecommunication Engineering
2012

Doctoral Dissertation by the University of Navarra-TECNUN

©Mikel Hernaez Arrazola, 2012

Printed in the Printing Office, TECNUN
Donostia-San Sebastián

Acknowledgements

For the sake of my parents, the least I can do is to allow them to understand at least one page of this dissertation. Therefore, I will continue in Spanish.

Primeramente, me gustaría agradecer a Pedro Crespo la oportunidad que me dio de trabajar con los mejores. Su pasión por la investigación es enormemente contagiosa y hace que ser estudiante suyo sea un lujo sólo alcanzable por unos privilegiados. ¡Muchas gracias por darme la oportunidad de ser uno de ellos! Además, en estos últimos años no sólo he aprendido muchísimo en el ámbito académico y personal, sino que también en el ámbito físico. Nunca podré olvidar cuando entró en el despacho y dijo: “No puede ser que el jefe esté mucho más delgado y en mejor forma física que sus estudiantes...” Desde ese día me propuse subir en bici a Miramón y lo sigo cumpliendo. ¡Muchas gracias Pedro!

A Javi Del Ser, tenerle como co-director ha sido todo un lujazo y un privilegio. ¡Muchas gracias Javi! Nunca olvidaré las charlas ilustrativas y motivadoras en Mondragón y Zamudio, ya que esas charlas han sido las semillas de las que han brotado los artículos publicados. Ha sido un grandísimo maestro del que he aprendido una barbaridad. Eskerrik asko!

A mis compañeros de despacho. Eskerrik asko Xabi, hiru urte hauetan gure artean eduki ditugun elkarrizketekin asko ikasi dut. Ez dut inoiz ahaztuko PW=P dela! A Iker (Alustiza) por aguantar las infinitas veces que me he metido con su tierra y con el rap. Eskerrik asko bioi!

A Aitor, María y Ana, gracias por aguantar mis chapas en mis visitas a vuestros despachos. Eskerrak aunitz, muchas gracias!

A Iker y Andoni, por aguantarme casi las 24 horas del día. Las infinitas visitas al despacho (gracias Christoph), los fines de semana, los domingos con *el conquis*, las sesiones de cine... y tantísimas cosas que me han animado durante estos últimos años. ¡Un gúgol de gracias!

A todos los de nuestra generación del CEIT (que como sois un montón no me voy a poner a nombrarlos a todos que si no no termino la tesis a tiempo...), simplemente porque sois lo mejor del CEIT (y TECNUN).

Gracias a vosotros ir a currar cada día era infinitamente mejor. Y porque gracias a vosotros las cenas y viajes de curro han sido memorables.

A la asociación de amigos de la universidad de Navarra por financiarme los primeros dos años de esta aventura.

A Carol Cullinane por su infinita paciencia. Los viernes por la mañana siempre empezaban con una sonrisa. Thanks!

Mención especial a Inaxio y Martintxo, por estar ahí los fines de semana aguantándome, y por esas inolvidables escapadas culinarias, ¡un millón de gracias! Siempre nos quedará Ibardin (aunque a Inaxio no le guste mucho el trayecto...).

Al resto de la cuadrilla (Iñi, Unai, Ruiz, Rami, Yarza y Garay) porque aunque estéis desperdigados por el mundo, sé que siempre estaréis ahí.

A Alexia, Haitz y Yago (hay que volver a Bealin!), Jorge y Jose Angel, Luleå Family, y a otros tantos que se me habrán olvidado mencionar, por aguantar mis tonterías y hacerme reír estos años, danke schön, thank you, eskerrikasko, grazie mile, tesekkurerler, moltes gràcies, merci beaucoup, muchas gracias, tack så mycket, dziękuję!

A la ama y el aita, por ser los mejores aitas que se puedan tener. Muchas gracias por estar siempre ahí y sobre todo por apoyarme incondicionalmente en todas las decisiones que he tomado en mi vida. De corazón, muchísimas gracias. ¡Os quiero!

A Alexander y Bárbara, por ser unos hermanos fuera de serie. Aquí pondría una ristra de palabras malsonantes que reflejarían todo lo que os quiero, pero por decencia os las imagináis, sólo decir que terminaría con un ***** amos! jejeje.

Para terminar se suele poner la típica frase: “por último pero no por eso menos importante bla bla bla”, yo la voy a cambiar un poco:

Por último y porque es la más importante, a Idoia. El apoyo que me has dado estos años, incluso en la distancia, ha hecho posible esta tesis. Sin tí nada de esto hubiese pasado. ¡No existe una expresión en castellano que refleje lo enormemente agradecido que te estoy! ;>

Summary

The goal of this thesis is to propose and design network and channel coding schemes for relay networks so that the promised gains dictated by network information theory (as upper or lower bounds) can be approximated. To that end, network coding and channel coding are jointly designed with the aim of exploiting the redundancy existing in the Multiple-Access Relay Channel (MARC) and Multihop networks for a better error protection.

To this end, through this dissertation we will present a plurality of five technical papers (Papers I-V, in Appendix A-E, respectively) in the field of joint network-channel coding for relay networks.

In Papers I and II, two joint network-channel coding scheme for the Time-Division Decode-and-Forward Multiple Access Relay Channel are proposed. In both schemes: 1) the relay linearly combines the encoded sequences transmitted by the sources; and 2) the decoding at the destination is performed by applying the Sum Product Algorithm over the derived factor graph of the Joint Network-Channel code.

In particular, Paper I presents a scheme based on Bit Interleaved Coded Modulation with non-binary Low Density Parity Check codes as channel codes. We showed that the proposed scheme outperforms its binary counterpart and performs close to the outage probability (cut-set bound) in all the simulated scenarios.

Paper II utilizes convolutional codes as channel codes. By performing a tailored selection of the coefficient of the linear combination, we are able to improve the overall performance with respect to a random choice. Simulation results showed that the proposed scheme outperformed the reference schemes found in the literature and the one presented in Paper I by using short-length codewords.

Regarding Paper III, it proposes a decode-combine-forward scheme for the multi-hop transmission in ad-hoc wireless networks, where the information generated by two independent sources has to be sent to a common destination based on multiple-relay cooperation. To this end, the proposed

scheme blends together LDPC channel coding with linear combination of blocks of data over a finite field.

On the other hand, Paper IV proposes a new scheme that clearly outperforms the scheme presented in Paper III, and consequently, the schemes found in the literature. The proposed scheme is based on distributing the method presented in Paper II among the different relays, so that in its corresponding hop each relay linearly combines (each one using a different linear combination) and forwards the source data.

Finally, Paper V introduces a channel coding design framework for short-length codewords which can achieve lower error floors than previous designs found in the literature. By adapting the joint code proposed in Paper II to the point-to-point scenario, we designed a channel code that is based on concatenating the output of two convolutional codes with a linear combination in \mathbb{F}_{2^q} . The main advantage of the proposed scheme is that one could choose error floors lower than the ones in previous schemes, (and consequently outperforming these schemes at high SNRs), with an SNR waterfall degradation of less than 0.5 dB at mid-range BERs.

Summarizing, the collection of papers presented in this dissertation will show that already proposed coding schemes found in the literature can be clearly outperformed by efficiently combining channel coding and network coding over a variety of network scenarios, such as the point-to-point (Paper V), Multiple-Access Relay Channel (Paper I and II) and multi-hop scenarios (Paper III and IV).

Glossary

AF	<i>Amplify-and-Forward</i>
AWGN	<i>Additive White Gaussian Noise</i>
BER	<i>Bit Error Rate</i>
BICM	<i>Bit Interleaved Coded Modulation</i>
BICM-ID	<i>Bit Interleaved Coded Modulation with Iterative Decoding</i>
BPSK	<i>Binary Phase Shift Keying</i>
CC	<i>Convolutional Code</i>
CDF	<i>Cumulative Distribution Function</i>
CF	<i>Compress-and-Forward</i>
CFER	<i>Common Frame Error Rate</i>
CSI	<i>Channel State Information</i>
C-MARC	<i>Constrained Multiple Access Relay Channel</i>
CRC	<i>Cyclic Redundancy Check</i>
DF	<i>Decode-and-Forward</i>
EXIT	<i>EXtrinsic Information Transfer</i>
FER	<i>Frame Error Rate</i>
IEEE	<i>Institute of Electrical and Electronic Engineers</i>
i.i.d.	<i>independent and identically distributed</i>
JNBICM-ID	<i>Joint Network-Bit Interleaved Coded Modulation with Iterative Decoding</i>
JNCC	<i>Joint Network-Channel Code</i>
LDPC	<i>Low-Density Parity-Check Code</i>
LT-LDPC	<i>Lower-Triangular Low-Density Parity-Check Code</i>

MAP	<i>Maximum A Posteriori</i>
MARC	<i>Multiple Access Relay Channel</i>
MIMO	<i>Multiple Input–Multiple Output</i>
ML	<i>Maximum Likelihood</i>
NC	<i>Network Coding</i>
O-MARC	<i>Orthogonal Multiple Access Relay Channel</i>
PAM	<i>Pulse Amplitude Modulation</i>
pdf	<i>probability density function</i>
PHY	<i>Physical layer</i>
pmf	<i>probability mass function</i>
PSK	<i>Phase Shift Keying</i>
P/S	<i>Parallel to Serial converter</i>
QAM	<i>Quadrature Amplitude Modulation</i>
RSC	<i>Recursive Systematic Code</i>
RSI	<i>Relay State Information</i>
rv	<i>random variable</i>
S/P	<i>Serial to Parallel converter</i>
SNR	<i>Signal to Noise Ratio</i>
SPA	<i>Sum-Product Algorithm</i>
TDMA	<i>Time-Division Multiple-Access</i>
WiMAX	<i>Worldwide Interoperability for Microwave Access</i>
XOR	<i>eXclusive OR</i>

Notation

Let $(\Omega, \beta, \mathcal{P})$ be the underlying probability space where all the random variables (r.v.) are defined. We use uppercase when referring to r.v. and lowercase when referring to realizations of r.v. In addition, we use boldface or preferably, a bracketed sequence of symbols (e.g. $\{X_k\}_{k=1}^N$) when referring to vectors; and boldface with an underline to refer to matrices (with some exceptions which will be clear from the context). For discrete r.v., we denote the probability mass function (p.m.f.) of the discrete r.v. X as $P_X(x) \triangleq \mathcal{P}\{\omega : X(w) = x\}$. For continuous r.v., we denote the probability density function (p.d.f.) of the continuous r.v. X as $p_X(x)$. However, when the context is clear, we use $P(x)$ and $p(x)$ for p.m.f. and p.d.f., respectively.

All the symbols used through this dissertation are defined before been used; however, some of them might be used far after their definition. Hence, a list of the most repeated symbols is provided below.

$\sim X_i$	All the variables involved in the computation except X_i .
$\psi(X) \setminus f_j$	All the elements in the set $\Psi(X)$ except f_j .
$\mu_{X_i \rightarrow f_j}(x_i)$	Message from node X_i to node f_j .
$\hat{f}_i(x_i)$	Marginal function associated to X_i .
$\{U_t\}_{t=1}^N$	Sequence of N random variables.
$\mathbb{1}[\cdot]$	Indicator function.
\mathcal{U}	Alphabet of the random variable U .

$ \mathcal{U} $	Cardinal of the alphabet \mathcal{U} .
$ \cdot $	Absolute value of a variable.
$\ \cdot\ $	Euclidean norm.
E_b	Energy per information bit.
E_s	Energy per complex dimension.
ρ	Spectral efficiency [bits per complex dimension].
C	Capacity.
$\mathbb{E}[\cdot]$	Expected value of a random variable.
$\mathcal{N}_{\mathbb{C}}(m, \sigma^2)$	Complex Normal distribution with mean m and variance σ^2 .
$\mathcal{N}(m, \sigma^2)$	Normal distribution with mean m and variance σ^2 .
$*$	Convolution.
v	Number of memory elements of a Convolutional Code.
\oplus	Modulus addition.
\otimes	Modulus multiplication.
H	Parity-check Matrix.
T	Transpose operator.
Π	Interleaver function.

Contents

List of Figures	xiii
List of Tables	xvii
1 Introduction	1
1.1 Organization of the Dissertation	3
2 Preliminaries	7
2.1 Communication Theory - Channel Coding and Decoding	7
2.2 Factor Graphs and the Sum-Product Algorithm	10
2.2.1 Factor Graphs	10
2.2.2 Sum-Product Algorithm	12
2.2.3 Factor Graphs in Channel Decoding	16
2.3 Gaussian Fading Channel Model	17
2.4 Information Theoretic Foundations - Channel Capacity	19
2.5 Channel Codes	23
2.5.1 Convolutional Codes	23
2.5.1.1 Decoding Convolutional Codes	26
2.5.2 Low-Density Parity-Check (LDPC) Codes	29
2.5.2.1 Decoding LDPC codes	31
2.6 Network Coding	34
2.6.1 Network and Channel Coding	35
2.6.1.1 Separated Network-Channel Coding	35
2.6.1.2 Joint Network-Channel Coding	36
3 Joint Network-Channel Coding Schemes for the Multiple-Access Relay channel	39
3.1 Multiple Access Relay Channel	39
3.1.1 Network Coding in MARCs	41
3.2 State of the art on TD-DF-MARC	42

3.3	Main contributions	43
3.3.1	Paper I	43
3.3.2	Paper II	45
4	Joint Network-Channel Coding Schemes for Multihop Wireless Networks	49
4.1	Multihop Wireless Networks	49
4.2	Progressive Network Coding for Multihop Wireless Networks	51
4.3	Main Contributions	53
4.3.1	Paper III	54
4.3.2	Paper IV	55
5	A Flexible Channel Coding Approach for Short-Length Codewords	59
5.1	Paper V	59
6	Conclusions and Future Lines	63
6.1	Conclusions	63
6.2	Future Lines	65
	References	67
A	Paper I	77
B	Paper II	95
C	Paper III	125
D	Paper IV	141
E	Paper V	155
F	Derivation of the outage probability of the TD-DF-MARC	171
F.1	Cut-set Bounds for the C-DF-MARC	171
F.2	Cut-set Bounds for the TD-DF-MARC	173
F.3	Outage probability derivation	174
G	Publications	177

List of Figures

1.1	Multiple Access Relay Channel (left) and Multihop Wireless Network (right).	4
2.1	Communication scenario with encoding and decoding functions.	8
2.2	Factor graph representing the global function $f(x_1, x_2, x_3, x_4, x_5)$	11
2.3	(a) Factor Graph of the factorized $f(\cdot)$; (b) Rearrangement of (a) for the sake of clarity.	12
2.4	Messages used for the marginalization of $\hat{f}_1(x_1)$	14
2.5	Messages necessary for calculating all possible marginal functions for $f(\cdot)$	15
2.6	Capacity in bits per channel use for multiple signal constellations with different alphabet size and uniform distribution in the AWGN channel. For reference, the channel capacity with Gaussian inputs is shown in dashed lines.	21
2.7	Encoder (set of filters) for $G_2(x)$	24
2.8	State diagram and Trellis representation of $G_2(x)$	25
2.9	Factor graph of a convolutional code	27
2.10	Message designation for the BCJR algorithm.	29
2.11	Factor graph representing the joint probability of (2.27) and the associated messages.	33
2.12	Example of superiority of network coding over routing.	35
2.13	Separated Network-Channel coding scheme.	36
3.1	Example of a Multiple Access Relay Network.	40
3.2	Example of diversity gain over a 2-user time-division MARC.	42
3.3	Schematic diagram of the transmitter for source \mathcal{S}_i , with $i \in \{1, 2\}$	43

3.4	Factor graph of the proposed joint network-channel code for source \mathcal{S}_1 . $\mathbb{1}[\cdot]$ denotes the indicator function, whereas $\mathbf{x} \perp \mathbf{H}_z^T$ stands for orthogonality between vector x and compounding non-binary LDPC parity-check matrix \mathbf{H}_z , with $z \in \{1, \dots, N-K\}$ (see Appendix A)	45
3.5	Factor graph of the proposed joint network-channel code.	46
3.6	Factor graph representing the factorization of the global function representing the network coding, i.e. the oversize check nodes of Figure 3.5.	47
4.1	The considered Multihop Wireless Network.	50
4.2	Parity-check matrix at the destination of the scheme proposed in [BL06]. The submatrices for each relay node are also shown.	52
4.3	Factor Graph at the destination of the scheme proposed in [BL06].	53
4.4	Factor graph employed for the decoding at each node in Paper III.	55
4.5	Factor graph employed for the decoding at each node in Paper IV.	56
5.1	Encoder associated to the proposed code.	61
5.2	EXIT Chart of the proposed code for different linear combinations functions (a) and unequal energy allocation parameter Λ (b).	62
A.1	Block diagram of the considered 2-user MARC scenario.	81
A.2	Schematic diagram of the transmitter for source \mathcal{S}_i , with $i \in \{1, 2\}$	82
A.3	Block diagram of the Joint Network-BICM Iterative Decoder.	85
A.4	Factor graph of the JNBICM-ID for source \mathcal{S}_1 . $\mathbb{1}[\cdot]$ denotes the indicator function, whereas $\mathbf{x} \perp \mathbf{H}_z^T$ stands for orthogonality between vector x and compounding non-binary LDPC parity-check matrix \mathbf{H}_z , with $z \in \{1, \dots, N-K\}$	88
A.5	CFER versus E_b/N_0 of the proposed JNBICM scheme for different values of q and m	90
B.1	Block diagram of the considered 2-user TD-DF-MARC scenario.	99
B.2	Factor Graph of the Proposed JNCC.	104

B.3	Factor Graph representing the factorization of $p(\mathbf{y}_l x_i^m)$, i.e. the network check node \mathcal{NC}_l	108
B.4	EXIT charts for different network decoders and convolutional codes.	111
B.5	EXIT curves of 100 system usages for $q = 2$ and $\mathbf{h} = (2, 3)$	113
B.6	CDF of $T_{\mathbf{h}}^q(0)$ and $T_{\mathbf{h}}^q(1)$ for $q = 3$ and all possible values of \mathbf{h}	114
B.7	Outage probabilities and PER performance of the proposed approach when the CC2 convolutional code is used.	117
B.8	Outage probabilities and PER performance of the proposed approach when the CC6 convolutional code is used in scenario A (left) and C (right).	118
B.9	PER performance of the proposed schemes for the erroneous source-relay channel setup when the CC2 convolutional code and $\mathbf{h} = (6, 6)$ is used. Also plotted the point-to-point and the SNCC schemes.	121
C.1	Network model.	129
C.2	Factor graph employed for the decoding.	131
C.3	Performance of the proposed system for $ \mathcal{R} = 0, \dots, 3$	134
C.4	Simulation results: (a) Bit error rate (BER) of the proposed scheme versus E_b/N_0 assuming non ideal relays. For comparison purposes, the performance of Ref1 scheme is also shown in the figure. (b) BER of the proposed scheme versus E_b/N_0 assuming ideal relays. For comparison purposes, the performance of Ref2 scheme is also shown in the figure.	135
C.5	(a) and (c) Factor Graph and Parity-check matrix, respectively, of Ref1 scheme. (b) and (d) Factor Graph and Parity-check matrix, respectively, of Ref2 scheme.	138
D.1	Network model.	145
D.2	Factor graph employed for the decoding.	149
D.3	Performance of the proposed scheme at the destination for different amount of iterations at the relays and 100 iterations at the destination.	151
D.4	BER performance of the proposed scheme at all the nodes for 100 Iterations. Also plotted the performance of [HCD11] at the destination.	152
E.1	Encoder associated to the proposed code.	160
E.2	Factor graph of the proposed decoder.	163

List of Tables

2.1	Message meaning and BCJR designation.	28
2.2	Messages in the factor graph and their respective meaning.	32
3.1	Gaps to the outage probabilities in dB for a 2-memory block convolutional code and a network coding over $GF(2^3)$	48
B.1	Gaps to the outage probabilities in dB.	119
C.1	Parameters for the simulation: K : block length (bl) of information bits; N : bl. of channel code bits; R : channel code rate; R_s : channel-network code rate at the relays; ρ_S : system spectral efficiency.	135

CHAPTER 1

Introduction

Since Shannon's landmark 1948 paper [Sha48], the problem of efficient data communication over the point-to-point Gaussian channel has driven much of communication and coding research in the half of the last century. Shannon's most celebrated result was the explicit computation of the capacity of the additive Gaussian noise channel. His result posed a magnificent challenge to succeeding generations of researchers. Only in the past decade, with the discovery of turbo codes, can we say that methods of approaching capacity have been found for practically all linear Gaussian channels (e.g. Low-Density Parity Check codes, Turbo codes...).

The advent of Internet and wireless communications has shifted the activity of information theorists towards what is known as Network Information Theory. Network Information Theory aims to establish the fundamental limits on information flow in networks and the optimal coding schemes that achieve these limits. It extends Shannon's fundamental theorems to general networks with multiple sources and destinations and share resources. Recent works have dealt, among others, with new wireless network models and new approaches to coding these networks.

The main advantage of the wireless medium over wireline is that it allows the user to be mobile and to communicate in all areas covered by the base stations. Moreover, the costs to establish the wireless infrastructure have the potential to be cheaper because it is not necessary to install wires

from the base station to each user. However, the bandwidth suitable for the aforementioned mobile communication scenario is a scarce resource and the transmission power is usually very limited. To overcome these limitations, extensions to the point-to-point communication scheme are considered. One of such possible extensions is given by the use of relays, which we study throughout this work.

The purpose of the relays is to support the communication between the mobile and base station. The most common characteristic of the relays are: i) they do not generate new data, ii) they are simpler than base stations in terms of transmit power requirements, size and cost, and iii) contrary to base stations, relays do not have a wired connection to the outside network. These characteristics provide the relays with a high installing flexibility, as for example: fixed relays could be installed in traffic lights or for street crossings; whereas mobile relays could be installed on trains or taxis. Next we summarize the main advantages of wireless relaying networks over point-to-point schemes.

- The relay is located in such way that the relay-destination link is of better quality than the source-destination link, so that relaying could deliver higher data rates than the point-to-point scenario. Moreover, the clever positioning of the relays increases the probability of a line-of-sight connection, especially on the link between a fixed relay and the base station. This allows the use of parts of the spectrum which are not used currently due to their vulnerability against non-line-of-sight conditions.
- Both the small-scale fading due to multipath propagation and the large-scale fading due to shadowing can be assumed independent for the source-sink and the relay-sink links. Hence, since the sink can receive both the signal from the source and the relay, relaying promises diversity gains and increments in the robustness of the communication system. As a consequence, the mobile station can save transmission energy (higher battery life).

Given the above, we focus on relay networks with broadcast transmissions that operate in Time-Division-Multiple-Access (TDMA) mode, where the sources and the relays convey their data by using orthogonal channels. Although the time-division scheme involves a suboptimal use of the available bandwidth, it avoids interferences in the network and allows an easier

implementation, thanks to the use of half-duplex relays and the lack of stringent synchronization constraints.

In addition, we consider the Decode-and-Forward (DF) decoding strategy at the relays, as it offers a higher code design flexibility. The following two relay networks architectures are considered (see Figure 1.1):

- (i) The Multiple Access Relay Channel (MARC, see [HSOB05]), where both sources and the relay convey their data by using three orthogonal channels. Hence, for two sources the total transmission time is divided into three time slots, one for each transmitting node.
- (ii) The multihop network, where the data transmission between the source and the corresponding destination is realized with the aid of intermediate nodes (relays). We design the system in TDMA mode and consider the DF decoding strategy; thus, at each intermediate node the received signal is decoded, re-encoded and forwarded. Hence, the total available transmission time is divided into several orthogonal time-slots, one for each node.

The goal of this thesis is to propose and design network and channel coding schemes for these relay networks so that the promised gains dictated by network information theory (as upper or lower bounds) can be approximated. To that end, network coding and channel coding are jointly designed with the aim of exploiting the redundancy existing in the MARC and Multihop networks for a better error protection.

1.1 ORGANIZATION OF THE DISSERTATION

The dissertation is organized as a plurality of five technical papers (Papers I-V shown in Appendix A-E, respectively), which are presented through Chapters 3-5 and where papers addressing similar topics are collected together. Throughout each of these chapters, we begin by introducing the network model considered. This is followed by addressing the state of the art together with the main contributions made by the corresponding papers. Finally, we draw some conclusions and present the future work.

Thus, the structure of this dissertation is as follows:

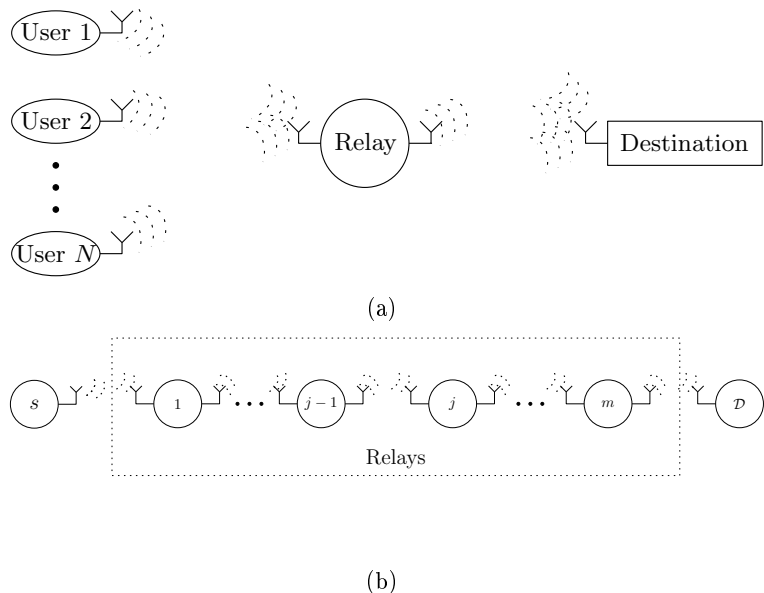


Figure 1.1: Multiple Access Relay Channel (left) and Multihop Wireless Network (right).

- **Chapter 2** summarizes the required background knowledge to understand the presented technical papers including: It reviews the basics of Communication Theory and the channel codes used in this thesis, and it provides a brief introduction to Network Coding. The aim of this chapter is to make the dissertation self-contained; however, due to the variety of different concepts covered by the technical papers presented in this work, in some cases we may refer to the literature for further detail.
- **Chapter 3** briefly introduces the Multiple-Access Relay Channel (MARC) and presents the main advantages of performing network coding in this network. Following, the state of the art regarding the design of joint network-channel codes for the Time-Division Decode-and-Forward Multiple Access Relay Channel (TD-DF-MARC) is presented. An insightful review of Papers I and II (Appendix A and B, respectively), where two novel joint network-channel schemes are proposed, is also included in this chapter. In both cases the relay linearly

combines – over a non-binary finite field – the coded sequences from the source nodes. We show that both schemes outperform the previous schemes described in the state of the art in terms of the gap to the outage probability (outer bound). Moreover, as the work presented in Paper II is an improvement of the work in Paper I, we also highlight the main differences between both.

- **Chapter 4** contains a comprehensive overview of the Multihop networks and an insightful review of the coding scheme known as Progressive Network Coding. Papers III and IV (Appendix C and D, respectively) are summarized in subsequent sections of this chapter. On the one hand, Paper III proposes a decode-combine-forward scheme for the multi-hop transmission in ad-hoc wireless networks, where the information generated by two independent sources has to be sent to a common destination based on multiple-relay cooperation. To this end, the proposed scheme blends together LDPC channel coding with linear combination of blocks of data over a finite field. The proposed scheme outperforms similar schemes found in the literature. On the other hand, Paper IV based on a concept presented in Paper II proposes a new scheme that clearly outperforms the scheme presented in Paper III, and consequently, the schemes found in the literature.
- **Chapter 5** presents Paper V (Appendix E). It proposes a channel coding scheme for the transmission of short length codewords in AWGN point to point links. In this sense, this paper differs from the main topics of the previous chapters for it does not involve relay networks. However, the idea behind the proposed approach is derived from the work of Paper III. The chapter begins by a brief introduction of the state of the art in iterative short-length codes. It then presents Paper V, where a new channel coding approach for the transmission of short-length codewords that permits balancing the tradeoff between the bit error rate floor and waterfall region by modifying a single real-valued parameter is proposed. It is based on combining convolutional coding with a q -ary linear combination and unequal energy allocation. Simulation results suggest that for very low bit-error rates the proposed scheme will exhibit lower error floors than previous approaches found in the literature.
- Finally, **Chapter 6** concludes the dissertation by summarizing its main contributions and by making some future remarks.

CHAPTER 2

Preliminaries

This chapter provides the reference background for the dissertation. It reviews the basics of Communication Theory and the channel codes used in this thesis, and it provides a brief introduction to Network Coding. The different network models considered in the papers are presented in their respective chapters.

2.1 COMMUNICATION THEORY - CHANNEL CODING AND DECODING

Let $(\Omega, \beta, \mathcal{P})$ be the underlying probability space where all the random variables (r.v.) are defined. We use uppercase when referring to r.v. and lowercase when referring to realizations of r.v. In addition, we use boldface when referring to vectors, and boldface with an underline to refer to matrices. For discrete r.v., we denote the probability mass function (p.m.f.) of the discrete r.v. X as $P_X(x) \triangleq \mathcal{P}\{\omega : X(\omega) = x\}$. For continuous r.v., we denote the probability density function (p.d.f.) of the continuous r.v. X as $p_X(x)$. However, when the context is clear, we use $P(x)$ and $p(x)$ for p.m.f. and p.d.f., respectively.

We consider the communication scenario depicted in Figure 2.1. In this work, it is assumed that the source is modeled as an i.i.d. discrete time

random process with a binary alphabet $P_U(0) = P_U(1) = 0.5$. A message $\mathbf{u}_m \in \{0, 1\}^K$ is formed by a block of K source symbols.

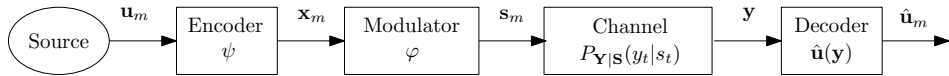


Figure 2.1: Communication scenario with encoding and decoding functions.

The encoder is assumed to be an invertible mapping ψ that assigns each message \mathbf{u}_m ($m \in \{1, \dots, 2^K\}$) to a codeword $\mathbf{x}_m \in \mathcal{X}^N$, i.e.,

$$\psi : \{0, 1\}^K \rightarrow \mathcal{X}^N.$$

Notice that this mapping can be formulated as $P(\mathbf{x}_m | \mathbf{u}_m)$, where in case of a deterministic mapping this probability is given by the indicator function, i.e.

$$P(\mathbf{x}_m | \mathbf{u}_m) = \mathbb{1} [\mathbf{x}_m = \psi(\mathbf{u}_m)], \quad (2.1)$$

where $\mathbb{1}[\cdot]$ is equal to 1 if the statement between brackets is true, and 0 otherwise.

After the channel encoder, a modulator $\varphi(\cdot) : \mathcal{X}^N \rightarrow \mathcal{S}^M$ (where \mathcal{S} is a finite channel alphabet) maps the encoded sequence into the sequence $\mathbf{s}_m = \varphi(\mathbf{x}_m)$ to be transmitted. Observe that $M = N$ when $|\mathcal{S}| = |\mathcal{X}|$.

We consider discrete memoryless channels $\{\mathcal{S}, P_{Y|S}(y|s), \mathcal{Y}\}$ modeled by a family of discrete conditional probability distributions with input and output alphabets \mathcal{S} and \mathcal{Y} , respectively. The channel is stationary and memoryless in the sense that when it is used M times with input $\mathbf{S}_m \in \mathcal{S}^M$, the output $Y_t \in \mathcal{Y}$ given $(S_1, \dots, S_t, Y_1, \dots, Y_{t-1})$ is distributed according to

$$P(y_t | s_1, \dots, s_t, y_1, \dots, y_{t-1}) = P(y_t | s_t).$$

It can be shown that when this channel is used without feedback, the memoryless property implies

$$P_{\mathbf{Y}|\mathbf{S}}(\mathbf{y}|\mathbf{s}) = \prod_{t=1}^M P_{Y|S}(y_t | s_t). \quad (2.2)$$

At this point, the joint probability of \mathbf{U} , \mathbf{X} , \mathbf{S} and \mathbf{Y} can be factorized as

$$P(\mathbf{u}, \mathbf{x}, \mathbf{s}, \mathbf{y}) = P(\mathbf{u}) \cdot P(\mathbf{x}|\mathbf{u}) \cdot P(\mathbf{s}|\mathbf{u}, \mathbf{x}) \cdot P(\mathbf{y}|\mathbf{u}, \mathbf{x}, \mathbf{s}). \quad (2.3)$$

Since by construction $\mathbf{U} \leftrightarrow \mathbf{X} \leftrightarrow \mathbf{S} \leftrightarrow \mathbf{Y}$ forms a Markov chain, the joint probability $P(\mathbf{u}, \mathbf{x}, \mathbf{s}, \mathbf{y})$ is simply given by

$$P(\mathbf{u}, \mathbf{x}, \mathbf{s}, \mathbf{y}) = \underbrace{P(\mathbf{u})}_{\text{Source}} \cdot \underbrace{P(\mathbf{x}|\mathbf{u})}_{\text{Code}} \cdot \underbrace{P(\mathbf{s}|\mathbf{x})}_{\text{Modulation}} \cdot \underbrace{P(\mathbf{y}|\mathbf{s})}_{\text{Channel}}, \quad (2.4)$$

where it can be observed that the first factor depends directly on the source, the second one on the used coding technique, the third one on the modulation and the forth one on the characteristics of the channel.

Finally, the decoder block maps the channel output \mathbf{y} to a message sequence $\hat{\mathbf{u}}_m$, that is, $\hat{\mathbf{u}}(\mathbf{y}) : \mathcal{Y}^M \rightarrow \{0, 1\}^K$. In the following, and unless strictly necessary, we drop the subindex m in the sequences and simply write \mathbf{s} , \mathbf{x} and \mathbf{u} . Given the received sequence \mathbf{y} , the decoding function that minimize the block error probability $\mathbf{P}_e \triangleq \mathcal{P}\{\omega : \hat{\mathbf{u}}(\mathbf{Y}(\omega)) \neq \mathbf{u} | \mathbf{U}(\omega) = \mathbf{u}\}$ is the block-wise Maximum a Posteriori (MAP) rule and is given by

$$\hat{\mathbf{u}}(\mathbf{y}) \triangleq \arg \max_{\mathbf{u} \in \{0, 1\}^K} P(\mathbf{u}|\mathbf{y}). \quad (2.5)$$

Applying the Bayes theorem to (2.5) and since $p(\mathbf{y})$ is not involved in the maximization, the above rule can be written as

$$\hat{\mathbf{u}}(\mathbf{y}) \triangleq \arg \max_{\mathbf{u} \in \{0, 1\}^K} \sum_{\substack{\mathbf{x} \in \mathcal{X}^N \\ \mathbf{s} \in \mathcal{S}^M}} P(\mathbf{u}, \mathbf{x}, \mathbf{s}, \mathbf{y}), \quad (2.6)$$

which is equivalent to [Von03]

$$\hat{\mathbf{u}}(\mathbf{y}) \triangleq \arg \max_{\mathbf{u} \in \{0, 1\}^K} \max_{\substack{\mathbf{x} \in \mathcal{X}^N \\ \mathbf{s} \in \mathcal{S}^M}} P(\mathbf{u}, \mathbf{x}, \mathbf{s}, \mathbf{y}). \quad (2.7)$$

On the other hand, if the objective is to minimize the symbol-wise error probability, i.e. $P_e \triangleq \mathcal{P}\{\hat{u}_i(\mathbf{Y}(\omega)) \neq u_i | U_i(\omega) = u_i\}$, we have that the

symbol-wise MAP decoding rule is given by

$$\hat{u}_i(\mathbf{y}) \triangleq \arg \max_{u_i \in \{0,1\}} P(u_i, \mathbf{y}) \quad (2.8)$$

$$= \arg \max_{u_i \in \{0,1\}} \sum_{u_1} \cdots \sum_{u_{i-1}} \sum_{u_{i+1}} \cdots \sum_{u_K} \sum_{\mathbf{x} \in \mathcal{X}^N} \sum_{\mathbf{s} \in \mathcal{S}^M} P(\mathbf{u}, \mathbf{x}, \mathbf{s}, \mathbf{y}) \quad (2.9)$$

$$= \arg \max_{u_i \in \{0,1\}} \sum_{\sim u_i} P(\mathbf{u}, \mathbf{x}, \mathbf{s}, \mathbf{y}), \quad i = 1, \dots, K \quad (2.10)$$

As explained in the next section, an efficient way for computing the above MAP rules is as follows:

- 1) Represent the joint probability $P(\mathbf{u}, \mathbf{x}, \mathbf{s}, \mathbf{y})$ as a factor graph.
- 2) The block-wise decoding is now obtained by the Max-Product algorithm [KFL01] executed over this factor graph. Notice that when the code is a Convolutional code the Max-Product algorithm reduces to the Viterbi algorithm. On the other hand, the symbol-wise decoding is obtained by running instead the Sum-Product Algorithm [KFL01].

When using iterative codes, one needs to compute the symbol-wise probabilities as these probabilities are used by the other compounding codes. Therefore, in this work we will exclusively consider the symbol-wise decoding. In the next section factor graphs and the Sum-Product Algorithm, are explained in detail.

2.2 FACTOR GRAPHS AND THE SUM-PRODUCT ALGORITHM

2.2.1 FACTOR GRAPHS

A factor graph [KFL01, Von03] represents a multivariate function. Let $f(x_1, x_2, x_3, x_4, x_5)$ be a function of a set of variables $\{X_1, X_2, X_3, X_4, X_5\}$. In Fig. 2.2 the *global*¹ function $f(x_1, x_2, x_3, x_4, x_5)$ is represented, where filled squares represent function nodes and empty circles symbolize variable nodes. An edge connects a function node to a variable node if and only if the corresponding variable is an argument of the function. Note that a

¹The term *global* refers to the multivariate function to be factorized, whereas the term *local* refers to the compounding functions of the factorized version of the *global* function.

factor graph is always bipartite: edges are only allowed between vertices of different types.

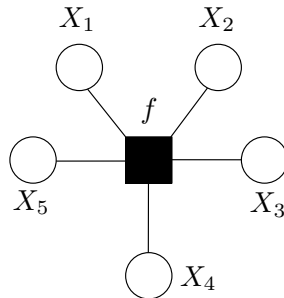


Figure 2.2: Factor graph representing the global function $f(x_1, x_2, x_3, x_4, x_5)$.

Factor graphs become interesting when the represented function can be factorized as a product of several *local*¹ functions. Let us assume that the global function mentioned above, $f(x_1, x_2, x_3, x_4, x_5)$, factors as

$$f(x_1, x_2, x_3, x_4, x_5) = f_A(x_1) \cdot f_B(x_2) \cdot f_C(x_1, x_2, x_3) \cdot f_D(x_3, x_4) \cdot f_E(x_3, x_5).$$

Now, the factor graph can be expanded to that depicted in Figure 2.3 (a), where f_A, f_B, f_C, f_D, f_E are the local functions. Even though the resulting graph is unique, different drawings can describe the same factorization of a given function, some more pleasing than others, as the one shown in Figure 2.3 (b).

The Sum-Product Algorithm (SPA) is what makes the factor graphs so attractive for the decoding problem in a communication system. It is essentially a set of rules and procedures for message passing over factor graphs that allows for an efficient calculation of the marginals of the joint probability distribution that characterizes the whole communication system. Concretely, the decomposition of the joint (global) function $f(\cdot)$ into several simpler local functions, together with its factor graph representation is what allows the SPA to efficiently compute the marginal functions needed for the Maximum a posteriori estimation, as shown in Section 2.1.

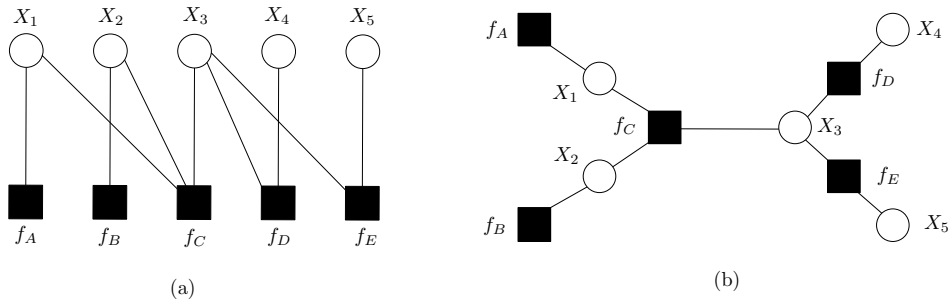


Figure 2.3: (a) Factor Graph of the factorized $f(\cdot)$; (b) Rearrangement of (a) for the sake of clarity.

2.2.2 SUM-PRODUCT ALGORITHM

The SPA consists of a set of rules for transferring messages through the edges of a factor graph, aimed at computing marginals of the global function describing the factor graph. This algorithm significantly simplifies the complexity of their calculations. For the sake of simplicity, the application of the algorithm over a cycle-free graph (i.e. factor *trees*) is first described, followed by the application of the SPA over cycle graphs.

The Sum-Product Algorithm over Non-cyclic Factor Graphs

Let us consider again the factor graph in Figure 2.3, with its global function

$$f(x_1, x_2, x_3, x_4, x_5) = f_A(x_1) \cdot f_B(x_2) \cdot f_C(x_1, x_2, x_3) \cdot f_D(x_3, x_4) \cdot f_E(x_3, x_5).$$

Assume that we are interested in calculating the marginal function $\hat{f}_1(x_1)$, where

$$\hat{f}_1(x_1) = \sum_{x_2, x_3, x_4, x_5} f(x_1, x_2, x_3, x_4, x_5) = \sum_{\sim x_1} f(x_1, x_2, x_3, x_4, x_5), \quad (2.11)$$

with $\sum_{\sim x_1}$ being the sum over all variables except x_1 . The SPA exploits the factorized structure of $f(\cdot)$ in such a way that the computation of the marginals is efficiently achieved by exchanging messages among the nodes of its factor graph under the fulfilment of certain rules. Let us pose first some useful definitions:

- The neighbor set operator $\psi(X_i)$ applied on a variable node X_i , returns the set of function nodes f_j which are connected to, whereas $\psi(X_i) \setminus f_k$ returns $\{f_j\}_{j \neq k}$ (i.e. the connected ones except f_k).
- The messages associated to the variable node X_i and variable node f_j are denoted as $\mu_{X_i \rightarrow f_j}(x_i)$ and $\mu_{f_j \rightarrow X_i}(x_i)$, where $f_j \in \psi(X_i)$ and $X_i \in \psi(f_j)$. The arrow indicates the direction of the exchanged message.

These messages are propagated through all edges of the graph obeying the rules imposed by the algorithm. The messages can be reused to compute different marginal functions. Thus, when the factor graph has no cycles, each message has to be computed only once, rather than once per marginalization. The rules for the computation of variable and function nodes are as follow:

Computation of variable-to-function message: The message from variable node X_i to function node f_j is computed as

$$\mu_{X_i \rightarrow f_j}(x_i) = \prod_{f_k \in \psi(X_i) \setminus f_j} \mu_{f_k \rightarrow X_i}(x_i). \quad (2.12)$$

Computation of function-to-variable message: The message from function node f_j to variable node X_i is computed as

$$\mu_{f_j \rightarrow X_i}(x_i) = \sum_{X_k \in \psi(f_j) \setminus X_i} f_j(x_k) \cdot \mu_{X_k \rightarrow f_j}(x_k). \quad (2.13)$$

Computation of the marginal functions: The desired marginal function $\hat{f}_i(x_i)$ is computed as

$$\hat{f}_i(x_i) = \prod_{f_j \in \psi(X_i)} \mu_{f_j \rightarrow X_i}(x_i). \quad (2.14)$$

The application of the set of rules is exemplified in Figure 2.4, where the messages necessary for calculating the marginal function $\hat{f}_1(x_1)$ are plotted. If we break the expression for $\hat{f}_1(x_1)$ down into its compounding factors, it can be seen that

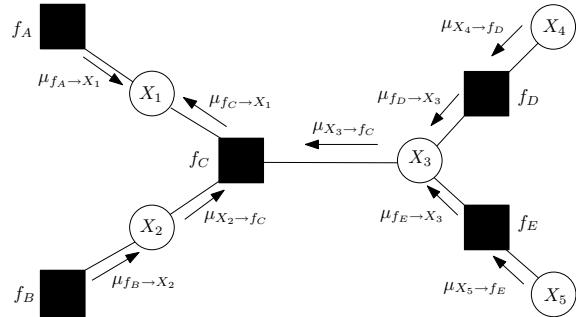


Figure 2.4: Messages used for the marginalization of $\hat{f}_1(x_1)$.

Therefore, the marginalization of X_1 is given by,

$$\hat{f}_1(x_1) = \mu_{f_A \rightarrow X_1}(x_1) \cdot \mu_{f_G \rightarrow X_1}(x_1). \quad (2.15)$$

Figure 2.5 represents all the necessary messages for calculating $\hat{f}_1(x_1)$, $\hat{f}_2(x_2)$, $\hat{f}_3(x_3)$, $\hat{f}_4(x_4)$ and $\hat{f}_5(x_5)$. Observe that the execution of the algorithm comprises a finite number of steps due to the lack of cycles in the underlying factor graph. As a result, any desired marginal of $f(\cdot)$ can be computed exactly. However, as explained in the next section, the algorithm does not take into account the presence of loops among the edges of a cyclic graph, as often occurs in e.g. the design of parallel concatenated coding schemes (see Section 2.5). In this case the algorithm has no natural termination and consequently, the marginalizations are not exact (suboptimal).

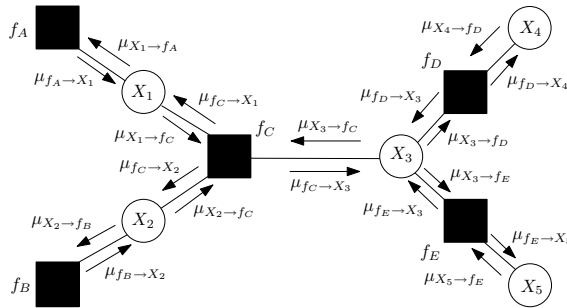


Figure 2.5: Messages necessary for calculating all possible marginal functions for $f(\cdot)$.

The Sum-Product algorithm over Cyclic Factor Graphs

If there exists cycles in the factor graph, an exact marginalization of the global function is not possible, since there are no finite number of steps in the algorithm [Mac03]. Unfortunately, the majority of the factor graphs used in communication systems are loopy. However, the SPA can still be executed on a cyclic factor graph, as the generic rules of the algorithm are locally executed in each node. In this case the algorithm would iterate with no natural termination, resulting in an inexact calculation of the marginal functions. Therefore, it yields a sub-optimal marginalization algorithm.

However, the performance of the SPA in the field of the iterative decoders of communication systems has proven to be surprisingly satisfactory by stopping the message updating after some iterations [RU08]. Moreover, the length of the codeword is a critical parameter when designing iterative decoders, since it is related to the length of the shortest cycle of the underlying graph [RU08]. Some examples of decoders with cycles are the ones used in Turbo codes [BGT93] and Low-Density-Parity-Check (LDPC) codes [RU01], the latter explained in this chapter.

Summarizing, the decoding of a received noisy sequence proceeds, in general, according to the following scheme:

- All messages are initialized.

- Messages are updated according to an update schedule: (2.12) and (2.13). This schedule may vary from step to step.
- After each step the marginal functions of the symbols to be decoded are computed: (2.14).
- A sequence is obtained by taking decisions based on the current marginal function.
- After obtaining the sequence, a decision should be made: continue with the decoding process until a specific number of iterations is achieved or stop if the sequence fulfils some conditions.

2.2.3 FACTOR GRAPHS IN CHANNEL DECODING

This Section applies the factor graphs and SPA to the communication problem presented at the end of Section 2.1. As argued in the insight around (2.10), the symbol-wise MAP rule is given by

$$\hat{u}_i(\mathbf{y}) = \underbrace{\arg \max_{u_i \in \{0,1\}}}_{\text{Decision taking}} \underbrace{\sum_{\sim u_i} \underbrace{P(\mathbf{u}, \mathbf{x}, \mathbf{s}, \mathbf{y})}_{\text{Factor Graph (product)}}}_{\text{Sum}} \underbrace{\text{Sum-Product algorithm}}_{\text{Decision about symbol } u_i \text{ based on symbol-wise decoding}} \quad (2.16)$$

A huge advantage can be taken by applying the SPA algorithm through the factor graph representing the global function $P(\mathbf{u}, \mathbf{x}, \mathbf{s}, \mathbf{y})$ and consequently, by computing efficiently the required marginals for each variable node U_i . As seen in Section 2.1, the joint probability can be further factorized as

$$P(\mathbf{u}, \mathbf{x}, \mathbf{s}, \mathbf{y}) = \underbrace{\prod_{i=1}^K P(u_i)}_{\text{Source}} \cdot \underbrace{\mathbb{1}[\mathbf{x} = \psi(\mathbf{u})]}_{\text{Code}} \cdot \underbrace{\mathbb{1}[\mathbf{s} = \varphi(\mathbf{x})]}_{\text{Modulation}} \cdot \underbrace{\prod_{t=1}^M P(y_t | s_t)}_{\text{Channel}}, \quad (2.17)$$

This factorization of the global function $P(\mathbf{u}, \mathbf{x}, \mathbf{s}, \mathbf{y})$ indicates that the overall factor graph would be formed by: (i) the function nodes of local functions representing the source, code, modulation and channel; and (ii) the variable nodes representing the sequences $\{U_i\}$ (source sequence), $\{X_l\}$ (encoded sequence), $\{S_t\}$ (modulated sequence) and $\{Y_t\}$ (channel observations).

In words, the process of performing a MAP decision in the proposed communication scenario can be summarized in the following three-stage approach:

- A) The joint probability distribution $P(\mathbf{u}, \mathbf{x}, \mathbf{s}, \mathbf{y})$ is represented by a factor graph composed of four sub-graphs representing the source, code, modulation and channel.
- B) Messages are passed through the resulting factor graph (Sum-Product Algorithm) in order to obtain the marginals required to make a symbol-wise MAP decision.
- C) The MAP decision is taken based on the calculated marginals.

Observe that the marginals are exact for non-cyclic graphs and not exact in case of cyclic graphs. In the latter case, step B and C can be performed iteratively, yielding successively refined estimations of u_i .

In the next sections we will present the channel model

$$P(\mathbf{y}|\mathbf{s}) = \prod_{t=1}^M P(y_t|s_t)$$

and the channel codes ($P(\mathbf{x}|\mathbf{u})$) used throughout this dissertation.

2.3 GAUSSIAN FADING CHANNEL MODEL

We consider the following discrete-time complex channel whose complex output at time t is given by (sampled baseband representation of a passband continuous time Gaussian channel without Inter-Symbol Interference (ISI) [Pro00])

$$Y_t = \beta_t \sqrt{d^{-\delta}} S_t + \tilde{Z}_t,$$

where S_t is the complex-valued channel input at time t , drawn from some complex constellation \mathcal{S} (e.g, Quadrature Amplitude Modulation (QAM) [Pro00]); β_t denotes the complex process modeling the multiplicative fading; and \tilde{Z}_t the complex process modeling the additive noise. It is assumed that the additive Gaussian noise $\{\tilde{Z}_t\}$ are i.i.d. circularly-symmetric complex Gaussian random variables of zero mean and variance N_0 meaning that

$$\tilde{Z} \sim \mathcal{N}_{\mathbb{C}}(0, N_0) \Leftrightarrow p_{\tilde{Z}}(z) = \frac{1}{\pi N_0} e^{-\frac{|z|^2}{N_0}} \quad (z \in \mathbb{C}).$$

Finally, the real constant d is the distance² between the transmitting and the receiving node and δ is the attenuation exponent. The latter is usually set between 2 (free space communications) and 4 (lossy environments such as urban areas) [Gol05].

In general, a fast fading process $\{\beta_t\}$ is modeled as a unit-variance, stationary, complex-Gaussian process of arbitrary spectral distribution function, where $(\beta_t - \bar{\beta})$ follows a circularly symmetric complex-Gaussian distribution (the overline operator denotes mean) [NM93]. However, in this thesis we assume a block constant fading model (slow fading), where the gains β_t are assumed to be constant over each transmitted block of length N . That is, $\beta_t = \alpha_l \forall t \in \{(l-1)N+1, \dots, lN\}$, with $l = 1, 2, \dots$, where the process of block gains $\{\alpha_l\}$ is a i.i.d. stationary complex-Gaussian process of variance 1 and with $(\alpha_l - \bar{\alpha})$ being circularly symmetric complex-Gaussian distributed. Notice that, in this case the fading process $\{\beta_t\}$ is not any longer stationary. For the sake of notation, within a block we will drop the sub-index l and denote α_l as α .

Furthermore, under the additional assumption of perfect channel state information (coherent detection), the above channel reduces to

$$Y_t = |\alpha| \sqrt{d^{-\delta}} S_t + Z_t, \quad (2.18)$$

where as before $Z_t \sim \mathcal{N}_{\mathbb{C}}(0, N_0)$.

It is also assumed that $|\alpha|$ is Rayleigh distributed as (i.e. the process $\{\alpha_l\}$ has zero-mean)

$$p_{|\alpha|}(a) = 2a \cdot e^{(-a^2)}.$$

Notice that the complex random variable Y , when conditioned by $|\alpha|$ and S , remains circularly symmetric and therefore its conditional pdf is given by

$$p(y|s, |\alpha|) = \frac{1}{\pi N_0} \exp \left(-\frac{|y - |\alpha| \cdot \sqrt{d^{-\delta}} \cdot s|^2}{N_0} \right). \quad (2.19)$$

To be consistent with the notation used so far, we shall denote the channel transition probability simply as $p(y|s)$, where the possible conditioning with respect to $|\alpha|$ is implicitly understood and will be set clear from the context.

²We refer to each paper in the appendix for the particular definition of distance

In the following, we will denote the average Signal-to-Noise Ratio (SNR) as E_s/N_0 , where E_s is the energy per complex dimension of the transmitted symbol s_t . Moreover, the energy per information bit E_b is given by $E_b = E_s \rho$, where ρ is the spectral efficiency of the system (in [bits/complex dimension]).

Before introducing the channel codes used through this dissertation, we will first introduce the channel capacity, that is, the maximum bits per channel use that can be transmitted through a channel.

2.4 INFORMATION THEORETIC FOUNDATIONS - CHANNEL CAPACITY

Let us first start with the non-fading Gaussian channel. This channel is obtained by letting $\alpha = 1$ with probability 1 and setting d to 1 in (2.18). Its conditional pdf is therefore given by

$$p(y|s) = \frac{1}{\pi N_0} \exp\left(-\frac{|y-s|^2}{N_0}\right). \quad (2.20)$$

The input sequence \mathbf{S} (codeword) to this channel results from encoding and modulating the source binary sequence $\mathbf{U} \in \{0,1\}^K$. Here the input symbols S of the channel can take any complex value without any restriction, i.e., $\mathbf{S} \in \mathbb{C}^N$.

Observe that under this assumption of no restriction, the capacity of the AWGN channel is infinite (reliable communication can be achieved with $K \rightarrow \infty$ and for any finite N). This changes by imposing some restrictions to the input symbols. The most common limitation in the input of such channels is the average transmitted energy, that is,

$$\frac{1}{N} \sum_{t=1}^N |s_t|^2 \leq E_s.$$

A coding rate $R = K/N$ (or a spectral efficiency ρ in bits per one-complex dimension) is said to be achievable for a Gaussian channel with power constraint E_s if, for all $\epsilon > 0$ and all sufficiently large N , there exist codes of length N with: codewords satisfying the power constraint; rate not smaller than R (i.e. with at least $[2^{RN}]$ messages); and error probability $\mathbf{P}_e < \epsilon$ [CT06]. The capacity is the maximum of all achievable

rates. For these channels, Shannon's theorem yields the capacity C in [bits/channel use or complex dimension] formula [Sha48]

$$C = \max_{p_S(\cdot): \mathbb{E}[|S|^2] \leq E_s} I(S; Y) = \log(1 + E_s/N_0), \quad (2.21)$$

where $I(S; Y)$ denotes the mutual information between S and Y , with \mathbb{E} denoting the expectation of a random variable. The above expression gives the maximum spectral efficiency or coding rate that is achievable for the gaussian channel given a $SNR = E_s/N_0$.

The achievability of (2.21) is proved by a Random Coding argument [CT06]. This implies that with high probability a good code could be obtained by randomly and independently generating each component of the 2^K codewords according to a complex-Gaussian distribution, $S \sim \mathcal{N}_{\mathbb{C}}(0, E_s)$. If for practical considerations, the channel symbols were instead drawn uniformly from the

$$\mathcal{S} = M^2\text{-QAM} = [\pm d, \pm 3d, \dots, \pm(M-1)d] \times [\pm d, \pm 3d, \dots, \pm(M-1)d]$$

constellation³ with M even and $M^2 \gg 2^\rho$, then one will incur in a penalty loss of up to 1.53 db in SNR (shaping gap [Jr.92]) as the symbol distributions are not longer Gaussian. It should be said that this penalty is negligible for spectral efficiencies less than 2, and in these cases, it turns out that M^2 can be chosen as low as 4 ($M = 2$). Figure 2.6 shows this fact where the capacities C (Gaussian distributed input) and $C_{\mathcal{S}}$ (Uniformly distributed input in \mathcal{S}) are plotted for multiple signal constellations in the AWGN channel, as a function of $SNR = E_s/N_0$.

On the other hand, for spectral efficiencies larger than 2, this loss could still be avoided if for example we partition the N complex dimensions of a codeword into κ blocks of L complex dimensions (i.e., $N = \kappa L$ for some large κ and L). Now, a subsequence of L complex symbols belonging to a codeword is obtained by uniformly drawing a point (vector of $2L$ real dimensions) from the set of M^{2L} lattice points of the integer lattice $2d\mathbb{Z}^{2L} + (d, d, \dots, d) = \mathcal{A}$, that lay inside a centered sphere \bigoplus . In this case d ($2d$ is the minimum distances between points of \mathcal{A}) is chosen so that the average energy of the lattice points inside \bigoplus is satisfied, i.e.,

³That is, the points of the $d > 0$ scaled and (d, d) displaced, integer lattice $2\mathbb{Z}^2$ laying inside of a square of length dM . Notice that the minimum distance between constellation points d is related to the E_s by $d^2 = \frac{3E_s}{M^2 - 1}$.

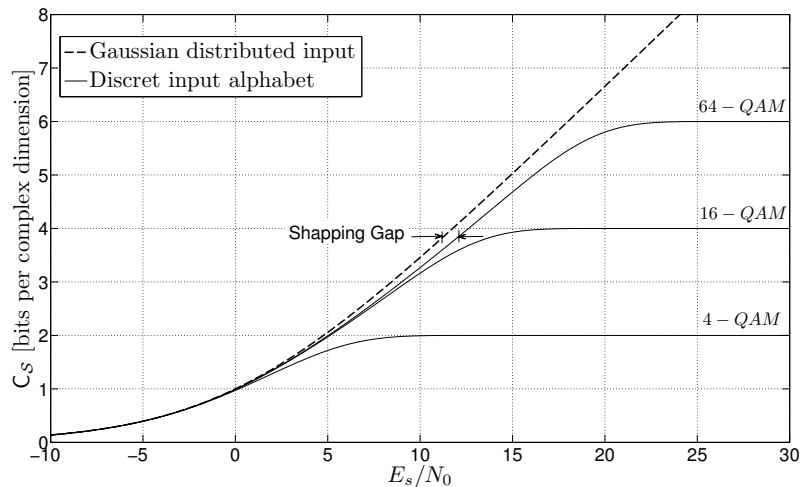


Figure 2.6: Capacity in bits per channel use for multiple signal constellations with different alphabet size and uniform distribution in the AWGN channel. For reference, the channel capacity with Gaussian inputs is shown in dashed lines.

$$\frac{1}{L} \frac{1}{M^{2L}} \sum_{i=1}^{M^{2L}} \|\mathbf{s}_i\|^2 = E_s, \quad \mathbf{s}_i \in \mathcal{A} \cap \oplus$$

A codeword is then obtained by independently repeating this process κ times⁴. The reason for reducing the shaping gap in this case is the fact [Fis02] that as the dimensionality of the $2L$ -sphere goes to infinity, the distribution induced by projecting in any complex dimension a point uniformly chosen inside the sphere, converges to the 2 real dimension Gaussian distribution.

Although, the generation of a random code will attain with high probability a capacity close to (2.21), the encoding and corresponding decoding will not be computationally feasible for large N . This is the reason to design well structured codes. For example, for spectral efficiencies lower than 2 one

⁴Notice that when $L = 1$ this selection reduces to the previous component-wise random selection.

uses Convolutional codes, linear block codes, or their iterative counterparts Turbo codes and LDPC codes, respectively [Moo05]. Similarly, for spectral efficiencies larger than 2, good channel codes are obtained by packing the points of a *good AWGN channel coding* $2N$ -dimensional lattice (or sphere-bound-achieving) inside a sphere. In this sense, one uses Coset codes and Trellis codes which are analogous to block and convolutional codes, respectively [Jr.92].

Let us now focus in the channel model presented in the previous section. Under the assumption of block fading, the capacity given in (2.21) is now a random variable depending on the instantaneous values of $|\alpha|^2$, which are exponentially distributed (i.e. $|\alpha|^2 \in \mathbb{R}^+$). That is,

$$C(|\alpha|^2 E_s / N_0) = \log(1 + |\alpha|^2 \cdot E_s / N_0). \quad (2.22)$$

Notice that in a block constant fading channel, one codes over a single block and the notion of channel capacity is in general not well defined. To deal with coding under slow fading, several coding options have been proposed in the literature [GK12], namely, the compound channel approach and the outage capacity approach:

- **Compound channel approach.** This approach consists on coding against the worst possible channel to guarantee reliable communication over every possible value of fading. The Shannon capacity under this coding approach is given by what is called in information theory the compound channel capacity. In our Gaussian fading model, the compound capacity reduces to

$$C_{CC} = \inf_{|\alpha| \in \mathcal{F}} C(|\alpha|^2 \cdot E_s / N_0) = 0,$$

where \mathcal{F} denotes the support of the pdf of the considered fading. Under our additional assumption of a Rayleigh distribution for $|\alpha|$, $\mathcal{F} = \mathbb{R}^+$ and consequently the above capacity is 0. Therefore, this approach is useless in our case. The following coding approach should be used instead.

- **Outage capacity approach.** In this approach, we transmit at a some target rate and tolerate some information loss due to low fading

realizations. We refer to the event of not being able to reliable transmit information due to the fading as *outage*. If the probability of such a event is low, then reliable communication can be performed most of the time. More precisely, if we can tolerate an outage probability P_{outage} , then we can communicate at any rate lower than the outage capacity given by,

$$C_{\text{outage}} = \max_{a: \mathcal{P}\{|\alpha|^2 < a\} \leq P_{\text{outage}}} C(a \cdot E_s/N_0).$$

Through this dissertation we will use the outage probability as a benchmark for comparing the performance of different systems.

2.5 CHANNEL CODES

2.5.1 CONVOLUTIONAL CODES

Convolutional codes are linear codes whose encoding can be regarded as a filtering (or convolution) operation in \mathbb{F}_2 . Thus, a convolutional encoder may be viewed as a set of digital (LTI - Linear Time Invariant) filters with the code sequence composed by the multiplexed filter outputs. For the sake of simplicity only rate- $1/n$ binary convolutional codes are considered, although the extension to rate- k/n codes is trivial. Nevertheless, we refer to [Moo05] for an insightful tutorial on convolutional codes.

A rate $R = 1/n$ convolutional code is characterized by a $1 \times n$ matrix function $G(x)$, referred to as the encoding function matrix. The elements of $G(x)$ can be polynomial or rational functions and represent the different digital filters. An encoder with only polynomial entries in its encoding function matrix is said to be a feed-forward, FIR or non-recursive encoder. On the contrary, if $G(x)$ is composed at least by one rational function, the encoder is said to be feedback, IIR or recursive. If a replica of the input sequence is kept unchanged in any of the n output sequences, then the encoder is said to be systematic. For this to happen, one of the elements of $G(x)$ must be equal to 1. Let us consider the encoding functions

$$\begin{aligned} G_1(x) &= [1 + x + x^3 \quad 1 + x + x^2 + x^3], \\ G_2(x) &= [1 \quad \frac{1+x^2}{1+x+x^2}]. \end{aligned} \tag{2.23}$$

It is clear that $G_1(x)$ is a non-recursive non-systematic encoder, while $G_2(x)$ is a systematic recursive encoder.

Moreover, for non-recursive encoders (FIR filters), it is common to indicate the polynomials as vectors representing the impulse response of the encoder, e.g., $G_1(x) = [1101 \ 1111] = [q_1 \ q_2]$, where q_j , $j = 1, \dots, n$ represents the impulse response of the j th digital filter. Following this notation, the transfer function of any convolutional code is usually written in octal form. In this case⁵ $G_1(x) \equiv (15, 17)_8$, and $G_2(x) \equiv (1, 5/7)_8$.

Regarding the filter representation of a convolutional code, we define the constraint length as the maximum exponent of the encoding function and denote it L . Thus, the number of memory elements v needed for implementing the filters is determined by the constraint length of the encoder as $v = L - 1$. Figure 2.7 shows the set of filters used to implement $G_2(x)$, where for this particular encoding function, the constraint length is $L = 3$, and therefore it has $v = 2$ memory elements.

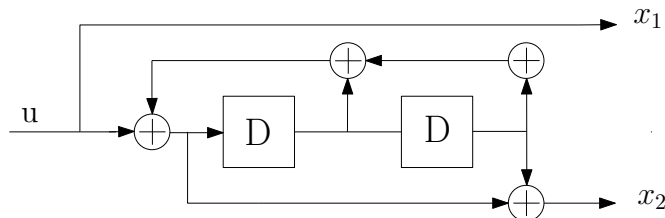


Figure 2.7: Encoder (set of filters) for $G_2(x)$.

To improve the performance of the convolutional code for short-length sequences, it is usual to drive the encoder such that all memory elements finish the encoding operation containing a zero, i.e. to terminate in the all-zero state. To this end, for the non-recursive (feed-forward) encoder (e.g. $G_1(x)$) it suffices to insert v additional zeros after the input sequence, although less than v might be needed. However, this strategy is not possible for the recursive (RSC) encoder due to the feedback. Fortunately, a simple strategy has been developed in [DP95] which overcomes this problem.

Let us now focus on other representations of convolutional codes. A convolutional encoder can also be seen as a finite-state machine. Therefore, it may be characterized by a finite state-transition diagram with 2^v states, one per possible values of the memory blocks (see Figure 2.8(a)). The state diagram represents the connections from states at one time instant to states

⁵The subindex 8 in the definition of the code stands for *octal*

at the next time instant. The possible transitions of states are shown by connecting them by an edge, indicating the input/output that generates that transition. Although the state diagram completely characterizes the encoder, one cannot easily use it for tracking the encoder transitions as a function of time since the diagram cannot represent time history. To solve this issue, another extremely useful representation is the Trellis diagram (see Figure 2.8(b)), which adds the dimension of time to the state diagram. The main advantage of this representation is that finding a codeword corresponding to a given input sequence is straightforward. By convention, the first state is always the zero state. To move through the trellis, one has to start in this first state, and depending of the input value (0 or 1), move to the next state from left to right. In Figure 2.8 these two representations are shown for $G_2(x)$. This encoding function leads to a state-machine with $2^v = 4$ different states.

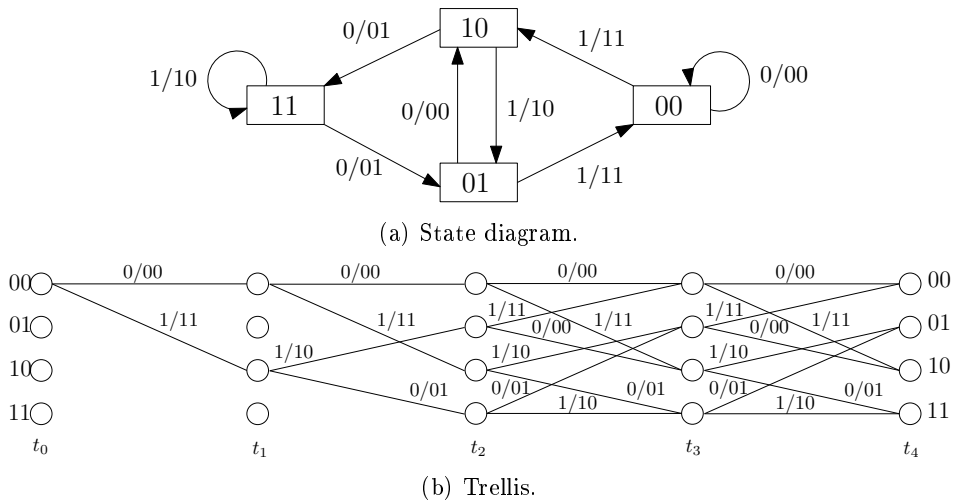


Figure 2.8: State diagram and Trellis representation of $G_2(x)$.

Finally, another useful representation is through the factor graph describing the factorization of the encoding (global) function $P(\mathbf{x}|\mathbf{u})$, i.e. the probability function taking value 1 if a codeword is associated to the input sequence and 0, otherwise. This factorization can be used for decoding by executing the SPA on it, as we will next explain.

2.5.1.1 Decoding Convolutional Codes

Several algorithms have been developed for decoding convolutional codes. The most widely used is the Viterbi algorithm, which is a maximum likelihood sequence estimator (an illustrative example can be found in [Moo05]). Another decoding algorithm is the symbol-wise MAP decoder frequently referred as the BCJR algorithm, which takes its name from its inventors Bahl, Cocke, Jelinek and Raviv (BCJR [BCJR74]). In many aspects, the BCJR algorithm is similar to the Viterbi algorithm. However, the Viterbi algorithm results in an overall decision on an entire sequence of bits (or codeword) at the end of the algorithm, and there is no way of determining the reliability of the decoder decisions on the individual bits. The BCJR algorithm, on the other hand, computes soft outputs in the form of posterior probabilities for each of the message bits [Moo05]. This fact makes the BCJR algorithm ideally suited for decoding iterative codes, as in the latter, the soft decisions on the individual bits are needed to be passed to the other compounding codes.

Finally, executing the SPA over the associated factor graph also leads to an efficient and exact symbol-wise MAP decoding. Moreover, we will next show that the latter is equivalent to the BCJR algorithm.

Consider a rate- $1/n$ convolutional code. Thus, at each instant i ($i = 1, \dots, K$), for the input bit u_i the encoder generates the n -length sequence \mathbf{x}_i . We denote \mathbf{y}_i to the n channel observations associated to \mathbf{x}_i . Regarding the states of the convolutional code, at each i the state of the encoder is set to Φ_i . We denote $Q = 2^v$, where v is the memory of the encoder, to the total number of states (i.e. $\Phi_i \in Q$). It is assumed that the encoder starts in the zero-state and when the encoder is terminated, the last state, namely Φ_K , is also the zero-state. Otherwise, it is assumed that the encoder could terminate in any state with equal probability. The sequence of states associated with the input sequence is $\{\Phi_0, \Phi_1, \dots, \Phi_K\}$. In a concrete instant $i + 1$, there is a transition from state $\Phi_i = p$ to state $\Phi_{i+1} = q$. The unique input u_i which causes this transition is denoted by $u^{(p,q)}$, and the output by $\mathbf{x}^{(p,q)}$.

The goal of the decoder is to determine the symbol-wise posterior probabilities of the input $P_{U_i}(b|\mathbf{y})$, that is, the probability that the input at instant i takes on some value $b \in \{0, 1\}$ given the entire received sequence \mathbf{y} . As seen in section 2.1, this probability can be obtained by marginaliz-

ing the joint probability $p(\mathbf{u}, \mathbf{x}, \mathbf{y})$, which can be efficiently computed by running the SPA through the factor graph.

Consider the factor graph depicted in Figure 2.9, where for simplicity the input sequence is only three bits long. The states are typically considered hidden, as they are not directly observable. Thus, they are depicted in the factor graph as double circles. The local functions $T_i(\phi_i, \phi_{i+1}, u_i, \mathbf{x}_i)$ describe the transitions allowed in the Trellis, indicating which combination of variables in its argument are valid, that is,

$$T_i(\phi_i, \phi_{i+1}, u_i, \mathbf{x}_i) = \mathbb{1} [\text{for } \phi_i = p \text{ and } \phi_{i+1} = q, \text{ then } u_i = u^{(p,q)} \text{ and } \mathbf{x}_i = \mathbf{x}^{(p,q)}].$$

Observe that the associated factor graph does not have cycles, and therefore, the exact marginal probability $P_{U_i}(b|\mathbf{y})$ will be computed after one iteration.

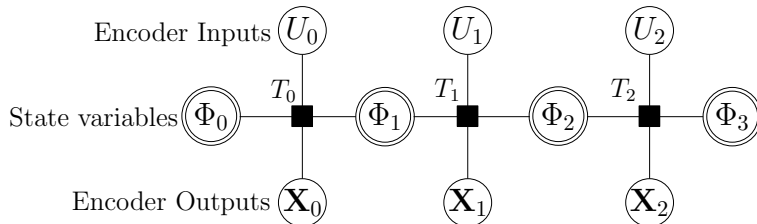


Figure 2.9: Factor graph of a convolutional code

Consider now the message passing algorithm starting at the left end of the factor graph. Table 2.1 shows all the messages together with their meaning. To begin with, nodes representing Φ_0 and \mathbf{X}_0 send their respective messages. Note that $\mu_{T_0 \rightarrow \Phi_0}(\phi_0)$ is actually known since the convolutional encoder starts in the zero-state. Moreover, if the convolutional code is forced to terminate in the all zero-state, then $\mu_{\Phi_K \rightarrow T_{K-1}}(\phi_K)$ is also known. Nevertheless, the corresponding nodes will be left as a variable nodes. At this point, the node T_0 has messages from all but one of its edges and can send out a message.

$$\mu_{T_i \rightarrow \Phi_{i+1}}(\phi_{i+1}) = \sum_{\sim \phi_{i+1}} T_i(\phi_i, u_i, \mathbf{x}_i, \phi_{i+1}) \mu_{T_i \rightarrow \Phi_i}(\phi_i) \mu_{\mathbf{x}_i \rightarrow T_i}(\mathbf{x}_i) \quad (2.24)$$

Equivalently, starting at the right and working backwards, the message passing rules yields

$$\mu_{\Phi_i \rightarrow T_i}(\phi_i) = \sum_{\sim \phi_i} T_i(\phi_i, u_i, \mathbf{x}_i, \phi_{i+1}) \mu_{\mathbf{x}_i \rightarrow T_i}(\mathbf{x}_i) \mu_{\Phi_{i+1} \rightarrow T_i}(\phi_{i+1}) \quad (2.25)$$

Having computed the $\mu_{T_i \rightarrow \Phi_{i+1}}(\phi_{i+1})$ and $\mu_{\Phi_i \rightarrow T_i}(\phi_i)$ at a node T_i , we can now compute the message to be sent to u_i as

$$\begin{aligned} \mu_{T_i \rightarrow U_i}(u_i = b) &= \sum_{\sim u_i} T_i(\phi_i, u_i = b, \mathbf{x}_i, \phi_{i+1}) \mu_{T_i \rightarrow \Phi_i}(\phi_i) \cdot \\ &\quad \cdot \mu_{\mathbf{x}_i \rightarrow T_i}(\mathbf{x}_i) \mu_{\Phi_{i+1} \rightarrow T_i}(\phi_{i+1}) \end{aligned} \quad (2.26)$$

The last equation correspond to the marginal probability $P_{U_i}(b|\mathbf{y})$ and it is used to estimated the source bits.

Finally, if the messages through the factor graph are renamed according to Table 2.1 (Figure 2.10 shows these messages in the corresponding edge of the graph), the SPA yields the BCJR algorithm as described in [Moo05, Section 14.3.7], which shows the optimality of the SPA applied in cycle-free factor graphs.

Message	Meaning	BCJR Designation
$\mu_{T_i \rightarrow \Phi_{i+1}}(\phi_{i+1})$	$P(\Phi_{i+1} = \phi_{i+1}, \mathbf{y}_1, \dots, \mathbf{y}_i)$	$\alpha(\phi_{i+1})$
$\mu_{\mathbf{x}_i \rightarrow T_i}(\mathbf{x}_i)$	$P(\mathbf{x}_i \mathbf{y}_i)$	$\gamma(\mathbf{x}_i)$
$\mu_{\Phi_{i+1} \rightarrow T_i}(\phi_{i+1})$	$P(\Phi_i = \phi_i, \mathbf{y}_{i+1}, \dots, \mathbf{y}_K)$	$\beta(\phi_{i+1})$
$\mu_{T_i \rightarrow U_i}(u_i = b)$	$P_{U_i}(b \mathbf{y})$	$\delta(u_i = b)$

Table 2.1: Message meaning and BCJR designation.

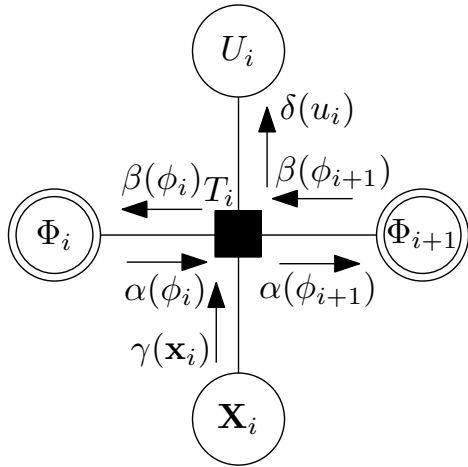


Figure 2.10: Message designation for the BCJR algorithm.

2.5.2 LOW-DENSITY PARITY-CHECK (LDPC) CODES

Let us first define the basics of a linear block code \mathcal{C} . A generator matrix G is a $K \times N$ matrix of rank K consisting of a set of linearly independent binary vectors. This set forms a basis for \mathcal{C} ; that is, $\{\mathcal{C} = \mathbf{u}G, \forall \mathbf{u} \in GF(2)^K\}$. Thus, a codeword \mathbf{x} can be obtained as $\mathbf{x} = \mathbf{u}G$. Analogously, the code \mathcal{C} can be seen as the null space over $GF(2)$ of the parity-check matrix H that fulfils $HG = 0$. Hence, we have that

$$\mathbf{x}H^T = 0 \quad \forall \mathbf{x} \in \mathcal{C}.$$

If we denote the parity matrix as

$$H = \begin{bmatrix} \mathbf{h}_1 \\ \vdots \\ \mathbf{h}_{N-M} \end{bmatrix},$$

the equation $\mathbf{x}\mathbf{h}_i^T = 0$ is said to be a linear parity-check constraint on the codeword \mathbf{x} . We use the notation $z_m = \mathbf{x}\mathbf{h}_i^T$ and call z_m a parity check or, more simply, a check. Finally, we define the weight of a binary vector as the number of non-zero elements in it. Then, the column weight of a column of a matrix is the weight of the column; similarly for row weight.

Having posed the above definitions, a Low-Density Parity-Check (LDPC) code is a linear block code with a very sparse⁶ parity-check matrix H . For reasons to be made clear below, the parity check matrix should also be such that no two columns have more than one row in which elements in both columns are nonzero (this corresponds to cycles of length four in the corresponding graph). Typically, N is taken to be quite large (such as $N > 10000$) while the column weight is held at around 3 or 4, so the density of 1s in the matrix is quite low (a column weight of 2 has been found to be ineffective [Mac99]).

An LDPC code is said to be regular if, in the parity check matrix, the column weights are all the same and the row weights are all the same. On the other hand, a LDPC code is said to be irregular if it has a parity check matrix in which the column weight (resp. row weight) may vary from column to column (resp. row to row). It is worth mentioning that the best known LDPC codes are irregular; and gains up to 0.5 dB compared to regular codes are attainable [RU08]. Thus, the correct choice of a good parity-check matrix is crucial for the performance of the system.

Once the parity-check matrix is built, the construction of the corresponding generator matrix G is not an easy task [RU08]. Fortunately, in some cases, there are two main ways to avoid the construction of G : i) to assume, due to the linearity of the code, that the transmitted codeword is always $\mathbf{x} = \mathbf{0}$, i.e., the all zeros codeword; ii) to generate random codewords and compute $z_m = \mathbf{x}\mathbf{h}_m^T$, $m = 1, \dots, N - M$. In this case, the matrix H no longer generates the null space since most of the checks $z_m \neq 0$. However the decoding algorithm can be easily adapted in order to take into account the new values of z_m [Mac03]. In this thesis we use the latter approach in Paper III.

Moreover, since the topic of this thesis is not focused on the construction of such good matrices, we opt to use the weight distributions already verified in [IPG] and we generate both G and H through the open software offered in [Mac]. We refer to [RU01] for an insight on the construction of parity-check matrices which lead to LDPC codes with very good performance and to [RU08] for further information on LDPC coding techniques.

⁶A matrix is said to be sparse if the proportion of non-zero entries is less than 1/2.

2.5.2.1 Decoding LDPC codes

Let us start defining some notation in order to be consistent with the notation used in the literature. Bits are indexed by n or n' (e.g., $x_{n'}$) and the checks are indexed by m or m' (e.g., z_m). We denote the set of bits n that participate in check m by $\mathcal{N}_m \triangleq \{n : H_{mn} = 1\}$. Thus, we can write the m th check as $z_m = \sum_{n \in \mathcal{N}_m} x_n$. Similarly we denote the set of checks in which bit n participates, $\mathcal{M}_n \triangleq \{m : H_{mn} = 1\}$. We denote a set \mathcal{N}_m with bit n excluded by $\mathcal{N}_m \setminus n$. Finally, for the sake of clarity, in some cases we opt to write $P(x = b)$ instead of $P_X(b)$, with $b \in \{0, 1\}$.

In addition, we simplify the symbol-wise MAP rule as follows: We omit the use of the modulator φ and \mathbf{s} ; we consider $\mathcal{X} = \{0, 1\}$; and, as the encoder is an invertible function, we aim at estimating the transmitted codeword $\hat{\mathbf{x}}$.

Therefore, the rule in (2.10) is now given by

$$\hat{x}_t = \arg \max_{x_n \in \{0, 1\}} \sum_{\sim x_n} p(\mathbf{y}, \mathbf{x}). \quad (2.27)$$

For memoryless channels, the above probability can be further factorized as

$$p(\mathbf{y}, \mathbf{x}) = \mathbb{1}[z_1 = 0, z_2 = 0, \dots, z_M = 0] \prod_{n=1}^N p(y_n | x_n). \quad (2.28)$$

where the indicator function represents whether the sequence \mathbf{x} belongs to the code or not, i.e., $\mathbf{x} \in \mathcal{C}$.

We now expand the indicator function of the above equation as

$$\mathbb{1}[z_1 = 0, z_2 = 0, \dots, z_M = 0] = \prod_{m=1}^M \mathbb{1}[z_m = 0] \quad (2.29)$$

Although not explicitly show, it is clear that $\mathbb{1}[z_m = 0]$ is a function of the encoded symbols $X_n \in \mathcal{N}_m$. Finally, combining (2.28) and (2.29) we have that the joint probability of (2.27) is given by

$$p(\mathbf{y}, \mathbf{x}) = \prod_{m=1}^M \mathbb{1}[z_m = 0] \prod_{n=1}^N p(y_n | x_n) \quad (2.30)$$

and its factor graph representation is shown in Figure 2.11, where, with a little abuse of notation, we have denoted $\mathbb{1}[z_m = 0]$ as z_m and $p(y_n|x_n = b)$ as $p_n(b)$.

Observe that the factor graph corresponding to (2.29) also represents the parity-check matrix. That is, the factor nodes z_m (also known as check nodes) and the variable nodes X_n (known as bit nodes) represent the rows and columns of H , respectively. Each of the edges in the graph represent that the n th bit is involved in the m th check, i.e., that $H_{mn} = 1$. The graph associated with the parity check matrix H is also called a Tanner graph.

Now, the symbol-wise MAP rule (2.27) can be efficiently computed by applying the SPA described in Section 2.2 in the factor graph representing the joint probability (Figure 2.11). Table 2.2 shows the different messages passed over the factor graph with its respective meaning. If the factor graph is a tree⁷ (that is, cycle-free), the SPA yields an exact symbol-wise MAP rule computation. However, it was shown in [RU08] that finite-length tree-like LDPC codes have bad performance (due to the large number of codewords of weight 2).

Fortunately, thorough analysis of large-cycle graphs have shown that the approximate algorithm still provides effective decoding capability and that the complexity of the decoding is linear in the code length [RU08]. Nevertheless, it is crucial to remove the 4-length cycles from the graph (and consequently from the matrix H), since they strongly degrade the decoding performance [RU08]. Therefore, as mention above, the parity check matrix should be such that no two columns have more than one row in which elements in both columns are non-zero.

Message	Meaning
$\mu_{z_m \rightarrow X_n}(x_n = b)$	$P(z_m = 0 \mathbf{y}, x_n = b)$
$\mu_{X_n \rightarrow z_m}(b)$	$P(x_n = b \mathbf{y}, \{z_{m'} = 0\}_{m' \in \mathcal{M}_n \setminus m})$
$\mu_{p_n \rightarrow X_n}(x_n = b)$	$P(y_n x_n = b)$

Table 2.2: Messages in the factor graph and their respective meaning.

⁷It is shown in [RU08] that when $N \rightarrow \infty$, the graph is in fact a tree, i.e., the probability of having a cycle in the graph tends to zero.

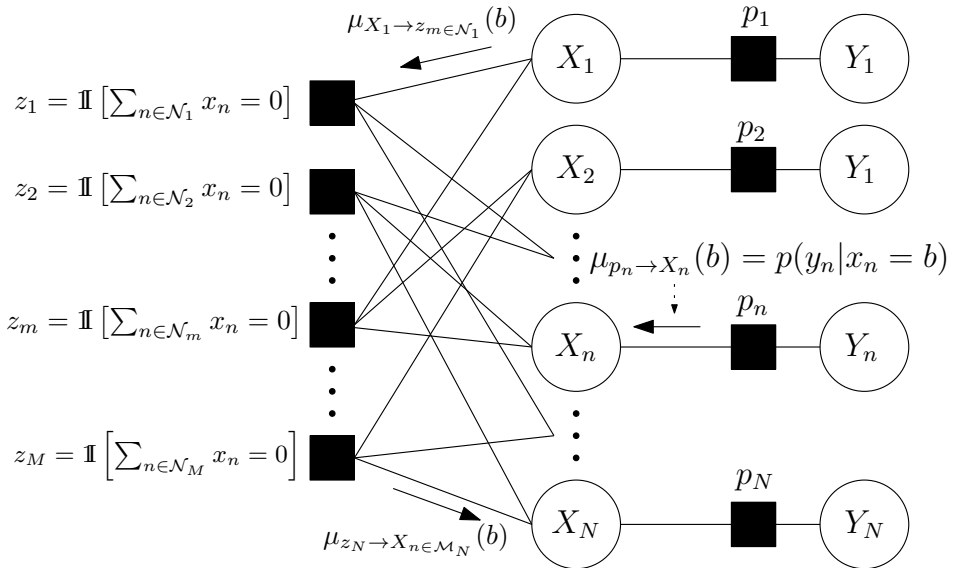


Figure 2.11: Factor graph representing the joint probability of (2.27) and the associated messages.

At this point, the iterative decoding algorithm is initialized by setting

$$\mu_{X_n \rightarrow z_m}(b) = \mu_{p_n \rightarrow X_n}(b) = p(Y_n = y | X_n = b).$$

That is, the conditional probability on the checks is set to the channel likelihood probability. Then, all the messages in the factor graph are computed as described in Section 2.2 (one iteration). After every iteration, the posterior probability of each encoded symbol x_n is computed as

$$P(x_n = b | \mathbf{y}, \{z_m\}_{m \in \mathcal{M}_n}) = \mu_{p_n \rightarrow X_n}(b) \cdot \prod_{m \in \mathcal{M}_n} \mu_{z_m \rightarrow X_n}(b). \quad (2.31)$$

These posterior probabilities are used to make decisions on b : if for $b = 1$ (2.31) is larger than 0.5, then a decision is made to set $\hat{x}_n = 1$; and $\hat{x}_n = 0$, otherwise. Finally, if $\mathbf{x}H^T = 0$, that is, all checks are simultaneously satisfied, the decoding is finished. Otherwise, the algorithm performs another iteration. If the halting condition is not fulfilled after a given number of iterations, the algorithm stops and a decoding error is declared.

After having described the channel codes used in this work, we now present a short introduction to network coding, as in the next chapters we

will present papers that design joint network-channel coding schemes to improve the error correction in wireless relay networks.

2.6 NETWORK CODING

Layered architecture models, as the Open Systems Interconnection (OSI) basic reference model [Zim80], allow to handle the complexity of large communication networks. Each layer fulfils its specific tasks and delivers a more abstract and simpler model of the network to its upper layer. This allows to split the design of the communication network into several easier design problems. Nevertheless, a layered design approach can be in general suboptimal in comparison to a cross-layer design approach, where several layers are designed jointly, as it was shown in [Hau08].

The basic idea of network coding is that the intermediate nodes in a network are not only allowed to route but also to perform simple coding operations, as for example, the combination of the incoming data. Network coding was first proposed to operate in the network layer (see OSI model [Zim80]), once the channel coding had transformed the noisy point-to-point links into error free links [ACLY00]. Although in a unicast network (one source and one sink) routing the information allows to achieve the maximum throughput (Max-Flow Min-Cut theorem [FF56]); it was shown in [ACLY00] that in multicast networks (one source, several sinks) it is, in general, necessary to perform network coding to achieve the multicast capacity.

The canonical example for the superiority of network coding over routing in multicast networks is the "Butterfly Network" [ACLY00], which is depicted in Figure 2.12. In the example, the source \mathcal{S} wants to transmit both bits u_1 and u_2 to both sinks \mathcal{D}_1 and \mathcal{D}_2 . Each of the error-free links can transmit (receive) only one bit per time-unit per outgoing (incoming) channel. As shown in Figure 2.12 (left), if network coding is not allowed, 5 time instants are needed to transmit both bits from the source to the sinks. On the other hand, if network coding is allowed, in the third time instant, the bottleneck node \mathcal{B} can combine both incoming bits using a modulo-2 addition into the bit u_3 (i.e. $u_3 = u_1 \oplus u_2$) and transmit it. Afterwards, the node \mathcal{C} transmits u_3 to both sinks. Finally, the sinks can recover the remaining bit (u_2 the sink \mathcal{D}_1 and u_1 the sink \mathcal{D}_2) by performing another modulo-2 addition between the two received bits (i.e. $u_2 = u_1 \oplus u_3$ and

$u_1 = u_2 \oplus u_3$). This process is depicted in Figure 2.12 (right). Therefore, in the latter case all links are used only once, saving one time instant.

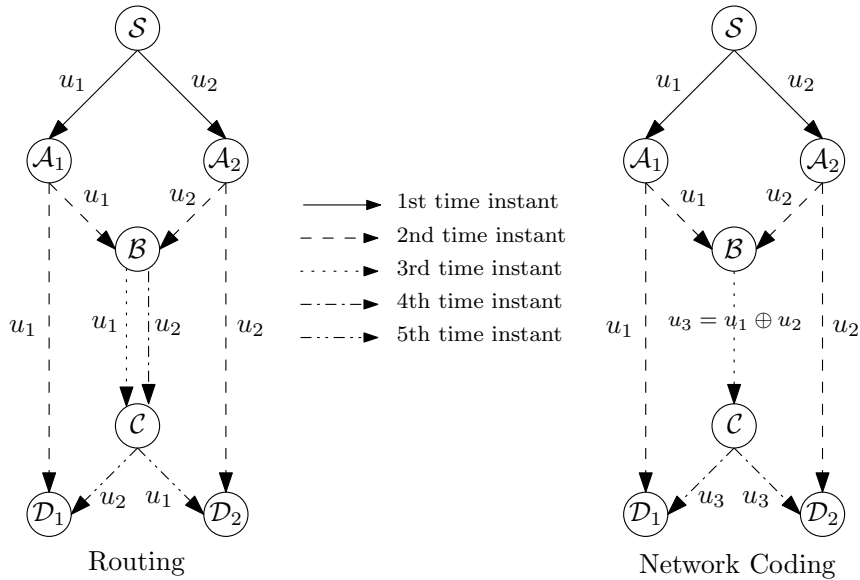


Figure 2.12: Example of superiority of network coding over routing.

2.6.1 NETWORK AND CHANNEL CODING

In the previous part of this section we have shown the throughput gain obtained by using network coding in error-free links. Now, we will consider networks with noisy point-to-point links [TF04]. To protect the information against errors, channel coding has to be considered. We now describe the two possibilities for combining network coding and channel coding, namely, Separated or Joint network-channel coding.

2.6.1.1 Separated Network-Channel Coding

In general, in the separated network and channel coding approach, the channel coding is performed in the physical layer (lowest layer of the OSI model) to protect the point-to-point links from errors, whereas the network coding is independently computed in the network layer to increase the throughput. In particular, for AWGN channels the channel coding aims

at converting the physical channels into error-free channels. This could be achieved for example by using a sufficiently low rate. Observe that the example mentioned above (Figure 2.12) would be a particular case, in which the channel coding has converted the noisy point-to-point links into error-free links; and hence, the network layer works over error-free links. Figure 2.13 shows the separate network-channel coding scheme performed at the node B of the previous example.

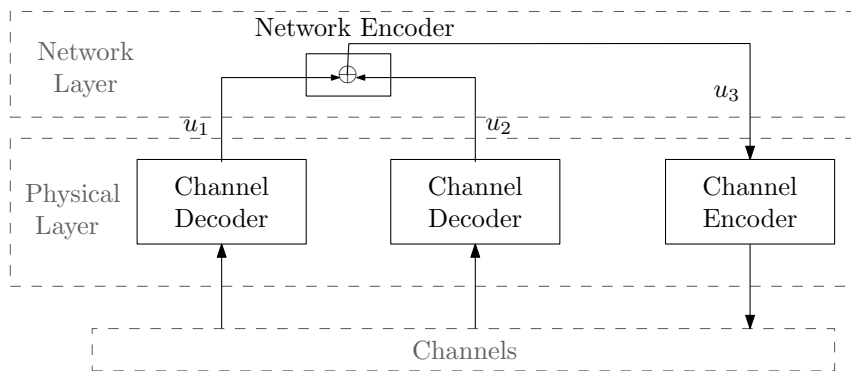


Figure 2.13: Separated Network-Channel coding scheme.

However, for channels with fading, if a link is in a deep fade the channel code will not be able to correctly decode the message. Therefore, instead of converting the point-to-point channels into error-free channels, the channel coding will convert them into erasure channels. That is, the decoder will pass either an erasure, if the channel was in a deep fade; or hard decisions of the received bits, otherwise.

2.6.1.2 Joint Network-Channel Coding

Joint network coding and channel coding is a more general approach than separated network-channel coding. Instead of splitting the overall problem into two separated tasks, error protection and network information transfer are considered jointly. That is, instead of guaranteeing the error-free transmission for each point-to-point link, we are only interested to guarantee error-free decoding at the nodes. In this sense, if a node has more than one incoming link, error-free decoding at the sink can be possible even

if error-free decoding of the point-to-point links is not possible. Hence, joint network-channel coding is useful, if the network code contains redundancy.

Analogous to joint source-channel coding where the remaining redundancy after the source encoding helps the channel code to combat noise, joint network-channel coding allows to exploit the redundancy in the network code to support the channel code for a better error protection. To that end, we will perform joint network-channel decoding by iteratively passing soft information between channel decoders and the network decoder.

While a separated network-channel coding approach seems sufficient for wireline networks, a joint network-channel coding approach is required for efficient information transfer in wireless networks with broadcast transmissions [EMH⁺03].

Finally, in the papers presented through this dissertation we will show the usefulness and the design of joint network-channel codes for specific wireless relay networks. We will show that the proposed joint network-channel coding schemes outperform not only the separate approach but also the joint schemes found in the literature.

CHAPTER 3

Joint Network-Channel Coding Schemes for the Multiple-Access Relay channel

In this chapter we first briefly introduce the Multiple-Access Relay Channel (MARC) and present the main advantages of performing network coding on this network. Following, the state of the art regarding the design of joint network-channel codes for the Time-Division Decode-and-Forward Multiple Access Relay Channel (TD-DF-MARC) is presented. Finally, we conclude the chapter with an insightful review of the main contributions of Papers I and II (Appendix A and B, respectively), where two novel joint network-channel schemes are proposed.

3.1 MULTIPLE ACCESS RELAY CHANNEL

The Multiple Access Relay Channel (MARC) is a communication scenario where several information sources forward data to a single common destination with the help of an intermediate relay [KW00]. As an example, consider a wireless cellular network where a relay station helps to transmit data to a base station, as depicted in Figure 3.1.

In order to survey the different types of MARC channels proposed so far in the literature, we first start with some definitions. If a node can both

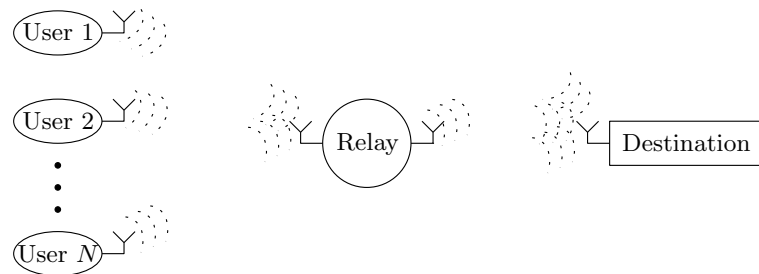


Figure 3.1: Example of a Multiple Access Relay Network.

transmit and receive at the same time instant, it is said that the node works in full duplex mode. On the other hand, if at a given time instant a node can only transmit or receive data, it is said that it works in half duplex mode. In addition, it is often convenient to divide the total transmission time used by the system in different orthogonal time slots, and then, assign the transmission times of each of the compounding nodes to the different time slots.

Thus, in this scenario, the relay can work either in full [KW00,KGG05] or half duplex mode. For the half duplex mode, the following transmission strategies have been proposed: i) the Constrained MARC (C-MARC [SKM04]), where the sources transmit during the first time slot and coordinate with the relay during the second time slot by transmitting information; ii) the Orthogonal MARC (O-MARC, see [SLPM07, SLMP11]), where the sources and the relay transmit over two orthogonal channels; and iii) the Time-Division MARC (TD-MARC, see [HSOB05]), where both the sources and the relay convey their data using three orthogonal channels, i.e. for two sources the total transmission time is divided into three time slots, one for each transmitting node.

On the other hand, during the last decade the well-known relaying strategies Decode-and-Forward (DF), Compress-and-Forward (CF) and Amplify and Forward (AF) originally developed for the conventional relay channel [CG79] have been applied to the aforementioned MARC models in a number of contributions (see e.g. [KW00, KGG05, SKM04, SLPM07, SLMP11] and references therein).

Regarding the implementation of our proposed coding schemes, a Time-Division multiplexing strategy has been considered. Although a time-division scheme involves a suboptimal use of the available bandwidth, it allows for an easier implementation in practical systems thanks to the use of half-duplex relays and the lack of stringent synchronization constraints. Similarly, the DF strategy is preferred over the CF and AF as it offers a higher code design flexibility. Therefore, in the following we focus specifically on the 2-user TD-MARC with a DF relaying strategy (hereafter coined as TD-DF-MARC). Before reviewing the practical schemes proposed in the literature for the TD-DF-MARC, we first present, with the aid of an illustrative example, the advantages of performing network coding in wireless MARCs.

3.1.1 NETWORK CODING IN MARCS

As mentioned in Chapter 2, Section 2.6, in fading environments (i.e. wireless channels) the network coding becomes a very powerful tool for increasing the diversity in the system. The following example shows how, if network coding is used, the data from the sources can be recovered at the destination even if one of the links suffering from block fading is in a deep fade.

In this context, we consider a TD-MARC as depicted in Figure 3.1 for $N = 2$ (i.e. a 2-user MARC). We assume the channels ending at the relay are error-free, whereas the three channels ending at the destination are independent random block fading channels. Finally, we consider a separate network-channel coding scheme, which means that the decoder will pass to the network layer either an erasure, if a link is in a deep fade, or otherwise a hard decision of the transmitted bits (see Chapter 2, Section 2.6).

As depicted in Figure 3.2, bits u_1 and u_2 from sources \mathcal{S}_1 and \mathcal{S}_2 , respectively, are transmitted to the destination with the aid of the relay \mathcal{R} . Thus, in the first time slot source \mathcal{S}_1 broadcasts u_1 , which is received by both the relay and the destination. Similarly, during the second time slot, the source \mathcal{S}_2 broadcasts u_2 . In the third time slot, the relay performs network encoding and transmits $u_R = u_1 \oplus u_2$ to the destination. Therefore, after the three time slots, the destination node can recover both bits even in the case where one of the three channels was in a deep fade (i.e. the channel was erased).

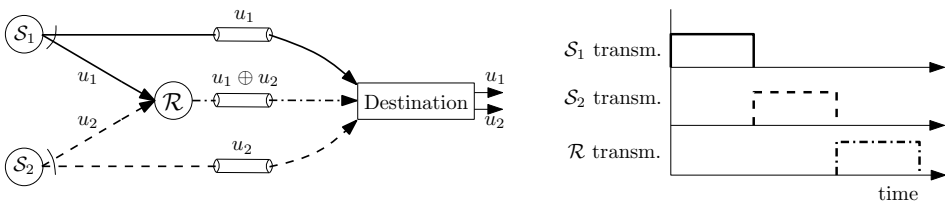


Figure 3.2: Example of diversity gain over a 2-user time-division MARC.

Motivated by the previous example, several works have shown how the redundancy provided by network coding can be used to help the channel code to improve the error protection. This is done by blending together controlled redundancy for forward error correction and in-network mixing of input data at the relay. In this context, we next present several recent contributions on joint network-channel coding schemes for TD-DF-MARC subject to flat fading.

3.2 STATE OF THE ART ON TD-DF-MARC

In [HSOB05] a joint network-channel coding scheme for TD-DF-MARC was first considered. The authors proposed distributed regular LDPC codes as the joint network-channel code at the relay node, where the destination jointly decodes the messages from the sources with the aid of the information sent from the relay, as opposed to [CKL06] where the two messages transmitted from the sources are separately decoded. In [HD06] the authors follow the same idea by proposing a turbo-code-based joint network-channel coding scheme. Parallel to these proposals, the authors in [NNLN07] propose a similar scheme for high-order modulations. More recently, a joint coding scheme based on WiMax LDPC codes was presented in [CHZK09], whereas in [YW10, IIO11] two schemes based on turbo codes were investigated. Furthermore, some joint non-binary coding schemes have been recently reported in [XS09] (non-binary network coding) and [GHW⁺09] (non-binary network and channel coding). Finally, in [YK07, ZKBW09] the authors propose a joint network-channel coding scheme where the relay transmits the soft values resulting from its decoding procedure over AWGN channels.

Motivated by the works presented above, we developed two joint network-channel coding schemes for the TD-DF-MARC [HCD11, HCD12]. In Paper I (Appendix A, [HCD11]) we propose a scheme which combines Bit-Interleaved Coded Modulation (BICM) [FMC08] based on non-binary LDPC codes (also known as $GF(2^q)$ -LDPC) [DM98], along with the linear combination of blocks of data at the relay. In Paper II (Appendix B, [HCD12]) the relay linearly combines – over a non-binary finite field – the already convolutionally encoded sequences from the source nodes. In both cases the iterative decoding procedure at the common destination is performed by running the Sum-Product Algorithm (see Chapter 2) on the factor graph describing the proposed joint network-channel code. We next present the main contributions of both papers.

3.3 MAIN CONTRIBUTIONS

3.3.1 PAPER I

In this paper we propose the use of a BICM scheme consisting of the concatenation of a non-binary LDPC code, a pseudorandom interleaver and a symbol mapper, for joint network-channel coding over the 2-user quasi-static flat-fading TD-DF-MARC. Figure 3.3 shows the schematic of each source. We refer to Appendix A for the notation used in the figure.

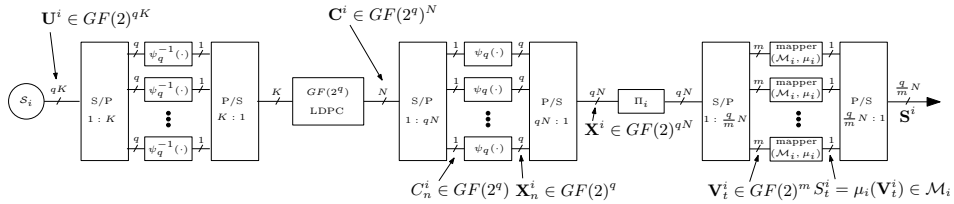


Figure 3.3: Schematic diagram of the transmitter for source S_i , with $i \in \{1, 2\}$.

The output of the symbol mapper at each sender is then broadcasted to the relay and the destination during its corresponding time slot. During the third time slot, the relay decodes the messages from both transmitters by employing a BICM iterative decoder (BICM-ID) [FMC08], which exchanges information between a soft demapper and the corresponding channel decoder. Once the received sequences have been correctly decoded, the relay

combines the estimated symbols into a single signal by employing the aforementioned BICM scheme, and transmits the resulting joint network-channel coded sequence to the distant receiver.

After receiving all the transmitted sequences, the common destination decodes and estimates both source messages. The iterative decoding procedure at the common destination is based on iteratively exchanging soft information between a pair of BICM-ID through a joint soft channel demapper, which is detailed by means of factor graphs and the Sum-Product Algorithm (SPA). Figure 3.4 shows the factor graph of the joint decoder at the destination.

Extensive Monte Carlo simulations were carried out by considering a variety of overall spectral efficiencies ρ_s [bits per complex dimension]. Based on such simulation results it is concluded that the proposed approach performs significantly close to the corresponding outage probability (whose derivation is shown in Appendix F).

However, the performance gain provided by $GF(2^q)$ -LDPC codes comes together with an increase in the decoding complexity. A straightforward implementation of the SPA has complexity $O(N \cdot 2^{2q})$, where N denotes the block length; this can be reduced to $O(N \cdot q2^q)$ by performing a Fourier domain implementation of the SPA [DM98]. Recently, the computational load has been reduced to $O(N \cdot n_m 2^{n_m})$, with $n_m \ll q$ [VDV⁺10]. However, since the values of q in this paper are small, the Fourier-domain SPA has been used for decoding.

Even though it is not shown in the paper, the proposed scheme is closer to its corresponding outage curve than the previous schemes to their corresponding ones. However, we did not consider including this comparison since the block length of the transmitted sequences was considerably higher than the one in the other schemes. This drawback, together with the high complexity of non-binary LDPC codes, were the main motivations to continue improving the proposed scheme. Thus, we chose to consider the convolutional codes as channel codes. The main motivations for this choice were that: i) The capability of convolutional codes to be terminated allowed the transmission of short-length codewords (see Chapter 2, Section 2.5.1); and ii) Due to their non-iterative nature, the use of convolutional codes allowed for an easier traceability of the performance of the joint code through iterations. These considerations gave rise to the paper that is presented next.

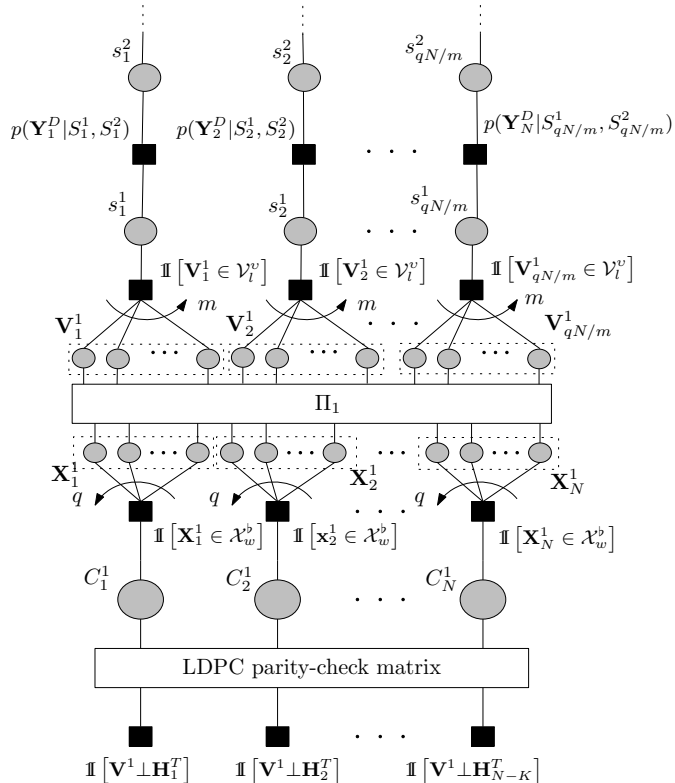


Figure 3.4: Factor graph of the proposed joint network-channel code for source \mathcal{S}_1 . $\mathbb{1}[\cdot]$ denotes the indicator function, whereas $\mathbf{x} \perp \mathbf{H}_z^T$ stands for orthogonality between vector \mathbf{x} and compounding non-binary LDPC parity-check matrix \mathbf{H}_z , with $z \in \{1, \dots, N-K\}$ (see Appendix A).

3.3.2 PAPER II

In this paper we propose a scheme that considerably reduced, with respect to the previous paper, the complexity of the encoders, since simple convolutional codes are used as channel codes. Observe that the complexity of the decoder at the relay is also reduced as it does not need to perform iterations in order to decode. After decoding the messages received from both sources, the relay linearly combines them over a non-binary finite field (i.e. $GF(2^q)$, $q \in \mathbb{N}$), and forwards the obtained sequence to the destination.

The iterative decoding procedure at the common destination is performed by running the SPA on the factor graph describing the proposed joint network-channel code, which is compounded by three sub-factor graphs: two describing the channel codes of each source, and a third describing the network coding operation performed at the relay node. Figure 3.5 shows the factor graph where the oversize check nodes represent the global function associated to the network coding performed at the relay. Through the paper, this function is factorized yielding the graph of Figure 3.6 that represents its factorize version. Finally, in both figures the messages of the SPA (i.e. the local probabilities) are also shown.

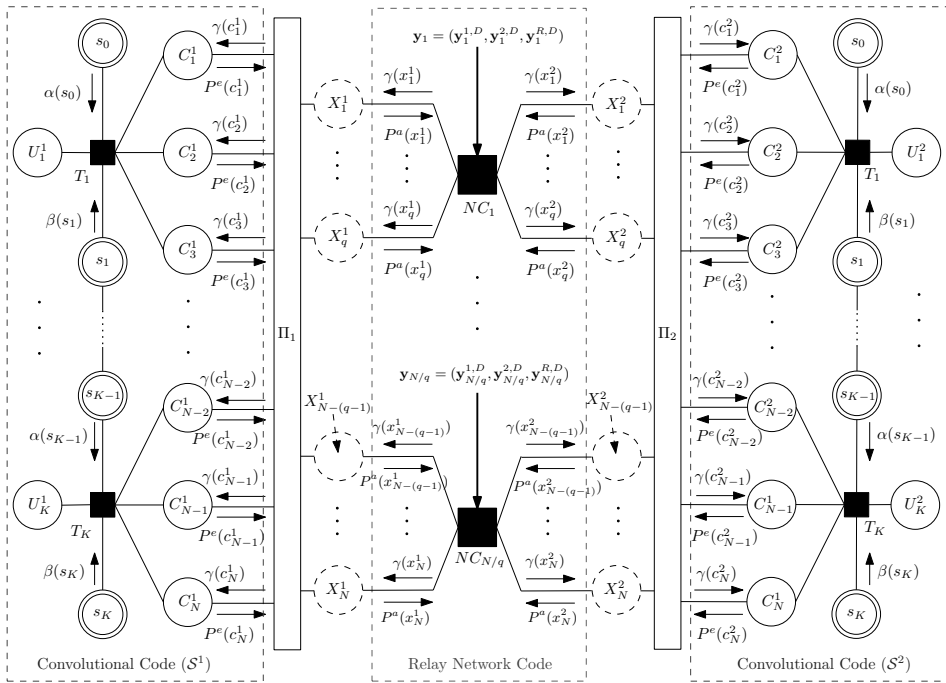


Figure 3.5: Factor graph of the proposed joint network-channel code.

The key contributions of this scheme over the state of the art on this topic are as follows:

- The proposed scheme does not perform channel coding on the already network-coded bits, reducing the complexity at the relay node without

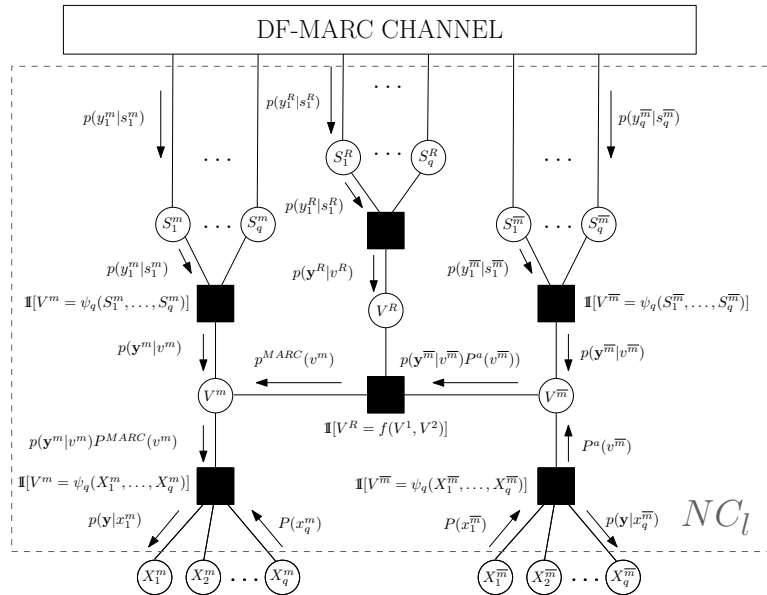


Figure 3.6: Factor graph representing the factorization of the global function representing the network coding, i.e. the over-size check nodes of Figure 3.5.

compromising performance. To our knowledge, all practical schemes for fading channels found in the related literature¹ perform channel coding on the already network-coded bits.

- It is shown that a tailored selection of the set of coefficients used in the network coding operation, namely, the Network Coding (NC) coefficients, outperforms a random choice as done in [GHW⁺09]. This selection is performed by matching the EXtrinsic Information Transfer (EXIT, [Ten99, Hag04]) functions of the compounding codes on the EXIT chart.
- Contrary to previous literature, the proposed joint network-channel code allows the sources to use completely different channel codes, at the sole expense of an increased complexity when choosing the NC-coefficients through EXIT-curve matching.

¹In [YK07] a similar coding procedure at the relay is proposed; however, their study is restricted to AWGN channels and binary network coding.

- The work presented here considers convolutional codes at both source nodes. As a consequence of the previous point, both convolutional codes can be independently terminated. This fact allows us to use very short-length codewords, making the scheme particularly attractive for low-latency applications.

Finally, regarding the performance of the system, Monte Carlo simulations show that the proposed scheme outperforms, in terms of its gap to the corresponding outage probability upper bounds (see Appendix F), the previously published schemes for all the scenarios (see Table 3.1). Moreover, the proposed system achieves these results by using short-length codewords: 144 complex dimensions per use of TD-DF-MARC in contrast to the 2176 utilized in [CHZK09], the 6000 utilized in [HSOB05, HD06] or the 27000 utilized in Paper I ([HCD11]), which makes our proposal particularly attractive for low-latency applications.

Table 3.1: Gaps to the outage probabilities in dB for a 2-memory block convolutional code and a network coding over $GF(2^3)$.

Scenario	q=3, CC2	[HCD11]	[HSOB05]	[HD06]	[CHZK09]
A	1.39 dB	-	3.4 dB	2.7 dB	-
B	1.64 dB	1.7 dB	-	-	4.8 dB
C	2.04 dB	-	-	5.2 dB	-

CHAPTER 4

Joint Network-Channel Coding Schemes for Multihop Wireless Networks

This chapter contains a comprehensive overview of the Multihop networks and an knowledgeable review of the coding scheme known as Progressive Network Coding. To conclude, the main contributions of Papers III and IV (Appendix C and D, respectively), where two novel coding schemes are proposed, are summarized in the subsequent sections.

4.1 MULTIHOP WIRELESS NETWORKS

Multihop transmission in mesh networks is an effective method for establishing connectivity between the nodes of a network where direct transmission is not feasible or power efficient. In a multihop network, the data transmission between the source and the corresponding destination is realized with the aid of a certain number of intermediate nodes (relays). Since the pioneer work of Ahlswede et al. [ACLY00], where the term Network Coding was coined, several works have focused on improving the throughput through multihop networks. Theoretical studies such as [LYC03, KM03, EMH⁺03] have proposed several different approaches for network coding. These works have been followed by practical network coding schemes as in [KRW⁺08].

In the general context of multihop transmission in mesh networks, we specifically consider pure multihop networks where a straight-line geometry and unity distance between two consecutive nodes is imposed. Although simple, the line network is not unrealistic since after a route is found from the source to the destination (for example by using the relay selection algorithm proposed in [BB10]), the relay nodes along the route form essentially a line network. Nevertheless, the straight-line geometry assumption is a bit rigid, but it is imposed in order to easily compute the distances between nodes and evaluate the corresponding signal attenuations. We further consider the Decode-and-Forward (DF) decoding strategy, where at each intermediate node the received signal is decoded, re-encoded and forwarded. In order to avoid possible interferences in the network, we also impose the system to work in Time-Division-Multiple-Access (TDMA) mode. Thus, the total available transmission time is divided into several orthogonal time-slots, one for each node.

In addition, the nodes are assumed to work in Half-duplex mode; hence, a node can either receive or transmit data, but not both at the same time. Besides, it is also assumed that the nodes have only one omnidirectional and forwards-oriented transmitting antenna so that data are transmitted in a progressive way, i.e. one node can listen to all the previous nodes but not to the following ones. Finally, due to the wireless nature of the signals, Rayleigh fading and path loss attenuation is considered. Figure 4.1 depicts the considered multihop wireless network.

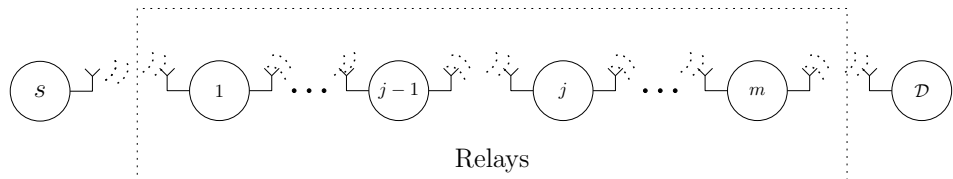


Figure 4.1: The considered Multihop Wireless Network.

These networks have been the focus of an intense research in the recent years (e.g. [BB10, MMJV⁺10, WMG10] and reference therein). Among the several theoretical aspects, the problem of finding the optimal route

through the one-dimensional multihop network was addressed in [BB10] where efficient-routing protocols, for a variety of power allocations in the relay nodes under fading conditions, are proposed. Moreover, in [MMJV⁺10] an analytical expression for the end-to-end average bit error rate from the statistical point of view is presented, whereas in [WMG10] the authors developed a unified framework for evaluating the exact ergodic capacity of the considered network.

In this work two joint network-channel applied to pure multihop networks are presented. Although a flurry of research has been developed in theoretical analysis of these networks, to the knowledge of the authors, only a reduced number of works have addressed joint network-channel coding solutions, aside from the traditional repetition-forward. One of such practical schemes was proposed by Bao et al. in [BL06] and named by the authors as *progressive network coding*. For comparison purposes with our schemes, we next review their proposed *progressive network coding* system.

4.2 PROGRESSIVE NETWORK CODING FOR MULTIHOP WIRELESS NETWORKS

Progressive network coding [BL06] was proposed as an extension of coded cooperation [HN02] to multihop networks. This scheme allows each relay node in the network: to gather all the messages transmitted from previous nodes, to jointly decode segments, to re-encode messages and finally to transmit a different (sub-) codeword. In other words, at each hop, the network code is strengthened by including new parity bits and additional checks. The destination receives all the (sub-)codewords from the original source as well as those from each and every participating relay and performs the SPA algorithm over the factor graph describing the entire coding scheme. Due to the nature of progressive network coding, it requires the code to be flexible, or more precisely, to seek a family of rate-compatible or structurally-embedded codes.

To that end, the authors in [BL08] proposed the use of distributed lower-triangular low-density parity-check (LT-LDPC) codes. The parity check matrix of a systematic LT-LDPC code consists of two parts, a sparse (and random) matrix P on the left and a sparse lower triangular matrix Q with all ones in the main diagonal on the right, i.e. $H = [P \ Q]$. Adapting this code in the progressive network coding framework, the H matrix is decomposed

to sub matrices, such that each node uses the sub matrix corresponding to the previous node to decode the data and use the submatrix corresponding to itself to encode and generate a new set of parity bits. Figure 4.2 shows parity-check matrix H as seen at the destination. The submatrices for decoding at each node are obtained from the matrix H as shown in the figure.

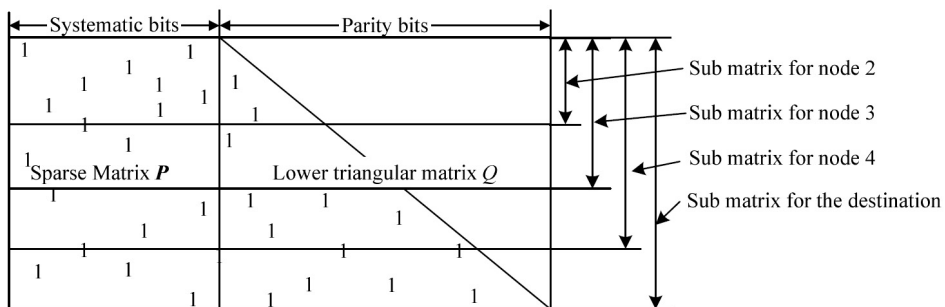


Figure 4.2: Parity-check matrix at the destination of the scheme proposed in [BL06]. The submatrices for each relay node are also shown.

To conclude, Figure 4.3 shows the associated factor graph used for decoding at the destination. The dashed lines in the factor graph indicate that there cannot exist a connection between a variable node and an upper check node due to the triangular nature of the parity-check matrix [BL06].

Note that, when fading is considered, the information about the systematic bits is highly probable to be lost due to the path loss attenuation suffered by the signal coming from the source. Therefore, in fading environments, an increase in the transmitted power is needed in order to reduce the probability of the systematic bits to be erased, and consequently, to avoid a decoding failure.

Motivated by this drawback, we inferred that an adaptation of the scheme presented in Paper I to the multihop scenario could solve the above addressed problem, leading to a performance improvement. Therefore, progressive network coding (denoted as Ref1 scheme in Paper III) is used as benchmark for the verification of the performance of the schemes proposed in both of the papers presented in this chapter.

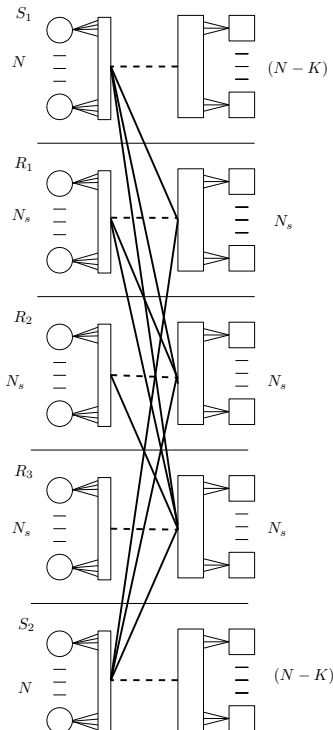


Figure 4.3: Factor Graph at the destination of the scheme proposed in [BL06].

4.3 MAIN CONTRIBUTIONS

Based on the work carried out in Paper I, Paper III (Appendix C) proposes a decode-combine-forward scheme for the multihop transmission in ad-hoc wireless networks, where the information generated by two independent sources has to be sent to a common destination based on multiple-relay cooperation.

Analogously, Paper IV (Appendix D) uses the improvements presented in previous Paper II and proposes a new scheme that clearly outperforms, using blocks of 13 information bits, the scheme presented in Paper III that uses blocks of 1500 information bits.

4.3.1 PAPER III

We consider the scenario where two source nodes want to transmit their independent information to a far distant destination using relay nodes along the way. To that aim, the binary symbols of each source are channel encoded by an LDPC code and high-order modulated before being transmitted. At each relay node, the following operations are performed: decode, combine (linear combination over a finite field) and forward transmission. We first focus on the latter two. The estimated source sequences are encoded by using the same LDPC code as the sources. Then, the resulting binary encoded blocks are partitioned into sub-blocks before being mapped into the elements of a finite field and linearly combined using random linear coefficients (coined in the paper as *local encoding vector*). Finally, the resulting sequence of non-binary elements is mapped into a M^2 -QAM constellation and forward transmitted.

Similarly as done in Paper I, the decoding scheme at each node is based on applying the Sum-Product algorithm to a compound factor graph (where the LDPC decoders and the network coding scheme are blend together) describing the joint probability of the communication scheme at the corresponding node. Figure 4.4 depicts the factor graph used for decoding. Observe that since binary LDPC codes are used, the resulting factor graph is simpler than the one of Paper I, which is shown in Chapter 3, Figure 3.4.

In order to asses the performance of the proposed scheme, we compare it with: 1) The scheme presented in Section 4.2 and proposed by Bao et al. in [BL06]¹, and 2) An adaptation of the one proposed by Hausl et al. in [HSOB05] for multiple access relay channels.

Simulation results reveal that the proposed decode-combine-and-forward scheme clearly outperforms these reference systems by more than 7 dB. Moreover, due to the decode step in the proposed scheme, a failure (or deep fade) of a node has a smaller impact in performance than in the corresponding reference scheme.

¹ Although in [BL06] the system was proposed for one source, the extension to two sources is straightforward.

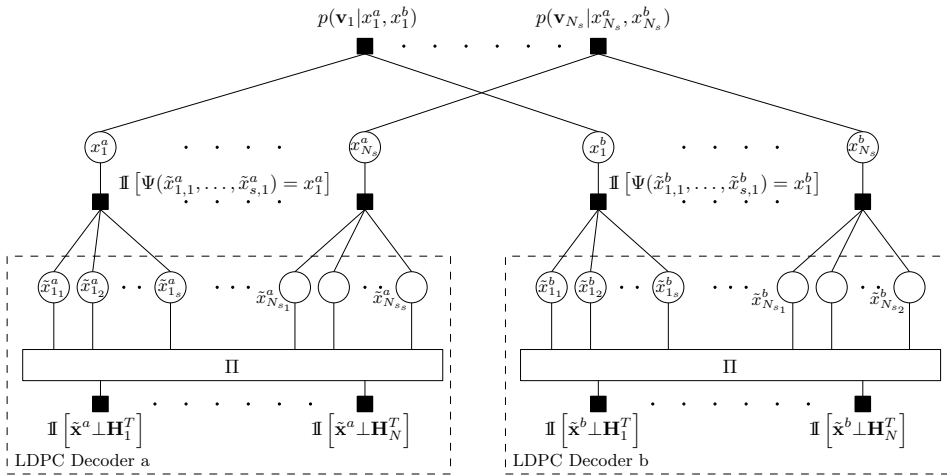


Figure 4.4: Factor graph employed for the decoding at each node in Paper III.

4.3.2 PAPER IV

A DF scheme is proposed to transmit the information generated by the source² to the destination. Like most DF schemes, at each relay node the proposed scheme can be divided into two parts: the decode part, where the information sequence is estimated; and the forward part, where the estimated sequence is encoded and forwarded. In particular, the forward part at the source node is implemented in a different manner than the ones produced at the relay nodes and therefore, it will be explained first.

The sequence generated by the source is: first encoded by a convolutional code; then, interleaved by a random spread interleaver and mapped into the sequence of complex symbols chosen from a 2^q -ary signal constellation according to a given bit-to-symbol mapping (e.g. Gray mapping); and finally, transmitted.

At each relay node, the decode part, which will be explained later, outputs the estimated information sequence, which is encoded and interleaved using the aforementioned convolutional code and interleaver, respectively. The resulting binary sequence is partitioned into several sub-sequences and

²Observe that, as opposed to Paper III, a unique source is considered.

each of them is mapped into a non-binary element. Next, the non-binary symbols are paired off and each pair is linearly combined to form new non-binary symbols. Finally, the new non-binary symbols are mapped into signal points of a 2^q -ary constellation and transmitted. Due to pairing and the linear combination, the sequences transmitted by the relays have half the length of the one transmitted by the source.

Regarding the decode part, Figure 4.5 shows the factor graph used for the decoding together with some of the messages that appear in the SPA while decoding. We refer to Appendix D for further information about the notation of used in the figure.

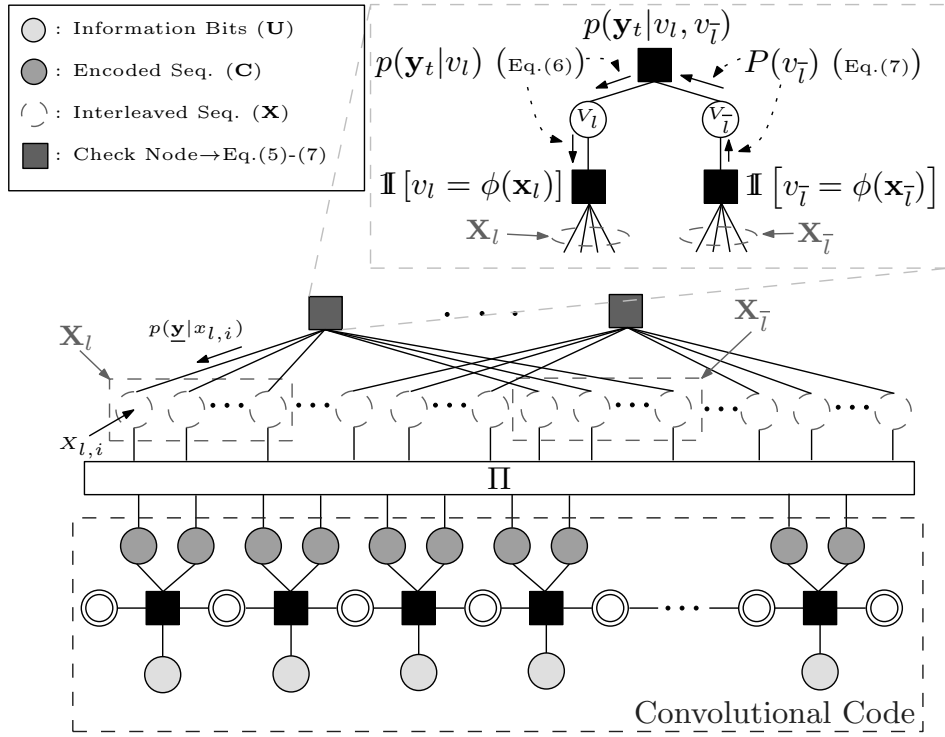


Figure 4.5: Factor graph employed for the decoding at each node in Paper IV.

Simulation results show that the proposed scheme clearly outperforms the scheme proposed in Paper III by more than 3dBs. Moreover, this gain is obtained using a total of 20 complex dimensions in comparison with the 4500

used in the reference scheme ([BL06] and the ones therein). This fact makes the proposed scheme particularly attractive for low-latency applications.

CHAPTER 5

A Flexible Channel Coding Approach for Short-Length Codewords

This chapter presents the last paper of this thesis, Paper V (Appendix E). The theme of this paper differs from the previous papers in the sense that it proposes an iterative coding scheme for the transmission of short-length codewords over the point-to-point AWGN channel, rather than a coding scheme for multihop networks. However, it should be said the idea behind the new point-to-point coding scheme comes from a modification of the work of Paper II, this is the reason for presenting it here. The chapter begins with a brief introduction of the state of the art in iterative channel codes using short-length codewords.

5.1 PAPER V

Iteratively decodable (i.e. Turbo-like) channel codes such as Low Density Parity-Check (LDPC) [RU01] or Turbo codes [BGT93], have been widely shown to perform near capacity for the AWGN channel when used with codeword lengths beyond 10^6 . However, such codes can be impractical in scenarios which demand low latencies (e.g. real-time video delivery), mainly due to their associated decoding complexity and limited technological resources of the underlying hardware. This rationale motivates the

upsurge of research on short-length codes (i.e. codes with codewords of several hundreds to few thousands coded symbols) to the above scenarios.

However, when dealing with short-length codewords the capacity approaching performance of LDPC or Turbo codes may severely degrade due to: 1) the widening of the waterfall region; and 2) the high error floors obtained under this condition (see [DPT⁺02, Ric03, SZ10] for LDPC codes and [GCP⁺01] for Turbo codes), the latter mainly because of their poor minimum distance. The shorter the codeword is, the higher the error floor and the wider the waterfall region will be [Ric03]. Several contributions [XB04, HEA05, ZLT10] have focused on reducing these error floors on LDPC codes. In [ZLT10], a design technique is proposed to produce short-length parity-check matrices for LDPC codes that leads to error floors of 10^{-7} bit error rate at $E_b/N_0 = 2.2$ dBs, outperforming [XB04, HEA05]. Regarding turbo codes, in [FB09], the authors proposed rate variable turbo codes with error floors of 10^{-5} packet error rate at $E_b/N_0 = 3.5$ dBs, both of them using codewords of 2000 symbols.

In our work (Paper V) we propose an alternative channel coding approach for short-length codewords which can achieve lower error floors than the previous schemes [XB04, HEA05, ZLT10]. The location of the error floor can be easily set by varying the energy allocation of the encoded binary symbols (i.e. at the output of the modulation). As drawback, the lower the error floor is, the higher the SNR of the waterfall region will be. Thus, when choosing a error floor lower than the one in the previous schemes, our code will outperform them for BERs lower than its error floor (with a SNR waterfall degradation of less than 0.5 dB at $\text{BER} = 10^{-4}$). On the other hand, when selecting an error floor higher than the error floors of [XB04, HEA05, ZLT10] (10^{-7}), say 10^{-5} , the loss in performance at $\text{BER} = 10^{-4}$ is negligible.

As mentioned above, the proposed code is based on a technique derived from Paper II (Appendix B). It appends to the convolutionally-encoded bits from the source extra parity bits generated by linearly combining over a non-binary finite field the originally encoded symbols. Figure 5.1 shows the schematic of the encoder. As seen in the figure, the overall rate is reduced from K/N to $2K/3N$ by appending the extra parity bits generated by the combining function $V^3 = f_{\mathbf{h}}(V^1, V^2)$.

Since the performance of short length convolutional codes improve when they are terminated (assuming bitwise MAP decoding), the proposed scheme

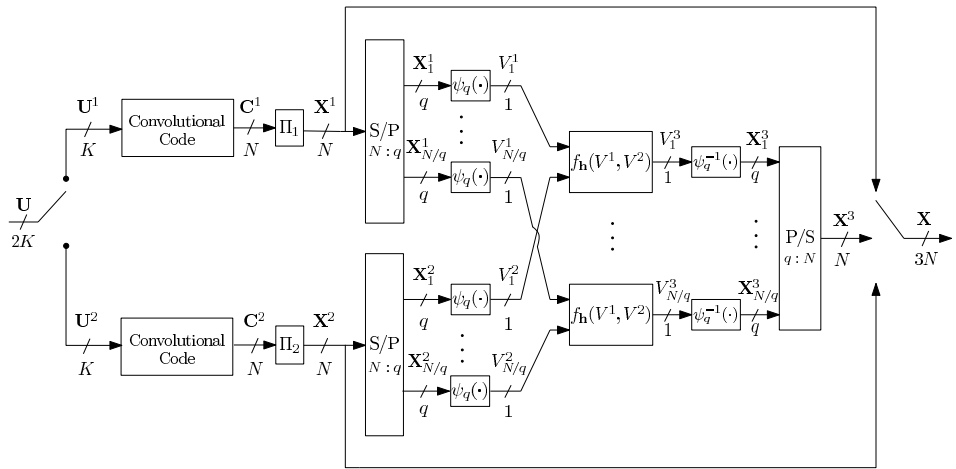


Figure 5.1: Encoder associated to the proposed code.

uses independent source input sequences so that both convolutional codes can be terminated. However, to increase performance, a dependency between the output of the convolutional codes has to be introduced. This is the reason for using the linear combination stage. Observe that if a convolutional code was used instead of the linear combination block for introducing this dependency (similar as in Turbo codes or in [BRG09], where a design framework for multiple parallel concatenated codes is developed), this code could not be terminated, leading to a performance degradation when using short-length codewords. Moreover, using a linear combination also permits a high and simple design flexibility, (see Figure 5.2).

A closer look at the encoder reveals the similarities with the code presented in Paper II, that is, the latter can be seen as a distributed version (among the sources and the relay) of the one presented here. Therefore, the associated factor graphs are similar for both schemes. We refer to Appendix E for the figure.

In order to choose the parameters of the code and the energy allocation of the encoded binary symbols, we propose the use of EXIT charts as done in [BRG09, PS06], where the authors proposed several channel code approaches based on EXIT charts for long-length codewords (65000 and 240000 in [BRG09] and [PS06], respectively). Although, EXIT charts pro-

vides good code convergence predictions only for long-length codewords, it can give us a good insight into how the parameters of the code should be chosen in order to achieve the different error floors. Figure 5.2 shows the EXIT charts for different linear combinations (a) and different energy allocations among the encoded symbols (b).

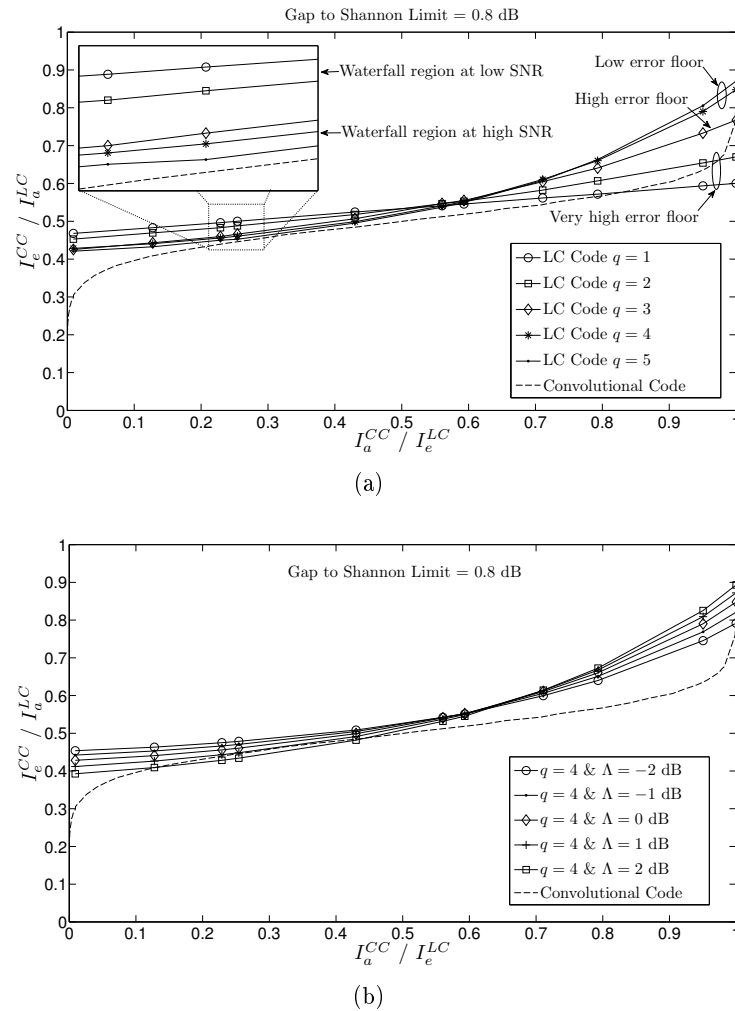


Figure 5.2: EXIT Chart of the proposed code for different linear combinations functions (a) and unequal energy allocation parameter Λ (b).

CHAPTER 6

Conclusions and Future Lines

We next present a brief summary of the main conclusions drawn from the work presented in this thesis and examine possible future research lines.

6.1 CONCLUSIONS

- In Papers I and II (Appendix A and B, respectively), two joint network-channel coding scheme for the Time-Division Decode-and-Forward Multiple Access Relay Channel are proposed. In both schemes: 1) the relay linearly combines the encoded sequences transmitted by the sources; and 2) the decoding at the destination is performed by applying the Sum Product Algorithm over the derived factor graph of the Joint Network-Channel code.

In particular, Paper I presents a scheme based on Bit Interleaved Coded Modulation with non-binary Low Density Parity Check codes as channel codes. We showed that the proposed scheme outperforms its binary counterpart and performs close to the outage probability (cut-set bound) in all the simulated scenarios. As a drawback, very long (65000) codeword are needed for a reliable transmission. This fact was the main motivation for continuing improving the scheme, resulting in Paper II.

Paper II utilizes convolutional codes as channel codes. The use of a non-iterative code such as the convolutional code, allowed us to

easily track the exchange of information through the factor graph used at the decoder. Furthermore, by performing a tailored selection of the coefficient of the linear combination, we were able to improve the overall performance with respect to a random choice. Simulation results show that the proposed scheme outperformed the reference schemes found in the literature and the one presented in Paper I by using short-length codewords: 144 complex dimensions per use of TD-DF-MARC in contrast to the 2176 utilized in [CHZK09], the 6000 utilized in [HSOB05,HD06] or the 27000 utilized in [HCD11] (Paper I).

- Regarding Paper III, it proposes a decode-combine-forward scheme for the pure multi-hop transmission in ad-hoc wireless networks, where the information generated by two independent sources has to be sent to a common destination based on multiple-relay cooperation. To this end, the proposed scheme blends together LDPC channel coding with linear combination of blocks of data over a finite field. The proposed scheme outperforms similar schemes, which can be found in the literature. On the other hand, Paper IV proposes a new scheme that clearly outperforms the scheme presented in Paper III, and consequently, the schemes found in the literature. The proposed scheme is based on distributing the method presented in Paper II among the different relays, so that in its corresponding hop each relay linearly combines (each one using a different linear combination) and forwards the source data. As in Paper II, this gain is obtained using short-length codewords: a total of 20 complex dimensions in comparison with the 4500 used in the reference scheme (Paper III, [BL06] and the ones therein). This fact makes the proposed scheme particularly attractive for low-latency applications.
- Finally, Paper V (Appendix E) introduces a channel coding design framework for short-length codewords which can achieve lower error floors than previous designs found in the literature. By adapting the joint code proposed in Paper II to the point-to-point scenario, we designed a channel code that is based on concatenating the output of two convolutional codes $\mathbf{X}_1, \mathbf{X}_2$ with a linear combination in \mathbb{F}_{2^q} of \mathbf{X}_1 and \mathbf{X}_2 . It allows a tradeoff between error floor and waterfall region by simply varying the energy allocation of the encoded sequences. Notice that the main advantage of the proposed scheme is that one could choose error floors lower than the ones in previous schemes,

(and consequently outperforming these schemes at high SNRs), with an SNR waterfall degradation of less than 0.5 dB at mid-range BERs. On the other hand, when selecting higher error floors (10^{-5}), the loss performance in the waterfall region is negligible.

6.2 FUTURE LINES

The collection of papers presented in this dissertation have shown that by efficiently combining channel coding and network coding over a variety of networks scenarios such as the point-to-point (Paper V), Multiple-Access Relay Channel (Paper I and II) and multihop scenarios (Paper III and IV), clearly outperforms other coding schemes found in the literature. Since we are dealing with relay nodes, we have assumed that these nodes do not generate their own data but use all their resources exclusively to aid the sources to reach their destinations.

In scenarios where some of the nodes in the network are also able to transmit their own data, [NHH, HN06] have shown the superiority of collaboration among nodes for sending their data when compared to non-collaboration. For example, [JHHN04, BL08] have proposed several node collaboration schemes in dense networks. Therefore, a reasonable future research line would be to adapt the present codes to cover node collaboration.

Regarding possible improvements of the work presented in this thesis, there are several possibilities:

- Paper I could be improved by applying the EXIT chart analysis of Paper II with the goal of optimizing both the coefficients of the linear combination and the degree distribution of parity check matrix.
- In Paper II, a deeper analysis (beyond the EXIT chart) of the behavior of the joint code for different linear coefficients could be done. For example, analyzing the underlying code generated by the linear combination in terms of distance among codewords and bit error probability.
- Finally, a hardware implementation of Paper IV and V in practical communication systems could show the feasibility of the proposed schemes in real world applications.

References

- [ACLY00] R. Ahlswede, N. Cai, S.-Y. R. Li, and R. W. Yeung. Network Information Flow. *IEEE Transactions on Information Theory*, 46(4):1204–1216, July 2000.
- [BB10] R. Babaee and N.C. Beaulieu. Cross-layer design for multihop wireless relaying networks. *IEEE Transactions on Wireless Communications*, 9(11):3522 –3531, november 2010.
- [BCJR74] L. Bahl, J. Cocke, F. Jelinek, and J. Raviv. Optimal Decoding of Linear Codes for Minimizing Symbol Error Rate (Corresp.). *IEEE Transactions on Information Theory*, 20(2):284–287, March 1974.
- [BGT93] C. Berrou, A. Glavieux, and P. Thitimajshima. Near Shannon Limit Error-Correcting Coding and Decoding: Turbo-Codes. In *1993 IEEE International Conference on Communications, ICC'93*, 1993.
- [BL06] X. Bao and J. Li. Progressive network coding for message-forwarding in ad-hoc wireless networks. In *2006 3rd Annual IEEE Communications Society on Sensor and Ad Hoc Communications and Networks, SECON'06*, volume 1, pages 207 –215, sept. 2006.
- [BL08] X. Bao and J. Li. Adaptive network coded cooperation (ancc) for wireless relay networks: matching code-on-graph with network-on-graph. *IEEE Transactions on Wireless Communications*, 7(2):574 –583, february 2008.
- [BRG05] F. Brännström, L. K. Rasmussen, and A. J. Grant. Convergence Analysis and Optimal Scheduling for Multiple Concatenated Codes. *IEEE Transactions on Information Theory*, 51(9):3354–3364, September 2005.
- [BRG09] F. Brännström, L. K. Rasmussen, and A. J. Grant. Optimal Puncturing Ratios and Energy Allocation for Multiple Parallel Concatenated Codes. *IEEE Transactions on Information Theory*, 55(5):2062–2077, May 2009.

- [CG79] T. Cover and A. E. Gamal. Capacity Theorems for the Relay Channel. *IEEE Transactions on Information Theory*,, 25(5):572–584, September 1979.
- [CHZK09] L. Chebli, C. Hausl, G. Zeitler, and R. Koetter. Cooperative Uplink of Two Mobile Stations with Network Coding Based on the WiMax LDPC Code. In *2009 IEEE Global Communication Conference, GLOBECOM’09*, December 2009.
- [CKL06] Y. Chen, S. Kishore, and J. Li. Wireless Diversity through Network Coding. In *2006 IEEE Wireless Communications and Networking Conference, WCNC’06*, April 2006.
- [CT06] T. M. Cover and J. A. Thomas. *Elements of Information Theory*. Wiley Series in Telecommunications and Signal Processing, 2006.
- [CTB98] G. Caire, G. Taricco, and E. Biglieri. Bit-interleaved Coded Modulation. *IEEE Transaction on Information Theory*, 44:927–946, May 1998.
- [Cui11] J. Cui. The Capacity of Gaussian Orthogonal Multiple-Access Relay Channel. *IEEE Communications Letters*, 15(4):365–367, April 2011.
- [CYJ03] P.A. Chou, Y.Wu, and K. Jain. Practical network coding. In *Forty-First Annual Allerton Conference on Communication, Control, and Computing*, 2003.
- [DCKGG07] J. Del Ser, P.M. Crespo, B.H. Khalaj, and J. Gutierrez-Gutierrez. On combining distributed joint source-channel-network coding and turbo equalization in multiple access relay networks. In *Third IEEE International Conference on Wireless and Mobile Computing, Networking and Communications, WiMOB’07.*, page 18, oct. 2007.
- [DF07] D. Declercq and M. Fossorier. Decoding Algorithms for Nonbinary LDPC Codes Over $GF(q)$. *IEEE Transactions on Communications*, 55(4):633–643, April 2007.
- [DM98] M.C. Davey and D. MacKay. Low-density parity check codes over $gf(q)$. *IEEE Communications Letters*, 2(6):165 –167, jun 1998.

- [DMC⁺09] J. Del Ser, M. Mendicute, P.M. Crespo, S. Gil-Lopez, and I. Olabarrieta. Joint source-channel network decoding and blind estimation of correlated sensor using concatenated zigzag codes. In *Springer Lecture Notes in Computer Science*, volume 5793/2009, pages 30–41, September 2009.
- [DP95] D. Disvalar and F. Pollara. Turbo Codes for Deep-Space Communications. In *TDA Progress Report 42-120*, February 1995.
- [DPT⁺02] C. Di, D. Proietti, I.E. Telatar, T.J. Richardson, and R.L. Urbanke. Finite-length analysis of low-density parity-check codes on the binary erasure channel. *IEEE Transactions on Information Theory*, 48(6):1570 –1579, jun 2002.
- [EMH⁺03] M. Effros, M. Medard, T. Ho, S. Ray, D. Karger, and R. Koetter. Linear Network Codes: A Unified Framework for Source, Channel and Network Coding. In *DIMACS Series in Discrete Mathematics and Theoretical Computer Science*, 2003.
- [FB09] M. Ferrari and S. Bellini. Rate variable, multi-binary turbo codes with controlled error-floor. *IEEE Transactions on Communications*, 57(5):1209 –1214, may 2009.
- [FF56] L. Ford and D. Fulkerson. Maximal flow through a network. *Canadian Journal of Mathematics*, 8(3):399–404, Aug. 1956.
- [Fis02] R. F. H. Fisher. *Precoding and Signal Shaping for Digital Transmission*. Wiley-Interscience, 2002.
- [FMC08] A. G. Fabregas, A. Martinez, and G. Caire. *Bit-Interleaved Coded Modulation*. Now Publishers Inc., 2008.
- [Gal62] R. Gallager. Low-density parity-check codes. *IRE Transactions on Information Theory*, 8(1):21 –28, january 1962.
- [GCP⁺01] R. Garello, F. Chiaraluce, P. Pierleoni, M. Scaloni, and S. Benedetto. On Error Floor and Free Distance of Turbo Codes. In *2001 IEEE International Conference on Communications, ICC'01*, June 2001.
- [GHW⁺09] Z. Guo, J. Huang, B. Wang, J.-H Cui, S. Zhou, and P. Willet. A Practical Joint Network-Channel Coding Scheme for Reliable Communication in Wireless Networks. In *The Tenth*

- ACM International Symposium on Mobile Ad Hoc Networking and Computing, MOBIHOC'09*, May 2009.
- [GK12] A. El Gamal and Y. H. Kim. *Network Information Theory*. Cambridge University Press, 2012.
 - [Gol05] A. Goldsmith. *Wireless Communications*. Cambridge University Press, 2005.
 - [GYW10] C. Gong, G. Yue, and X. Wang. Joint Channel and Network Code Design for Half-Duplex Multiple-Access Relay System. In *2010 IEEE International Conference on Communications, ICC'10*, May 2010.
 - [Hag04] J. Hagenauer. The EXIT Chart: Introduction to Extrinsic Information Transfer in Iterative Processing. In *2004 European Signal Processing Conference, EUSIPCO'04*, September 2004.
 - [Hau08] C. Hausl. *Joint Network-Channel Coding for Wireless Relay Channels*. PhD thesis, TU München, 2008.
 - [Hau09] C. Hausl. Joint network-channel coding for multiple-access relay channel based on turbo codes. volume 20, pages 175 – 181, Mar. 2009.
 - [HCD11] M. Hernaez, P. M. Crespo, and J. Del Ser. Joint Non-Binary LDPC-BICM and Network Coding with Iterative Decoding for the Multiple Access Relay Channel. In *2011 IEEE 73rd Vehicular Technology Conference: VTC'11-Spring*, May 2011.
 - [HCD12] M. Hernaez, P. M. Crespo, and J. Del Ser. On the Design of a Novel Joint Network-Channel Coding Scheme for Multiple Access Relay Channels. *IEEE Journal on Selected Areas in Communications*, Accepted for publication 2012.
 - [HD06] C. Hausl and P. Dupraz. Joint Network-Channel Coding for the Multiple-Access Relay Channel. In *2006 3rd Annual IEEE Communications Society on Sensor and Ad Hoc Communications and Networks, SECON'06*, September 2006.
 - [HEA05] X.-Y. Hu, E. Eleftheriou, and D.M. Arnold. Regular and irregular progressive edge-growth tanner graphs. *IEEE Transactions on Information Theory*, 51(1):386–398, January 2005.

- [HN02] T.E. Hunter and A. Nosratinia. Cooperation diversity through coding. In *2002 IEEE International Symposium on Information Theory, ISIT'02*, 2002.
- [HN06] T.E. Hunter and A. Nosratinia. Diversity through coded cooperation. *IEEE Transactions on Wireless Communications*, 5(2):283 – 289, feb. 2006.
- [HSOB05] C. Hausl, F. Schreckenbah, I. Oikonomidis, and G. Bauch. Iterative network and channel decoding on a tanner graph. In *Forty-Third Annual Allerton Conference on Communication, Control, and Computing, Allerton'05*, 2005.
- [IIO11] K. Ishii, K. Ishibashi, and H. Ochiai. Multiple-access Relay System based on Nested Distributed Turbo Code. In *2011 IEEE Radio and Wireless Symposium, RWS11*, January 2011.
- [ILH10] O. Iscan, I. Latif, and C. Hausl. Network Coded Multi-Way Relaying with Iterative Decoding. In *2010 IEEE International Symposium on Personal, Indoor and Mobile Radio Communications, PIMRC10*, September 2010.
- [IPG] EPFL Information Processing Group. ldpcopt. <http://ipgdemos.epfl.ch/ldpcopt/>, retrieved on March 2009.
- [JHHN04] M. Janani, A. Hedayat, T.E. Hunter, and A. Nosratinia. Coded cooperation in wireless communications: space-time transmission and iterative decoding. *IEEE Transactions on Signal Processing*, 52(2):362 – 371, feb. 2004.
- [Jr.92] G.D. Forney Jr. Trellis shaping. *IEEE Transactions on Information Theory*, 38(2):281 –300, mar 1992.
- [KFL01] F.R. Kschischang, B.J. Frey, and H.-A. Loeliger. Factor graphs and the sum-product algorithm. *IEEE Transactions on Information Theory*, 47(2):498 –519, feb 2001.
- [KGG05] G. Kramer, M. Gastpar, and P. Gupta. Cooperative Strategies and Capacity Theorems for Relay Networks. *IEEE Transactions on Information Theory*, 51(9):3037–3063, September 2005.

- [KM03] R. Koetter and M. Medard. An algebraic approach to network coding. *IEEE/ACM Transactions on Networking*, 11(5):782 – 795, oct. 2003.
- [KRW⁺08] S. Katti, H. Rahul, Hu Wenjun, D. Katabi, M. Medard, and J. Crowcroft. Xors in the air: Practical wireless network coding. *IEEE/ACM Transactions on Networking*, 16(3):497 –510, june 2008.
- [KW00] G. Kramer and A. J. Van Wijngaarden. On the White Gaussian Multiple-Access Relay Channel. In *2000 IEEE International Symposium on Information Theory, ISIT'00*, June 2000.
- [Lee04] J. W. Lee. Lower bound on BER of finite-length turbo codes based on EXIT characteristics. *IEEE Communications Letters*, pages 238–240, April 2004.
- [LTW04] J.N. Laneman, D.N.C. Tse, and G.W. Wornell. Cooperative diversity in wireless networks: Efficient protocols and outage behavior. *IEEE Transactions on Information Theory*, 50(12):3062 – 3080, dec. 2004.
- [LYC03] S.-Y. R. Li, R. W. Yeung, and N. Cai. Linear Network Coding. *IEEE Transactions on Information Theory*, 49(2):371– 381, February 2003.
- [Mac] D. J. Mackay. Ldpc codes resources. <http://www.inference.phy.cam.ac.uk/mackay/codes/>, retrieved on March 2009.
- [Mac99] D. J. Mackay. Good error-correcting codes based on very sparse matrices. *IEEE Transactions on Information Theory*, 45(2):399 – 431, February 1999.
- [Mac03] D. J. Mackay. *Information Theory, Inference, and Learning Algorithms*. Cambridge University Press, 2003.
- [MMJV⁺10] E. Morgado, I. Mora-Jimenez, J.J. Vinagre, J. Ramos, and A.J. Caamano. End-to-end average ber in multihop wireless networks over fading channels. *IEEE Transactions on Wireless Communications*, 9(8):2478 –2487, august 2010.
- [Moo05] T. K. Moon. *Error Correction Coding: Mathematical Methods and Algorithms*. Wiley-Interscience, 2005.

- [NHH] A. Nosratinia, T.E. Hunter, and A. Hedayat. *IEEE Communications Magazine*.
- [NM93] F.D. Neeser and J.L. Massey. Proper complex random processes with applications to information theory. *IEEE Transactions on Information Theory*, 39(4):1293 –1302, jul 1993.
- [NNLN07] H. T. Nguyen, H. H. Nguyen, and T. Le-Ngoc. A Joint Network-Channel Coding Scheme for Relay-Based Communications. In *2007 Canadian Conference on Electrical and Computer Engineering, CCECE07*, April 2007.
- [Pro00] J. G. Proakis. *Digital Communications*. McGraw-Hill Science/Engineering/Math, 2000.
- [PS06] S. Pfletschinger and F. Sanzi. Error Floor Removal for Bit-Interleaved Coded Modulation with Iterative Detection. *IEEE Transactions on Wireless Communications*, 5:3174–3181, Nov. 2006.
- [Ric03] T. Richardson. Error Floors of LDPC codes. In *Forty-first Annual Allerton Conference on Communication, Control, and Computing, Allerton'03*, October 2003.
- [RK06] N. Ratnakar and G. Kramer. The Multicast Capacity of Deterministic Relay Networks with No Interference. *IEEE Transactions on Information Theory*, 52(6):2425–2432, June 2006.
- [RU01] T. J. Richardson and R. Urbanke. The capacity of low-density parity-check codes under message-passing decoding. *IEEE Transactions on Information Theory*, 47:599–618, Feb. 2001.
- [RU08] T. Richardson and R. Urbanke. *Modern Coding Theory*. Cambridge University Press, 2008.
- [SA00] M. K. Simon and M.-S. Alouini. *Digital Communication over Fading Channels*. Wiley-Interscience, 2000.
- [SEA03] A. Sendonaris, E. Erkip, and B. Aazhang. User cooperation diversity - part i and ii. *IEEE Transactions on Communications*, 51(11):1927 – 1938, nov. 2003.
- [Sha48] C. E. Shannon. A Mathematical Theory of Communication. *The Bell System Technical Journal*, 27:379–423, July 1948.

- [SKM04] L. Sankaranarayanan, G. Kramer, and N. B. Mandayam. Hierarchical Sensor Networks: Capacity Bounds and Cooperative Strategies using the Multiple-Access Relay Channel Model. In *2004 1st Annual IEEE Communications Society on Sensor and Ad Hoc Communications and Networks, SECON'04*, October 2004.
- [SLMP11] L. Sankar, Y. Liang, N. Mandayam, and V. H. Poor. Fading Multiple Access Relay Channels: Achievable Rates and Opportunistic Scheduling. *IEEE Transactions on Information Theory*, 57(4):1911–1931, April 2011.
- [SLPM07] L. Sankar, Y. Liang, V. H. Poor, and N. Mandayam. Opportunistic Communications in an Orthogonal Multiaccess Relay Channel. In *2007 IEEE International Symposium on Information Theory, ISIT'07*, June 2007.
- [SMP09] L. Sankar, N.B. Mandayam, and H.V. Poor. On the sum-capacity of degraded gaussian multiple-access relay channels. *IEEE Transactions on Information Theory*, 55(12):5394 – 5411, dec. 2009.
- [SZ10] C. Schlegel and S. Zhang. On the dynamics of the error floor behavior in (regular) ldpc codes. *Information Theory, IEEE Transactions on*, 56(7):3248 –3264, july 2010.
- [Tan81] R. Tanner. A recursive approach to low complexity codes. *IEEE Transactions on Information Theory*, 27(5):533 – 547, sep 1981.
- [Ten99] S. Ten Brink. Convergence of Iterative Decoding. *IEEE Electronic Letters*, 35(10):806–808, May 1999.
- [TF04] D. Tuninetti and C. Fragouli. Processing along the way: forwarding vs. coding. In *International Symposium on Information Theory and its Applications, ISITA '04*, 2004.
- [TNS03] Yu-Chee Tseng, Sze-Yao Ni, and En-Yu Shih. Adaptive approaches to relieving broadcast storms in a wireless multihop mobile ad hoc network. *IEEE Transactions on Computers*, 52(5):545 – 557, may 2003.

- [VDV⁺10] A. Voicila, D. Declercq, F. Verdier, M. Fossorier, and P. Urard. Low-complexity decoding for non-binary ldpc codes in high order fields. *IEEE Transactions on Communications*, 58(5):1365–1375, may 2010.
- [Von03] P. O. Vontobel. *Algebraic Coding for Iterative Decoding*. PhD thesis, ETH Zurich, 2003.
- [WC02] B. Williams and T. Camps. Comparison of broadcasting techniques for mobile ad hoc networks. In *The Third ACM International Symposium on Mobile Ad Hoc Networking and Computing, MOBIHOC'02*, 2002.
- [WK07] D. H. Woldegebreal and H. Karl. Multiple-Access Relay Channel with Network Coding and Non-Ideal Source-Relay Channels. In *2007 IEEE International Symposium on Wireless Communication Systems, ISWCS07*, October 2007.
- [WMG10] O. Waqar, D.C. McLernon, and M. Ghogho. Exact evaluation of ergodic capacity for multihop variable-gain relay networks: A unified framework for generalized fading channels. *IEEE Transactions on Vehicular Technology*, 59(8):4181–4187, oct. 2010.
- [XB04] H. Xiao and A.H. Banihashemi. Improved progressive-edge-growth (peg) construction of irregular ldpc codes. *IEEE Communications Letters*, 8(12):715–717, December 2004.
- [XS09] M. Xiao and M. Skoglund. Design of Network Codes for Multiple-User Multiple-Relay Wireless Networks. In *2009 IEEE International Symposium on Information Theory, ISIT'09*, June-July 2009.
- [XS10] M. Xiao and M. Skoglund. Multiple-User Cooperative Communications Based on Linear Network Coding. *IEEE Transactions on Communications*, 58(12):3345–3351, December 2010.
- [YE07] M. Yuksel and E. Erkip. Diversity-Multiplexing Tradeoff in Half-Duplex Relay Systems. In *2007 IEEE International Conference on Communications, ICC'07*, June 2007.
- [YK07] S. Yang and R. Koetter. Network Coding over a Noisy Relay: a Belief Propagation Approach. In *2007 IEEE International Symposium on Information Theory, ISIT'07*, June 2007.

-
- [YW10] R. Yu and T. Wu. Joint Network Coding and Channel Coding for Cooperative Relay Communication System. In *2010 International Conference on Wireless Communications and Signal Processing, WCSP10*, October 2010.
 - [Zim80] H. Zimmermann. OS1 Reference Model-The ISO Model of Architecture for Open Systems Interconnection. *IEEE Transactions on Communications*,, 28(04), April 1980.
 - [ZKBW09] G. Zeitler, R. Koetter, G. Bauch, and J. Widmer. On quantizer Design for Soft Values in the Multiple-Access Relay Channel. In *2009 IEEE International Conference on Communications, ICC'09*, June 2009.
 - [ZLT10] X. Zheng, F. C. M. Lau, and C. K. Tse. Constructing Short-Length Irregular LDPC Codes with Low Error Floor. *IEEE Transactions on Communications*,, 58(10):2823–2834, October 2010.

APPENDIX A

Paper I

Title: Non-Binary LDPC-BICM and Network Coding with Iterative Decoding for the Multiple Access Relay Channel

Authors: Mikel Hernaez¹, Pedro M. Crespo¹ and Javier Del Ser²

Affiliation:¹ Centro De Estudios e Investigaciones Técnicas de Gipuzkoa (CEIT) and TECNUN (University of Navarra), 20008 Donostia-San Sebastián, Spain

Affiliation:² TELECOM Unit TECNALIA RESEARCH & INNOVATION P. Tecnológico, Ed. 202, 48170 Zamudio, Spain

Conference: *IEEE 73th Vehicular Technology Conference, IEEE VTC2011-Spring*, Budapest, Hungary, May 2009. DOI: 10.1109/VETECS.2011.5956367.

***NON-BINARY LDPC-BICM AND NETWORK CODING WITH
ITERATIVE DECODING
FOR THE MULTIPLE ACCESS RELAY CHANNEL***

Mikel Hernaez, *Student member, IEEE*, Pedro M. Crespo, *Senior member, IEEE*, and Javier Del Ser, *Member, IEEE*

¹ Centro De Estudios e Investigaciones Técnicas de Gipuzkoa (CEIT) and TECNUN (University of Navarra), 20008 Donostia-San Sebastián, Spain
E-mails: {mhernaez, pcrespo}@ceit.es

² TELECOM Unit TECNALIA RESEARCH & INNOVATION P.
Tecnológico, Ed. 202, 48170 Zamudio, Spain
E-mails: {javier.delser}@tecnalia.com.es

Abstract — In this paper we present a novel joint network-channel coding scheme for the time-division Multiple Access Relay Channel (MARC), which combines Bit-Interleaved Coded Modulation with iterative decoding (BICM-ID) based on non-binary Low-Density Parity Check (LDPC) codes, along with the linear combination of blocks of data at the relay. The common receiver iteratively exchanges soft information between a joint soft demapper and the LDPC decoder associated to the transmitting nodes. The performance of the proposed system is compared, in terms of Frame Error Rate (FER) and through intensive Monte Carlo simulations, with the corresponding theoretical outage rate for different values of the spectral efficiency ρ_s of the overall setup. Two main conclusions are drawn: 1) small FER degradation is obtained as ρ_s increases; and 2) no diversity is lost with respect to the theoretical outage rate.

I. INTRODUCTION

The Multiple Access Relay Channel (MARC) is a communication scenario where several information sources forward data to a single common destination with the help of an intermediate relay [13]. This channel has spurred a flurry of research in the last few years: for instance, in [10, 15, 17] it was shown that cooperation among nodes may improve the total transmission rate and increase the spatial diversity of the network. In [11, 18] the advantages of performing network coding at the relays were analyzed, while different coding strategies and capacity bounds for the MARC were analyzed in [12]. Further work on the MARC includes the derivation of the exact sum-capacity for the degraded gaussian MARC [16], as well as extensions to frequency-selective MARC [4] and correlated senders [5].

In this context, we specifically consider the time-division MARC, where each node in the network conveys its data by using time-orthogonal channels, i.e. the total transmission time is divided in N time slots, one for each transmitting node. This setup is depicted in Figure A.1. Although the time-division scheme results in a suboptimal use of the available bandwidth, it allows for an easier implementation in practical systems thanks to the use of half-duplex relays and the lack of stringent synchronization constraints. When dealing with this scenario, several contributions have focused on joint network-channel decoding schemes for MARC subject to flat fading as a means to efficiently exploit the spatial diversity at the relay. Joint network-channel codes blend together controlled redundancy for forward error correction and in-network mixing of input data at the relay. As such, the performance of binary Turbo [5, 8] and binary Low-Density Parity Check (LDPC) [2, 9] codes has been thoroughly explored for this scenario. On the other hand, non-binary codes were investigated for similar networks in [6, 20]. However, to the knowledge of the authors no application of non-binary coding schemes – known for their outstanding performance in point-to-point links with respect to their binary counterpart – to the MARC scenario has been reported so far in the related literature.

In this paper we propose the use of non-binary LDPC (also known as $GF(2^q)$ -LDPC) codes [3] for joint network-channel coding over the 2-user quasi-static flat-fading MARC. The performance gain provided by $GF(2^q)$ -LDPC codes comes together with a decoding complexity increase. A straightforward implementation of the Sum-Product Algorithm (SPA) [14] has complexity in $\mathcal{O}(2^{2q})$, although a Fourier domain implementation

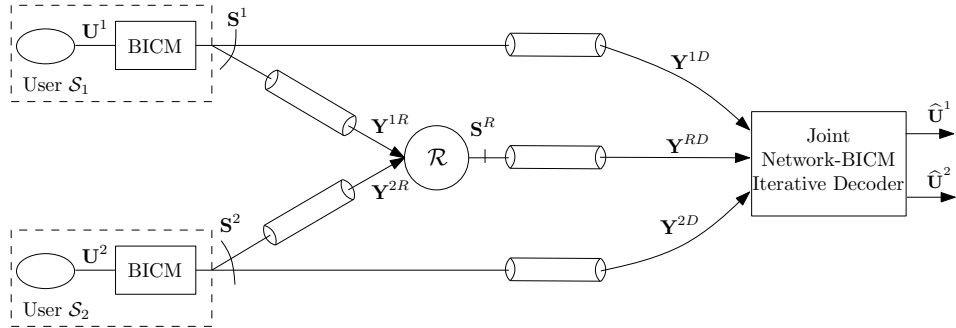


Figure A.1: Block diagram of the considered 2-user MARC scenario.

of the SPA reduces the complexity to $\mathcal{O}(q2^q)$ [3]. Recently the computational load has been reduced to $\mathcal{O}(n_m 2^{n_m})$, with $n_m \ll q$ [19]. However, since the values of q in this article are small, the Fourier domain SPA has been used for decoding.

Moreover, each transmitter utilizes a Bit-Interleaved Coded Modulation (BICM, see [1]) scheme consisting of the concatenation of a $GF(2^q)$ -LDPC encoder, a pseudorandom interleaver and a symbol mapper. The output of the symbol mapper at each sender is then broadcasted to the relay and the destination during its corresponding time slot. During the third time slot, the relay decodes the messages from both transmitters by employing a BICM iterative decoder (BICM-ID), which exchanges information between a soft demapper and the corresponding channel decoder. Once the received sequences have been correctly decoded, the relay combines the estimated symbols into a single signal by employing the aforementioned BICM scheme, and transmits the resulting joint network-channel coded sequence to the distant receiver.

After receiving all the transmitted sequences, the common destination decodes and estimates both source messages. The iterative decoding procedure at the common destination is based on iteratively exchanging soft information between a pair of BICM-ID through a joint soft channel demapper, which will be later detailed by means of factor graphs and the Sum-Product Algorithm (SPA, see [14]). Extensive Monte Carlo simulation results have been carried out by considering a variety of overall spectral efficiencies ρ_s [bits per complex dimension]. Based on such simulation results it is con-

cluded that the proposed approach performs significantly close to the corresponding outage rate at no diversity gain penalty.

The remainder of the manuscript is organized as follows: Section II introduces the system model, whereas the proposed decoding algorithm at the receiver is detailed in Section III. Next, Section IV discusses the obtained Monte Carlo simulation results, and finally Section V concludes the paper by drawing some concluding remarks.

II. SYSTEM MODEL

Referring to Figure A.1, for simplicity we have considered a symmetric scenario consisting of 2 unit-entropy information sources \mathcal{S}_1 and \mathcal{S}_2 , which generate statistically independent binary data segmented in blocks \mathbf{U}^1 and \mathbf{U}^2 of length qK , i.e. $\mathbf{U}^1 \in \{0, 1\}^{qK}$ and $\mathbf{U}^2 \in \{0, 1\}^{qK}$. As depicted in Figure A.2, at each transmitter, q consecutive bits of the corresponding source block \mathbf{U}^i are grouped and mapped¹ to a $GF(2^q)$ -symbol. The resulting K -length sequence is then channel-encoded by using the aforementioned $GF(2^q)$ -LDPC, giving rise to the non-binary codeword $\mathbf{C}^i \in GF(2^q)^N$, with $i \in \{1, 2\}$. The code rate is therefore given by $R = K/N$. Next, each encoded symbol in \mathbf{C}^i is mapped back to its binary equivalent, which yields the q -length binary subsequence $\mathbf{X}_n^i = \{X_n^i(1), \dots, X_n^i(q)\} = \psi_q(C_n^i) \in GF(2)^q$, where $n \in \{1, \dots, N\}$ and $\psi_x(\cdot) : GF(2^x) \rightarrow GF(2)^x$. The resulting binary codeword $\mathbf{X}^i \triangleq \{\mathbf{X}_n^i\}_{n=1}^N \in GF(2)^{qN}$ is parallel-to-serial converted and interleaved through a bitwise random interleaver Π_i .

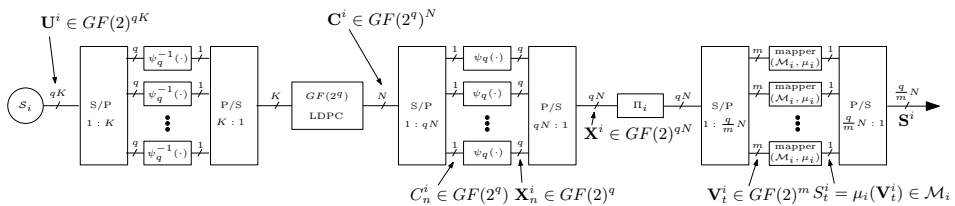


Figure A.2: Schematic diagram of the transmitter for source S_i , with $i \in \{1, 2\}$.

¹ For the binary transformation the left bit will be regarded as the most significant bit (MSB).

A second serial-to-parallel stage processes m consecutive bits of the interleaved encoded sequence to build the vector $\mathbf{V}_t^i \in GF(2)^m$, where $t \in \{1, \dots, qN/m\}$. Each vector $\mathbf{V}_t^i = \{V_t^i(1), \dots, V_t^i(m)\}$ is finally allocated to a signal $S_t^i = \mu_i(\mathbf{V}_t^i)$ chosen from a 2^m -ary signal constellation \mathcal{M}_i with mapping rule $\mu_i(\cdot)$. A Cyclic Redundancy Check (CRC) header is finally appended to the transmitted sequences $\mathbf{S}^i \triangleq \{S_t^i\}_{t=1}^{qN/m}$ to allow for error detection at the relay.

The symbol received by node $j \in \{R, D\}$ (R: Relay, D: Destination) from transmitter $i \in \{1, 2\}$ at time $t \in \{1, \dots, qN/m\}$ is given by

$$Y_t^{i,j} = A^{i,j} S_t^i + N_t^{i,j}, \quad (1)$$

where $A^{i,j} = \alpha_{i,j}/d_{i,j}^{\delta/2}$ represents the path loss and fading attenuation, with $d_{i,j}$ denoting the distance between nodes i and j and δ the attenuation exponent. In the above expression, $\alpha_{i,j}$ is Rayleigh distributed with $E[\alpha_{i,j}^2] = 1 \forall i, j$, whereas $N_t^{i,j}$ is modeled as a Gaussian random variable with zero mean and variance $N_0/2$. The value of $\alpha_{i,j}$ is assumed to remain constant within the duration of a transmitted block (i.e. quasi-static fading).

A. Relay Node

At the first and second time slots, the relay receives the channel sequences $\mathbf{Y}^{1,R} \triangleq \{Y_t^{1,R}\}_{t=1}^{qN/m}$ and $\mathbf{Y}^{2,R}$ from sources \mathcal{S}_1 and \mathcal{S}_2 , respectively. This intermediate node decodes both sequences by using a BICM-ID decoder, which is based on iteratively exchanging soft information between a soft demapper and the corresponding non-binary LDPC decoder. This procedure is similar to that performed at destination; therefore, we refer to Section III for a detailed explanation.

As a result, estimations $\hat{\mathbf{U}}^i$ for the original source sequences \mathbf{U}^i are obtained. The relay knows if the decoded sequences are error-free thanks to the CRC bits added to the original transmitted messages. In such a case, the relay proceeds with subsequent encoding procedures. We will however assume perfect decoding at the relay, which is not a very unrealistic assumption since the relay is usually closer to the sources than to the destination. Under this assumption, the relay follows the same encoding procedure as in the transmitters so as to reproduce the binary vectors \mathbf{V}_t^1 and \mathbf{V}_t^2 . However, at this node both vectors are mapped to symbols in $GF(2^m)$ and linearly combined over this field. That is, the *network-coded* vector \mathbf{V}_t^R is given by

$$\mathbf{V}_t^R = \psi_m(h_1 \otimes \psi_m^{-1}(\mathbf{V}_t^1) \oplus h_2 \otimes \psi_m^{-1}(\mathbf{V}_t^2)), \quad (2)$$

where $\psi_x^{-1}(\cdot) : GF(2)^x \rightarrow GF(2^x)$, $\mathbf{h} = (h_1, h_2) \in GF(2^m)^2$ denotes the set of coefficients of the linear combination, and \otimes and \oplus represent multiplication and summation over $GF(2^m)$, respectively.

Once the network coding operation in expression (2) is done, every network-coded vector \mathbf{V}_t^R is mapped to a signal $S_t^R = \mu_R(\mathbf{V}_t^R)$ from a 2^m -ary constellation \mathcal{M}_R with mapping rule $\mu_R(\cdot)$. The symbol transmitted by the relay node and received by the destination node at time t is thus given by

$$Y_t^{R,D} = A^{R,D} S_t^R + N_t^{R,D}, \quad (3)$$

where $A^{R,D}$ and $N_t^{R,D}$ are defined as in expression (1). Full channel state information (CSI) is assumed at the receiver.

III. JOINT NETWORK-BICM ITERATIVE DECODER

After processing at the relay, the destination receives the qN/m -length sequences $\mathbf{Y}^{i,D}$, with $i \in \{1, 2, R\}$, which are then processed through a Joint Network-BICM Iterative Decoder (JNBICM-ID) composed of a soft demapper and a non-binary LDPC channel decoder of each source. The decoding procedure iteratively exchanges soft information between the soft demapper and both LDPC decoders until a fixed number of iterations \mathcal{I} is reached. For the sake of simplicity in the notation, through this section we will denote the received symbols $\{Y_t^{1,D}, Y_t^{2,D}, Y_t^{R,D}\}$ at time instant t by \mathbf{Y}_t^D , and the three received blocks $\{\mathbf{Y}^{1,D}, \mathbf{Y}^{2,D}, \mathbf{Y}^{R,D}\}$ by \mathbf{Y}^D .

A. Soft Demapper

The aim of the soft demapper is to compute the *a priori* probabilities $p^a(\mathbf{X}_n^i(w))$, with $i \in \{1, 2\}$, $n \in \{1, \dots, N\}$ and $w \in \{1, \dots, q\}$ based on the received sequence set \mathbf{Y}^D . To that end, we will partition the soft demapper algorithm in two stages: (i) the channel soft demapper, which operates on the set \mathbf{Y}_t^D ; and (ii) the bitwise *a priori* probability computation, which is independently computed for each transmitter. While the latter reduces to the traditional BICM-ID decoder, the former takes advantage of the diversity given by the relay to jointly compute the conditional channel probabilities $p(\mathbf{Y}_t^D | S_t^i)$ of the transmitted symbols from each source. Next, we will elaborate on such compounding stages in reference to Figure A.3:

In the channel soft demapper (i), at each time instant t the demapper processes the received signals \mathbf{Y}_t^D and calculates the symbol probability

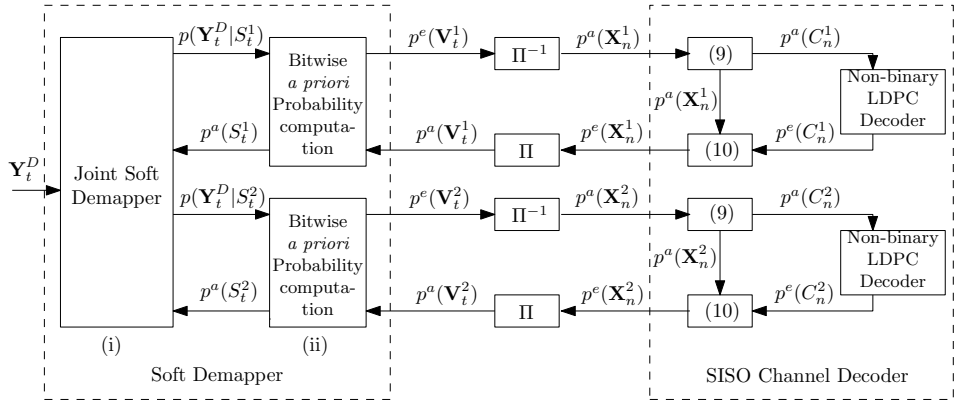


Figure A.3: Block diagram of the Joint Network-BICM Iterative Decoder.

$p(\mathbf{Y}_t^D | S_t^i) \forall t \in \{1, \dots, qN/m\}$. On that purpose, it first computes the joint likelihood probability $p(\mathbf{Y}_t^D | S_t^1, S_t^2)$ as

$$p(\mathbf{Y}_t^D | S_t^1, S_t^2) \propto \exp \left\{ -\frac{\sum_{j \in \{1,2,R\}} |Y_t^{j,D} - A^{j,D} S_t^j|^2}{N_0} \right\},$$

where S_t^R is as defined in Section II-A, and the proportionality accounts for the normalization $\sum p(\mathbf{Y}_t^D | S_t^1, S_t^2) = 1$. Notice that the signal S_t^R in the above expression is a function of the signals S_t^1 and S_t^2 as explained in Section II. Next, the resulting probability is marginalized, yielding the symbol likelihoods

$$p(\mathbf{Y}_t^D | S_t^i) = \sum_{S_t^{\sim i} \in \mathcal{M}_{\sim i}} p(\mathbf{Y}_t^D | S_t^1, S_t^2) p^a(S_t^{\sim i}) \quad (4)$$

where $\sim i$ denotes the complement of $i \in \{1, 2\}$, and $p^a(S_t^{\sim i})$ is the *a priori* probability of the signal point $S_t^{\sim i} \in \mathcal{M}_{\sim i}$ fed back from the second stage of the soft demapper and given by expression (8). Observe that at the relay, a similar channel demapping procedure is performed to obtain the symbol probability $p(Y_t^{i,R} | S_t^i)$, which is given by

$$p(Y_t^{i,R} | S_t^i) \propto \exp \left\{ -\frac{|Y_t^{i,R} - A^{i,R} S_t^i|^2}{N_0} \right\}, \quad (5)$$

Note that this probability is computed independently for each source. As for the second stage of the soft demapper (ii), first recall that the interleaved

version of the codeword \mathbf{X}^i is split in m -length binary vectors \mathbf{V}_t^i , which are then mapped to a signal point as $S_t^i = \mu_i(\mathbf{V}_t^i)$. Hence, by using the symbol probabilities provided by the channel soft demapper (and given by expression (4)), the bitwise *extrinsic* probabilities are defined as

$$\begin{aligned} p^e(V_t^i(l) = v) &\triangleq p(V_t^i(l) = v | \mathbf{Y}_t^D) / p(V_t^i(l) = v) \\ &\propto \sum_{\mathbf{V}_t^i \in \mathcal{V}_l^v} p(\mathbf{Y}_t^D | \mathbf{V}_t^i) p(\mathbf{V}_t^i | V_t^i(l) = v), \end{aligned} \quad (6)$$

where $l \in \{1, \dots, m\}$, $v \in \{0, 1\}$, $p(\mathbf{Y}_t^D | \mathbf{V}_t^i) = p(\mathbf{Y}_t^D | S_t^i = \mu_i(\mathbf{V}_t^i))$ and thereby given by expression (4) (at the receiver) and (5) (at the relay), and \mathcal{V}_l^v denotes the subset of binary vectors $\mathbf{V} \in GF(2)^m$ whose l -th position $V(l)$ has value v , i.e. $\mathcal{V}_l^v = \{\mathbf{V} \in \{0, 1\}^m | V(l) = v\}$. On the other hand, the conditional probabilities $p(\mathbf{V}_t^i | V_t^i(l) = v)$ are computed based on the output soft information of the coded bits from the corresponding LDPC decoder as

$$p(\mathbf{V}_t^i | V_t^i(l) = v) = \prod_{\substack{l'=1 \\ l' \neq l}}^m p^a(V_t^i(l')), \quad (7)$$

assuming independencies, where $p^a(V_t^i(l))$ are the *a priori* probabilities of the coded bits fed back from the LDPC decoder, and given in expression (11). Notice that the *extrinsic* probabilities $p^e(V_t^i(l))$ must be deinterleaved through Π_i before entering the corresponding $GF(2^q)$ -LDPC channel decoder. This yields the *a priori* probability $p^a(X_n^i(w)) = \Pi_i^{-1}[p^e(V_t^i(l))]$, with $n \in \{1, \dots, N\}$, $w \in \{1, \dots, q\}$ and $i \in \{1, 2\}$.

Besides, at the destination this second stage of the soft demapper compiles all the *a priori* probabilities of the coded bits and computes the *a priori* probabilities of each channel symbol S_t^i as

$$p^a(S_t^i) = p^a(\mathbf{V}_t^i = \mu_i^{-1}(S_t^i)) = \prod_{l=1}^m p^a(V_t^i(l)), \quad (8)$$

where $p^a(V_t^i(l))$ is given by expression (11).

B. Non-binary LDPC Decoding

As mentioned in Section I and II, $GF(2^q)$ -LDPC codes are utilized as channel encoders at all transmitters. Since we are using non-binary codes, the *a priori* probabilities of the encoded $GF(2^q)$ -symbols $C_n^i = \psi_q^{-1}(\mathbf{X}_n^i) \in$

$GF(2^q)$ must be computed based on the binary probabilities $p^a(\mathbf{X}_n^i)$ generated by the soft demapper. Such probabilities are given by

$$p^a(C_n^i) = p^a(\mathbf{X}_n^i = \psi_q(C_n^i)) = \prod_{w=1}^q p^a(X_n^i(w)), \quad (9)$$

which are then fed to the corresponding LDPC decoder as a priori information on the coded symbols. Next, a single iteration of the non-binary LDPC is performed (see [19]), which produces the *extrinsic* probabilities $p^e(C_n^i)$ of the $GF(2^q)$ -symbols $\{C_n^i\}_{n=1}^N$. Next, in order to compute the estimates $\widehat{\mathbf{U}}^i$ for the information bits \mathbf{U}^i , we need to compute the *extrinsic* probabilities of each binary symbol as

$$p^e(X_n^i(w) = b) \triangleq \sum_{\mathbf{X}_n^i \in \mathcal{X}_w^b} p^e(\mathbf{X}_n^i) \prod_{\substack{w'=1 \\ w' \neq w}}^q p^a(X_n^i(w')), \quad (10)$$

where $p^e(\mathbf{X}_n^i) = p^e(C_n^i = \psi_q^{-1}(\mathbf{X}_n^i))$, $p^a(X_n^i(w))$ is the output probability from the soft demapper, and \mathcal{X}_w^b denotes the subset of vectors $\mathbf{X} \in GF(2)^q$ whose w -th position has value $b \in \{0, 1\}$, i.e. $\mathcal{X}_w^b = \{\mathbf{X} \in \{0, 1\}^q | X(w) = b\}$. Finally, the decoder estimates $\widehat{\mathbf{U}}^i$ based on the binary equivalent of the estimation of $X_n^i(w)$, which is obtained through a hard decision on the *a posteriori* probability $p^a(x_n^i(w)) \cdot p^e(x_n^i(w))$. Besides, the *extrinsic* probabilities in expression (10) are interleaved so as to render the *a priori* binary probabilities entering the soft demapper, i.e.

$$p^a(V_t^i(l)) = \Pi_i [p^e(X_n^i(w))]. \quad (11)$$

Notice that when $q = 1$ (i.e. binary LDPC codes), the *extrinsic* probabilities output by the LDPC decoder reduce to the *extrinsic* probabilities of expression (11); consequently, there is no need for either expression (9) or (10).

All the expressions detailed in this section can be derived from the application of the SPA algorithm over the factor graph depicted in Figure A.4. It is important to remark that the joint likelihood probabilities (represented by the topmost check nodes in Figure A.4) implicitly considers the correlation between transmitted symbols S_t^1 and S_t^2 through the linear network coding operation at the relay (expression (2)).

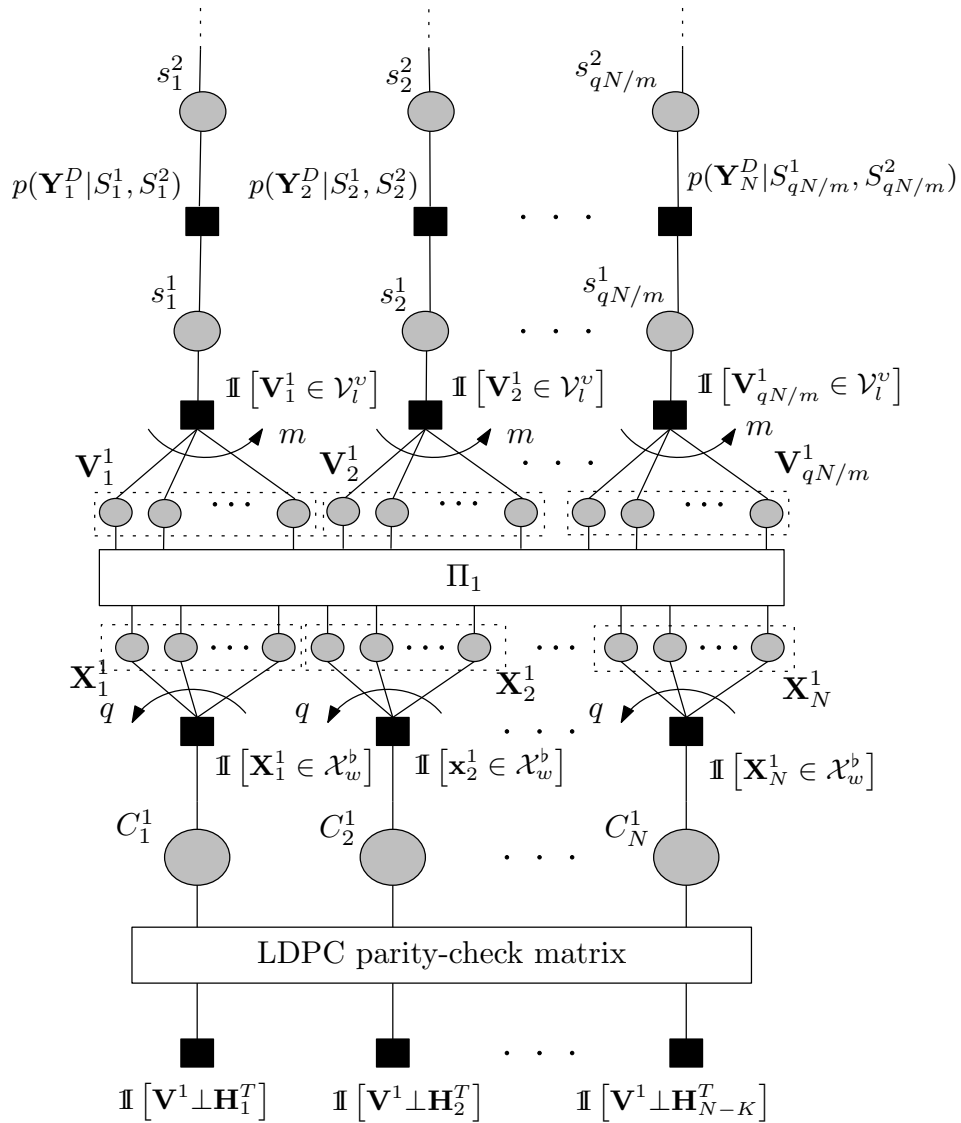


Figure A.4: Factor graph of the JNBICM-ID for source \mathcal{S}_1 . $\mathbb{I}[\cdot]$ denotes the indicator function, whereas $\mathbf{x} \perp \mathbf{H}_z^T$ stands for orthogonality between vector x and compounding non-binary LDPC parity-check matrix \mathbf{H}_z , with $z \in \{1, \dots, N - K\}$.

IV. RESULTS

In order to assess the performance of the proposed approach, Monte Carlo simulations have been done for different values of q and m . The distances between nodes have been set to $d_{1,D} = d_{2,D}$, $d_{1,R} = d_{1,D}/4$, and $d_{R,D} = 3 \cdot d_{1,D}/4$, whereas the attenuation exponent δ equals 3.52. Each source \mathcal{S}_i generates information blocks of $K = 6000$ bits, and a irregular $GF(2^q)$ -LDPC code of rate $R = 1/3$ is utilized at each transmitter. Due to the lack of central control and cooperation among the sources, we will further assume that both transmitters and the relay use Gray-mapped 2^m -ary Pulse Amplitude Modulation (PAM). We have considered $m \in \{1, 2, 3\}$; since the spectral efficiency of the system ρ_s (in bits per complex dimension) depends on m , we have that

$$\rho_s = 4m/9 \text{ [bits per complex dimension].} \quad (12)$$

We adopt the *Common Frame Error Rate* (CFER) as the performance metric, which is compared to the ultimate outage rate (i.e. when gaussian input is assumed) as defined in [7]. The Sum-Product algorithm over the factor graph in Figure A.4 is halted after $\mathcal{I} = 50$ iterations. For all the considered scenarios the vector $\mathbf{h} = (h_1, h_2)$ has been selected based on exhaustive simulations. Not shown for brevity, these simulations show that a maximum performance gain of around 2 dB at $\text{CFER} = 10^{-2}$ is achieved by selecting a fixed *but* optimized value of \mathbf{h} instead of randomly generating \mathbf{h} at every transmission.

The results are summarized in Figure A.5, where the CFER versus E_b/N_0 – with E_b denoting energy per source bit – is displayed for $m \in \{1, 2, 3\}$ (corr. 2-PAM, 4-PAM and 8-PAM) and $q \in \{1, 2, 3\}$. First notice that the maximum achievable diversity gain is achieved for all the simulated cases, since the slopes of the simulated curves are equal to that of the corresponding outage rate. Also notice that the performance of our proposed system for $q = 2$ is significantly close to the corresponding outage rate. Finally observe that for all values of m , using non-binary LDPC codes entails a significant performance gain with respect to the binary LDPC case, e.g. for $m = 2$ and $\text{CFER} = 10^{-2}$ the gap between $GF(4)$ -LDPC coding ($q = 2$) and binary LDPC coding ($q = 1$) is approximately 3.2 dB. A slight performance degradation is obtained for $q = 3$. The reason being that as q increases, the number of check nodes interconnecting the LDPC factor

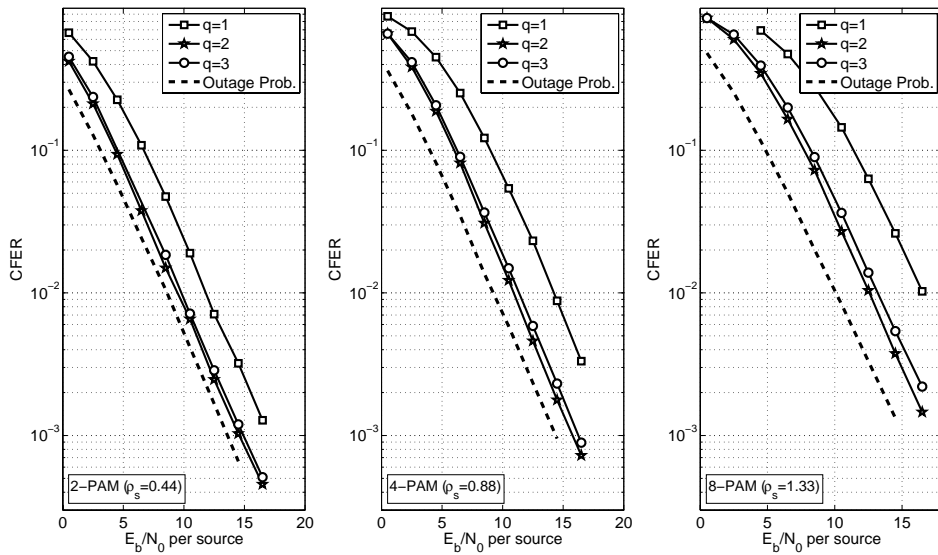


Figure A.5: CFER versus E_b/N_0 of the proposed JNBICM scheme for different values of q and m .

graph to that of the soft demapper decreases. Consequently, short-length cycles are more likely to appear between such factor graphs, which gets even more likely if m also increases. The rationale follows by noting that the performance of the SPA is known to degrade when applied to cyclic factor graphs with low girth (i.e. with small length of the shortest cycle).

VI. CONCLUDING REMARKS

In this manuscript we have presented a novel Joint Network-Bit Interleaved Coded Modulation scheme for the time-division 2-user MARC with orthogonal quasi-static fading channels. The proposed scheme combines linear network coding with Bit-Interleaved Coded Modulation (BICM) using non-binary LDPC codes in order to exploit the spatial diversity of the setup. The common receiver is based on iteratively exchanging soft information between a soft demapper and the soft-input-soft-output (SISO) non-binary LDPC decoders corresponding to each source. Monte Carlo simulations have verified, on one hand, that the proposed approach based on non-binary LDPC codes outperforms its binary coding counterpart at no

loss in diversity. Future research will be conducted towards optimizing the LDPC parity check matrices and the mapping rules $\mu_i(\cdot)$ ($i \in \{1, 2, R\}$) via EXIT charts.

REFERENCES

- [1] G. Caire, G. Taricco, and E. Biglieri. Bit-interleaved Coded Modulation. *IEEE Transaction on Information Theory*, 44:927–946, May 1998.
- [2] L. Chebli, C. Hausl, G. Zeitler, and R. Koetter. Cooperative Uplink of Two Mobile Stations with Network Coding Based on the WiMax LDPC Code. In *2009 IEEE Global Communication Conference, GLOBECOM'09*, December 2009.
- [3] M.C. Davey and D. MacKay. Low-density parity check codes over $gf(q)$. *IEEE Communications Letters*, 2(6):165 –167, jun 1998.
- [4] J. Del Ser, P.M. Crespo, B.H. Khalaj, and J. Gutierrez-Gutierrez. On combining distributed joint source-channel-network coding and turbo equalization in multiple access relay networks. In *Third IEEE International Conference on Wireless and Mobile Computing, Networking and Communications, WiMOB'07.*, page 18, oct. 2007.
- [5] J. Del Ser, M. Mendicute, P.M. Crespo, S. Gil-Lopez, and I. Olabarrieta. Joint source-channel network decoding and blind estimation of correlated sensor using concatenated zigzag codes. In *Springer Lecture Notes in Computer Science*, volume 5793/2009, pages 30–41, September 2009.
- [6] Z. Guo, J. Huang, B. Wang, J.-H Cui, S. Zhou, and P. Willet. A Practical Joint Network-Channel Coding Scheme for Reliable Communication in Wireless Networks. In *The Tenth ACM International Symposium on Mobile Ad Hoc Networking and Computing, MOBIHOC'09*, May 2009.
- [7] C. Hausl. *Joint Network-Channel Coding for Wireless Relay Channels*. PhD thesis, TU München, 2008.
- [8] C. Hausl. Joint network-channel coding for multiple-access relay channel based on turbo codes. volume 20, pages 175 – 181, Mar. 2009.

- [9] C. Hausl, F. Schreckenbah, I. Oikonomidis, and G. Bauch. Iterative network and channel decoding on a tanner graph. In *Forty-Third Annual Allerton Conference on Communication, Control, and Computing, Allerton'05*, 2005.
- [10] T.E. Hunter and A. Nosratinia. Cooperation diversity through coding. In *2002 IEEE International Symposium on Information Theory, ISIT'02*, 2002.
- [11] R. Koetter and M. Medard. An algebraic approach to network coding. *IEEE/ACM Transactions on Networking*, 11(5):782 – 795, oct. 2003.
- [12] G. Kramer, M. Gastpar, and P. Gupta. Cooperative Strategies and Capacity Theorems for Relay Networks. *IEEE Transactions on Information Theory*, 51(9):3037–3063, September 2005.
- [13] G. Kramer and A. J. Van Wijngaarden. On the White Gaussian Multiple-Access Relay Channel. In *2000 IEEE International Symposium on Information Theory, ISIT'00*, June 2000.
- [14] F.R. Kschischang, B.J. Frey, and H.-A. Loeliger. Factor graphs and the sum-product algorithm. *IEEE Transactions on Information Theory*, 47(2):498 –519, feb 2001.
- [15] J.N. Laneman, D.N.C. Tse, and G.W. Wornell. Cooperative diversity in wireless networks: Efficient protocols and outage behavior. *IEEE Transactions on Information Theory*, 50(12):3062 – 3080, dec. 2004.
- [16] L. Sankar, N.B. Mandayam, and H.V. Poor. On the sum-capacity of degraded gaussian multiple-access relay channels. *IEEE Transactions on Information Theory*, 55(12):5394 –5411, dec. 2009.
- [17] A. Sendonaris, E. Erkip, and B. Aazhang. User cooperation diversity - part i and ii. *IEEE Transactions on Communications*, 51(11):1927 – 1938, nov. 2003.
- [18] D. Tuninetti and C. Fragouli. Processing along the way: forwarding vs. coding. In *International Symposium on Information Theory and its Applications, ISITA'04*, 2004.
- [19] A. Voicila, D. Declercq, F. Verdier, M. Fossorier, and P. Urard. Low-complexity decoding for non-binary ldpc codes in high order fields. *IEEE Transactions on Communications*, 58(5):1365 –1375, may 2010.

- [20] M. Xiao and M. Skoglund. Design of Network Codes for Multiple-User Multiple-Relay Wireless Networks. In *2009 IEEE International Symposium on Information Theory, ISIT'09*, June-July 2009.

APPENDIX B

Paper II

-
- Title:** On the Design of a Novel Joint Network-Channel Coding Scheme for the Multiple Access Relay Channel
- Authors:** Mikel Hernaez¹, Pedro M. Crespo¹ and Javier Del Ser²
- Affiliation:**¹ Centro De Estudios e Investigaciones Técnicas de Gipuzkoa (CEIT) and TECNUN (University of Navarra), 20008 Donostia-San Sebastián, Spain
- Affiliation:**² TELECOM Unit TECNALIA RESEARCH & INNOVATION P. Tecnológico, Ed. 202, 48170 Zamudio, Spain
-
- Journal:** *IEEE Journal on Selected Areas in Communications*, Accepted for publication, 3rd Quarter 2012
-

***ON THE DESIGN OF A NOVEL JOINT
NETWORK-CHANNEL CODING SCHEME FOR THE
MULTIPLE ACCESS RELAY CHANNEL***

Mikel Hernaez, *Student member, IEEE*, Pedro M. Crespo, *Senior member, IEEE*, and Javier Del Ser, *Senior member, IEEE*

¹ Centro De Estudios e Investigaciones Técnicas de Gipuzkoa (CEIT) and TECNUN (University of Navarra), 20008 Donostia-San Sebastián, Spain
E-mails: {mhernaez, pcrespo}@ceit.es

² TELECOM Unit TECNALIA RESEARCH & INNOVATION P.
Tecnológico, Ed. 202, 48170 Zamudio, Spain
E-mails: {javier.delser}@tecnalia.com.es

Abstract — This paper proposes a novel joint non-binary network channel code for the Time-Division Decode-and-Forward Multiple Access Relay Channel (TD-DF-MARC), where the relay linearly combines – over a non-binary finite field – the coded sequences from the source nodes. A method based on an EXIT chart analysis is derived for selecting the best coefficients of the linear combination. Moreover, it is shown that for different setups of the system, different coefficients should be chosen in order to improve the performance. This conclusion contrasts with previous works where a random selection was considered. Monte Carlo simulations show that the proposed scheme outperforms, in terms of its gap to the outage probabilities, the previously published joint network-channel coding approaches. Besides, this gain is achieved by using very short-length codewords, which makes the scheme particularly attractive for low-latency applications.

Keywords—Fading multiple access relay channel, joint network-channel code, iterative decoding, EXIT charts..

I. INTRODUCTION

Node cooperation has been widely shown to improve the performance of wireless networks with several terminals by increasing the robustness of the system to channel variations such as deep fades, as well as by enabling significant energy savings. The essence of node cooperation lies in jointly processing the in-network information by all the constituent nodes of the network, which allows improving the spectral and power efficiency of wireless networks and ultimately, attaining the desired diversity-multiplexing tradeoff without requiring additional complexity (e.g. co-located multiterminal MIMO schemes).

A particular example of relay cooperation in multi-terminal networks is the so-called Multiple-Access Relay Channel (MARC). The MARC is a communication scenario where two or more information sources forward data to a single common destination with the help of an intermediate relay [18]. In this scenario, the relay can work in full [17, 18] or half duplex mode. For the half duplex mode, the following transmission strategies have been proposed: i) the Constrained MARC (C-MARC [25]), where the sources transmit during the first time slot and coordinate with the relay during the second time slot by transmitting information; ii) the Orthogonal MARC (O-MARC, see [23, 24]), where the sources and the relay transmit over two orthogonal channels; and iii) the Time-Division MARC (TD-MARC, see [14]), where both sources and the relay convey their data by using three orthogonal channels, i.e. for two sources the total transmission time is divided into three time slots, one for each transmitting node. On the other hand, during the last decade the well-known relaying strategies Decode-and-Forward (DF), Compress-and Forward (CF) and Amplify-and-Forward (AF) originally developed for the conventional relay channel [7] have been applied to the aforementioned MARC models in a number of contributions (see e.g. [17, 18, 23–25] and references therein).

When dealing with practical coding schemes for the MARC scenario, the TD-MARC, along with a DF strategy, has been widely studied in the related literature [5, 10, 13–16, 21, 27–30]. Although the time-division scheme involves a suboptimal use of the available bandwidth, it allows for an easier implementation in practical systems thanks to the use of half-duplex relays and the lack of stringent synchronization constraints. Besides, the DF strategy offers a higher code design flexibility. In this work we specifically focus on the 2-user TD-MARC with a DF relaying strategy (hereafter

coined as TD-DF-MARC), which is schematically depicted in Figure B.1. It is important to note that the capacity bounds for this model can be derived from the capacity bounds of the O-MARC [12, 25].

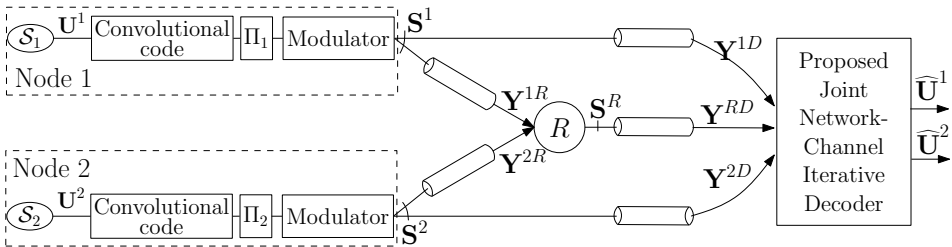


Figure B.1: Block diagram of the considered 2-user TD-DF-MARC scenario.

In the MARC we are interested in maximizing the information conveyed by the relay node. To this end, network coding [1, 20] has become a widely used technique to complement channel coding schemes used for combating channel-induced errors. Combining the data from both sources at the intermediate relay node embodies a practical tool for approaching the capacity bounds of the TD-DF-MARC scenario. However, by treating network and channel coding separately some performance loss is expected, since the network decoder cannot use the output soft information computed by the channel decodes. Likewise, the channel code cannot exploit the redundant information provided by the network code. This observation is further supported by the findings in [8, 22], where it was shown that in general, capacity can only be achieved by conceiving channel and network coding as a single non-separated data processing stage.

In this context, several practical joint network-channel coding schemes have been recently proposed [5, 9, 10, 13–16, 21, 27–30]. In [14] joint network-channel coding for TD-DF-MARC model was first considered. The authors proposed distributed regular LDPC codes as the joint network-channel code at the relay node, where the destination jointly decodes the messages from the sources with the aid of the information sent from the relay, as opposed to [6] where the two messages transmitted from the sources were separately decoded. In [13] the authors follow the same idea by proposing a turbo-code-based joint network-channel coding scheme. Parallel to these proposals, the authors in [21] proposed a similar scheme for high-order modulations. More recently a joint coding scheme based on WiMax

LDPC codes was presented in [5], whereas in [16, 29] two schemes based on turbo codes were investigated. Furthermore, some joint non-binary coding schemes have been recently reported in [27] (non-binary network coding) and [10, 15] (non-binary network and channel coding). Finally, in [28, 30] the authors proposed a joint network-channel coding scheme where the relay transmits the soft values resulting from its decoding procedure over AWGN channels.

The present work joins the upsurge of research on the TD-DF-MARC scenario by proposing a novel Joint Network-Channel Code (JNCC) where the relay linearly combines – over a non-binary finite field – the coded sequences from the source nodes. The iterative decoding procedure at the common destination is performed by running the Sum-Product Algorithm (SPA [19]) on the factor graph describing the proposed JNCC, which is compounded by three sub-factor graphs: two describing the channel codes of each source, and a third describing the network coding operation performed at the relay node. Specifically, the key contributions of this manuscript over the state of the art on this topic are as follows:

- The proposed scheme does not perform channel coding on the already network-coded bits, reducing the complexity at the relay node without compromising performance. To the knowledge of the authors, all practical schemes for fading channels found in the related literature¹ perform channel coding on the already network-coded bits.
- It is shown that a tailored selection of the set of coefficients used in the network coding operation, namely, the Network Coding (NC) coefficients, outperforms a random choice as done in [10]. This selection is performed by matching the EXtrinsic Information Transfer (EXIT, [11, 26]) functions of the compounding codes on the EXIT chart.
- Contrary to previous literature, the JNCC allows the sources to use completely different channel codes, at the sole expense of an increased complexity when choosing the NC-coefficients through EXIT-curve matching.
- The work presented here considers convolutional codes at both source nodes. As a consequence of the previous point, both convolutional

¹In [28] a similar coding procedure at the relay is proposed; however, their study is restricted to AWGN channels and binary network coding.

codes can be independently terminated. This fact allows us to use very short-length codewords, making the scheme particularly attractive for low-latency applications.

The remainder of the manuscript is organized as follows: Section II introduces the system model, whereas the decoding algorithm of the proposed JNCC is detailed in Section III. In Section IV an analysis on the influence of the NC-coefficients is performed through EXIT charts. Section V discusses the obtained Monte Carlo simulation results, and finally Section VI ends the paper by drawing some concluding remarks.

II. SYSTEM MODEL

Let $(\Omega, \beta, \mathcal{P})$ be the underlying probability space where all the random variables (r.v.) are defined. We use uppercase when referring to r.v. and lowercase when referring to realizations of r.v. In addition, we use boldface when referring to vectors; thus, uppercase and boldface refer to random vectors. For discrete r.v., we denote the probability mass function (p.m.f.) of the discrete r.v. X as $P_X(x) \triangleq \mathcal{P}\{X = x\}$. For continuous r.v., we denote the probability density function (p.d.f.) of the continuous r.v. X as $p_X(x)$. However, when the context is clear, we use $P(x)$ and $p(x)$ for p.m.f. and p.d.f., respectively.

Referring to Figure B.1, for simplicity we have considered a symmetric scenario consisting of 2 unit-entropy binary information sources \mathcal{S}_1 and \mathcal{S}_2 , which generate blocks $\mathbf{U}^1 \in \{0, 1\}^K$ and $\mathbf{U}^2 \in \{0, 1\}^K$ of length K . As depicted in this figure, at each transmitter the sequence is channel-coded by a convolutional code, producing the codeword $\mathbf{C}^m \triangleq \{\mathbf{C}_t^m\}_{t=1}^N \in \{0, 1\}^N$, with $m \in \{1, 2\}$ denoting the source index. The code rate is therefore given by $R = K/N$. Each codeword is then interleaved yielding the interleaved codeword $\mathbf{X}^m = \Pi_m(\mathbf{C}^m)$, where Π_1 and Π_2 are two different random spread interleavers with a spread factor equal to $q \in \mathbb{N}$. Finally, the codeword is modulated, resulting in the transmitted sequence $\mathbf{S}^m \triangleq \{S_t^m\}_{t=1}^N$, which is transmitted over $M = N/2$ complex dimensions (i.e. N real dimensions). During the first and second time slots source \mathcal{S}_1 and \mathcal{S}_2 transmit to both the relay and destination nodes the sequence \mathbf{S}^1 and \mathbf{S}^2 , respectively. The third time slot is used by the relay to process the data from the sources and transmit the resulting coded data to destination.

Regarding the links between nodes, we denote as $d_{k,j}$ the distance from transmitter $k \in \{1, 2, R\}$ (R: Relay) to receiver $j \in \{R, D\}$ (D: Destination). Moreover, considering the power at the end of the source-destination link P_0 as the reference, the received power at the end of each link will be given by $P_0 \cdot (d_{S,D}/d_{k,j})^\delta$, where δ denotes an attenuation exponent. In what follows, and without loss of generality, the distances are normalized with respect to $d_{S,D} = 1$ and we consider $P_0 = 1$. Thus, the attenuation undergone by the signals due to the distance-dependant propagation losses of a given link can be expressed as $d_{k,j}^{-\delta}$. Therefore the received symbol per real dimension at each receiver is given by

$$Y_t^{m,j} = \alpha_{k,j}^{k,j} \cdot \sqrt{d_{k,j}^{-\delta}} \cdot S_t^k + N_t^{k,j}, \quad (1)$$

where $\alpha_{k,j}$ is Rayleigh distributed with $E[\alpha_{k,j}^2] = 1 \forall k, j$, and $\{N_t^{k,j}\}_{t=1}^N$ are modelled as real Gaussian i.i.d. random variables with zero mean and variance $N_0^{k,j}/2$. The values of $\{\alpha_{k,j}\}$ are assumed to remain constant within the duration of a transmitted block (i.e. quasi-static fading). Moreover, full channel state information (CSI) is assumed at the receivers.

A. Relay Node

Consider the set of all 2^q polynomials $\rho(z)$ of degree $q-1$ with coefficients lying in $GF(2)$ (the binary Galois field). Let $g(z)$ be a prime polynomial (i.e., monic and irreducible polynomial) of order q . Then, this set becomes a finite field, $GF(2^q)$, by defining the addition \oplus and multiplication \otimes rules as the mod $g(z)$ remainder of the sum and product of two polynomials, respectively. Notice that since the mod $g(z)$ addition rule is just componentwise addition of coefficients in $GF(2)$, $GF(2^q)$ under addition is isomorphic to the vector space $(GF(2))^q$ of binary q -tuples with mod 2 elementwise addition, denoted hereafter as \wedge . Therefore, there is a one-to-one mapping $\psi_q : (GF(2))^q \rightarrow GF(2^q)$ defined as $\psi_q(a_0, \dots, a_{q-1}) = \sum_{k=0}^{q-1} a_k z^k$ such that $\psi_q(\mathbf{a}) \oplus \psi_q(\mathbf{b}) = \psi_q(\mathbf{a} \wedge \mathbf{b})$, where $\mathbf{a}, \mathbf{b} \in (GF(2))^q$. In addition, we index the elements $\rho_i \in GF(2^q)$, $i \in \{0, \dots, 2^q - 1\}$ by the base-10 notation of the corresponding binary tuple (a_0, \dots, a_{q-1}) . In the following we refer to the elements of the finite field $GF(2^q)$ as *non-binary* symbols.

In the first and second time slots the relay receives the channel sequences $\mathbf{Y}^{1,R} \triangleq \{Y_t^{1,R}\}_{t=1}^N$ and $\mathbf{Y}^{2,R}$ from sources \mathcal{S}^1 and \mathcal{S}^2 , respectively and it deinterleaves them. Then, it executes the BCJR algorithm [2] twice in order to obtain the estimations $\widehat{\mathbf{C}}^1$ and $\widehat{\mathbf{C}}^2$ of the source channel-coded sequences,

which are then interleaved in order to obtain the estimated interleaved coded bits $\widehat{\mathbf{X}}^1$ and $\widehat{\mathbf{X}}^2$.

Each of the interleaved coded sequences $\widehat{\mathbf{X}}^1$ and $\widehat{\mathbf{X}}^2$ is partitioned into N/q sub-sequences of length q . We denote as $V^m = \psi_q(\{\widehat{X}_i^m\}_{i=1}^q) \in GF(2^q)$ to the non-binary symbol associated to the corresponding sub-sequence. The non-binary symbol of the relay V^R is now computed as the linear combination of the non-binary symbols corresponding to each source, i.e.

$$V^R \triangleq \psi_q(\psi_q^{-1}(h^1 \otimes V^1) \wedge \psi_q^{-1}(h^2 \otimes V^2)) \triangleq f(V^1, V^2), \quad (2)$$

where $\mathbf{h} = (h^1, h^2)$ and $h^m \in \{\rho_i\}_{i=1}^{2^q-1}$ represents the NC-coefficients used in the linear combination. Finally, the modulated symbols associated to each sub-sequence are computed as $\{S_i^R\}_{i=1}^q = 2 \cdot \psi_q^{-1}(V^R) - 1$ and the transmitted signal \mathbf{S}^R is obtained by concatenating the N/q resulting modulated sub-sequences.

III. ITERATIVE JOINT NETWORK-CHANNEL DECODER

The destination receives the channel outputs $\mathbf{Y} \triangleq (\mathbf{Y}^{1,D}, \mathbf{Y}^{2,D}, \mathbf{Y}^{R,D})$. The aim of the JNCC decoder is to find the source binary symbols $\{U_k^m\}_{k=1}^K$ that maximize the conditional probability $P(u_k^m|\mathbf{y})$, which is obtained by marginalizing the joint conditional probability $P(\mathbf{u}^m|\mathbf{y})$. This marginalization is efficiently computed by applying the SPA over the factor graph describing $P(\mathbf{u}^m|\mathbf{y})$. Figure B.2 shows the three compounding sub-factor graphs of the proposed JNCC: two describing the source convolutional codes, and the third one describing the network code used at the relay. As explained in Section II-A, the factor graph of the relay network code is in turn composed of N/q parallel and identical factor nodes, depicted in Figure B.2 as the oversized factor nodes which we hereafter refer to as *network* check nodes and labelled with \mathcal{NC}_l , $l \in \{1, \dots, N/q\}$. Furthermore, we define $\mathbf{y}_l \triangleq (\mathbf{y}_l^{1,D}, \mathbf{y}_l^{2,D}, \mathbf{y}_l^{R,D})$ as those components of \mathbf{Y} associated to the network check node \mathcal{NC}_l . In the next subsection the derivation of the factor graph corresponding to one of these network check nodes is explained, which is then incorporated into the overall factor graph plotted in Figure B.2.

Since the overall factor graph of the JNCC has loops, the SPA is iteratively run between the sub-factor graphs corresponding to the relay network

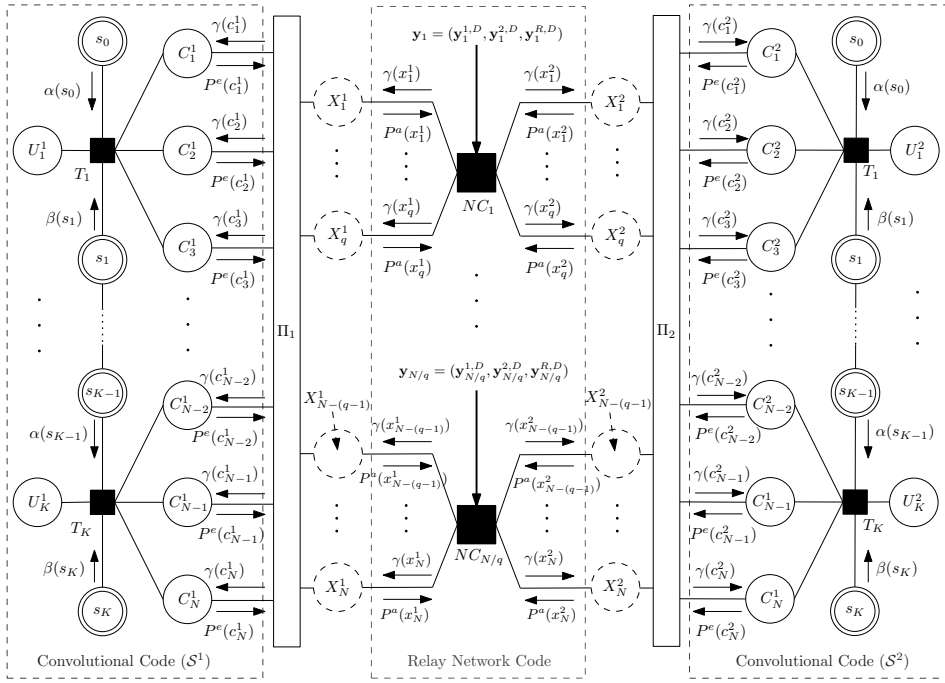


Figure B.2: Factor Graph of the Proposed JNCC.

code and the convolutional codes. After a fixed number of iterations \mathcal{I} , the U_k^m is computed as

$$P(u_k^m | \mathbf{y}) \propto \sum_{\sim u_k^m} T_k(s_k, u_k^m, \mathbf{c}_k^m, s_{k+1}) \alpha(s_k) \beta(s_{k+1}) \prod_{t: c_t^m \in \mathbf{c}_k^m} \gamma(c_t^m), \quad (3)$$

where α and β are the forward and backward messages passed from the adjacent state nodes to the factor node T_k given by the Trellis of the convolutional code; \mathbf{c}_k^m are the coded bits c_t^m associated to u_k^m ; and γ are the messages passed from the variable nodes c_t^m to T_k (i.e. the likelihoods). Note that in the case of not having a relay, the likelihoods γ are given by $\gamma(c_t^m) = p(y_t^{m,D} | c_t^m)$. However, when the relay is present, these likelihoods now depend on the messages passed by the network check nodes associated to the interleaved binary symbol $x_{\Pi_{m-1}(t)}^m$, i.e. $\gamma(c_t^m) = \gamma(x_{\Pi_{m-1}(t)}^m)$, where $\gamma(x_t^m) \propto p(\mathbf{y}_l | x_t^m)$. In the next subsection a factorized form of $p(\mathbf{y}_l | x_t^m)$ is derived.

A. Factorization of $p(\mathbf{y}_l|x_t^m)$

In this section the factorization of the conditional probability $p(\mathbf{y}_l|x_t^m)$ is derived. As before, the upper index j refers to the random variables associated with both sources and the relay, whereas the index m only refers to variables associated to the sources, i.e. $j \in \{1, 2, R\}$ and $m \in \{1, 2\}$. Besides we use index \bar{m} to refer to the complement of m , i.e. $\bar{m} = 3 - m$. As $p(\mathbf{y}_l|x_t^m)$ only depends on the bits belonging to the corresponding pair of sub-codewords of length q , we focus on any given pair $\{\mathbf{X}^m\}_{m=1,2}$, where $\mathbf{X}^m = (X_1^m, \dots, X_q^m)$. Thus, we use the subindex i to denote the position of a given bit inside its corresponding sub-codeword. For the sake of simplicity we drop the super index D from the set of received signals $\mathbf{Y} = \{\mathbf{Y}^{j,D}\}_{j=1,2,R}$ and rewrite the channel random variables for a given sub-codeword as $\mathbf{Y}_l^j = \{Y_{l,i}^j\}_{i=1}^q$.

In order to compute $p(\mathbf{y}_l|x_i^m)$, let us first focus on the *a priori* information provided by the channel decoder. The sequence of random variables $\{X_i^m\}_{i=1}^q$ is assumed to be i.i.d. based on the fact that a spread interleaver is used to suppress strong dependencies (4-length cycles in the underlying factor graph) between the bits belonging to the same sub-codeword. Moreover, the p.m.f of its associated non-binary symbol $V^m = \psi_q(X_1^m, \dots, X_q^m)$ is given by

$$P_{V^m}(v) \triangleq \sum_{x_1^m, \dots, x_q^m} \mathbb{1}[v = \psi_q(x_1^m, \dots, x_q^m)] \prod_{i=1}^q P_{X_i^m}^a(x_i^m), \quad (4)$$

where the last factor represents the *a priori* probabilities of $\{X_i^m\}_{i=1}^q$.

As shown in expression (2), the non-binary symbols V^1 and V^2 are linearly combined over the finite field $GF(2^q)$, producing the non-binary symbol V^R . Therefore, the non-binary symbols joint p.m.f. can be factorized as

$$P(v^1, v^2, v^R) = P(v^R|v^1, v^2)P(v^2|v^1)P(v^1) \quad (5)$$

$$= P(v^1)P(v^2)\mathbb{1}[v^R = f(v^1, v^2)], \quad (6)$$

where $V^R = f(V^1, V^2)$ is the linear combination defined in (2). Now let us focus on the information coming from the channels. Due to the TDMA

scheme, the following Markov chains are verified:

$$\begin{aligned}\mathbf{Y}_l^1 &\Leftrightarrow V^1 \Leftrightarrow (V^2, V^R, \mathbf{Y}_l^2, \mathbf{Y}_l^R), \\ \mathbf{Y}_l^2 &\Leftrightarrow V^2 \Leftrightarrow (V^1, V^R, \mathbf{Y}_l^1, \mathbf{Y}_l^R), \\ \mathbf{Y}_l^R &\Leftrightarrow V^R \Leftrightarrow (V^1, V^2, \mathbf{Y}_l^1, \mathbf{Y}_l^2).\end{aligned}$$

Hence, we have

$$p(\mathbf{y}_l | v^1, v^2, v^R) = p(\mathbf{y}_l^1 | v^1)p(\mathbf{y}_l^2 | v^2)p(\mathbf{y}_l^R | v^R). \quad (7)$$

Furthermore, the non-binary symbols can also be expressed by the corresponding modulated symbols $\{S_i^j\}_{i=1}^q \in \{\pm 1\}^q$ as

$$V^j = \psi_q \left(\left\{ (1 + S_i^j)/2 \right\}_{i=1}^q \right) \triangleq \theta_q \left(\{S_i^j\}_{i=1}^q \right),$$

yielding

$$p(\mathbf{y}_l^j | v^j) \propto \sum_{s_1^j, \dots, s_q^j} \mathbb{1} \left[v^j = \theta_q(s_1^j, \dots, s_q^j) \right] \prod_{i=1}^q p(y_{l,i}^j | s_i^j), \quad (8)$$

where the last product is due to the memoryless channel assumption made in this work, with

$$p(y_{l,i}^j | s_i^j) \propto \exp \left(-\frac{\left(y_{l,i}^j - \alpha^{j,D} \cdot \sqrt{d_{j,D}} \cdot s_i^j \right)^2}{N_0} \right). \quad (9)$$

Now, from expressions (6) and (7) and by applying the Bayes theorem, we obtain the joint *a posteriori* p.d.f. of the non-binary symbols as

$$\begin{aligned}p(v^1, v^2, v^R | \mathbf{y}_l) &\propto p(\mathbf{y}_l^1 | v^1)p(\mathbf{y}_l^2 | v^2)p(\mathbf{y}_l^R | v^R) \\ &\cdot \mathbb{1} [v^R = f(v^1, v^2)] \frac{P^a(v^1)P^a(v^2)}{p(\mathbf{y}_l)}. \quad (10)\end{aligned}$$

Likewise, one can compute the *a posteriori* p.m.f. $P(v^m | \mathbf{y}_l)$ of the non-binary symbol associated to a given source by marginalizing the previous equation. Thus,

$$\begin{aligned}P(v^m | \mathbf{y}_l) &= p(\mathbf{y}_l^m | v^m)P^a(v^m) \\ &\cdot \sum_{v^{\bar{m}}, v^R} \mathbb{1} [v^R = f(v^1, v^2)] \frac{p(\mathbf{y}_l^{\bar{m}} | v^{\bar{m}})P^a(v^{\bar{m}})p(\mathbf{y}_l^R | v^R)}{p(\mathbf{y}_l)}. \quad (11)\end{aligned}$$

On the other hand, following a similar reasoning as in (4), we obtain

$$P(x_1^m, \dots, x_q^m | \mathbf{y}_l) = \sum_{v^m} \mathbb{1} [v^m = \psi_q(x_1^m, \dots, x_q^m)] P(v^m | \mathbf{y}_l), \quad (12)$$

from which we can compute the bitwise channel conditional p.d.f. by marginalizing and applying again the Bayes Theorem, i.e.

$$p(\mathbf{y}_l | x_i^m) = \sum_{\sim x_i^m, v^m} P(v^m | \mathbf{y}_l) \mathbb{1} [v^m = \psi_q(x_1^m, \dots, x_q^m)] \frac{p(\mathbf{y}_l)}{P(x_i^m)}, \quad (13)$$

where $\sim x_i^m \triangleq \{x_j^m\}_{\forall j \neq i}$. Finally, combining (11) and (13), we get

$$\begin{aligned} p(\mathbf{y}_l | x_i^m) &= \sum_{\sim x_i^m, v^m} \mathbb{1} [v^k = \psi_q(x_1^m, \dots, x_q^m)] \cdot \\ &\quad \cdot p(\mathbf{y}_l^m | v^m) \prod_{i' \neq i} P^a(x_{i'}^m) P^{\text{MARC}}(v^m), \end{aligned} \quad (14)$$

with

$$P^{\text{MARC}}(v^m) \triangleq \sum_{v^{\overline{m}}, v^R} \mathbb{1} [v^R = f(v^1, v^2)] \cdot p(\mathbf{y}_l^{\overline{m}} | v^{\overline{m}}) P^a(v^{\overline{m}}) p(\mathbf{y}_l^R | v^R). \quad (15)$$

The factorized form of $p(\mathbf{y}_l | x_i^m)$ given in expression (14) is graphically represented by the factor graph depicted in Figure B.3, where for the sake of clarity the sub-index l is dropped. The application of the SPA over the factor graph of Figure B.3 allows for a efficient computation of the likelihoods $\gamma(x_t^m)$. To be concise, the SPA iterates between the sub-factor graphs corresponding to the relay network code and the convolutional codes. It should be remarked that if the probability $p(\mathbf{y}_l^R | v^R)$ (message) is not dependent on the data from source m (e.g., when the NC coefficients are set to zero or the relay-destination channel is in deep fade), then $P^{\text{MARC}}(v^m)$ will be uniformly distributed and consequently the exchange of messages between both convolutional decoders ($P^{\text{MARC}}(v^m)$) will not improve the performance of the decoder (see Fig. B.3).

Although the factor graph shown in Fig. B.2 has been constructed for convolutional codes, it could be easily modified if iteratively decodable codes (e.g. LDPC, Turbo) are used, by facing their outer codes with the

Relay Network code subgraph. However, care should now be taken when programming the decoder activation scheduling.

In [3] scheduling algorithms for both parallel and serially concatenated codes with several compounding graphs are proposed. We further refer to [3] for algorithms that find the fastest convergent code activation schedule. Finally, a particular case where non-binary LDPC codes were used as channel codes was published by current authors in [15].

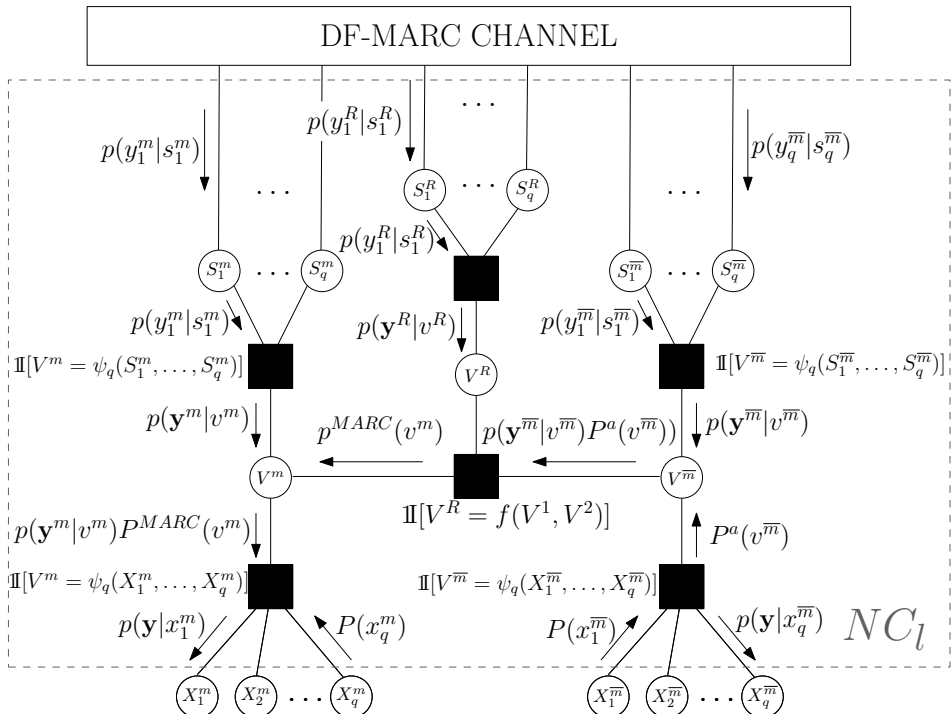


Figure B.3: Factor Graph representing the factorization of $p(\mathbf{y}_l|x_i^m)$, i.e. the network check node $\mathcal{N}\mathcal{C}_l$.

In the next section, the EXIT charts of the proposed JNCC are used to obtain a pair of NC-coefficients that optimizes the performance of the system. To simplify the exposition, the optimization procedure next presented assumes that both sources are detected with no errors at the relay, in line with the assumptions made in the related literature [5, 14, 15, 21].

IV. ANALYSIS OF THE RELAY NETWORK CODE BASED ON EXIT CHARTS

An additional insight can be gained through an analysis of the NC-coefficient based on the interchange of mutual informations between the output of the channel decoders and the output of the relay network decoder. Due to the iterative nature of the decoding algorithm, EXtrinsic Information Transfer (EXIT, see [11]) charts are a good method for visually exploring this iterative exchange of information. Given a code, the EXIT function associated is defined by the relation between the *a priori* mutual information at the input of the decoder (commonly denoted as I_a) and the corresponding extrinsic mutual information I_e at its output, i.e. $I_e = T(I_a)$. For further information on EXIT charts we refer [11] and references therein to the reader.

We will denote the transfer function of the network code for a given q and \mathbf{h} as $I_e^{\text{NC}} = T_{\mathbf{h}}^q(I_a^{\text{NC}})$. Notice that, $T_{\mathbf{h}}^q(0)$ and $T_{\mathbf{h}}^q(1)$ represent the extrinsic information at the output of the network decoder with no *a priori* and full *a priori* information about the information bits, respectively. Moreover, since the mutual information at the input of the channel decoders is equal to the mutual information at the output of the network decoder, i.e. $I_a^{\text{CC}} = I_e^{\text{NC}}$, the extrinsic mutual information at the output of the convolutional decoders is given by $I_e^{\text{CC}} = T^{\text{CC}}(I_e^{\text{NC}})$. Thus, for a successful decoding procedure, there must be an open gap between both EXIT curves so that the iterative decoding can proceed from $I_e^{\text{CC}} = 0$ to $I_e^{\text{CC}} = 1$ ². When both transfer functions intersect, the iterative process will stop at a given extrinsic mutual information of the source bits $I_e^{\text{CC}} < 1$. A crossing yielding $I_e^{\text{CC}} \leq 0.5$ will be referred to as early-crossing and as late-crossing, otherwise (i.e., $0.5 < I_e^{\text{CC}} < 1$). Since the transfer functions are monotonically increasing, the higher the value $T_{\mathbf{h}}^q(0)$ is, the later the early-crossing will occur. On the other hand, and if no early-crossing occurs, the higher the value of $T_{\mathbf{h}}^q(1)$ is, the closer I_e^{CC} will be to one.

Next, we justify the reason why the NC coefficients have a greater impact on the value of $T_{\mathbf{h}}^q(1)$ than on $T_{\mathbf{h}}^q(0)$. When no *a priori* information is available at the network decoder, all its information comes from the sources-and relay-destination links. On the other hand, when full *a priori* information is available, only the information provided by the relay-destination

²Although for a perfectly successful decoding the final I_e^{CC} should be equal to one, we also consider the values of $I_e^{\text{CC}} \approx 1$ that yield to negligible error floors.

link is relevant, since the information regarding the coded messages from the sources is fully supplied by the channel decoders. In addition, from the Area Theorem of EXIT charts [11], which states that the area below the transfer function depends only on the rate of the encoder, the area below the transfer functions will be constant $\forall q, \mathbf{h}$. Consequently, the transfer functions of those NC-coefficients with a large value of $T_{\mathbf{h}}^q(1)$ are expected to be flat shaped at low values of I_e^{NC} , and steep shaped at values near one.

To corroborate the above, let us first assume AWGN channels (i.e. $\boldsymbol{\alpha} = (1, 1, 1)$). Figure B.4 plots the EXIT chart of a network check node for different NC-coefficients and values of q , along with the transfer function of a 2^2 -state (CC2) and a 2^6 -state (CC6) convolutional code with same transmission rate $1/3$. Note that by the symmetry of the network, it is sufficient to consider only those NC-coefficients $\mathbf{h} = (\rho_i, \rho_j)$ with indexes verifying $1 \leq i \leq j \leq 2^q - 1$. For the sake of clarity, we will denote $\mathbf{h} = (\rho_i, \rho_j)$ by (i, j) . From this figure, it can be observed that the transfer function corresponding to $\mathbf{h} = (1, 1)$ (i.e. raw XOR-network coding) maximizes $T_{\mathbf{h}}^q(0)$ and minimizes $T_{\mathbf{h}}^q(1)$ for all q . Also observe that for high values of q and for some NC coefficients, the initial flat shape of the plotted transfer functions curves induces an early-crossing with the curve of CC2, and consequently the system requires more energy per symbol to open the gap between these curves. In this case, one may opt to select NC-coefficients that increase the value of $T_{\mathbf{h}}^q(0)$, so the early-crossing could be avoided. As a drawback, a higher error floor due to their associated lower $T_{\mathbf{h}}^q(1)$ is expected. As highlighted in the figures, such alternate coefficients are given by $\mathbf{h} = (2, 2)$ ($q = 2$), $\mathbf{h} = (6, 6)$ ($q = 3$), $\mathbf{h} = (7, 7)$ ($q = 4$) and $\mathbf{h} = (14, 15)$ ($q = 5$).

Therefore, for AWGN channels we can conclude that by a proper choice of the coefficients an iterative gain will be achieved when using a linear combination of the estimated symbols, as it was also stated in [28]. This contrasts with the more commonly used scheme based on a channel encoder at the relay. Moreover, from the variety of transfer functions generated by the family of NC coefficients, it is also concluded that a tailored non-binary linear combination at the relay can outperform 1) the XOR coding method (i.e. $\mathbf{h} = (1, 1)$) first proposed in [6, 28, 29]; and 2) a random choice of such parameters as was proposed in [10, 27].

Before considering the more general case of fading channels, observe that the proposed soft-output network decoder can be seen as N/q parallel systematic codes $\mathcal{W}(\mathbf{h})$; each of them having the $3q$ -length codewords $\mathbf{W} =$

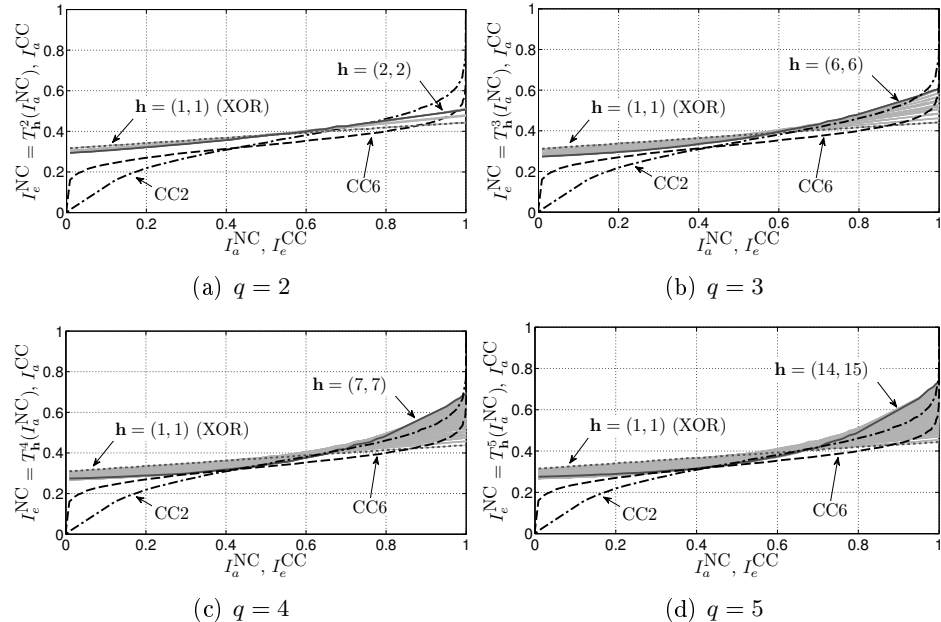


Figure B.4: EXIT charts for different network decoders and convolutional codes.

$(\{X_i^1\}_{i=1}^q, \{X_i^2\}_{i=1}^q, \{X_i^R\}_{i=1}^q)$ where its systematic bits $(\{X_i^1\}_{i=1}^q, \{X_i^2\}_{i=1}^q)$ correspond to the interleaved bits of the sub-sequences from sources \mathcal{S}^1 and \mathcal{S}^2 , respectively, and its parity bits, $\{X_i^R\}_{i=1}^q$, correspond to the bits generated by the relay. Hence, each pair of NC-coefficients generates a particular code $\mathcal{W}(\mathbf{h})$ with a different distance spectrum and therefore, different transfer functions. Moreover, the relation among these functions depends solely on their distance spectrum and it is independent of the quality of the channels.

We now look at Rayleigh fading links. In this case, different realization of the coefficients of the Rayleigh fading $\boldsymbol{\alpha}$ will produce differently shaped transfer functions, making $T_{\mathbf{h}}^q$ a random mapping from $\mathbb{R} \rightarrow \mathbb{R}$. If the channel between the relay and the destination is in a deep fade, no gain is obtained by iterating (since $P^{\text{MARC}}(\cdot)$ is uniform), and a late-crossing might occur (given that $T_{\mathbf{h}}^q(0)$ is high enough). On the other hand, if a deep fade occurs in both source-destination channels, an early-crossing

could be produced due to the low value of $T_{\mathbf{h}}^q(0)$. Both situations are shown in Figure B.5, which plots the EXIT curves of 100 channel realizations for $q = 2$ and $\mathbf{h} = (2, 3)$. In this Figure, the curves corresponding to two fading realizations producing an early- and late-crossings, have been highlighted for clarity. Since a decoding error is produced when a crossing occurs, the probability of a failed decoding event could be approximated by $\mathcal{P}\{\text{failed decoding}\} \approx \mathcal{P}\{\text{early-crossing}\} + \mathcal{P}\{\text{late-crossing}\}$.

It should be mentioned that the $\mathcal{P}\{\text{early-crossing}\}$ strongly depends on the quality of the channels whereas $\mathcal{P}\{\text{late-crossing}\}$ is not so dependant. The reason being that increasing the received signal-to-noise ratio will reduce the probability of an early-crossing, since the decoder would be fed during the first iteration with more reliable channel information. However, the late-crossing probability will not be significantly reduced since the influence of the information provided by both source-destination channels decreases as the channel decoders begin to provide *a priori* information regarding the source encoded bits. Therefore, as the signal-to-noise ratio increases, the late-crossing probability starts to dominate the failure probability, and hence, beyond a certain value of the signal-to-noise ratio, the early-crossing probability becomes negligible, regardless of the channel code used.

In addition, the failure probability will also depend on the type of convolutional code used and as shown in Fig. B.5, the more complex the code is, the larger the value of $T_{\mathbf{h}}^q(0)$ should be in order to avoid early-crossings. On the contrary, the less complex the code is, the higher the value of $T_{\mathbf{h}}^q(1)$ should be in order to avoid late-crossings. Therefore, the value of $T_{\mathbf{h}}^q(0)$ and $T_{\mathbf{h}}^q(1)$ will strongly determine the failure probability of the proposed decoder. To analyze the crossing probabilities one has to statistically characterize the behavior of the random variables $T_{\mathbf{h}}^q(0)$ and $T_{\mathbf{h}}^q(1)$ for different values of q and NC-coefficients. To that end, we next show that the distribution of these random variables depend on the path-loss gain suffered by the signal coming from the relay (i.e. the position of the relay).

For $T_{\mathbf{h}}^q(1)$ (i.e., the full *a priori* case) the extrinsic information generated by the network check nodes (i.e., $P^{\text{MARC}}(\cdot)$) depends on the quality of the relay-destination channel through the check node associated to the linear combination. Therefore, in the limit when the SNR of the relay-destination channel tends to infinity, the probability of $\mathcal{P}(T_{\mathbf{h}}^q(1) = 1)$ tends to one. As a consequence, the slope of transfer functions will increase since $T_{\mathbf{h}}^q(0)$

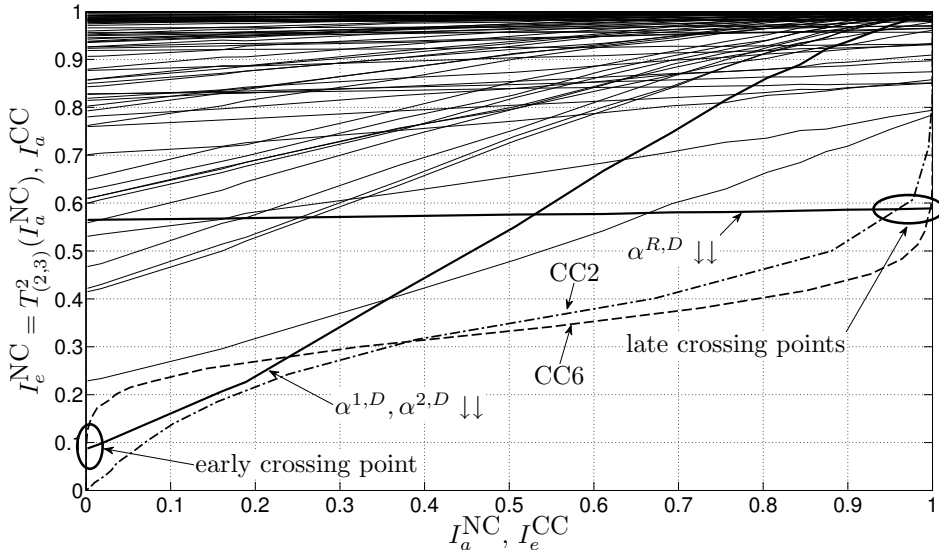


Figure B.5: EXIT curves of 100 system usages for $q = 2$ and $\mathbf{h} = (2, 3)$.

remains fairly constant; and consequently, some of the early-crossings will be avoided.

To make this analysis clearer, Figure B.6 shows the Cumulative Distribution Function (CDF) of $T_{\mathbf{h}}^q(0)$ and $T_{\mathbf{h}}^q(1)$ for $q = 3$ and all combinations of \mathbf{h} for the cases where: the relay and the sources are at the same distance to the destination (0 dB gain), and the relay is placed at half distance between the sources and destination (10 dB gain). As mentioned for the AWGN case, it can be observed that the choice of a different value of \mathbf{h} has a stronger impact on $T_{\mathbf{h}}^q(1)$ than on $(T_{\mathbf{h}}^q(0))$. Also, increasing the quality of the relay-destination channel leads to an increase in the values of the realizations of $T_{\mathbf{h}}^q(1)$, which in turn diminishes $\mathcal{P}\{T_{\mathbf{h}}^q(1) < x\}$ for any $x \in [0, 1]$. Moreover, $\mathcal{P}\{T_{\mathbf{h}}^q(0) < x\}$ does not significantly change as the gain in the relay-destination link is varied.

Observe from Figure B.6 that given a q , there is a particular value \mathbf{h}_1^* (shown as solid lines) that minimizes³ $\mathcal{P}\{T_{\mathbf{h}}^q(1) < x\}$, $\forall x \in [0, 1]$ regardless

³The minimization is performed by an exhaustive search over all possible $\mathbf{h} \in GF(2^q)$ (Figure B.6).

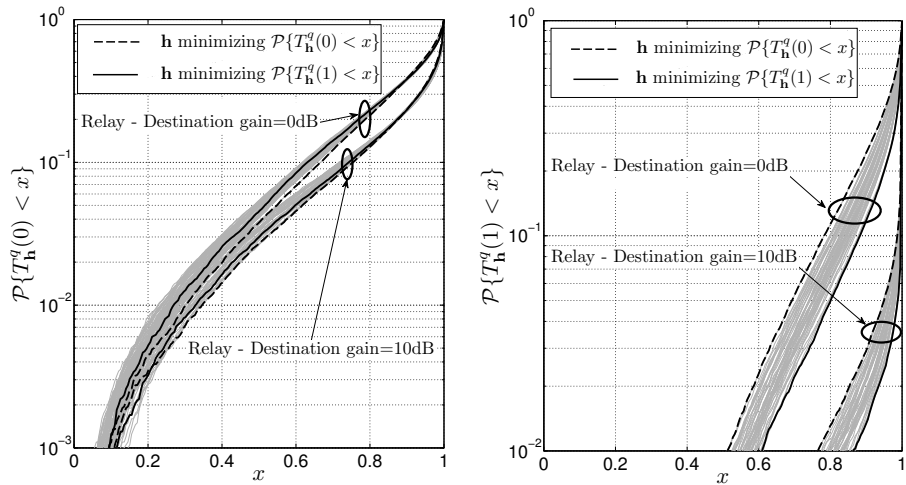


Figure B.6: CDF of $T_h^q(0)$ and $T_h^q(1)$ for $q = 3$ and all possible values of \mathbf{h} .

the quality of the channels. Similarly, there is a value \mathbf{h}_0^* (shown as dashed lines) that minimizes $\mathcal{P}\{T_h^q(0) < x\}, \forall x \in [0, 1]$.

At this point, by denoting the smaller SNR value that makes the term $\mathcal{P}\{\text{late-crossing}\}$ to dominate the system performance as SNR_{th} , the best choice of NC-coefficients is \mathbf{h}_1^* when $SNR \geq SNR_{th}$, and \mathbf{h}_0^* , otherwise. Based on this, the steps for selecting the NC-coefficients can be summarized as follows: 1) find the values of \mathbf{h}_0^* and \mathbf{h}_1^* ; 2) estimate by Monte Carlo simulations the value of SNR_{th} ; and 3) choose \mathbf{h}_0^* or \mathbf{h}_1^* depending on the operating region of the system.

In conclusion, the value of a good \mathbf{h} will depend on the channel codes, the relay position and channel conditions. This corroborates the previous statement that a random choice of the NC-coefficient might lead to some performance degradation.

Finally, note that if the channel codes are composed of several sub-graphs (e.g. LDPC or Turbo codes), several transfer functions (one for each compounding subgraph) are obtained and a direct representation of these functions will result in an N -dimensional EXIT chart. By converting the N -dimensional EXIT chart into a two-dimensional EXIT chart, for ex-

ample by using the EXIT Chart Projection Algorithm proposed in [3], the above analysis could still be applied.

V. SIMULATION RESULTS

In order to asses the performance of the proposed scheme and to corroborate the conclusions from the previous analysis, several sets of simulations have been performed. We have considered a symmetric scenario where both source nodes are placed at the same distance from the destination nodes, i.e. $d_{1,D} = d_{2,D}$. Regarding the relay position, three different scenarios are defined:

- A) The relay and the sources are deployed at identical distance from the destination, (i.e., $SNR_{R,D} = SNR_{1,D} + 0\text{dB}$). This setup was used in [13, 14].
- B) The distance between the relay and the destination is three quarters of the source-destination distance ($SNR_{R,D} = SNR_{1,D} + 4.4\text{dB}$) as used in [5, 15].
- C) The relay is set at approximately half the distance between the sources and the destination ($SNR_{R,D} = SNR_{1,D} + 10\text{dB}$). This setup was also considered in [13].

The channel codes used at both source nodes are identical, non systematic convolutional codes of rate $1/3$. Two types of convolutional codes are considered: a 2^2 -state $[5, 7, 7]_8$ code⁴ (heretofore denoted as CC2), and a 2^6 -state $[554, 624, 764]_8$ code (correspondingly, CC6). A zero-bit termination tail is appended at each source sequence. We use packets of $K = 32$ bits (i.e. we use $M = 32 \cdot 3/2 = 48$), and the interleavers have been randomly generated and are independent of each other. We have considered 4-QAM⁵, which leads to an spectral efficiency of $\rho = 4/9$ [bits per complex dimension], and the number of iteration for the SPA has been set to $\mathcal{I} = 15$. Finally, from the region of achievable decode-and-forward rates of the TD-MARC given in [12], (derived from the capacity bounds of the C-MARC

⁴The subindex 8 in the definition of the code stands for *octal*.

⁵Further improvement can be expected with higher order modulation schemes and by applying the so-called Bit-Interleaved Coded Modulation (BICM [4]) technique. However, this research line lies beyond the scope of this manuscript.

in [25]), a set of upper bounds on the outage probabilities has been obtained by specifying the actual packet lengths of the source information bits and the transmitted sequences ($K = 32$, $M = 48$). These outage probability bounds are used as an information-theoretic benchmark for the Packet Error Rate (PER), where a packet is in error if one or both sources packets are erroneously decoded.

Based on the analysis carried out in Section IV, the NC-coefficients for $q = 3$ that minimizes $\mathcal{P}\{T_{\mathbf{h}}^q(1) < x\}$ and $\mathcal{P}\{T_{\mathbf{h}}^q(0) < x\}$ are given by $\mathbf{h} = (6, 6)$ and $\mathbf{h} = (1, 1)$, respectively. To corroborate the optimality of these values a first set of simulations have been done for scenarios A and C (Fig. B.7-B.8). Since we are mainly interested in the selection of the NC coefficients, in these simulations error-free links between the sources and the relay are assumed. Nevertheless, the noisy source-relay link case is also discussed later in this section.

By using the channel code CC2, Figure B.7 plots the end-to-end PER versus $E_b/N_0 = SNR - 10 \log_{10} \rho$ (in dB) for all possible values of \mathbf{h} and for scenarios A (lefthand plot) and C (righthand plot). It can be observed that in scenario A, and for all values of SNR, the coefficients $\mathbf{h} = (6, 6)$ (i.e. \mathbf{h}_1^*) are the optimal choice. For scenario C, \mathbf{h}_1^* is still optimal in the range $SNR > SNR_{th}$ (recall that SNR_{th} denotes the SNR at the crossing of the curves for \mathbf{h}_1^* and \mathbf{h}_0^*); however, for $SNR < SNR_{th}$ the optimal choice is $\mathbf{h} = (1, 1)$ (i.e. \mathbf{h}_0^*). This corroborates what was stated in Section IV, that the use of low-complexity codes reduces the influence of $\mathcal{P}\{\text{early-crossing}\}$, leading to low values of SNR_{th} (in scenario A $SNR_{th} < 0$ and in scenario C $SNR_{th} \approx 3$). Moreover, it can be seen that as the quality of the relay-destination link increases (going from scenario A to C), the value of SNR_{th} increases; as also stated in Section IV.

Figure B.8 shows a similar analysis on the PER when using the CC6 code, instead. It can be observed that in both scenarios SNR_{th} arise at high values of SNR, since \mathbf{h}_0^* outperforms \mathbf{h}_1^* for the SNR ranges of interest (in scenario A and C, the crossing occurs at $SNR > 20$ dB and $SNR > 16$ dB, respectively), corroborating the fact that we are using high-complexity convolutional codes (see Section IV).

Furthermore, these results show that as the relay is placed toward the destination, a tailored selection of the NC-coefficients improves the performance of the system; e.g. in scenario C, gains of 1.3dB and 1.5dB, with respect to the worst selection, can be achieved when using CC2 and CC6,

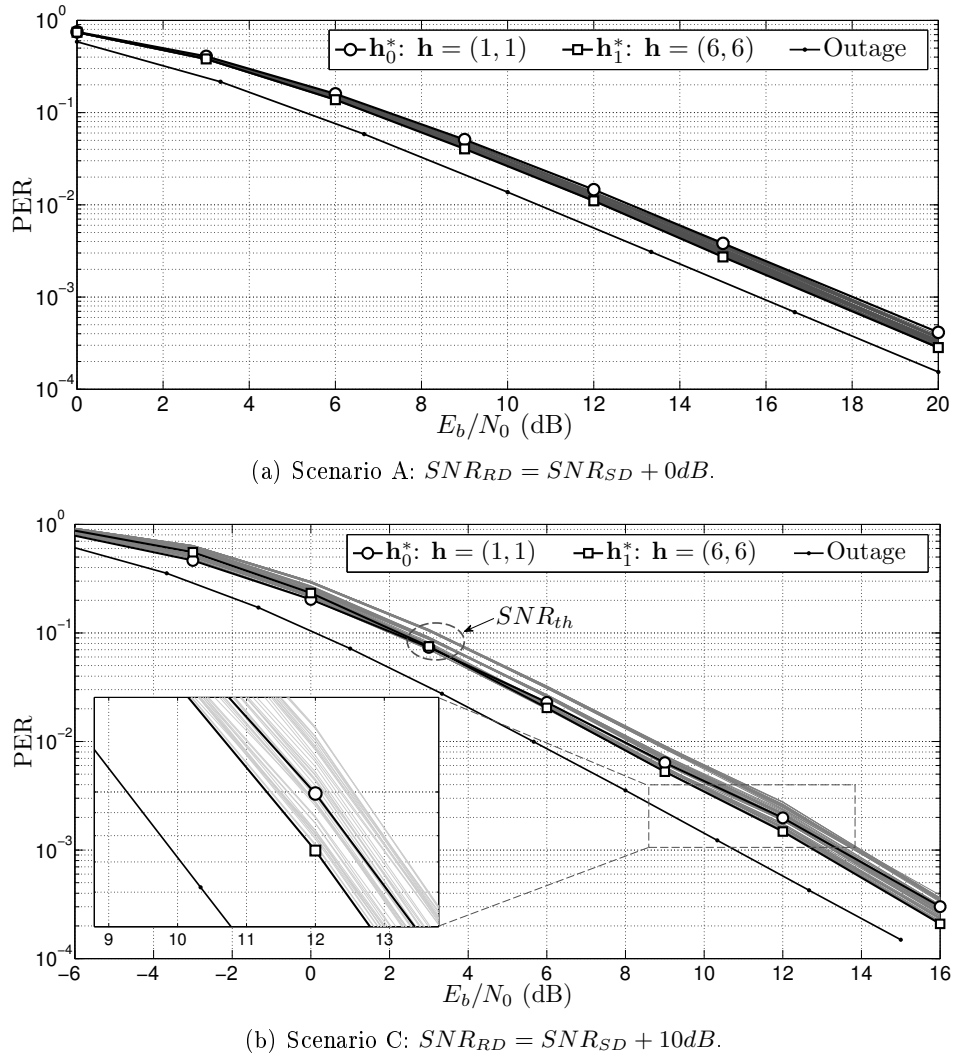


Figure B.7: Outage probabilities and PER performance of the proposed approach when the CC2 convolutional code is used.

respectively . One can also conclude from the figures that, since the performances for the different coefficients are roughly uniformly distributed

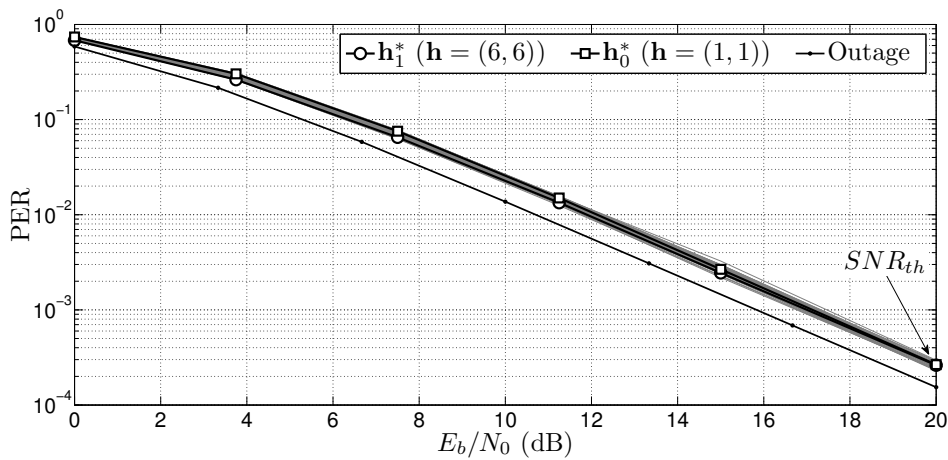
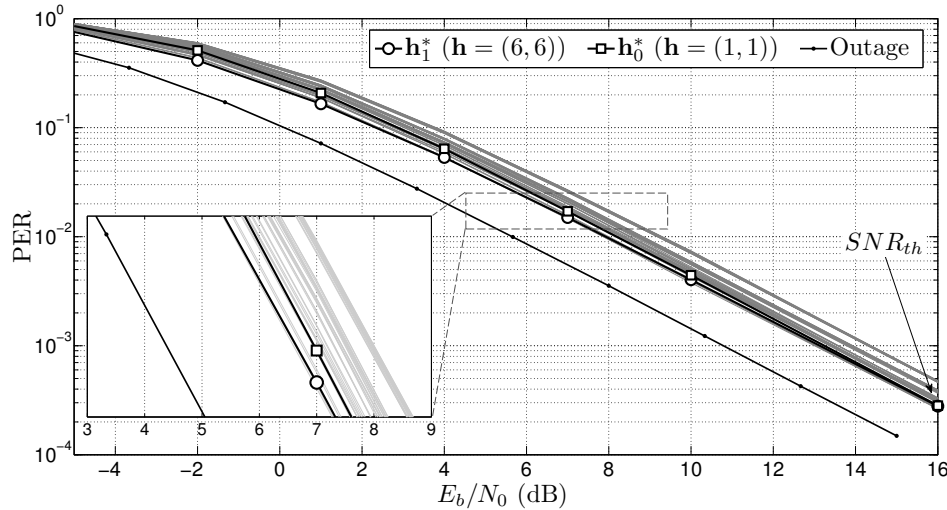
(a) Scenario A: $SNR_{RD} = SNR_{SD} + 0\text{dB}$.(b) Scenario C: $SNR_{RD} = SNR_{SD} + 10\text{dB}$.

Figure B.8: Outage probabilities and PER performance of the proposed approach when the CC6 convolutional code is used in scenario A (left) and C (right).

between the best and worst case scenarios, a gain of 0.75dB (scenario C and CC6) is obtained with respect to the random choice of coefficients.

The next set of simulation compares the gap between the performance of the proposed system with respect to the outage probability. This gap is also computed for different schemes found in the literature, all having a spectral efficiency less than 2 (bits per complex dimension). It should be mentioned that all these schemes [5, 13–15] were analyzed assuming error free source-relay channels. Therefore, the outage probabilities (upper bounds) for scenarios A,B,C has been computed with the later assumption and for unconstrained channel inputs (Gaussian).

These gaps are given in Table B.1, where the first two columns refer to our scheme. Observe that the proposed scheme outperforms all the reference schemes. Moreover, the proposed system achieves these results by using short-length codewords: 144 complex dimensions per use of TD-DF-MARC in contrast to the 2176 utilized in [5], the 6000 utilized in [13, 14] or the 27000 utilized in [15].

Table B.1: Gaps to the outage probabilities in dB.

Scenario	q=3, CC2	q=1, CC6	[15]	[14]	[13]	[5]
A	1.39	1.44	-	3.4	2.7	-
B	1.64	1.64	1.7	-	-	4.8
C	2.04	2.36	-	-	5.2	-

Finally, we consider the case where non-ideal source-relay channels are used. An unchanged implementation of the proposed scheme will lead to error propagation at the decoder and as a result a degradation on the performance as shown in Figure B.9. Moreover, at high SNRs, the closer the relay to the destination is, the stronger the impact of the error propagation will be. However, since the error propagation also degrades the outage probability as shown in Fig. B.9, the gap between the performance of the unchanged scheme and the new outage probability curve [12] is still small, and is in fact negligible at high SNRs. We conclude that our scheme is still robust when non ideal channel error propagation occurs.

An alternative scheme to cope with the error propagation at the destination is as follows. This scheme assumes that the destination node knows if an error has occurred at the relay (Relay State Information, RSI), e.g, by using an additional low rate error free relay-destination channel. To this end, a cyclic redundancy check (CRC) is added at the end of the source

transmitted sequences, so that the relay can detect if any residual errors have occurred in $\widehat{\mathbf{X}}^1$ and $\widehat{\mathbf{X}}^2$. If errors are detected in $\widehat{\mathbf{X}}^m$, the relay sets h^m to 0 (i.e. the sequence transmitted by the relay only conveys information from \mathcal{S}^{3-i}) and the relay communicates that an error has been produced to the destination. The decoder sets at the network check node, h^m to 0, avoiding in this way error propagation through channel decoders. However, some performance degradation is still expected since $P^{\text{MARC}}(v^m)$ (see Fig. B.3) is now uniformly distributed and therefore no iteration gain will be obtained. The performance of the RSI scheme is shown in Figure B.9 together with the corresponding outage probability. One can observe that the performance loss with respect to the error-free case is negligible.

To conclude, Figure B.9 also shows the performance of: 1) the traditional separated network-channel coding scheme (SNCC, [12]); and 2) the point-to-point scenario using the same spectral efficiency as in the above simulations. In the former, as explained in [12], the channel decoders at the destination converts each incoming AWGN channel with fading into a Bit-Erasure Channel which outputs either the correctly decoded symbol or a erasure if the channel was in a deep fade. Thus, the source information bits can be correctly decoded (using the XOR function with the correct bits) if at least two out of the three channels are not in a deep fade. For the sake of clarity we have only consider the scenario A for the simulations of the SNCC scheme.

VI. CONCLUSIONS

This paper proposes a novel joint network-channel coding scheme for the Decode-and-Forward Time-Division Multiple Access Relay Channel. Specifically, we have designed a Joint-Network-Channel code which does not perform channel coding on the already network-coded bits, reducing the complexity at the relay node without compromising performance. A method for selecting the best pair of coefficients of the linear combination is derived based on an EXIT charts analysis. Moreover, the proposed code allows the sources to use completely different channel codes, at the sole expense of an increased complexity on the EXIT chart analysis. The decoding at the destination is performed by applying the SPA over the derived factor graph of the JNCC code. Monte Carlo simulations show that the proposed scheme outperforms, in terms of its gap to the corresponding outage probability upper bounds, the previously published schemes for the same network

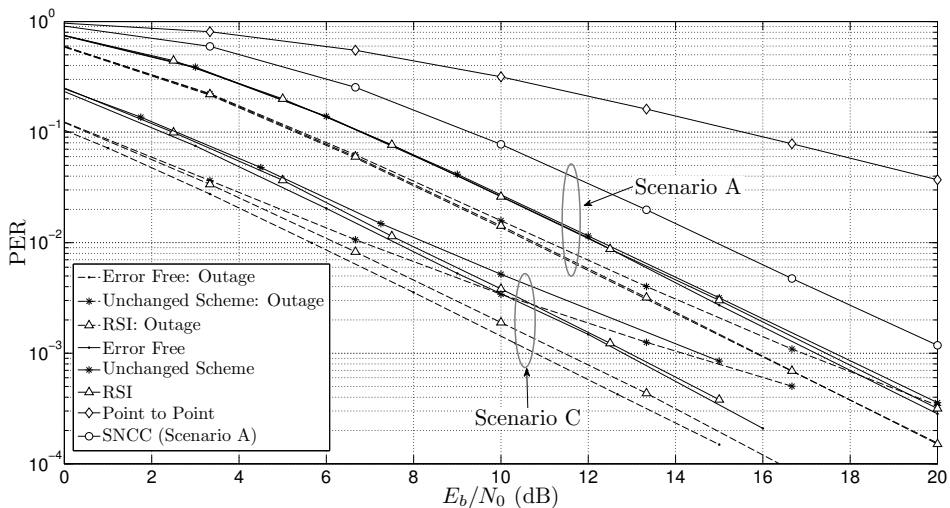


Figure B.9: PER performance of the proposed schemes for the erroneous source-relay channel setup when the CC2 convolutional code and $\mathbf{h} = (6, 6)$ is used. Also plotted the point-to-point and the SNCC schemes.

setup. Besides, this gain is achieved by using short-length codewords, which makes our proposal particularly attractive for low-latency applications.

REFERENCES

- [1] R. Ahlswede, N. Cai, S.-Y. R. Li, and R. W. Yeung. Network Information Flow. *IEEE Transactions on Information Theory*, 46(4):1204–1216, July 2000.
- [2] L. Bahl, J. Cocke, F. Jelinek, and J. Raviv. Optimal Decoding of Linear Codes for Minimizing Symbol Error Rate (Corresp.). *IEEE Transactions on Information Theory*, 20(2):284–287, March 1974.
- [3] F. Brännström, L. K. Rasmussen, and A. J. Grant. Convergence Analysis and Optimal Scheduling for Multiple Concatenated Codes. *IEEE Transactions on Information Theory*, 51(9):3354–3364, September 2005.

- [4] G. Caire, G. Taricco, and E. Biglieri. Bit-interleaved Coded Modulation. *IEEE Transaction on Information Theory*, 44:927–946, May 1998.
- [5] L. Chebli, C. Hausl, G. Zeitler, and R. Koetter. Cooperative Uplink of Two Mobile Stations with Network Coding Based on the WiMax LDPC Code. In *2009 IEEE Global Communication Conference, GLOBECOM'09*, December 2009.
- [6] Y. Chen, S. Kishore, and J. Li. Wireless Diversity through Network Coding. In *2006 IEEE Wireless Communications and Networking Conference, WCNC'06*, April 2006.
- [7] T. Cover and A. E. Gamal. Capacity Theorems for the Relay Channel. *IEEE Transactions on Information Theory*, 25(5):572–584, September 1979.
- [8] M. Effros, M. Medard, T. Ho, S. Ray, D. Karger, and R. Koetter. Linear Network Codes: A Unified Framework for Source, Channel and Network Coding. In *DIMACS Series in Discrete Mathematics and Theoretical Computer Science*, 2003.
- [9] C. Gong, G. Yue, and X. Wang. Joint Channel and Network Code Design for Half-Duplex Multiple-Access Relay System. In *2010 IEEE International Conference on Communications, ICC'10*, May 2010.
- [10] Z. Guo, J. Huang, B. Wang, J.-H Cui, S. Zhou, and P. Willet. A Practical Joint Network-Channel Coding Scheme for Reliable Communication in Wireless Networks. In *The Tenth ACM International Symposium on Mobile Ad Hoc Networking and Computing, MOBIHOC'09*, May 2009.
- [11] J. Hagenauer. The EXIT Chart: Introduction to Extrinsic Information Transfer in Iterative Processing. In *2004 European Signal Processing Conference, EUSIPCO'04*, September 2004.
- [12] C. Hausl. *Joint Network-Channel Coding for Wireless Relay Channels*. PhD thesis, TU München, 2008.
- [13] C. Hausl and P. Dupraz. Joint Network-Channel Coding for the Multiple-Access Relay Channel. In *2006 3rd Annual IEEE Communications Society on Sensor and Ad Hoc Communications and Networks, SECON'06*, September 2006.

- [14] C. Hausl, F. Schreckenbah, I. Oikonomidis, and G. Bauch. Iterative network and channel decoding on a tanner graph. In *Forty-Third Annual Allerton Conference on Communication, Control, and Computing, Allerton'05*, 2005.
- [15] M. Hernaez, P. M. Crespo, and J. Del Ser. Joint Non-Binary LDPC-BICM and Network Coding with Iterative Decoding for the Multiple Access Relay Channel. In *2011 IEEE 73rd Vehicular Technology Conference: VTC'11-Spring*, May 2011.
- [16] K. Ishii, K. Ishibashi, and H. Ochiai. Multiple-access Relay System based on Nested Distributed Turbo Code. In *2011 IEEE Radio and Wireless Symposium, RWS11*, January 2011.
- [17] G. Kramer, M. Gastpar, and P. Gupta. Cooperative Strategies and Capacity Theorems for Relay Networks. *IEEE Transactions on Information Theory*, 51(9):3037–3063, September 2005.
- [18] G. Kramer and A. J. Van Wijngaarden. On the White Gaussian Multiple-Access Relay Channel. In *2000 IEEE International Symposium on Information Theory, ISIT'00*, June 2000.
- [19] F.R. Kschischang, B.J. Frey, and H.-A. Loeliger. Factor graphs and the sum-product algorithm. *IEEE Transactions on Information Theory*, 47(2):498 –519, feb 2001.
- [20] S.-Y. R. Li, R. W. Yeung, and N. Cai. Linear Network Coding. *IEEE Transactions on Information Theory*, 49(2):371–381, February 2003.
- [21] H. T. Nguyen, H. H. Nguyen, and T. Le-Ngoc. A Joint Network-Channel Coding Scheme for Relay-Based Communications. In *2007 Canadian Conference on Electrical and Computer Engineering, CCECE07*, April 2007.
- [22] N. Ratnakar and G. Kramer. The Multicast Capacity of Deterministic Relay Networks with No Interference. *IEEE Transactions on Information Theory*, 52(6):2425–2432, June 2006.
- [23] L. Sankar, Y. Liang, N. Mandayam, and V. H. Poor. Fading Multiple Access Relay Channels: Achievable Rates and Opportunistic Scheduling. *IEEE Transactions on Information Theory*, 57(4):1911–1931, April 2011.

- [24] L. Sankar, Y. Liang, V. H. Poor, and N. Mandayam. Opportunistic Communications in an Orthogonal Multiaccess Relay Channel. In *2007 IEEE International Symposium on Information Theory, ISIT'07*, June 2007.
- [25] L. Sankaranarayanan, G. Kramer, and N. B. Mandayam. Hierarchical Sensor Networks: Capacity Bounds and Cooperative Strategies using the Multiple-Access Relay Channel Model. In *2004 1st Annual IEEE Communications Society on Sensor and Ad Hoc Communications and Networks, SECON'04*, October 2004.
- [26] S. Ten Brink. Convergence of Iterative Decoding. *IEEE Electronic Letters*, 35(10):806–808, May 1999.
- [27] M. Xiao and M. Skoglund. Design of Network Codes for Multiple-User Multiple-Relay Wireless Networks. In *2009 IEEE International Symposium on Information Theory, ISIT'09*, June-July 2009.
- [28] S. Yang and R. Koetter. Network Coding over a Noisy Relay: a Belief Propagation Approach. In *2007 IEEE International Symposium on Information Theory, ISIT'07*, June 2007.
- [29] R. Yu and T. Wu. Joint Network Coding and Channel Coding for Co-operative Relay Communication System. In *2010 International Conference on Wireless Communications and Signal Processing, WCSP10*, October 2010.
- [30] G. Zeitler, R. Koetter, G. Bauch, and J. Widmer. On quantizer Design for Soft Values in the Multiple-Access Relay Channel. In *2009 IEEE International Conference on Communications, ICC'09*, June 2009.

APPENDIX C

Paper III

Title: A Novel Scheme for Message-Forwarding in Multi-Hop Ad-Hoc Wireless Networks

Authors: Mikel Hernaez and Pedro M. Crespo

Affiliation: Centro De Estudios e Investigaciones Técnicas de Gipuzkoa (CEIT) and TECNUN (University of Navarra), 20008 Donostia-San Sebastián, Spain

Conference: *IEEE 73th Vehicular Technology Conference, IEEE VTC2011-Spring*, Budapest, Hungary, May 2009. DOI: 10.1109/VETECS.2011.5956446.

A NOVEL SCHEME FOR MESSAGE-FORWARDING IN MULTI-HOP AD-HOC WIRELESS NETWORKS

Mikel Hernaez, *Student member, IEEE*, and Pedro M. Crespo, *Senior member, IEEE*

Centro De Estudios e Investigaciones Técnicas de Gipuzkoa (CEIT) and
TECNUN (University of Navarra), 20008 Donostia-San Sebastián, Spain
E-mails: {mhernaez, pcrespo}@ceit.es

Abstract — In this paper, we propose a novel *decode-combine-forward* scheme for the multi-hop transmission in ad-hoc wireless networks, where the information generated by two independent sources has to be sent to a common destination based on multiple-relay cooperation. The proposed scheme blends together LDPC channel coding with linear combination of blocks of data over a finite field. The performance of the proposed system is compared with two reference schemes previously proposed on the literature. We provide simulation results which show that our scheme clearly outperforms these reference systems.

I. INTRODUCTION

Ad-hoc networks can improve the system performance significantly by relaying signals in multiple hops between the sources and the destination without any central control. Multihop wireless networks have been the focus of an intense research effort in recent times, [1,8,11]. Moreover, a large number of papers appeared in the literature addressing the routing problem in ad-hoc networks (see, for example, [10, 12] and the references therein). Most of the routing strategies proposed so far are based on the traditional *store-and-forward* mechanism, or, on the *repetition-forward* framework. In this context we consider a multihop wireless network where path attenuation and block Rayleigh fading is assumed. In particular, we have considered the scenario where two source nodes want to transmit their independent information to a far distant receiver node using relay nodes along the way. Progressive transmission left to right (from source to destination) is also assumed.

The binary symbols of each source are channel encoded by LDPC codes [4] and high-order modulated before being transmitted. At each relay node, the following operations are performed: decode, combine (linear combination over a finite field) and forward transmission. The decoding scheme at each node is based on applying the sum-product algorithm to a compound factor graph [9] (where the LDPC decoders and the network coding scheme are blend together) describing the joint probability of the communication scheme at the corresponding node. The performance of the proposed system is compared with previous schemes in the literature addressing similar problems [2], [5].

The rest of the paper is organized as follows. Section II introduces the network model considered. Section III describes the proposed *decode-combine-forward* scheme. In Section IV the performance of the proposed system is evaluated by Monte-Carlo simulations and finally Section V concludes the paper.

II. NETWORK MODEL

We study the problem where two users a and b want to transmit data to a destination located at a certain distance and segmented by n hops, with the aid of $n - 1$ relays. Without loss of generality, we will assume unity

distance between two consecutive nodes. For the sake of simplicity, we have imposed a straight-line geometry, so we can easily compute distances and signal attenuations between nodes. Half-duplex system is also considered, thus a node can either receive or transmit data, but not both at the same time. Since data is transmitted in a progressive way, one node can listen to all the previous nodes, but not to the following ones.

Let $\mathcal{N} = \{a, b, 1, \dots, n-1, n\}$ denote the set of nodes in the network, where n is the destination node. We define $\mathcal{S} = \{a, b\} \subset \mathcal{N}$, $\mathcal{R} = \{1, \dots, n-1\} \subset \mathcal{N}$ and $\mathcal{D} = \{n\} \subset \mathcal{N}$ as the subset formed by the sources, the relays and the destination, respectively. Moreover, for $j = 1, \dots, n$ we define the subsets $\mathcal{T}_j = \{a, b, 1, \dots, j-1\} \subset \mathcal{N}$ as the subset of nodes from which node j receives their transmitted symbols. Figure C.1 depicts the network model. Regarding the Quality of Service (QoS), the proposed scheme works under TDMA; so that the destination performs the decoding algorithm after $|\mathcal{N}| - 1$ time slots. Therefore, the end-to-end delay increases proportionally with the number of relays used for the retransmission of the data blocks generated by the sources.

Users a and b transmit statistically independent binary data that is segmented in blocks \mathbf{U}^a and \mathbf{U}^b of length K .

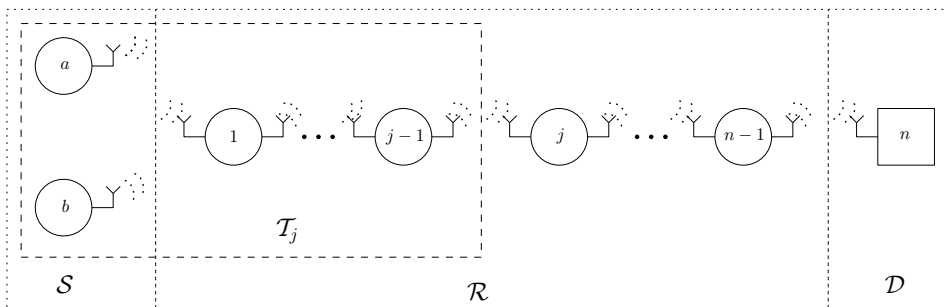


Figure C.1: Network model.

Regarding the links between nodes, we consider independent (orthogonal) quasi-static Rayleigh flat-fading channels where the T -sampled baseband (complex) link input-output ($X-Y$) relation from node i to node j at time k is given by

$$Y_k = |\alpha^{ij}| \sqrt{\beta^{ij}} X_k + N_k^{ij}$$

with $\beta = l^{-\delta}$ modeling a path loss attenuation, l being the number of hops (units) between the transmitter and the receiver node and δ being set to 4. The Rayleigh coefficient α and the additive Gaussian noise N_k are circularly symmetric complex Gaussian random variables of zero mean and variance one and N_0 , respectively. A realization of α is assumed to remain constant for the duration of the transmitted block.

III. PROPOSED DECODE-COMBINE-FORWARD SCHEME

A *decode-combine-forward* scheme is proposed to transmit the source information blocks $\mathbf{U}^a \in \{0, 1\}^K$ and $\mathbf{U}^b \in \{0, 1\}^K$ to the destination. Nevertheless, the *decode-combine-forward* scheme is not fully implemented in all the nodes. The *combine-forward* part is performed by nodes $\mathcal{S} \cup \mathcal{R}$ (i.e. nodes with a transmitting antenna), while the *decode* part is implemented by nodes $\mathcal{R} \cup \mathcal{D}$ (i.e. nodes with a receiving antenna). Notice that only the relay nodes $\mathcal{R} = \{1, 2, \dots, n - 1\}$ fully perform the *decode-combine-forward* scheme. Next, we describe this process.

[*Decode*] Each node $j \in \mathcal{R} \cup \mathcal{D}$ receives the blocks sent by the nodes $i \in \mathcal{T}_j$ (i.e. all the nodes located at its left, see Fig. 1). Based on these observations, the node j estimates the source blocks \mathbf{U}^a and \mathbf{U}^b , denoted by $\widehat{\mathbf{U}}^{aj}$ and $\widehat{\mathbf{U}}^{bj}$, respectively. A detailed decoding explanation is postponed to the next subsection.

[*Combine-Forward*] At each node $j \in \mathcal{S} \cup \mathcal{R}$, the source generated block \mathbf{U}^k (for nodes in \mathcal{S}) or the previously decoded source blocks $\widehat{\mathbf{U}}^{aj}$ and $\widehat{\mathbf{U}}^{bj}$ (for nodes in \mathcal{R}) are LDPC encoded by using the same rate $R = K/N$ LDPC code. The resulting binary encoded blocks, $\tilde{\mathbf{X}}^a$ and $\tilde{\mathbf{X}}^b$, are partitioned into sub-blocks of length s before being mapped into the elements of the finite field \mathbb{F}_{2^s} . We denote by $\mathbf{X}^i \in \mathbb{F}_{2^s}^{N_s}$ ($i = a, b$) with $N_s = N/s$ the corresponding mapped blocks. Before transmission, these blocks are linearly combined in the vector space $\mathbb{F}_{2^s}^{N_s}$ over the field \mathbb{F}_{2^s} . That is,

$$\mathbf{Y}^j = h_a^j \mathbf{X}^a + h_b^j \mathbf{X}^b. \quad (1)$$

where the *local encoding vector* [3] coefficients, $\mathbf{h}^j = (h_a^j, h_b^j)$, $\mathbf{h}^j \in \mathbb{F}_{2^s}^2$, are randomly¹ generated by the node. However, and unlike in the relays, the

¹We will constrain the election to $\{h_i^j\}_{i=a}^b \neq 0$

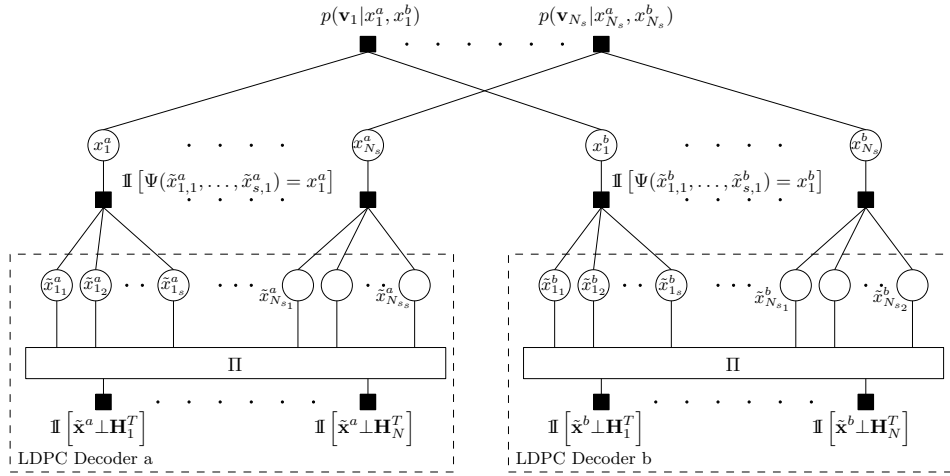


Figure C.2: Factor graph employed for the decoding.

local encoding vectors at the source nodes a and b are fixed to $(1,0)$ and $(0,1)$, respectively.

Both \mathbf{Y}^j and \mathbf{h}^j are forward transmitted by node j using a 2^s -QAM constellation. It is assumed that all the receiving nodes are able to perfectly recover² \mathbf{h}^j .

At each time instant k , $k \in \{1, \dots, N_s\}$, we denote the modulated Y_k^j symbol by $\Phi(Y_k^j) \in 2^s$ -QAM. The sample transmitted by node j and received by node i at time k is

$$V_k^i = |\alpha^{ij}| \cdot \sqrt{\beta^{ij}} \cdot \Phi(Y_k^j) + N_k^{ij}, \quad (2)$$

where α^{ij} , β^{ij} and N_k^{ij} have been defined in Section II.

A. Decode

Let us consider an arbitrary node $j \in \mathcal{R} \cup \mathcal{D}$. Notice that this node will have $m = |\mathcal{T}_j|$ incoming links. Denote by $(\mathbf{v}^1, \dots, \mathbf{v}^m)$ the corresponding received packets. Next, we will explain the proposed decoding method.

²For example, this can be done by channel encoding these coefficients. Notice that if $N_s \gg 2$ the overhead will be small.

The aim of the decoder is to implement a bitwise MAP decoding. That is, to find the values of $\tilde{\mathbf{x}}^a$ and $\tilde{\mathbf{x}}^b$ that are most likely given $(\mathbf{v}^1, \dots, \mathbf{v}^m)$, i.e. the $(\tilde{\mathbf{x}}^a, \tilde{\mathbf{x}}^b)$ that maximizes $P_{\tilde{\mathbf{x}}^a, \tilde{\mathbf{x}}^b | \mathbf{v}^1, \dots, \mathbf{v}^m}(\tilde{\mathbf{x}}^a, \tilde{\mathbf{x}}^b | \mathbf{v}^1, \dots, \mathbf{v}^m)$. For the sake of simplicity $P_Z(z)$ will be denoted by $p(z)$.

$$\widehat{\tilde{x}_k^i} = \arg \max_{\substack{\tilde{x}_k^i \\ \sim \tilde{x}_k^i}} \sum p(\tilde{\mathbf{x}}^a, \tilde{\mathbf{x}}^b | \mathbf{v}^1, \dots, \mathbf{v}^m) \quad (3)$$

for $i \in \mathcal{S}$ and $k = 1, \dots, N$. Since both sources are independent and the channel is memoryless, the probability function can be factorized as shown in (4).

$$\begin{aligned} p(\tilde{\mathbf{x}}^a, \tilde{\mathbf{x}}^b | \mathbf{v}^1, \dots, \mathbf{v}^m) &\propto \prod_{k=1}^{N_s} p(v_k^1, \dots, v_k^m | x_k^1, x_k^2) \mathbb{I}[\Psi(\tilde{x}_{1,k}^a, \dots, \tilde{x}_{s,k}^a) = x_k^a] \cdot \\ &\quad \mathbb{I}[\Psi(\tilde{x}_{1,k}^b, \dots, \tilde{x}_{2,k}^b) = x_k^b] \cdot \prod_{i=1}^{N-K} \mathbb{I}[\tilde{\mathbf{x}}^a \perp \mathbf{H}_i^T] \mathbb{I}[\tilde{\mathbf{x}}^b \perp \mathbf{H}_i^T] \end{aligned} \quad (4)$$

where $\Psi : \mathbb{F}_2^s \rightarrow \mathbb{F}_{2^s}$ is the binary mapping³ and the first term is the joint likelihood probability. The last two terms represent the parity-check equations of both LDPC codes.

Let us focus on the joint likelihood probability $p(v_k^1, \dots, v_k^m | x_k^a, x_k^b)$. The following set of equations in (5) shows the relationship between $\{v_k^i\}_{i=1}^m$ and $\{x_k^i\}_{i=a}^b$.

$$\begin{bmatrix} v_k^1 \\ \vdots \\ v_k^m \end{bmatrix} = \begin{bmatrix} |\alpha^{1j}| & \dots & 0 \\ \vdots & \ddots & \vdots \\ 0 & \dots & |\alpha^{mj}| \end{bmatrix} \cdot \begin{bmatrix} \sqrt{\beta^{1j}} & \dots & 0 \\ \vdots & \ddots & \vdots \\ 0 & \dots & \sqrt{\beta^{mj}} \end{bmatrix} \cdot \Phi \left(\begin{bmatrix} h_a^1 & h_b^1 \\ \vdots & \vdots \\ h_a^m & h_b^m \end{bmatrix} \cdot \begin{bmatrix} x_k^a \\ x_k^b \end{bmatrix} \right) + \begin{bmatrix} n_k^1 \\ \vdots \\ n_k^m \end{bmatrix} \quad (5)$$

$$\mathbf{v}_k = \Lambda \cdot \Theta \cdot (\Pi \mathbf{x}_k) + \mathbf{n}_k$$

³For the binary transformation we will consider the left bit as the most significant bit.

Since CSI is available at the receiving node, i.e. $\Lambda \cdot \Theta$ is known, the conditional probability at the node j is given by

$$p(\mathbf{v}_k | x_k^a, x_k^b) = \mathcal{N}(\Lambda \cdot \Theta \cdot (\Pi \mathbf{x}_k), \sigma^2 I_{m \times m}). \quad (6)$$

Consequently,

$$p(\mathbf{v}_k | x_k^a, x_k^b) = \exp \left\{ \frac{-\sum_{i=1}^m \left\| v_k^i - |\alpha^{ij}| \sqrt{\beta^{ij}} \Phi(h_a^i x_k^a + h_b^i x_k^b) \right\|^2}{N_0} \right\}, \quad (7)$$

where $\|\cdot\|^2$ denotes the euclidean norm.

The marginalization of (3) can be efficiently performed by the Sum-Product algorithm (SPA) [7] applied to the factor graph (Figure C.2) derived from the factorization of (4). Notice from this factor graph that the likelihood probabilities of $\tilde{\mathbf{x}}^a$ and $\tilde{\mathbf{x}}^b$ are updated at each iteration. This contrasts to what it is done in a standard LDPC decoding algorithm.

V. RESULTS

In order to evaluate the performance of the proposed system, Monte Carlo simulations have been done for different values of $|\mathcal{R}|$, i.e. different number of relays. An irregular LDPC code with $d_v = 9$ and $d_c = 0.53x^2 + 0.3x^3 + 0.16x^{20}$ has been used as channel code. Each source generates $K = 1500$ bits and a total of 4500 baseband symbols (1 complex dimension) are transmitted through the system. Therefore, a spectral efficiency of $\rho_S = \frac{2}{3}$ bits per transmitted symbol (i.e., bits per complex dimension) is obtained. The Sum-Product algorithm performs 50 full iterations over the corresponding factor graph.

Figure C.3 plots the bit error rate (BER) versus $E_b/N_0 = E_s/(\rho_S N_0)$ for $|\mathcal{R}| = 0, \dots, 3$. For low SNRs, the achieved diversity at the destination (i.e. the slope of the BER curve) slowly increases with the number of relays. Thus, for small number of relays the increment of diversity is not significant due to the pathloss attenuation suffered by the signals. On the other hand, as the number of relays increases, the achieved diversity starts to increase since the pathloss attenuation becomes less significant due to the increment of incoming signals. For higher SNRs it can be seen how the

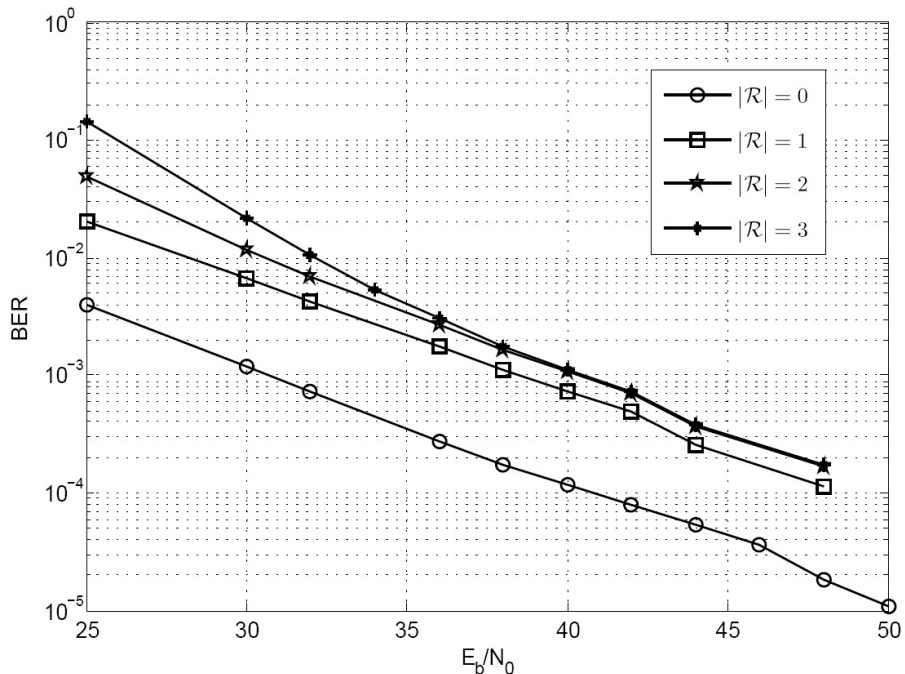


Figure C.3: Performance of the proposed system for $|\mathcal{R}| = 0, \dots, 3$.

BER differences reduce drastically as the number of relays increases. Notice that for $|\mathcal{R}| = 2$ and $|\mathcal{R}| = 3$ the BER curves even collapse. Therefore, for high SNRs, adding more relays in order to reach a distant point practically does not degrade the performance of the system, which makes the proposed system suitable for multi-hop wireless networks.

Moreover, for the particular case of having 3 relays, i.e.

$$\mathcal{N} = \{a, b, 1, 2, 3, 4\},$$

the performance of the proposed system is compared with the scheme proposed by *Bao et al.* in [2] and the one proposed by *Hausl et al.* in [5], which have been adapted to our network topology; hereafter, we will denote them as Ref1 and Ref2, respectively. To that end, two sets of simulations have been performed.

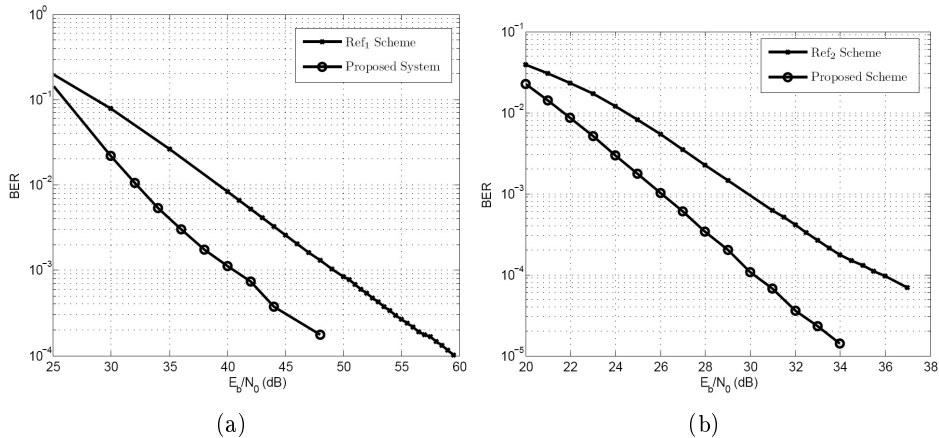


Figure C.4: Simulation results: (a) Bit error rate (BER) of the proposed scheme versus E_b/N_0 assuming non ideal relays. For comparison purposes, the performance of Ref1 scheme is also shown in the figure. (b) BER of the proposed scheme versus E_b/N_0 assuming ideal relays. For comparison purposes, the performance of Ref2 scheme is also shown in the figure.

Table C.1 summarizes the values of the parameters for the proposed and referenced schemes.

Table C.1: Parameters for the simulation: K : block length (bl) of information bits; N : bl . of channel code bits; R : channel code rate; R_s : channel-network code rate at the relays; ρ_S : system spectral efficiency.

System	s	K	N	R	R_s	ρ_S
Proposed Scheme	4	1500	3600	0.83	1.66	$2/3$
Ref1 Scheme	1	1500	2070	0.72	1.85	$2/3$
Ref2 Scheme	1	1500	1800	0.83	1.66	$2/3$

The first set of simulations is shown in Figure C.4(a), where the bit error rate (BER) versus $E_b/N_0 = E_s/(\rho_S N_0)$ is displayed for our scheme

and for the Ref1 scheme [2]. From these curves it can be observed that at a BER of 10^{-4} , the proposed system outperforms by approximately 10 dB in E_b/N_0 the Ref1 scheme. Also at low SNRs, the proposed scheme has a larger diversity gain. However, as the SNR increases this gain diminishes and ends up being the same. The keypoint of the obtained gain is that the relays do not transmit any systematic bit in the Ref1 scheme, which makes the scheme very sensitive to the fading. In the latter scheme the destination only receives information about the systematic bits through the messages transmitted by the sources. Thus, due to the pathloss, if a message transmitted by any source suffers from a deep fade, the destination will not have any information about the respective systematic bits.

The second set of simulations compares our system with a modification of the scheme proposed in [5] in the sense that more relays have been included (Ref2). For a fair comparison, and as it was done in [5], we will also assume perfect decoding at the relays. The BER versus E_b/N_0 results are displayed in Figure C.4(b). In this case, the E_b/N_0 gain is approximately 6 dB at a BER of 10^{-4} and the diversity gain is constant for all the SNRs. Notice that in the proposed scheme a higher order modulation is used, which allows the binary channel code to have a lower rate for the same total spectral efficiency. Moreover, the drawback of using a higher modulation is diminished by computing the joint likelihood probability $p(\mathbf{v}_k|x_k^a, x_k^b)$ using all the incoming messages as showed in (7). This could be the keypoint of the obtained gain with respect to the Ref2 scheme.

It is important to mention that all simulated schemes (i.e., proposed scheme, Ref1 and Ref2) use the same spectral efficiency to transmit the 1500 bits from each source, so they require the same bandwidth over the same network topology. Both reference schemes are briefly explained in the Appendix.

VI. CONCLUSION

We have investigated a novel *decode-combine-forward* scheme applied to ad-hoc wireless networks with orthogonal channels. The proposed scheme has been compared with two reference schemes previously described in the literature. Simulation results reveal that the *decode-combine-forward* scheme clearly outperforms these reference systems by more than 7 dB in E_b/N_0 . Due to the *decode* step in the proposed scheme, a failure (or deep

fade) of a node has a smaller impact in performance than in the corresponding reference scheme. This fact could also explain the observation that when pathloss-Rayleigh channels are considered, the proposed scheme achieves a higher diversity gain for low SNRs.

APPENDIX

A. Ref1 Scheme

The Ref1 scheme was first proposed in [2] as an extension of *coded cooperation* [6] to the multi-hop network. This scheme allows each relay node in the ad-hoc network to gather all the messages transmitted from previous nodes, to decode segments altogether, and to reencode and transmit a different (sub-) codeword. The destination receives all the (sub-)codewords from the original source⁴ as well as from each and every participating relay and performs the SPA algorithm over the factor graph associated to the network parity-check matrix.

Figures C.5(a) and C.5(c) show the associated factor graph and the network parity-check matrix, respectively. The dashed lines in the factor graph mean that there cannot exist a connection between a variable node and an upper check node due to the triangular nature of the parity-check matrix [2]. We will use packet length factors of 0.23, 0.23, 0.18, 0.18 and 0.18 for both sources and relays 1, 2, 3, respectively [2]. Since $K = 1500$, the packets from the sources and the relays have lengths of 2070 (1500 systematic bits and 570 parity bits) and 1620 (parity bits only), respectively.

B. Ref2 Scheme

It was first proposed for MARC (Multiple Access Relay Channels). The sources perform a channel coding with a low-density parity-check (LDPC) code and each relay performs a linear combination of the decoded bits and encodes them before transmitting. As in [5], we will consider the same length of the transmitted codewords for the sources and the relays. The destination receives the noisy versions of the signals transmitted by sources and relays, \mathbf{V}_i , $i \in \mathcal{T}_n$ and performs a joint channel-network decoding by

⁴Although in [2] the system was proposed for one source, the assumption of two sources is straightforward.

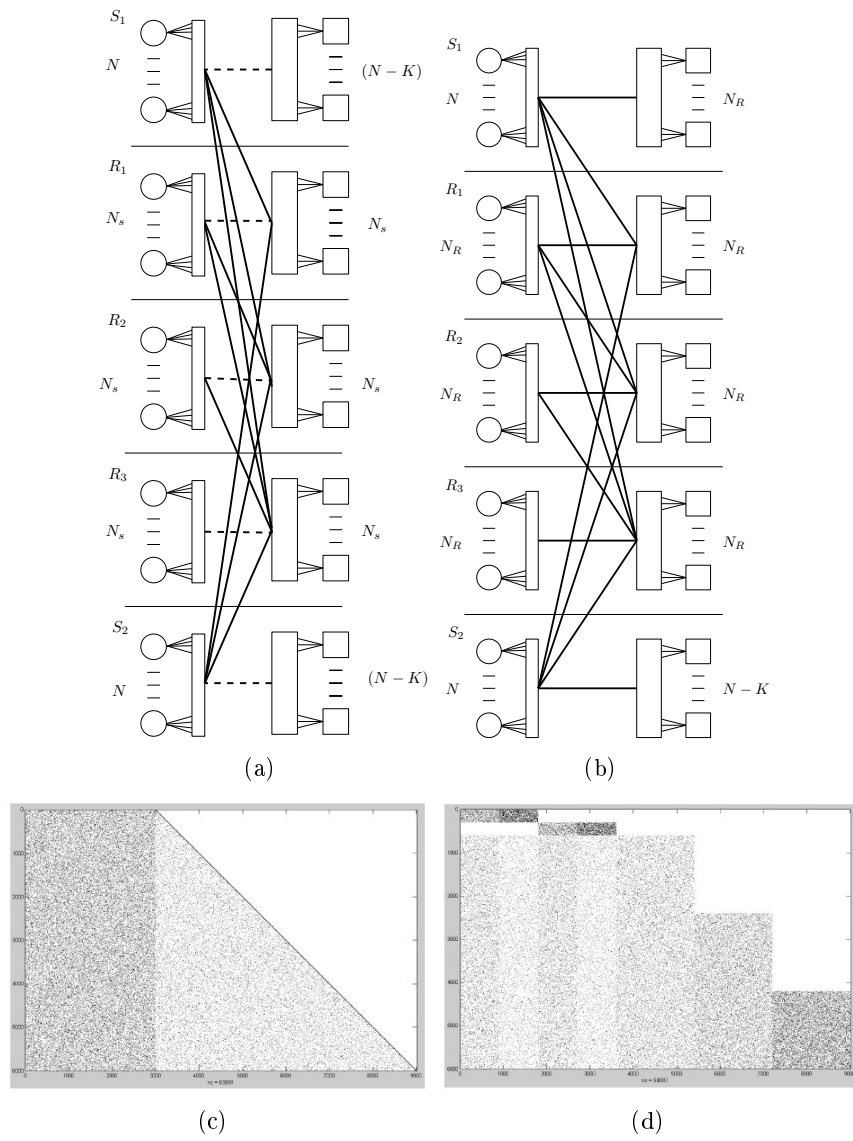


Figure C.5: (a) and (c) Factor Graph and Parity-check matrix, respectively, of Ref1 scheme. (b) and (d) Factor Graph and Parity-check matrix, respectively, of Ref2 scheme.

applying the Sum-Product Algorithm over the factor graph, which jointly

models the channel and network codes. Figures C.5(b) and C.5(d) show the factor graph and the parity-check matrix associated to this scheme, respectively.

REFERENCES

- [1] R. Babaee and N.C. Beaulieu. Cross-layer design for multihop wireless relaying networks. *IEEE Transactions on Wireless Communications*, 9(11):3522 –3531, november 2010.
- [2] X. Bao and J. Li. Progressive network coding for message-forwarding in ad-hoc wireless networks. In *2006 3rd Annual IEEE Communications Society on Sensor and Ad Hoc Communications and Networks, SECON'06*, volume 1, pages 207 –215, sept. 2006.
- [3] P.A. Chou, Y.Wu, and K. Jain. Practical network coding. In *Forty-First Annual Allerton Conference on Communication, Control, and Computing*, 2003.
- [4] R. Gallager. Low-density parity-check codes. *IRE Transactions on Information Theory*, 8(1):21 –28, january 1962.
- [5] C. Hausl, F. Schreckenbah, I. Oikonomidis, and G. Bauch. Iterative network and channel decoding on a tanner graph. In *Forty-Third Annual Allerton Conference on Communication, Control, and Computing, Allerton'05*, 2005.
- [6] T.E. Hunter and A. Nosratinia. Cooperation diversity through coding. In *2002 IEEE International Symposium on Information Theory, ISIT'02*, 2002.
- [7] F.R. Kschischang, B.J. Frey, and H.-A. Loeliger. Factor graphs and the sum-product algorithm. *IEEE Transactions on Information Theory*, 47(2):498 –519, feb 2001.
- [8] E. Morgado, I. Mora-Jimenez, J.J. Vinagre, J. Ramos, and A.J. Caamano. End-to-end average ber in multihop wireless networks over fading channels. *IEEE Transactions on Wireless Communications*, 9(8):2478 –2487, august 2010.
- [9] R. Tanner. A recursive approach to low complexity codes. *IEEE Transactions on Information Theory*, 27(5):533 – 547, sep 1981.

- [10] Yu-Chee Tseng, Sze-Yao Ni, and En-Yu Shih. Adaptive approaches to relieving broadcast storms in a wireless multihop mobile ad hoc network. *IEEE Transactions on Computers*, 52(5):545 – 557, may 2003.
- [11] O. Waqar, D.C. McLernon, and M. Ghogho. Exact evaluation of ergodic capacity for multihop variable-gain relay networks: A unified framework for generalized fading channels. *IEEE Transactions on Vehicular Technology*, 59(8):4181 –4187, oct. 2010.
- [12] B. Williams and T. Camps. Comparison of broadcasting techniques for mobile ad hoc networks. In *The Third ACM International Symposium on Mobile Ad Hoc Networking and Computing, MOBIHOC'02*, 2002.

APPENDIX D

Paper IV

Title: A Decode-and-Forward Scheme for Multihop Wireless Networks

Authors: Mikel Hernaez¹, Pedro M. Crespo¹ and Javier Del Ser²

Affiliation:¹ Centro De Estudios e Investigaciones Técnicas de Gipuzkoa (CEIT) and TECNUN (University of Navarra), 20008 Donostia-San Sebastián, Spain

Affiliation:² TELECOM Unit TECNALIA RESEARCH & INNOVATION P. Tecnológico, Ed. 202, 48170 Zamudio, Spain

Journal: *Springer Wireless Networks*, submitted 2012

A DECODE-AND-FORWARD SCHEME FOR MULTIHOP WIRELESS NETWORKS

Mikel Hernaez, *Student Member, IEEE*, Pedro M. Crespo, *Senior Member, IEEE*, and Javier Del Ser, *Senior Member, IEEE*

¹ Centro De Estudios e Investigaciones Técnicas de Gipuzkoa (CEIT) and TECNUN (University of Navarra), 20008 Donostia-San Sebastián, Spain

E-mails: {mhernaez, pcrespo}@ceit.es

² TELECOM Unit TECNALIA RESEARCH & INNOVATION P. Tecnológico, Ed. 202, 48170 Zamudio, Spain

E-mails: {javier.delser}@tecnalia.com.es

Abstract — In this paper, we propose a Decode-and-Forward (DF) relaying scheme for the multihop transmission in wireless networks, where the information generated by an independent source has to be sent to a far destination based on multiple-relay cooperation. The proposed DF scheme blends together Convolutional channel coding with linear combination of blocks of data over a finite field. The performance of the proposed system is compared with reference schemes previously proposed in the literature. We provide simulation results showing that using blocks of $K = 13$ information bits, our scheme clearly outperforms these reference schemes that use blocks of $K = 1500$ information bits. Moreover, we show that the proposed DF scheme is suitable for large multi-hop networks with relays that share their resources with other networks since: 1) a negligible performance degradation is obtained for adding more hops; and 2) most of the iterative gain at the decoding is achieved in less than 10 iterations.

I. INTRODUCTION

In a multihop network, the data transmission between the source and the corresponding destination is realized with the aid of intermediate nodes (relays). These networks have been the focus of an intense research in the recent years, where Multihop Communication has been shown to be an effective method for establishing connectivity between nodes of a network where direct transmission is not feasible due to coverage or battery life issues [1, 2, 6, 10, 11].

In [1, 10, 11] and references therein, several theoretical aspects of multihop network are presented. Concretely, in [1] efficient-routing protocols for several power allocations in fading are proposed. Once the route between source and destination is fixed (by for example, the protocols presented in [1]), the authors of the present work proposed in [6] a Decode-and-Forward (DF) relaying strategy based on a blend of Low-Density Parity-Check (LDPC) codes together with a linear combination of blocks of data over a finite field. We showed that for blocks of $K = 1500$ information bits, the proposed scheme outperformed two reference schemes based on previous works addressing similar problems [2, 5].

In the current manuscript we propose a DF relaying strategy which uses a terminated convolutional code and an improved version of the non-binary block-wise linear combination of [6]. At each node, the decoding scheme is based on applying the Sum-Product Algorithm (SPA) [8] to a factor graph [8] describing the *a posteriori* probability of the communication scenario at the corresponding node. By using blocks of only $K = 13$ information bits, the performance of the proposed scheme outperforms the scheme of [6] (and consequently, [2, 5]) where 1500 bits were used, making the proposed scheme particularly attractive for low-latency applications.

The rest of the manuscript is organized as follows: Section II introduces the network model, whereas the proposed DF scheme is presented in Section III. Section IV discusses the obtained Monte Carlo simulations results and finally, Section V concludes the paper and makes some future remarks.

II. NETWORK MODEL

We study the problem where a user wants to transmit data to a destination through a multihop wireless network. For the sake of simplicity,

we have imposed a straight-line geometry and unity distance between two consecutive nodes, so we can easily compute distances and signal attenuations between nodes. We consider the Decode-and-Forward (DF) decoding strategy, where at each intermediate node the received signal is decoded, re-encoded and forwarded. In order to avoid possible interferences in the network, we design the system in Time-Division-Multiple-Access (TDMA) mode. Thus, the total available transmission time is divided into several orthogonal time-slots, one for each node.

The nodes are assumed to work in Half-duplex mode; hence, a node can either receive or transmit data, but not both at the same time. Besides, we also assume that the nodes have only one omnidirectional and forwards-oriented transmitting antenna; therefore, the data is transmitted in a progressive way. That is, one node can listen to all the previous nodes but not to the following ones. Due to the wireless nature of the signals, we consider Rayleigh fading and path loss attenuation. Finally, due to the wireless environment and following [2, 6], we do not constrain the transmission range of each node to one hop, as done in [1, 10, 11].

Let $\mathcal{M} = \{s, 1, \dots, m-1, m\}$ denote the set of nodes in the network, where s and m are the source and destination nodes, respectively. We define $\mathcal{R} = \{1, \dots, m-1\} \subset \mathcal{M}$ as the subset formed by the intermediate nodes (relays), and $\mathcal{T}_j = \{s, 1, \dots, j-1\} \subset \mathcal{M}$ (for $j = 1, \dots, m$) as the subset of nodes from which node j receives their transmitted symbols. Figure D.1 depicts the network model.

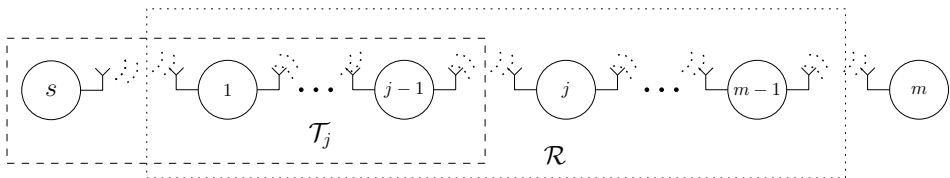


Figure D.1: Network model.

Regarding the links between nodes, we consider independent (orthogonal) quasi-static Rayleigh flat-fading channels (coherent detection at the receivers), where the t -sampled baseband (complex) link input-output (S -

Y) relation from node i to node j at time t is given by

$$Y_t = |\Lambda^{ij}| \sqrt{d_{ij}^{-\delta}} S_t + N_t^{ij} \quad (1)$$

with $d^{-\delta}$ modelling the path loss attenuation, where d is the number of hops (units) between the transmitting and the receiving node and δ is the attenuation exponent. The latter is usually set between 2 (free space communications) and 4 (lossy environments such as urban areas) [4]. The fading coefficient Λ and the additive Gaussian noise N_t are circularly symmetric complex Gaussian random variables of zero mean and variance one and N_0 , respectively. A realization of Λ is assumed to remain constant for the duration of the transmitted block.

III. PROPOSED DF SCHEME

Let $(\Omega, \beta, \mathcal{P})$ be the underlying probability space where all the random variables (r.v.) are defined. We use uppercase when referring to r.v. and lowercase when referring to realizations of r.v. In addition, we use boldface when referring to vectors, and boldface with an underline to refer to matrices. For discrete r.v., we denote the probability mass function (p.m.f.) of the discrete r.v. X as $P_X(x) \triangleq \mathcal{P}\{\omega : X(\omega) = x\}$. For continuous r.v., we denote the probability density function (p.d.f.) of the continuous r.v. X as $p_X(x)$. However, when the context is clear, we use $P(x)$ and $p(x)$ for p.m.f. and p.d.f., respectively.

A DF scheme is proposed to transmit the information generated by the source to the destination. Like most of the DF schemes, the proposed scheme can be divided into two parts: the decode part, where the information sequence is estimated; and the forward part, where the estimated sequence is encoded and forwarded. In this case, the forward part at the source node is implemented in a different manner than the ones at the relay nodes; therefore, it will be explained first.

We consider a unit-entropy binary source that generates information blocks $\mathbf{U} \in \{0, 1\}^K$. Then, the information sequence is encoded by a rate $R = K/N$ convolutional code. The resulting encoded binary codeword $\mathbf{C} \triangleq \{C_n\}_{n=1}^N \in \{0, 1\}^N$ is interleaved by a random spread interleaver Π yielding the interleaved sequence \mathbf{X} with $X_n = C_{\Pi(n)}$. Finally, \mathbf{X} is mapped into the sequence of symbols $\mathbf{S} \in \mathcal{S}^M$ chosen from the 2^q -ary signal

constellation \mathcal{S} according to the bit-to-symbol mapping $\mu : \{0,1\}^q \rightarrow \mathcal{S}$ (e.g. Gray mapping), thus, $M = N/q$.

Next, we present the proposed DF scheme performed at the relays. Even if the decode part is executed before the forward part, for the sake of understanding, we first present the latter. Furthermore, since we are presenting the operations performed at each relay node, we will intentionally omit any references to the particular node j . However, when considering the entire network we will use the upper index j to discern between different nodes.

A. Forward

At each node $j \in \mathcal{R}$, the decode part, which will be explained later, outputs the estimated information sequence $\widehat{\mathbf{U}}$, which is encoded and interleaved using the aforementioned convolutional code and interleave, respectively. The resulting binary sequence \mathbf{X} is partitioned into the q -length subsequences $\mathbf{X}_l \triangleq \{X_{lq+i}\}_{i=1}^q$, where $l = 0, \dots, M-1$. Let denote $\phi : \mathbb{F}_2^q \rightarrow \mathbb{F}_{2^q}$ to the mapping from a q -length binary sequence¹ into an element of \mathbb{F}_{2^q} . Thus, the non-binary symbols $\{V_l\}_{l=0}^{M-1} \in \mathbb{F}_{2^q}^M$ are computed from each subsequence as $V_l = \phi(\mathbf{X}_l)$.

Let us now denote $\bar{l} \triangleq |M/2 - l|$ and consider the set of pairs $\{(V_l, V_{\bar{l}}) : l = 0, \dots, M-1\}$. By symmetry, we have that

$$\{(V_l, V_{\bar{l}})\}_{l=0}^{M/2-1} = \{(V_l, V_{\bar{l}})\}_{l=M/2}^{M-1}.$$

Thus, at the relays we only consider $l = 0, \dots, M/2 - 1$. Each pair $(V_l, V_{\bar{l}})$ is linearly combined over the field \mathbb{F}_{2^q} and mapped into signal points of the 2^q -ary constellation \mathcal{S} . That is, for $t = 1, \dots, M/2$ and $l = t - 1$

$$S_t = \mu_{\mathbb{F}_{2^q}}(h_1 V_l + h_2 V_{\bar{l}}), \quad (2)$$

where $\mu_{\mathbb{F}_{2^q}}(x) \triangleq \mu(\phi^{-1}(x)) \forall x \in \mathbb{F}_{2^q}$. The network vector coefficients $\mathbf{h} = (h_1, h_2)$, with $\mathbf{h} \in \mathbb{F}_{2^q}^2$, are fixed by the network so that all the vector coefficients in the network are linearly independent. We further constrain the election to $\{h_i\}_{i=1,2} \neq 0$. Finally note that the sequences transmitted by the relays are half as short as the one transmitted by the source.

B. Decode

Let us consider an arbitrary node $j \in \mathcal{R} \cup m$ that receives the sequences sent by the nodes $i \in \mathcal{T}_j$ (i.e. all the nodes located at its left, see Fig. 1).

¹We consider the left bit as the most significant bit.

This node have $|\mathcal{T}_j|$ incoming links with received sequences $(\mathbf{y}^1, \dots, \mathbf{y}^{|\mathcal{T}_j|})$. For the sake of clarity, through this sub-section we define $\underline{\mathbf{y}} \triangleq (\mathbf{y}^1, \dots, \mathbf{y}^{|\mathcal{T}_j|})$ and denote \mathbf{y}_t as the $|\mathcal{T}_j|$ symbols received at time instant t , which are related to the elements V_l and $V_{\bar{l}}$ (see (1) and (2)).

The aim of the decoder is to implement a bitwise MAP decoding. That is, to find the values $\{u_k\}_{k=1}^K$ that are most likely given $\underline{\mathbf{y}}$, i.e.

$$\hat{u}_k = \arg \max_{u_k} \sum_{\sim u_k} P_{\mathbf{U}|\underline{\mathbf{Y}}}(\mathbf{u}|\underline{\mathbf{y}}) \quad (3)$$

where $\sim u_k \triangleq \{u_{k'}\}_{k' \neq k}$. Since a convolutional code is used as a channel code the above maximization can be rewritten as [9, Chapter 16]

$$\hat{u}_k = \arg \max_{u_k} \sum_{\sim u_k} T_k(s_k, u_k, \mathbf{c}_k, s_{k+1}) \alpha(s_k) \beta(s_{k+1}) \prod_{n: c_n \in \mathbf{c}_k} \gamma(c_n), \quad (4)$$

where α and β are the forward and backward messages passed from the adjacent state nodes to the factor node T_k given by the Trellis of the convolutional code; \mathbf{c}_k are the N/K coded bits $\{c_n\}$ associated to u_k ; and γ are the channel likelihoods about the coded bits. Due to the proposed forward part, these likelihoods are now proportional to the information about the interleaved binary symbols x_{lq+i} supplied by the $|\mathcal{T}_j|$ incoming links, i.e. $\gamma(c_n) = \gamma(x_{\Pi^{-1}(lq+i)})$, where $\gamma(x_{lq+i}) \propto p(\underline{\mathbf{y}}|x_{lq+i})$.

Since the channel is memoryless and assuming that the interleaved sequence is i.i.d., this probability can be factorize as

$$p(\underline{\mathbf{y}}|x_{lq+i}) \propto \sum_{\sim x_{lq+i}, v_l} p(\mathbf{y}_t|v_l) \mathbb{1}[v_l = \phi(\mathbf{x}_l)] \prod_{i' \neq i} P(x_{lq+i'}) \quad (5)$$

where

$$p(\mathbf{y}_t|v_l) = \sum_{v_{\bar{l}}} p(\mathbf{y}_t|v_l, v_{\bar{l}}) P(v_{\bar{l}}) \quad (6)$$

with

$$P(v_{\bar{l}}) = \sum_{\mathbf{x}_{\bar{l}}} \mathbb{1}[v_{\bar{l}} = \phi(\mathbf{x}_{\bar{l}})] \prod_{i=1}^q P(x_{\bar{l}q+i}), \quad (7)$$

and $\mathbb{1}[\cdot]$ is an indicator function taking value 1 if its argument is true and 0 otherwise.

Let us focus on the joint likelihood probability $p(\mathbf{y}_t|v_l, v_{\bar{l}})$. Using (2), applying maximum-ratio combining and since Λ and $d^{-\delta}$ are known at the receiver (see (1)), the conditional probability is given by

$$p(\mathbf{y}_t|v_l, v_{\bar{l}}) = \exp \left\{ \frac{-\sum_{i=1}^{|\mathcal{T}_j|} \left\| y_t^i - |\Lambda^{ij}| \sqrt{d_{ij}^{-\delta}} \mu_{\mathbb{F}_{2^q}}(h_1^i v_l + h_2^i v_{\bar{l}}) \right\|^2}{N_0} \right\}, \quad (8)$$

where $\|\cdot\|^2$ denotes the euclidean norm.

Therefore, the marginalization of (3) can be efficiently performed by the Sum-Product algorithm (SPA) applied to the factor graph (Figure D.2) derived from the factorization of $P_{\mathbf{U}|\underline{\mathbf{Y}}}(\mathbf{u}|\underline{\mathbf{y}})$ given by (4)-(7).

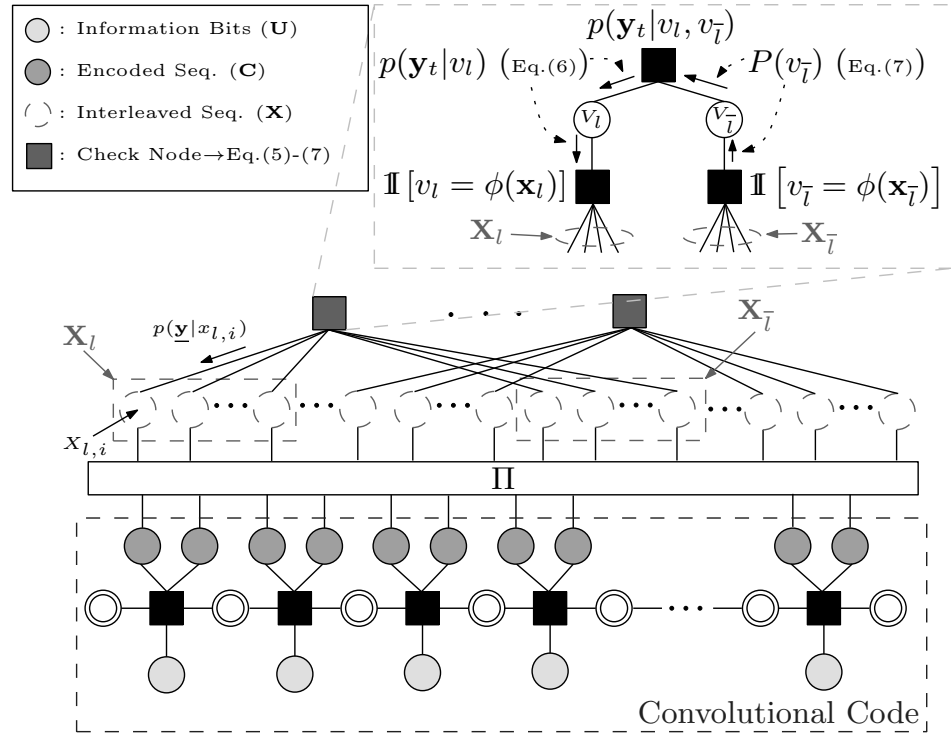


Figure D.2: Factor graph employed for the decoding.

IV. RESULTS

In order to assess the performance of the proposed code, several Monte Carlo simulations have been run using a 2^2 -state $[5, 7]_8$ non-systematic rate- $1/2$ convolutional code². Each source generates $K = 13$ information bits, and a zero-bit tail is appended at the source sequence in order to terminate the convolutional code properly. Specifically, we add 3 zeros so the block entering the convolutional code has 16 bits; and hence, the encoded sequence has $N = 32$ binary symbols. We have considered a 16-QAM constellation (i.e. $q = 4$ and $M = 8$ complex dimensions) and μ to be the Gray mapping. Finally, δ has been set to 4 and the interleaver $\Pi(\cdot)$ has been randomly generated with a spread factor of $q = 4$.

The number of nodes has been set to $|\mathcal{M}| = 5$. That is, the source transmits its message to the destination with the aid of three intermediate nodes that will relay the information sequence using the proposed DF scheme. Therefore, a total of 20 baseband symbols (i.e., complex dimensions) are transmitted through the system leading to a spectral efficiency of $\rho_S = \frac{13}{20}$ [information bits per complex dimension]. Finally, for the sake of simplicity, we have assumed equal power at each of the compounding nodes of the network.

An specially interesting network is that in which the relays share their resources with other networks. In this case, the number of iterations at the relays should be kept small to reduce their computational load. However, a performance degradation is expected for choosing a low number of iteration. To check this behaviour a first set of simulations has been performed. This is shown in Figure D.3, which plots the Packet-Error Rate (PER) versus $E_b/N_0 = E_s/(\rho_S N_0)$ at the destination (recall that node $j = 4$ is the destination), where we fix the number of iterations at the destination in 100, and vary the iterations performed at the relays in 1, 2, 10 and 100.

As seen in the figure, gains of 2dB, 3.5dB and 4dB are obtained with respect to a single iteration for letting the relays to iterate 2, 10 and 100 times, respectively. Notice that the change from 10 iterations to 100 iterations conveys a gain of only 0.5dB; hence, the gain obtained for performing more than 10 iterations is negligible, which makes the scheme suitable for relays with shared resources.

²The subindex 8 in the definition of the code stands for *octal*.

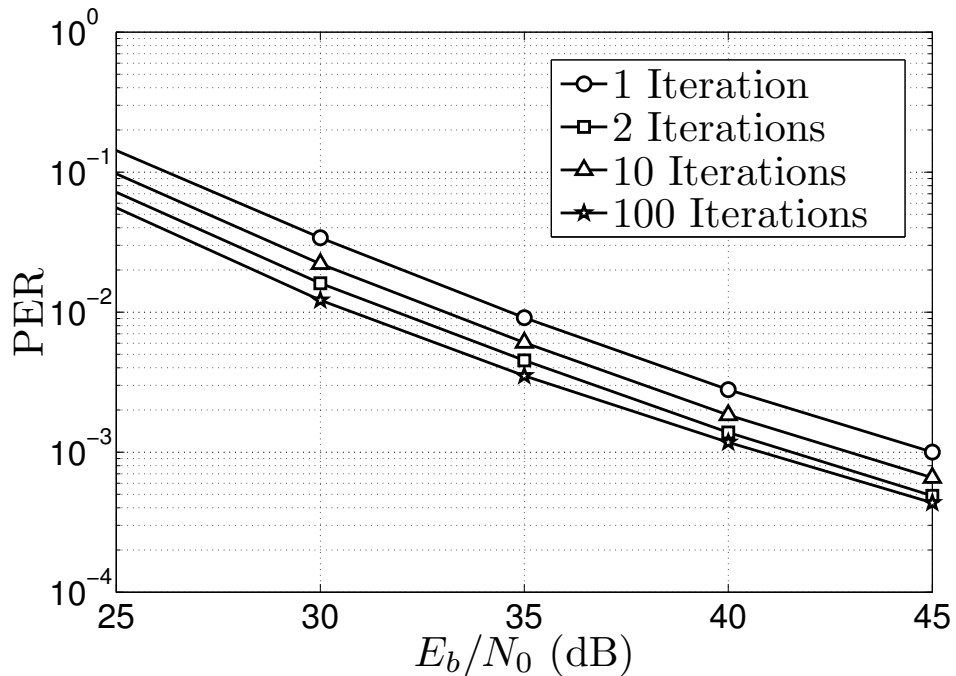


Figure D.3: Performance of the proposed scheme at the destination for different amount of iterations at the relays and 100 iterations at the destination.

The second set of simulations aims at analyzing the performance of the DF scheme for different number of hops. Figure D.4 shows the performance of the proposed scheme at the different nodes in the network, where the bit error rate (BER), after 100 iterations, versus E_b/N_0 is displayed. For comparison proposes, the BER performance of the schemes proposed in [2,6] at the destination ($j = 4$) are also plotted.

It can be observed that, after the first hop, the performance at high values of SNR for the different nodes is practically the same, which makes the proposed system very suitable for multihop wireless networks.

It can also be observed that, the proposed DF scheme outperforms the schemes presented in [6] and [2] in more than 3dB and 10dB, respectively. Moreover, side simulations show that when error-free links are assumed, the proposed scheme also outperforms both [6] and the adaptation of [5]

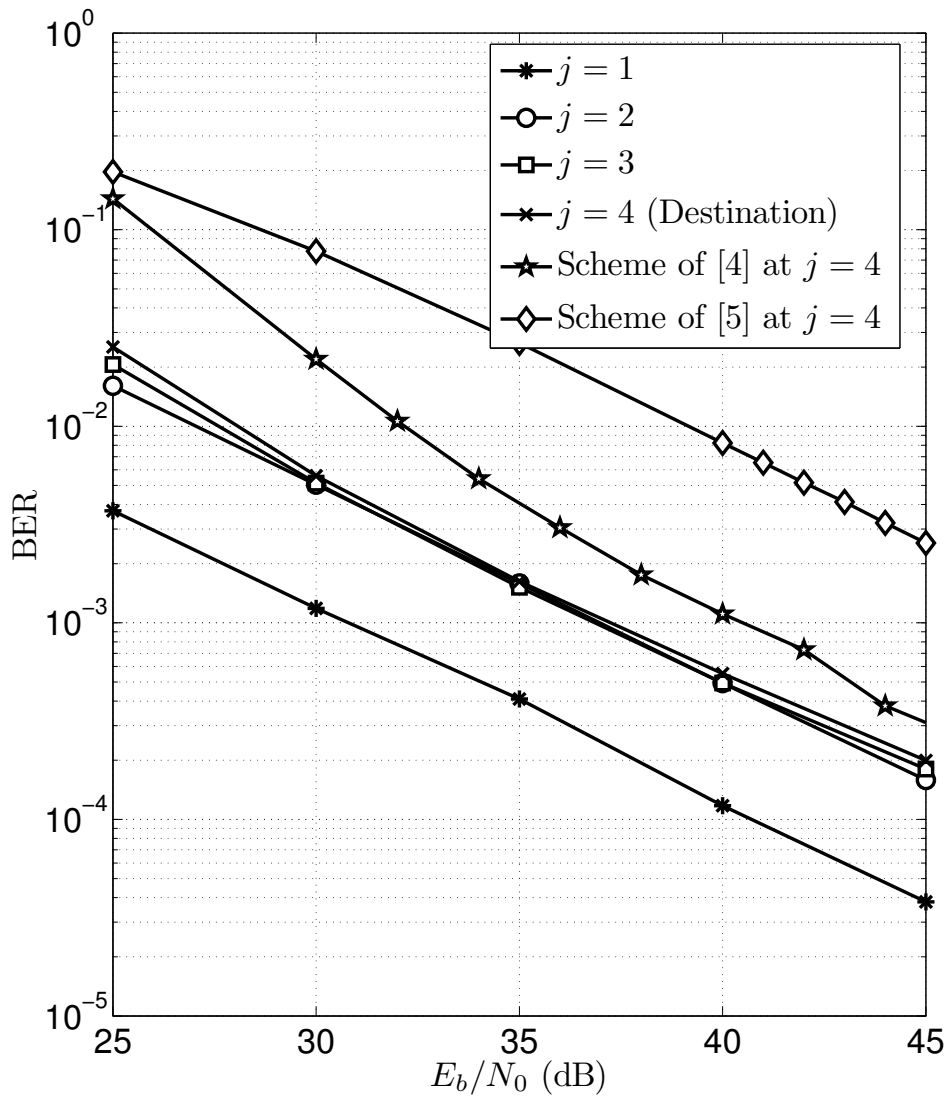


Figure D.4: BER performance of the proposed scheme at all the nodes for 100 Iterations. Also plotted the performance of [6] at the destination.

proposed in [6]. Finally, it is important to remark that, for the same spectral

efficiency, the proposed scheme uses a total of 20 complex dimensions in comparison to the 4500 used in the reference schemes.

V. CONCLUSIONS AND FUTURE REMARKS

We have presented a decode-and-forward scheme applied to multihop wireless networks with orthogonal channels. The proposed scheme blends together Convolutional channel coding with linear combination of blocks of data over a finite field. Simulation results reveal that the proposed DF scheme:

1. is suitable for large multi-hop networks as a negligible performance degradation is obtained for adding more hops;
2. is suitable for relays with shared resources since most of the iterative gain at the decoding is achieved in less than 10 iterations;
3. clearly outperforms previously proposed schemes; and
4. uses only a total of 20 complex dimensions in comparison with the 4500 used in the reference schemes, which makes the proposed scheme particularly attractive for low-latency applications.

Since this work aims at introducing a new scheme for multihop networks, we have considered the simple case of Gray mapping and arbitrarily chosen linearly independent network vector coefficients. However, we suspect that more iterative gain could be achieved by: i) carefully choosing the mapping μ as extensively done for bit interleaved coded modulation [3] and references therein; and ii) a tailored selection of the coefficients \mathbf{h} as suggested by the authors of the present work in [7].

REFERENCES

- [1] R. Babaee and N.C. Beaulieu. Cross-layer design for multihop wireless relaying networks. *IEEE Transactions on Wireless Communications*, 9(11):3522 –3531, november 2010.
- [2] X. Bao and J. Li. Progressive network coding for message-forwarding in ad-hoc wireless networks. In *2006 3rd Annual IEEE Communica-*

- tions Society on Sensor and Ad Hoc Communications and Networks, SECON'06*, volume 1, pages 207 –215, sept. 2006.
- [3] A. G. Fabregas, A. Martinez, and G. Caire. *Bit-Interleaved Coded Modulation*. Now Publishers Inc., 2008.
 - [4] A. Goldsmith. *Wireless Communications*. Cambridge University Press, 2005.
 - [5] C. Hausl, F. Schreckenbah, I. Oikonomidis, and G. Bauch. Iterative network and channel decoding on a tanner graph. In *Forty-Third Annual Allerton Conference on Communication, Control, and Computing, Allerton'05*, 2005.
 - [6] M. Hernaez, P. M. Crespo, and J. Del Ser. Joint Non-Binary LDPC-BICM and Network Coding with Iterative Decoding for the Multiple Access Relay Channel. In *2011 IEEE 73rd Vehicular Technology Conference: VTC'11-Spring*, May 2011.
 - [7] M. Hernaez, P. M. Crespo, and J. Del Ser. On the Design of a Novel Joint Network-Channel Coding Scheme for Multiple Access Relay Channels. *IEEE Journal on Selected Areas in Communications*, Accepted for publication 2012.
 - [8] F.R. Kschischang, B.J. Frey, and H.-A. Loeliger. Factor graphs and the sum-product algorithm. *IEEE Transactions on Information Theory*, 47(2):498 –519, feb 2001.
 - [9] T. K. Moon. *Error Correction Coding: Mathematical Methods and Algorithms*. Wiley-Interscience, 2005.
 - [10] E. Morgado, I. Mora-Jimenez, J.J. Vinagre, J. Ramos, and A.J. Caamano. End-to-end average ber in multihop wireless networks over fading channels. *IEEE Transactions on Wireless Communications*, 9(8):2478 –2487, august 2010.
 - [11] O. Waqar, D.C. McLernon, and M. Ghogho. Exact evaluation of ergodic capacity for multihop variable-gain relay networks: A unified framework for generalized fading channels. *IEEE Transactions on Vehicular Technology*, 59(8):4181 –4187, oct. 2010.

APPENDIX E

Paper V

Title: A Flexible Channel Coding Approach for Short-Length Codewords

Authors: Mikel Hernaez¹, Pedro M. Crespo¹ and Javier Del Ser²

Affiliation:¹ Centro De Estudios e Investigaciones Técnicas de Gipuzkoa (CEIT) and TECNUN (University of Navarra), 20008 Donostia-San Sebastián, Spain

Affiliation:² TELECOM Unit TECNALIA RESEARCH & INNOVATION P. Tecnológico, Ed. 202, 48170 Zamudio, Spain

Journal: *IEEE Communications Letters*, in 2nd Review 2012

A FLEXIBLE CHANNEL CODING APPROACH FOR SHORT-LENGTH CODEWORDS

Mikel Hernaez, *Student member, IEEE*, Pedro M. Crespo, *Senior member, IEEE*, and Javier Del Ser, *Senior member, IEEE*

¹ Centro De Estudios e Investigaciones Técnicas de Gipuzkoa (CEIT) and TECNUN (University of Navarra), 20008 Donostia-San Sebastián, Spain

E-mails: {mhernaez, pcrespo}@ceit.es

² TELECOM Unit TECNALIA RESEARCH & INNOVATION P.
Tecnológico, Ed. 202, 48170 Zamudio, Spain

E-mails: {javier.delser}@tecnalia.com.es

Abstract — This letter introduces a channel coding design framework for short-length codewords which can achieve lower error floor than previous approaches. The proposed code is based on combining convolutional coding with a q -ary linear combination and unequal energy allocation. Simulation results suggest that for very low bit-error rates the proposed system will exhibit lower error floors than previous approaches, with a small performance penalty at mid-range bit-error rates (BERs). On the other hand, when selecting an error floor higher than the previous approaches, the loss in performance at mid-range BERs is negligible.

I. INTRODUCTION

Iteratively decodable channel codes such as Low Density Parity-Check (LDPC) [9] or Turbo codes [1], have been widely shown to perform near capacity for the AWGN channel when used with codeword lengths beyond 10^6 . However, such codes can be impractical in scenarios which demand low latencies (e.g. real-time video delivery), mainly due to their associated decoding complexity and limited technological resources of the underlying hardware. This rationale motivates the upsurge of research on short-length codes (i.e. codes with codewords of several hundreds to few thousands coded symbols) to the above scenarios.

However, when dealing with short-length codewords the capacity approaching performance of LDPC or Turbo codes may severely degrade due to: 1) the widening of the waterfall region; and 2) the high error floors obtained under this condition (see [8] for LDPC codes and [3] for Turbo codes), mainly because of their poor minimum distance. The shorter the codeword is, the higher the error floor and the wider the waterfall region will be [8]. Several contributions ([7,10] and reference therein) have focused on reducing these error floors. In [10], a design technique is proposed to produce short-length parity-check matrices for LDPC codes that leads to error floors of 10^{-7} bit error rate at $E_b/N_0 = 2.2$ dBs, outperforming the previous approaches.

In this letter we propose an alternative channel coding approach for short-length codewords which can achieve lower error floors than [10] and reference therein. The location of the error floor can be easily set by varying the energy allocation of the encoded binary symbols (i.e. at the output of the modulation). As drawback, the lower the error floor is, the higher the SNR of the waterfall region will be. Thus, when choosing a error floor lower than the one in the previous schemes, our code will outperform them for BERs lower than its error floor (with a SNR waterfall degradation of less than 0.5 dB at $\text{BER} = 10^{-4}$). On the other hand, when selecting an error floor higher than those of [10] (10^{-7}), say 10^{-5} , the loss in performance at $\text{BER} = 10^{-4}$ is negligible.

To shed some light on the design parameters of the proposed code, we use Extrinsic Information Transfer (EXIT) charts [4]. Although, EXIT charts provides good BER convergence predictions only for long-length codewords, which is not our case, it gives us a good insight into how to choose the

parameters of the code in order to achieve the different error floors. For predicting BER convergence for short length codes, we refer to [6], where a method for computing lower bounds based on a EXIT *band* chart is proposed.

It should be mentioned that for long-length codewords (65000) the authors of [2] have used unequal energy allocation for shaping the curves of the EXIT charts in order to optimize the BER convergence of the designed code. As already said, we do not use EXIT charts together with unequal energy allocation to optimize BER convergence, but to predict the behavior of the waterfall versus error floor tradeoff for the different energy allocations.

The rest of the manuscript is organized as follows: Section II presents the system model, the proposed encoder and the corresponding decoder, whereas an analysis of the code based on EXIT charts is performed in Section III. Next, Section IV discusses the obtained Monte Carlo simulation results and ends the paper by drawing some concluding remarks.

II. PROPOSED CODE

To ease the understanding of the proposed code some definitions are first introduced. Consider the set of all 2^q polynomials $\rho(z)$ of degree $q - 1$ with coefficients lying in $GF(2)$ (the binary Galois field). Let $g(z)$ be a prime polynomial (i.e., monic and irreducible polynomial) of order q . Then, this set becomes a finite field, $GF(2^q)$, by defining the addition \oplus and multiplication \otimes rules as the mod $g(z)$ remainder of the sum and product of two polynomials, respectively. Notice that, since the mod $g(z)$ addition rule is just a componentwise addition of coefficients in $GF(2)$, $GF(2^q)$ under addition is isomorphic to the vector space $(GF(2))^q$ of binary q -tuples with mod 2 elementwise addition denoted hereafter as \wedge . Therefore, there is a one-to-one mapping $\psi_q : (GF(2))^q \rightarrow GF(2^q)$ defined as $\psi_q(a_0, \dots, a_{q-1}) = \sum_{k=0}^{q-1} a_k z^k$ such that $\psi_q(\mathbf{a}) \oplus \psi_q(\mathbf{b}) = \psi_q(\mathbf{a} \wedge \mathbf{b})$, where $\mathbf{a}, \mathbf{b} \in (GF(2))^q$. In addition, we index the elements $\rho_i \in GF(2^q)$, $i \in \{0, \dots, 2^q - 1\}$ by the base-10 notation of the corresponding binary tuple (a_0, \dots, a_{q-1}) . In the following we refer as *non-binary* symbols to the elements of the finite field $GF(2^q)$.

We consider a point-to-point scenario consisting of a binary unit-entropy information source \mathcal{S} , which generates blocks $\mathbf{U} \in \{0, 1\}^{2K}$. As depicted in Figure E.1, the sequence \mathbf{U} is divided into two sequences \mathbf{U}^1 and \mathbf{U}^2

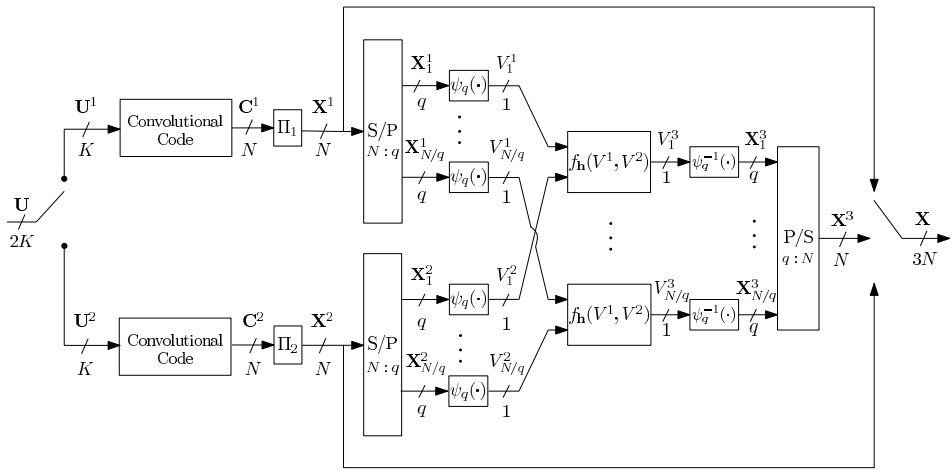


Figure E.1: Encoder associated to the proposed code.

of length K , which are channel-coded by a terminated convolutional code, producing the codewords $\mathbf{C}^m \triangleq \{C_t^m\}_{t=1}^N \in \{0,1\}^N$, with $m \in \{1,2\}$. Then, each codeword is interleaved yielding the interleaved codeword $\mathbf{X}^m = \Pi_m(\mathbf{C}^m)$, where Π_1 and Π_2 are two different spread interleavers with a spread factor equal to q . Next, each of the interleaved coded sequences \mathbf{X}^1 and \mathbf{X}^2 is split into q -length sub-sequences $\{\mathbf{X}_l^1\}_{l=1}^{N/q} \triangleq \{X_{l,1}^1, \dots, X_{l,q}^1\}_{l=1}^{N/q}$ and $\{\mathbf{X}_l^2\}_{l=1}^{N/q}$, respectively. We denote as $V_l^m = \psi_q(\mathbf{X}_l^m) \in GF(2^q)$ the non-binary symbol associated to the corresponding sub-sequence: the non-binary symbol V_l^3 is computed as the linear combination of the non-binary symbols V_l^1 and V_l^2 , i.e.

$$V_l^3 \triangleq \psi_q(\psi_q^{-1}(h^1 \otimes V_l^1) \wedge \psi_q^{-1}(h^2 \otimes V_l^2)) \triangleq f_{\mathbf{h}}(V_l^1, V_l^2), \quad (1)$$

where $\mathbf{h} = (h^1, h^2)$, $h^m \in \{\rho_i\}_{i=1}^{2^q-1}$ represents the coefficients used in the linear combination. Each sub-sequence \mathbf{X}_l^3 is computed from the associated non-binary symbols V_l^3 as $\mathbf{X}_l^3 = \psi_q^{-1}(V_l^3)$. In the following, we refer as Linear Combination (LC) code to the rate- $2/3$ code formed by the sub-codewords $(\mathbf{X}_l^1, \mathbf{X}_l^2, \mathbf{X}_l^3)$. Thus, there are N/q parallel LC codes. Finally, the sequence \mathbf{X}^3 is given by $\mathbf{X}^3 = \{\mathbf{X}_l^3\}_{l=1}^{N/q}$, and the final codeword $\mathbf{X} = \{X_t\}_{t=1}^{3N}$ is formed by $\mathbf{X} = (\mathbf{X}^1, \mathbf{X}^2, \mathbf{X}^3)$. Thus, the overall code rate is given by $2K/3N$.

Since the performance of short length convolutional codes improves when they are terminated (assuming bitwise MAP decoding), the proposed scheme uses independent source input sequences so that both convolutional codes can be terminated. However, to increase performance, a dependency between the output of the convolutional codes has to be introduced. This is the reason for using the linear combination step. Observe that if a convolutional code was used instead of the linear combination block for introducing this dependency (similar as in Turbo codes or in [2]), this code could not be terminated, leading to a performance degradation when using short-length codewords. Moreover, using a linear combination also permits a high and simple design flexibility, as shown later.

We apply unequal energy allocation between the sub-codewords associated to the terminated convolutional codes (\mathbf{X}^1 and \mathbf{X}^2) and the sub-codeword associated to the linear combination (\mathbf{X}^3). We denote as¹ $E_s^{cc} = E[(X^m)^2]$ the energy of the sub-codewords \mathbf{X}^1 and \mathbf{X}^2 , whereas $E_s^{lc} = E[(X^3)^2]$ and $\bar{E}_s = E[X^2]$ denote the energy of \mathbf{X}^3 and \mathbf{X} , respectively. Furthermore, without loss of generality, we assume $E_s^{lc} = \lambda E_s^{cc}$, with $\lambda > 0$ and define $\Lambda = 10 \log \lambda$ (dB). Thus, we have

$$E_s^{cc} = \frac{3}{2+\lambda} \bar{E}_s, \quad E_s^{lc} = \frac{3\lambda}{2+\lambda} \bar{E}_s. \quad (2)$$

This results in the modulated symbols $S_t = 2X_t - 1$, with $t = 1, \dots, 3N$, and average energy per symbol \bar{E}_s . The received symbol per real dimension at the receiver is given by $Y_t = S_t + N_t$, where $\{N_t\}_{t=1}^{3N}$ are modelled as real Gaussian i.i.d. random variables with zero mean and variance $N_0/2$.

A. Proposed Decoder

The destination receives the channel outputs $\mathbf{Y} = (\mathbf{Y}^1, \mathbf{Y}^2, \mathbf{Y}^3)$, where the subsequence \mathbf{Y}^j (with $j \in \{1, 2, 3\}$) represents the channel outputs associated to encoded symbols \mathbf{X}^j . The aim of the decoder is to estimate the source binary symbols $\widehat{\mathbf{U}} = (\{\widehat{U}_k^1\}_{k=1}^K, \{\widehat{U}_k^2\}_{k=1}^K)$ so that the conditional probability $P(u_k^m | \mathbf{y})$ ($m \in \{1, 2\}$) – which is obtained by marginalizing the joint conditional probability $P(\mathbf{u}^m | \mathbf{y})$ – is maximized. This marginalization is efficiently computed by applying the Sum-Product Algorithm (SPA, see [5]) to the factor graph describing $P(\mathbf{u}^m | \mathbf{y})$, which is shown in Figure E.2. Observe that such an overall factor graph is composed by three sub-factor graphs: two describing the convolutional codes, and a third one describing

¹ $E[\cdot]$ stands for expected value.

the LC code. Since this factor graph has loops, the SPA is iteratively run between the sub-factor graphs corresponding to the LC code and the convolutional codes. After a fixed number of iterations \mathcal{I} , the probability $P(u_k^m | \mathbf{y})$ based on which \widehat{U}_k^m is computed results proportional to

$$\sum_{\sim u_k^m} T_k(\mathbf{s}_k^m, u_k^m, \mathbf{c}_k^m, \mathbf{s}_{k+1}^m) \alpha(\mathbf{s}_k^m) \beta(\mathbf{s}_{k+1}^m) \prod_{t: c_t^m \in \mathbf{c}_k^m} \gamma(c_t^m),$$

where $\sim u_k^m \triangleq \{u_{k'}^m\}_{\forall k' \neq k}$; α and β are the messages passed from the adjacent state nodes to the factor node T_k given by the transitions in the Trellis describing the convolutional code; $\mathbf{c}_k^m = \{c_t^m\}_{t=(k-1)N/K}^{kN/K}$ (with $k \in \{1, \dots, K\}$) represents the coded bits associated to u_k^m ; and $\gamma(\cdot)$ are the likelihoods passed from the variable nodes c_t^m to T_k . These likelihoods depend on the messages passed by the LC-check nodes associated to the interleaved binary symbol $x_{\Pi_m^{-1}(t)}^m$, i.e. $\gamma(c_t^m) = \gamma(x_{\Pi_m^{-1}(t)}^m)$, where $\gamma(x_t^m) \propto p(\mathbf{y}_l | x_t^m)$ and $\mathbf{y}_l \triangleq (\mathbf{y}_l^1, \mathbf{y}_l^2, \mathbf{y}_l^3)$ (i.e. those components of \mathbf{Y} associated to the LC check node LC_l). It can be shown that such likelihoods can be further factorized as

$$\begin{aligned} p(\mathbf{y}_l | x_{l,i}^m) &= \sum_{\sim x_{l,i}^m, v_l^m} \mathbb{1}[v_l^m = \psi_q(x_{l,1}^m, \dots, x_{l,q}^m)] \cdot \\ &\quad p(\mathbf{y}_l^m | v_l^m) \prod_{i' \neq i} P^a(x_{l,i'}^m) P^{\text{LC}}(v_l^m), \end{aligned} \quad (3)$$

where $i \in \{1, \dots, q\}$, $\mathbb{1}[\cdot]$ is an indicator function taking value 1 if its argument is true and 0 otherwise, and

$$P^{\text{LC}}(v_l^m) \triangleq \sum_{v_l^m, v_l^3} \mathbb{1}[v_l^3 = f_{\mathbf{h}}(v_l^1, v_l^2)] p(\mathbf{y}_l^m | v_l^m) P^a(v_l^m) p(\mathbf{y}_l^3 | v_l^3), \quad (4)$$

with $\overline{m} = 3 - m$. Since the non-binary symbols can be also expressed by the modulated symbols $\{S_{l,i}^j\}_{i=1}^q \in \{\pm 1\}^q$ as

$$V_l^j = \psi_q \left(\left\{ (1 + S_{l,i}^j)/2 \right\}_{i=1}^q \right) \triangleq \theta_q \left(\{S_{l,i}^j\}_{i=1}^q \right),$$

we have that

$$p(\mathbf{y}_l^j | v_l^j) \propto \sum_{s_{l,1}^j, \dots, s_{l,q}^j} \mathbb{1}[v_l^j = \theta_q(s_{l,1}^j, \dots, s_{l,q}^j)] \prod_{i=1}^q \exp \left(\frac{-|y_{l,i}^j - s_{l,i}^j|^2}{N_0} \right). \quad (5)$$

In light of the above factorization, it is clear to see that the factor graph of the LC code is in turn composed of N/q parallel and identical sub-factor graphs LC_l , which are depicted, for $l = 1$ and $l = N/q$, in Figure E.2.

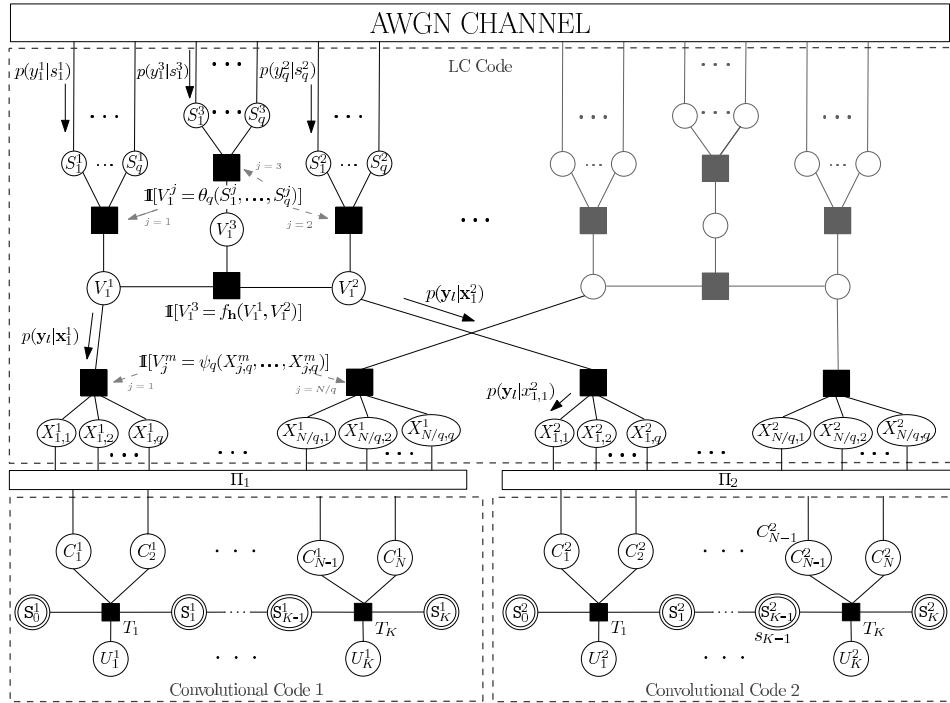


Figure E.2: Factor graph of the proposed decoder.

III. CODE ANALYSIS THROUGH EXIT CHARTS

The EXIT function of a code is defined as the relationship between the mutual information at the input of the decoder (commonly denoted as I_a) and the extrinsic mutual information I_e at its output, i.e. $I_e = T(I_a)$. For an iterative code, the chart plotting the transfer functions of the compounding sub-codes is called EXIT chart, and is known to be a powerful tool for designing and predicting the behavior of iterative codes [4].

We denote the transfer function of the LC-code for a given q and \mathbf{h} as $I_e^{\text{LC}} = T_{\mathbf{h}}^q(I_a^{\text{LC}})$. Notice, that for $I_a^{\text{LC}} = 0$ the value of $I_e^{\text{LC}} = T_{\mathbf{h}}^q(0)$ will also

depend on the Signal-to-Noise Ratio (SNR), since the channel observations \mathbf{y} are used by the LC-code (last term of (5) and Fig. E.2). As the mutual information at the input of the channel decoders I_a^{CC} is equal to I_e^{LC} , the extrinsic mutual information at the output of the convolutional decoders is given by $I_e^{\text{CC}} = T^{\text{CC}}(I_e^{\text{LC}})$. Thus, for a successful decoding procedure, there must be an open gap between both EXIT curves so that the iterative decoding can proceed from $I_e^{\text{CC}} = 0$ to $I_e^{\text{CC}} = 1$. When both transfer functions cross, the iterative process will stop at a given extrinsic mutual information of the source bits $I_e^{\text{CC}} < 1$.

Since the transfer functions are monotonically increasing functions, the higher the value of $T_{\mathbf{h}}^q(0)$ is, the smaller the required SNR to open a gap will be. On the other hand, if no crossing between curves has been produced, the higher the value of $T_{\mathbf{h}}^q(1)$ is, the closer I_e^{CC} will be to 1 yielding lower error floors (see Fig. E.3). Therefore, we are interested on having high values of both $T_{\mathbf{h}}^q(1)$ and $T_{\mathbf{h}}^q(0)$.

However, due to the Area Theorem of EXIT charts [4], which states that the area under the transfer function depends only on the rate of the encoder, it turns out that a high value of $T_{\mathbf{h}}^q(1)$ will yield a low value of $T_{\mathbf{h}}^q(0)$ and vice versa. Therefore, for a given q we select a \mathbf{h} that maximizes $T_{\mathbf{h}}^q(1) \cdot T_{\mathbf{h}}^q(0)$. The reason for such a choice is that we are interested in rejecting the \mathbf{hs} having very low values either of $T_{\mathbf{h}}^q(1)$ or $T_{\mathbf{h}}^q(0)$). For the sake of simplicity, this is done through exhaustive search over the $(q^2 - 1)^2$ possible values of \mathbf{h} .

Next, we justify the reason why the different linear combinations have a greater impact on the value of $T_{\mathbf{h}}^q(1)$ than on $T_{\mathbf{h}}^q(0)$. When $I_a^{\text{LC}} = 0$ all the information at the LC-Code comes equally from the channel observations associated to \mathbf{X}^1 , \mathbf{X}^2 and \mathbf{X}^3 . On the other hand, when $I_a^{\text{LC}} = 1$, only the information provided by the channel observations associated to \mathbf{X}^3 is relevant, as the information regarding \mathbf{X}^1 and \mathbf{X}^2 is fully supplied by the convolutional decoders.

Furthermore, variations on the unequal energy allocation parameter Λ are expected to affect to $T_{\mathbf{h}}^q(1)$ and $T_{\mathbf{h}}^q(0)$ similarly, given that Λ operates identically on \mathbf{X}^1 , \mathbf{X}^2 and \mathbf{X}^3 .

Figure E.3(a) shows that as q increases, the value of $T_{\mathbf{h}}^q(1)$ increases yielding lower error floors, but obtaining BER waterfall regions at higher SNRs. However, as shown in Fig. E.3(b), the tradeoff between the SNR at

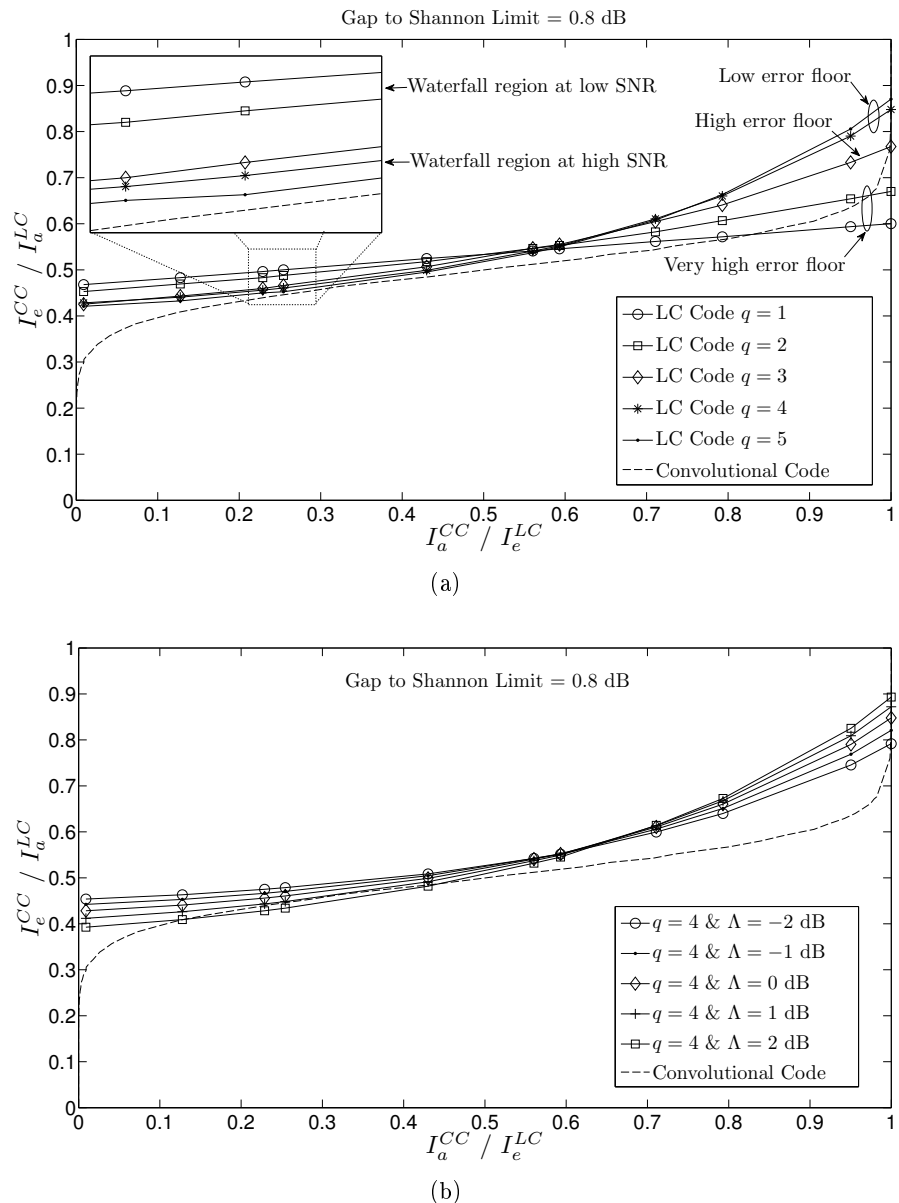


Figure E.3: EXIT Chart of different LC codes and a rate-1/2 Convolutional Code for different values of q (a) and Λ (b).

which waterfall regions occur and its associated BER floor can be balanced through the selection of Λ . By increasing Λ the value of $T_{\mathbf{h}}^q(1)$ is increased, leading to low error floors. However, the value of $T_{\mathbf{h}}^q(0)$ is decreased, hence obtaining BER waterfall regions at higher SNRs.

Finally, notice that for high values of q the tunnel is already opened at 0.8 dB from the Shannon Limit (see Section IV for its definition), in contrast to the 0.85 dB of [2, Figure 10], where unequal energy allocation is used for designing the codes. This implies that for large-length codewords both codes would have the waterfall region at similar SNRs.

IV. RESULTS

In order to assess the performance of the proposed code, several Monte Carlo simulations have been run using 6-memory-block $[554, 774]_8$ non-systematic rate-1/2 convolutional codes². The interleavers $\Pi_m(\cdot)$ have been randomly generated and are independent from each other. The source generates $2K = 648 + 2q$ information bits, then a 12-length zero-bit tail is appended in order to terminate both convolutional codes properly. We have considered binary unit-energy PAM modulation with transmitted blocks of $3N = 1980 + 6q$ real symbols. The dependency in q of the length of the sequences is imposed such that it is divisible by q , for all the considered qs . Note that the added bit tail reduces the overall spectral efficiency of the system to a spectral efficiency of $\rho = 2/3 - 8/N$ information bits per complex dimension. As benchmark, we show the gap (in dBs) between the performance of the proposed system and the limit given by Shannon for the AWGN channel, i.e. $10 \log_{10}(2^\rho - 1)$ in dB. Finally, $\mathcal{I} = 20$ iterations of the decoding algorithm have been considered and the decoding is stopped at every simulated SNR point when 100 errors have been obtained.

Figure E.4 plots the end-to-end Bit Error Rate (BER) of the system for different values of q and Λ . Observe that when Λ is set beyond a certain threshold, the waterfall region is produced at high SNRs and with no error floor detected in the simulations. On the other hand, for low values of Λ , waterfall regions at lower SNRs with higher error floors are obtain. This behavior was predicted by the EXIT charts in Section III, although it was performed for long-length sequences. Also observe that the system utilizing $q = 2$ is clearly outperformed by those using higher qs , as also predicted

²The subindex 8 in the definition of the code stands for *octal*.

by the EXIT charts due to the low values of $T_{\mathbf{h}}^q(1)$ resulting when $q = 2$ is chosen.

Also included in these plots are reference curves corresponding to the PEG, PEG-ACSE and PEG-ACE schemes analyzed in [10, Fig. 6], where 2000-symbol-length sequences are transmitted with a spectral efficiency of $\rho = 1$. Simulation results suggest that the proposed system will produce lower error floors than the irregular LDPC code proposed in [10] at a SNR waterfall degradation of less than 0.5 dB at $\text{BER} = 10^{-4}$ (e.g. see Fig. E.4(c), $\Lambda = 1$ dB). On the other hand, when the error floor is set to values around 10^{-6} , the performance loss at $\text{BER} = 10^{-4}$ with respect to [10] is negligible (e.g. see Fig. E.4(b), $\Lambda = -1$ dB or Fig. E.4(c), $\Lambda = -2, -3$ dB).

REFERENCES

- [1] C. Berrou, A. Glavieux, and P. Thitimajshima. Near Shannon Limit Error-Correcting Coding and Decoding: Turbo-Codes. In *1993 IEEE International Conference on Communications, ICC'93*, 1993.
- [2] F. Brännström, L. K. Rasmussen, and A. J. Grant. Optimal Puncturing Ratios and Energy Allocation for Multiple Parallel Concatenated Codes. *IEEE Transactions on Information Theory*, 55(5):2062–2077, May 2009.
- [3] R. Garello, F. Chiaraluce, P. Pierleoni, M. Scaloni, and S. Benedetto. On Error Floor and Free Distance of Turbo Codes. In *2001 IEEE International Conference on Communications, ICC'01*, June 2001.
- [4] J. Hagenauer. The EXIT Chart: Introduction to Extrinsic Information Transfer in Iterative Processing. In *2004 European Signal Processing Conference, EUSIPCO'04*, September 2004.
- [5] F.R. Kschischang, B.J. Frey, and H.-A. Loeliger. Factor graphs and the sum-product algorithm. *IEEE Transactions on Information Theory*, 47(2):498 –519, feb 2001.
- [6] J. W. Lee. Lower bound on BER of finite-length turbo codes based on EXIT characteristics. *IEEE Communications Letters*, pages 238–240, April 2004.

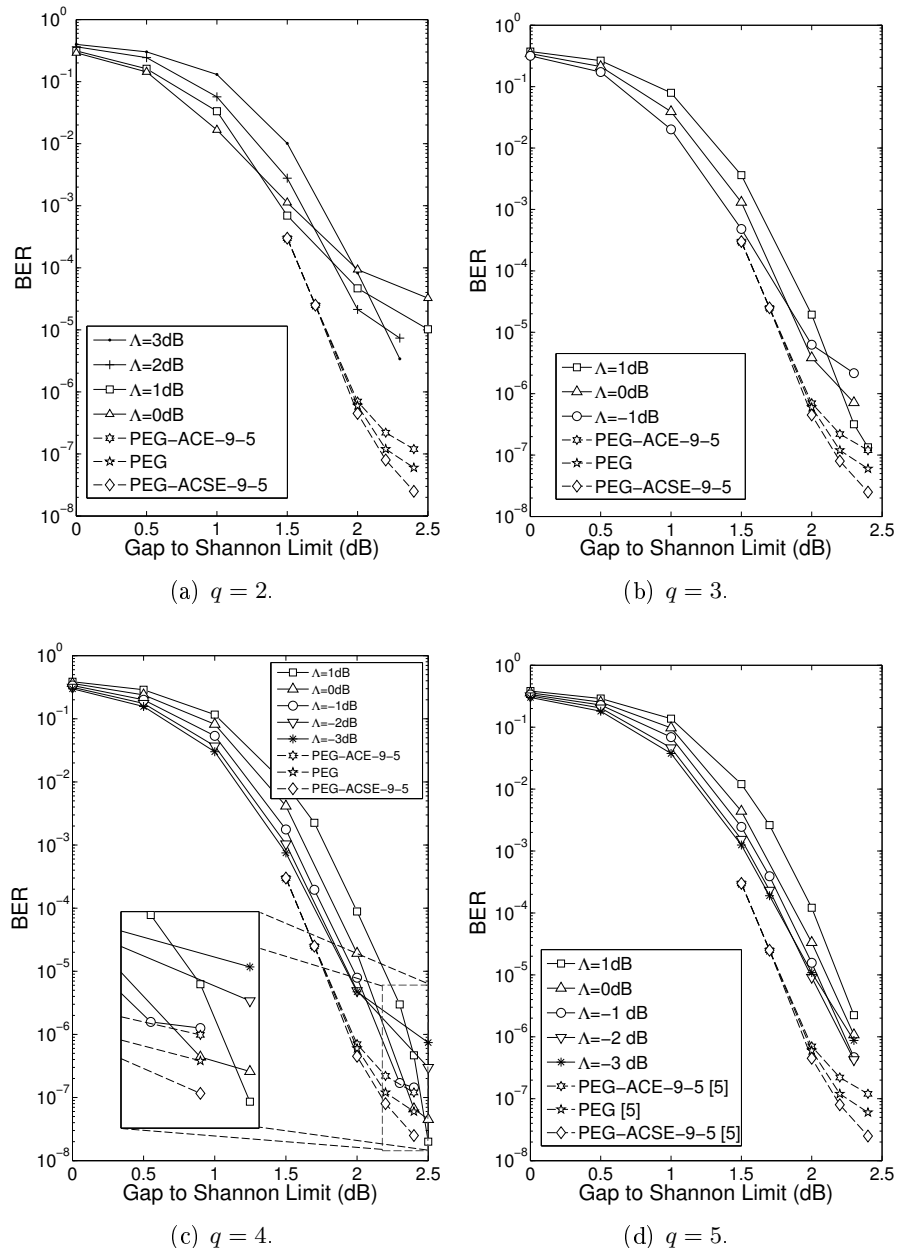


Figure E.4: BER performance of the proposed system with different values of q .

- [7] S. Pfletschinger and F. Sanzi. Error Floor Removal for Bit-Interleaved Coded Modulation with Iterative Detection. *IEEE Transactions on Wireless Communications*, 5:3174–3181, Nov. 2006.
- [8] T. Richardson. Error Floors of LDPC codes. In *Forty-first Annual Allerton Conference on Communication, Control, and Computing, Allerton'03*, October 2003.
- [9] T. J. Richardson and R. Urbanke. The capacity of low-density parity-check codes under message-passing decoding. *IEEE Transactions on Information Theory*, 47:599–618, Feb. 2001.
- [10] X. Zheng, F. C. M. Lau, and C. K. Tse. Constructing Short-Length Irregular LDPC Codes with Low Error Floor. *IEEE Transactions on Communications*, 58(10):2823–2834, October 2010.

APPENDIX F

Derivation of the outage probability of the TD-DF-MARC

Through this appendix we will derive the outage probability used as a benchmark in Papers I and II. Let us first start by reviewing the cut-set bounds for the Constrained-MARC with DF relaying strategy (C-DF-MARC) derived by Sankar et al. in [SKM04]

F.1 CUT-SET BOUNDS FOR THE C-DF-MARC

As defined in [SKM04], a 2-user-C-MARC is a MARC where the relay receives information from both sources (namely, \mathbf{X}^1 and \mathbf{X}^2) for a fraction α of the total time N and it is transmitting for the remaining fraction $\bar{\alpha} = 1 - \alpha$. One can view this channel as having two states: the relay is in the *receive* state for $t = 1, \dots, N_r$ symbols and in the *transmit* state for the remaining $t = N_r + 1, \dots, N$ symbols, where $N_r/N = \alpha$. The C-DF-MARC is a C-MARC where the relay decodes and forwards the messages from the source, and the sources do not send new information during the *transmit* state. Rather, they simply cooperate with the relay to aid the destination in decoding the message sent in the *receive* state. Figure F.1 shows the considered C-DF-MARC.

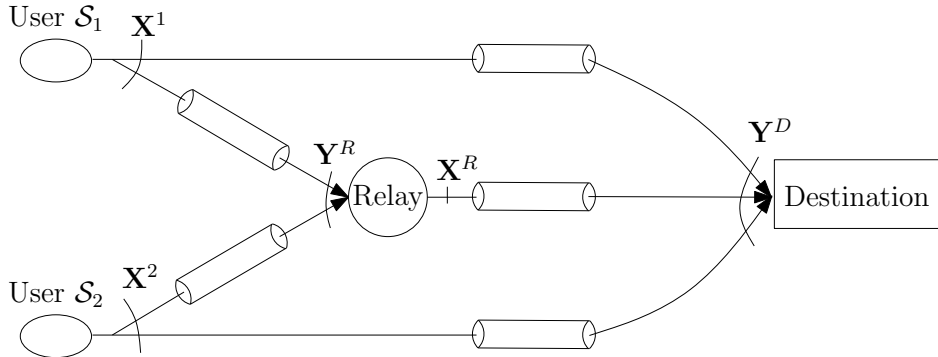


Figure F.1: 2-user C-DF-MARC

The output signals for a Gaussian C-DF-MARC are

$$Y_t^R = X_t^1 + X_t^2 + Z_t^R \quad (1)$$

$$Y_t^D = X_t^1 + X_t^2 + Z_t^D \quad (2)$$

in the *receive* state (i.e. $t = 1, \dots, N_r$), where Z_t is as defined in Chapter 2, Section 2.1. While in the *transmit* state (i.e. $t = N_r + 1, \dots, N$) we have

$$Y_t^R = 0 \quad (3)$$

$$Y_t^D = X_t^1 + X_t^2 + X_t^R + Z_t^D. \quad (4)$$

Finally, by defining $R_i = K_i/N$ [information bits per multiple-access relay channel use], with $i \in \{1, 2\}$, the resulting cut-set bounds can be obtained from the sum-rate bound of the 2-user DF-C-MARC given in [SKM04] as

$$R_1 \leq \max_{\alpha} \min \left(\begin{array}{c} \alpha I(X_1; Y_R | X_2), \\ \alpha I(X_1; Y_D | X_2) + \bar{\alpha} I(X_1 X_R; Y_D | X_2) \end{array} \right) \quad (5)$$

$$R_2 \leq \max_{\alpha} \min \left(\begin{array}{c} \alpha I(X_2; Y_R | X_1), \\ \alpha I(X_2; Y_D | X_1) + \bar{\alpha} I(X_2 X_R; Y_D | X_1) \end{array} \right) \quad (6)$$

$$R_1 + R_2 \leq \max_{\alpha} \min \left(\begin{array}{c} \alpha I(X_1 X_2; Y_R), \\ \alpha I(X_1 X_2; Y_D) + \bar{\alpha} I(X_1 X_2 X_R; Y_D) \end{array} \right). \quad (7)$$

F.2 CUT-SET BOUNDS FOR THE TD-DF-MARC

As proposed in [Hau08], for deriving the cut-set bounds for the TD-DF-MARC we based on assuming two C-DF-MARCs (namely, C-DF-MARC1 and C-DF-MARC2), which transmit in parallel. Then, some transmission are neglected such that we obtain our TD-DF-MARC model. In other words, the assumed parallel C-DF-MARC results in a four-time-phases MARC model, and then by neglecting some of the transmissions, the three orthogonal time slots of the TD-DF-MARC can be obtained.

Let us now define both C-DF-MARCs: C-DF-MARC1 transmits a total of $N^{(1)}$ symbols in the following manner. User 1 transmits $N_r^{(1)}$ symbols during the *receive* state, whereas the rest of the transmissions are neglected. Hence, the output signals in the *receive* state (i.e. $t = 1, \dots, N_r^{(1)}$) are

$$Y_t^R = X_t^1 + Z_t^R \quad (8)$$

$$Y_t^D = X_t^1 + Z_t^D. \quad (9)$$

While those in the transmit state (i.e. $t = N_r^{(1)} + 1, \dots, N^{(1)}$) are

$$Y_t^R = 0 \quad (10)$$

$$Y_t^D = 0. \quad (11)$$

Recalling that $K_1^{(1)} = R_1^{(1)} N^{(1)}$, for a fixed value of $N^{(1)}$ (i.e. a fixed value of $\alpha = N_r^{(1)}/N^{(1)}$), in this particular case the bounds (5)-(7) result to be

$$K_1^{(1)} \leq \min \left(\begin{array}{l} N_r^{(1)} I(X_1; Y_R), \\ N_r^{(1)} I(X_1; Y_D) \end{array} \right) \quad (12)$$

$$K_2^{(1)} = 0 \quad (13)$$

$$K_1^{(1)} + K_2^{(1)} \leq \min \left(\begin{array}{l} N_r^{(1)} I(X_1; Y_R), \\ N_r^{(1)} I(X_1; Y_D) \end{array} \right). \quad (14)$$

On the other hand, C-DF-MARC2 transmits a total of $N^{(2)}$ symbols in the following manner. During the *receive* phase, user 2 transmits $N_r^{(2)}$ symbols, while in the *transmit* phase just the relay transmits $N_r^{(2)} = N^{(2)} - N_r^{(2)}$ symbols. Thus, the output signals in the *receive* state (i.e. $t' = 1, \dots, N_r^{(2)}$) are

$$Y_{t'}^R = X_{t'}^2 + Z_{t'}^R \quad (15)$$

$$Y_{t'}^D = X_{t'}^2 + Z_{t'}^D. \quad (16)$$

While those in the *transmit* state (i.e. $t' = N_r^{(2)}, \dots, N^{(2)}$) are

$$Y_{t'}^R = 0 \quad (17)$$

$$Y_{t'}^D = X_{t'}^R + Z_{t'}^D. \quad (18)$$

Analogously as done for the C-DF-MARC1, the resulting cut-set bounds for the C-DF-MARC2 are

$$K_1^2 \leq \min \left(\begin{array}{l} 0, \\ N_R I(X_R; Y_D) \end{array} \right) \quad (19)$$

$$K_1^{(2)} \leq \min \left(\begin{array}{l} N_r^{(2)} I(X_2; Y_R), \\ N_r^{(2)} I(X_2; Y_D) + N_R I(X_R; Y_D) \end{array} \right) \quad (20)$$

$$K_2^{(2)} + K_2^{(2)} \leq \min \left(\begin{array}{l} N_r^{(2)} I(X_2; Y_R), \\ N_r^{(2)} I(X_2; Y_D) + N_t^{(2)} I(X_R; Y_D) \end{array} \right), \quad (21)$$

where $K_i^{(2)} = R_i^{(2)} N^{(2)}$, with $i \in \{1, 2\}$.

For the sake of notation, we rename $N_r^{(1)}$, $N_r^{(2)}$ and $N_\tau^{(2)}$ as N_1 , N_2 and N_R , respectively. Finally, by summing the corresponding cut-set bounds of each of the C-DF-MARCs we get the cut-set bounds of the TD-DF-MARC,

$$K_1 \leq \min \left(\begin{array}{l} N_1 I(X_1; Y_R), \\ N_1 I(X_1; Y_D) + N_R I(X_R; Y_D) \end{array} \right) \quad (22)$$

$$K_2 \leq \min \left(\begin{array}{l} N_2 I(X_2; Y_R), \\ N_2 I(X_2; Y_D) + N_R I(X_R; Y_D) \end{array} \right) \quad (23)$$

$$K_1 + K_2 \leq \min \left(\begin{array}{l} N_1 I(X_1; Y_R) + N_2 I(X_2; Y_R), \\ N_1 I(X_1; Y_D) + N_2 I(X_2; Y_D) + N_R I(X_R; Y_D) \end{array} \right), \quad (24)$$

where $K_i = K_i^{(1)} + K_i^{(2)}$, with $i \in \{1, 2\}$. Consequently, the data transmitted by the sources can be recovered at the destination with vanishing error probability if the above inequalities hold.

F.3 OUTAGE PROBABILITY DERIVATION

Let us now consider the particular channel given in Chapter 2, Equation (2.18). We denote by SNR_{iR} , SNR_{iD} (with $i \in \{1, 2\}$) and SNR_{RD}

to the mean signal-to-noise ratio at the sources-relay, sources-destination and relay-destination channels output, respectively. And we refer to γ_{1R} , γ_{2R} , γ_{1D} , γ_{2D} and γ_{RD} as the instantaneous SNRs at the respective channel outputs. The latter result from the product of a realization of a Rayleigh fading with the mean signal-to-noise ratio and the path-loss of the channel (see Chapter 2, Section 2.4). Finally we consider that the inputs of the compounding point-to-point channels are Gaussian distributed, yielding $I(X_i, Y_j) = C(\gamma_{i,j})$, with $i \in \{1, 2, R\}$, $j \in \{R, D\}$ and $C(\cdot)$ being the channel capacity given in information bits per complex dimension as defined in Chapter 2, Equation (2.21).

Substituting the above into (22)-(24), the total transmitted data can be reliably decoded at the destination, if the following inequalities hold:

$$K_1 \leq N_1 C(\gamma_{1R}) \quad (25)$$

$$K_2 \leq N_2 C(\gamma_{2R}) \quad (26)$$

$$K_1 + K_2 \leq N_1 C(\gamma_{1R}) + N_2 C(\gamma_{2R}) \quad (27)$$

$$K_1 \leq N_1 C(\gamma_{1D}) + N_R C(\gamma_{RD}) \quad (28)$$

$$K_2 \leq N_2 C(\gamma_{2D}) + N_R C(\gamma_{RD}) \quad (29)$$

$$K_1 + K_2 \leq N_1 C(\gamma_{1D}) + N_2 C(\gamma_{2D}) + N_R C(\gamma_{RD}). \quad (30)$$

Observe that (25)-(27) correspond to the cut-set bound of the multiple-access channel formed by the sources and the relay. Hence, this three conditions will be omitted when perfect decoding at the relay is assumed. Conditions (28)-(29) correspond to the set of links that completely cut each source from the sink, and condition (30) refers to the set of links that completely cut both sources from the sink. In addition, when error detection is available at the relay node, a reliable communication can also be established if the follow inequalities hold:

$$K_1 \leq N_1 C(\gamma_{1D}) \quad (31)$$

$$K_2 \leq N_2 C(\gamma_{2D}). \quad (32)$$

Due to the fading environment, the above point-to-point capacities $C(\gamma_{i,j})$ are random variables depending on their respective instantaneous signal-to-noise ratios. Therefore, the inequalities (25)-(32) may or may not hold depending on the instantaneous values of the fading random variables associated to each point-to-point channel. We say that the system is in outage

(or that the event OUT has occurred) if the destination cannot reliably decode the data transmitted by the sources, i.e. some inequalities do not hold.

For example, in case of assuming perfect decoding at the relay, an outage will occur when the events: i) none or more of the inequalities (28)-(30) fail to hold, and the event: ii) one or more of the inequalities (31)-(32) fail to hold, both happen together. Therefore, in case of assuming perfect decoding at the relay the event of not being in outage is given by

$$\begin{aligned} \overline{OUT} = & \left\{ \left([K_1 \leq N_1 C(\gamma_{1D}) + N_R C(\gamma_{RD})] \cap [K_2 \leq N_2 C(\gamma_{2D}) + N_R C(\gamma_{RD})] \right. \right. \\ & \cap [K_1 + K_2 \leq N_1 C(\gamma_{1D}) + N_2 C(\gamma_{2D}) + N_R C(\gamma_{RD})] \left. \right) \cup \\ & \left. \cup ([K_1 \leq N_1 C(\gamma_{1D})] \cap [K_2 \leq N_2 C(\gamma_{2D})]) \right\}. \quad (33) \end{aligned}$$

And the outage probability of the system is given by

$$\mathcal{P}\{OUT\} = 1 - \mathcal{P}\{\overline{OUT}\}. \quad (34)$$

APPENDIX G

Publications

INTERNATIONAL JOURNALS

- **M. Hernaez**, P. M. Crespo, J. Del Ser, "A Decode-and-Forward Scheme for Multihop Wireless Networks". *Springer Wireless Networks*, submitted 2012.
- **M. Hernaez**, P. M. Crespo, J. Del Ser, "A Flexible Channel Coding Approach for Short-Length Codewords". *IEEE Communications Letters*, in second review 2012.
- **M. Hernaez**, P. M. Crespo, J. Del Ser, "On the Design of a Novel Joint Network-Channel Coding Scheme for the Multiple Access Relay Channel". *IEEE Journal on Selected Areas in Communications*, accepted for publication, 3rd quarter 2012.
- **M. Hernaez**, P. M. Crespo, J. Del Ser, J. Garcia-Frias, "Serially-Concatenated LDGM Codes for Correlated Sources over Gaussian Broadcast Channels". *IEEE Communications Letters*, Vol 13, No. 10, 788-790, October 2009.
- **M. Hernaez**, P. M. Crespo, J. Del Ser, J. Garcia-Frias, "Erratum to Serially-Concatenated LDGM Codes for Correlated Sources over Gaussian Broadcast Channels", *IEEE Communications Letters*, Vol 14, No. 03, 235-235, March 2010.

- I. Alustiza, **M. Hernaez**, X. Insasusti, P.M. Crespo, "Teaching Information Theory via a Simulation Tool for Communications Systems", *IEEE Transactions on Education*, to be submitted 2012.
- I. Ochoa, P. Crespo, J. Del Ser and **M. Hernaez**, "Turbo Joint Source-Channel Coding of Non-Uniform Memoryless Sources in the Bandwidth-Limited Regime", *IEEE Communications Letters*, Vol. 14, No. 04, April 2010.
- I. Ochoa, P. Crespo and **M. Hernaez**, "LDPC Codes for Non-Uniform Memoryless Sources and Unequal Energy Allocation", *IEEE Communications Letters*, Vol. 14, No. 09, Sept. 2010.

INTERNATIONAL CONFERENCES

- **M. Hernaez**, P. Crespo and J. Del Ser, "Joint Non-Binary LDPC-BICM and Network Coding with Iterative Decoding for the Multiple Access Relay Channel", *2011 IEEE Vehicular Technology Conference*, Budapest (Hungary), May 2011.
- **M. Hernaez** and P. Crespo, "A Novel Scheme for Message-Forwarding in Multi-Hop Ad-Hoc Wireless Networks", *2011 IEEE Vehicular Technology Conference*, Budapest (Hungary), May 2011.
- I. Ochoa, P. Crespo, J. Del Ser and **M. Hernaez**, "Turbo Joint Source-Channel Coding of Cycle-Stationary Sources in the Bandwidth-Limited Regime", *The 2nd International Conference on Mobile Light-weight Wireless Systems (MOBILIGHT)*, Barcelona (Spain), May 2010.

NATIONAL CONFERENCES

- **M. Hernaez**, P. Crespo, J. Del Ser and I. Ochoa, "Códigos LDGM concatenados para la transmisión de fuentes correlacionadas para canales de difusión", *XXIV National Assembly of the International Union of Radio Science (URSI)*, Santander (Spain), September 2009.

Serially-Concatenated LDGM Codes for Correlated Sources
over Gaussian Broadcast Channels

M. Hernaez, P. M. Crespo, J. Del Ser and J. Garcia-Frias,
IEEE Communications Letters, Vol 13, No. 10, 788-790,
October 2009

Serially-Concatenated LDGM Codes for Correlated Sources over Gaussian Broadcast Channels

Mikel Hernaez, Pedro Crespo, Senior Member, IEEE, Javier Del Ser, and Javier Garcia-Frias, Senior Member, IEEE

Abstract—We propose a superposition scheme, based on the use of serially-concatenated LDGM codes, for the transmission of spatially correlated sources over Gaussian broadcast channels. The messages intended for each receiver are independently encoded using the same code. In this manner, a strong degree of correlation is kept between the encoded sequences, which are then modulated with different energies and symbolwise added. By properly designing the encoding process, simulation results show that our proposed scheme easily outperforms the suboptimal theoretical limit assuming separation between source and channel coding.

Index Terms—Gaussian broadcast channel, superposition coding, correlated sources, concatenated LDGM codes.

I. INTRODUCTION

IN THE Gaussian broadcast channel, first proposed in [1] and further studied in [2], the messages $w_1 \in \{1, 2, \dots, 2^{nR_1}\}$ and $w_2 \in \{1, 2, \dots, 2^{nR_2}\}$ generated by two information terminals with rates R_1 and R_2 , are encoded by using a single transmitted signal and sent over two AWGN channels to their corresponding receivers. This channel can be modeled as $Y_1 = X + N_1$ and $Y_2 = X + N_2$, where X denotes its input, Y_1 and Y_2 the corresponding outputs, and N_1 and N_2 are arbitrary correlated Gaussian random variables with variances σ_1^2 and $\sigma_2^2 = \beta\sigma_1^2$. Without loss of generality we will assume $\beta > 1$.

It is well known that the Gaussian broadcast channel belongs to the class of degraded broadcast channels, and its capacity is given by [2]

$$R_1 \leq \frac{1}{2} \log_2 \left(1 + \frac{\alpha E_c}{\sigma_1^2} \right), \quad R_2 \leq \frac{1}{2} \log_2 \left(1 + \frac{(1-\alpha)E_c}{\alpha E_c + \sigma_2^2} \right), \quad (1)$$

where $0 \leq \alpha \leq 1$ may be arbitrarily chosen to trade rate R_1 for R_2 as the transmitter wishes. To encode the messages, the optimum transmitter for independent sources [2], usually referred to as *superposition* scheme, generates two codebooks: one with average energy per symbol αE_c at rate R_1 , and another with energy $(1-\alpha)E_c$ at rate R_2 . Then, in order to send messages $w_1 \in \{1, 2, \dots, 2^{nR_1}\}$ and $w_2 \in \{1, 2, \dots, 2^{nR_2}\}$ to receivers 1 (Y_1) and 2 (Y_2), the transmitter takes a codeword $\mathbf{X}(w_1)$ from the first codebook and a codeword $\mathbf{X}(w_2)$ from the second codebook, and computes the sum $\mathbf{X} = \mathbf{X}(w_1) + \mathbf{X}(w_2)$ before sending it over the channel.

Manuscript received June 17, 2009. The associate editor coordinating the review of this letter and approving it for publication was V. Stankovic.

M. Hernaez and P. M. Crespo are with the Centro de Estudios e Investigaciones Técnicas de Gipuzkoa (CETI) and TECNUN (University of Navarra), 20009 San Sebastian, Spain (e-mail: {mhernaez, pcrespo}@ceit.es).

J. Del Ser is with TECNALIA-Robotiker, 48170 Zamudio, Spain (e-mail: jdelser@robotiker.es).

J. Garcia-Frias is with the University of Delaware, Newark, DE 19716, USA (e-mail: jgarcia@ee.udel.edu).

Digital Object Identifier 10.1109/LCOMM.2009.091289

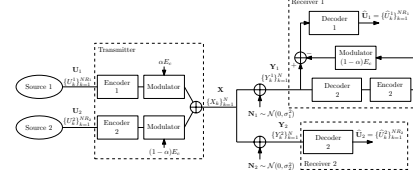


Fig. 1. Superposition scheme for the Gaussian broadcast channel.

In the decoding, the receiver associated to the channel Y_2 with higher noise variance σ_2^2 (hereafter *bad* receiver) looks through the second codebook to find the closest codeword to the receiver vector $\mathbf{Y}_2 = \mathbf{X} + \mathbf{N}_2$. Its effective Signal to Noise Ratio (SNR) is $(1-\alpha)E_c/(\alpha E_c + \sigma_2^2)$, since $\mathbf{X}(w_1)$ acts as a noise. On the other hand, the *good* receiver (i.e. that associated to Y_1) first decodes and reconstructs the codeword $\mathbf{X}(w_2)$ as $\hat{\mathbf{X}}(w_2)$, which can be accomplished due to its lower noise variance σ_1^2 . Then it subtracts this codeword from $\mathbf{Y}_1 = \mathbf{X} + \mathbf{N}_1$, and finally looks for the codeword in the first codebook closest to $\mathbf{Y}_1 - \hat{\mathbf{X}}(w_2)$.

In this context, several papers (e.g. [3], [4]) have presented practical superposition schemes for independent sources which outperform orthogonal schemes (i.e. time or frequency division multiplexing). However, in dense communication networks (e.g. sensor networks), the physical proximity between nodes leads to a certain degree of correlation between the data registered by the sensors. This correlation should be exploited in reception in order to improve the performance of the communication system. Based in recent results on the correlation-preserving properties of Serially-Concatenated Low-Density Generator Matrix Codes, (SC-LDGM [5], [6], [7]), this letter proposes the use of such codes for the transmission of spatially correlated sources through the Gaussian broadcast channel.

II. PROPOSED SYSTEM

The proposed transmission system is depicted in Figure 2. It is assumed that the spatially correlated multiterminal source $\{U_k^1, U_k^2\}_{k=1}^\infty$ is a sequence of independent and identically distributed pairs of binary random variables with distributions $Pr(U_k^1 = 0) = Pr(U_k^2 = 0) = 0.5$ and $Pr(U_k^1 \neq U_k^2) = p \ll 0.5$. Furthermore, the source symbols U_k^1 and U_k^2 are intended for the *good* and *bad* receiver, respectively. Terminal 1 and terminal 2 forms blocks $\mathbf{U}_1 = \{U_k^1\}_{k=1}^K$ and $\mathbf{U}_2 = \{U_k^2\}_{k=1}^K$ of K symbols, before being processed through two separated identical systematic SC-LDGM codes. Let \mathbf{C}_1 and \mathbf{C}_2 denote the corresponding output codewords, consisting of the systematic bits $C_n^i = U_n^i$ (for $n = 1, \dots, K$ and $i \in \{1, 2\}$), and the coded (parity) bits $\{C_n^i\}_{n=K+1}^N$. The

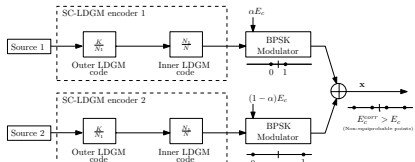


Fig. 2. Proposed transmitter for the Gaussian broadcast channel.

reason for using this kind of binary block codes is to preserve, as much as possible, the existing correlation between \mathbf{U}_1 and \mathbf{U}_2 into the output codewords \mathbf{C}_1 and \mathbf{C}_2 .

More specifically, a rate K/N systematic LDGM code is a linear binary code with generator matrix $\mathbf{G} = [\mathbf{I} \mathbf{P}]$, where \mathbf{I} denotes the identity matrix of order K , and \mathbf{P} is a $K \times (N-K)$ sparse matrix. A systematic SC-LDGM code is then built by concatenating two LDGM codes of rates K/N_1 and N_1/N , where the outer code has a rate close to 1 (i.e. $N_1 \approx K$). As in [5], [6], we will denote as (θ, ϑ) LDGM codes those codes in which all the K systematic bit nodes have degree θ , and each of the $N - K$ coded nodes has degree ϑ . In other words, the parity matrix \mathbf{P} of an (θ, ϑ) LDGM code has exactly θ non-zero entries per row and ϑ non-zero entries per column. In the proposed system, the same generator matrices have been used for both encoders. As already mentioned, the advantage of using this type of code is to keep the spatial correlation between the codewords associated to the messages sent by the spatially correlated multiterminal source. This fact is obvious for the systematic part of the codewords. Regarding the parity part of the codewords, it can be shown [7] that the probability for two parity bits, located at the same position in the corresponding two codewords, of being different is

$$p_c = \frac{1 - (1 - 2p)^\vartheta}{2}, \quad (2)$$

where p and ϑ have been previously defined. For very small values of p , (2) can be approximated as $p_c \approx \vartheta p$. Therefore, by choosing a small ϑ , the spatial correlation in the parity part of the codewords \mathbf{C}_1 and \mathbf{C}_2 can be preserved.

Before being added to form the transmitted symbol X_k , the encoded binary symbols C_k^1 and C_k^2 at the output of the two encoders are BPSK modulated to yield $X_k^1 = \sqrt{\alpha E_c} (2C_k^1 - 1)$ and $X_k^2 = \sqrt{(1 - \alpha) E_c} (2C_k^2 - 1)$. Notice that, due to the high level of correlation between C_k^1 and C_k^2 , the modulated symbols X_k^1 and X_k^2 will be added coherently with high probability¹. This in turn will improve the detection of the codewords at the corresponding receivers. The downside of this coherent addition is that the actual energy per symbol E_c^{corr} sent over the broadcast channel increases, since X_k^1 and X_k^2 are no longer independent. It can be easily shown that $E_c^{corr} = E_c(1 + \Delta_{exc})$, where

$$\Delta_{exc} = R_c \Delta_{sys} + (1 - R_c) \Delta_{par}, \quad (3)$$

$$\Delta_{sys} = (1 - 2p) 2 \sqrt{\alpha(1 - \alpha)}, \quad (4)$$

$$\Delta_{par} = (1 - 2p_c) 2 \sqrt{\alpha(1 - \alpha)}, \quad (5)$$

¹Probabilities $(1 - p)$ and $(1 - p_c)$ for the systematic and parity symbols, respectively.

with overall code rate $R_c = K/N$, and Δ_{sys} and Δ_{par} representing the excess energy fraction of the systematic and the parity symbols. In the above expression, the parity symbols introduced by the outer code have been neglected for two reasons: (i) as the outer rate is close to one, the outer parity symbols represent a small fraction of the transmitted codeword, and (ii) the number of ones per row in the outer parity-check matrix \mathbf{H} is considerably high (e.g. $\vartheta \approx 76$ in our simulations), thus the correlation is not preserved in these symbols.

III. DECODING PROCESS

The decoding procedure to estimate $\{U_k^1\}$ and $\{U_k^2\}$ at the corresponding receivers is based on the Sum-Product Algorithm (SPA) applied to the factor graphs that models the SC-LDGM codes [8]. These factor graphs are modified to take into account the existing correlation between terminals.

We begin by analyzing the decoding process of the *bad* receiver. An estimation of \mathbf{U}_2 , denoted as $\hat{\mathbf{U}}_2$, is obtained by applying the SPA algorithm over the graph of the SC-LDGM code (\mathcal{I} iterations over the inner code followed by \mathcal{T} iterations over the outer code). The *a priori* probabilities of the symbols U_k^2 are kept unchanged to 0.5, while the conditional channel probabilities $p(y_k^2|c_k^2)$ required by the factor graph are given by

$$p(y_k^2|c_k^2) = \begin{cases} (1 - p_{cor})f_{00} + p_{cor}f_{10} & \text{if } c_k^2 = 0, \\ (1 - p_{cor})f_{11} + p_{cor}f_{01} & \text{if } c_k^2 = 1, \end{cases} \quad (6)$$

where $p_{cor} = p$ for the channel symbols associated to the systematic part of the codeword, and $p_{cor} = p_c$ for those associated to the parity symbols of the codeword. The probability density functions f_{ij} are defined as

$$f_{ij} \triangleq \mathcal{N}\left((2i - 1)\sqrt{(1 - \alpha)E_c} + (2j - 1)\sqrt{\alpha E_c}, \sigma_2^2\right), \quad (7)$$

where $\mathcal{N}(\rho, \sigma^2)$ denotes a Gaussian probability density function with mean ρ and variance σ^2 . Hence, the correlation between sources is exploited in this receiver not as *side information* (the *a priori* probabilities of U_k^2 are unmodified), but intrinsically in the channel conditional probabilities used by the decoder.

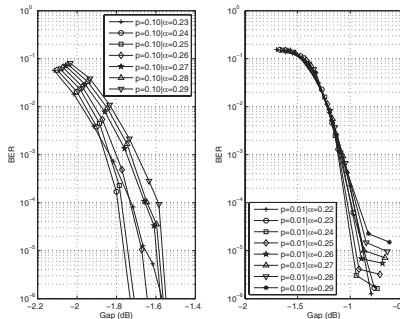
As explained in Section I, the *good* receiver first decodes the *bad* receiver's codeword \mathbf{C}_2 ($\sigma_1^2 \leq \sigma_2^2$) and then, after an appropriate scaling, subtracts it from the received signal, i.e. $\mathbf{Y}_1 - \sqrt{(1 - \alpha)E_c}\mathbf{C}_2$. Based on this sequence, and having an effective signal to noise ratio $\alpha E_c / \sigma_1^2$, the receiver obtains an estimation $\hat{\mathbf{U}}_1$ for \mathbf{U}_1 . In this case the *a priori* probabilities of the symbols U_k^1 are modified by the *a posteriori* probabilities of the symbols U_k^2 , introduced here as *side information*, i.e.

$$p(u_k^1) = p(u_k^1|u_k^2 = 0)p(u_k^2 = 0) + p(u_k^1|u_k^2 = 1)p(u_k^2 = 1),$$

where $p(u_k^1|u_k^2) = 1 - p$ if $u_k^1 = u_k^2$ and $p(u_k^1|u_k^2) = p$ if $u_k^1 \neq u_k^2$. On the other hand, the conditional channel probabilities are now given by $\mathcal{N}(\sqrt{\alpha E_c}, \sigma_1^2)$.

IV. SIMULATION RESULTS

In order to assess the performance of the proposed system, Monte Carlo simulations have been performed for different values of p and scale factor α . A serially-concatenated LDGM code has been used for both terminals, composed by a (4, 76)

Fig. 3. Gap to the separation limit for $p = 0.1$ (left) and $p = 0.01$ (right).

regular outer LDGM code and a (14, 7) regular inner LDGM code. The resulting overall code rate is $R_c \approx 0.316$. The input block size for all the simulations is kept fixed to $K = 9500$, and $\mathcal{I} = 100$ iterations have been considered for the decoding algorithm. The ratio between σ_2^2 and σ_1^2 is set to $\beta = 3$.

In order to define a point of reference, we will compare the E_c/σ_1^2 obtained by the proposed system with the one rendered by the theoretical limit when the suboptimal scheme based on separation between source and channel coding is considered. Specifically, since the *good* receiver can decode both messages (as opposed to the *bad* receiver), \mathbf{U}^1 would be compressed to $H(\mathbf{U}^1|\mathbf{U}^2)$ bits per source symbol, while \mathbf{U}^2 to its entropy $H(\mathbf{U}^2)$. Considering the same total rate R_c for both separated source-channel codes, the separation-achievable minimum E_c/σ_1^2 is obtained by using equality in expressions (1), and substituting R_1 and R_2 by $R_c H(\mathbf{U}^1|\mathbf{U}^2)$ and $R_c H(\mathbf{U}^2)$, respectively. By solving this system of equations, one obtains

$$\left[\frac{E_c}{\sigma_1^2} \right]_{\min} = \frac{2^{2R_c H(\mathbf{U}^1|\mathbf{U}^2)} - 1}{\alpha_*}, \quad (8)$$

with α_* given by

$$\alpha_* = \frac{2^{2R_c H(\mathbf{U}^1|\mathbf{U}^2)} - 1}{\beta (2^{2R_c H(\mathbf{U}^2)} - 1) - 2^{2R_c H(\mathbf{U}^2)} + 2^{2R_c H(\mathbf{U}^1|\mathbf{U}^2)}}, \quad (9)$$

where, from our multiterminal source assumption, we have that $H(\mathbf{U}^2) = 1$ and $H(\mathbf{U}^1|\mathbf{U}^2) = H(p)$, i.e. the entropy of a binary random variable with distribution $(p, 1-p)$.

Figure 3 plots the Bit Error Rate (BER), computed by averaging the BER at both receivers, versus the gap in dB to the separation-based limit for $p = 0.1$ (left) and $p = 0.01$ (right). That is,

$$\text{Gap} = 10 \log_{10} \frac{E_c^{\text{corr}}}{\sigma_1^2} - 10 \log_{10} \left[\frac{E_c}{\sigma_1^2} \right]_{\min} (\text{dB}), \quad (10)$$

where $E_c^{\text{corr}}/\sigma_1^2$ denotes the SNR required by our proposed system to achieve the corresponding BER level. Several values for the energy-splitting parameter α are considered (see Figure 2). Notice that in all simulated curves the proposed system

TABLE I
GAPS FOR SEVERAL VALUES OF THE CORRELATION PARAMETER.

p	0.25	0.2	0.15	0.10	0.05	0.01
α	0.28	0.28	0.26	0.24	0.24	0.24
Gap@ 10^{-5}	-1.05	-1.27	-1.6	-1.75	-1.48	-0.98

outperforms the separation-based limit (e.g. by around 1.75 dB at $\text{BER} = 10^{-5}$ for $p = 0.1$). For $p=0.1$ the best performance (in terms of waterfall, since no error floor is observed) is achieved by using a unique value of α ($\alpha = 0.24$). The same behavior (unique value of α for optimal performance) is also observed for $p > 0.1$. However, for high correlation levels ($0.05 \geq p > 0$) the selection of α is a tradeoff between the error floor level and the waterfall region (Figure 3, right).

Finally, Table I shows the *Gap* performance for different values of p at $\text{BER}=10^{-5}$. Also shown in the table are the corresponding optimum α_* 's. Again, in all cases the separation-based limit is outperformed. It is interesting to observe the gap inflection point at $p = 0.1$. This is due to the fact that, for a given E_c , increasing the correlation level (i.e., decreasing p) will increase the coherence effect and, in turn, improve the BER performance. However, at the same time the effective E_c^{corr} will also increase. There is a point (around $p = 0.1$) where the latter effect outgains the first effect.

V. CONCLUSION

We have proposed a superposition system for the transmission of two correlated sources over a Gaussian broadcast channel. Each information sequence is independently encoded using SC-LDGM codes, which allows preserving the correlation between the sources, and ultimately leads to a coherent signal addition at the superposition stage. The proposed system is able to outperform the theoretical limit assuming separation between source and channel coding.

ACKNOWLEDGMENT

This work was supported in part by the Spanish Ministry of Science and Innovation through the CONSOLIDACION 2010 programme (CSD20080010, www.comonsens.org).

REFERENCES

- [1] T. M. Cover, "Broadcast channels," *IEEE Trans. Inform. Theory*, vol. 18, no. 1, pp. 2–14, Jan. 1972.
- [2] T. M. Cover, "Comments on broadcast channels," *IEEE Trans. Inform. Theory*, vol. 44, no. 6, pp. 2524–2530, Oct. 1998.
- [3] T. W. Sun, R. D. Wesel, M. R. Shane, and D. Jaret, "Superposition turbo TCM for multi-rate broadcast," *IEEE Trans. Commun.*, vol. 52, pp. 368–371, Mar. 2004.
- [4] X. Wang and M. T. Orchard, "Design of superposition coded modulation for unequal protection," in *Proc. IEEE International Conference on Communications (ICC)*, pp. 412–416, June 2001.
- [5] W. Zhong and J. García-Frías, "Approaching Shannon performance by iterative decoding of linear codes with low-density generator matrix," *IEEE Commun. Lett.*, vol. 7, no. 6, pp. 266–268, June 2003.
- [6] W. Zhong and J. García-Frías, "LDGM codes for channel coding and joint source-channel coding of correlated sources," *EURASIP J. Applied Signal Processing*, vol. 44, no. 2, pp. 942–953, May 2005.
- [7] J. García-Frías, Y. Zhang, and W. Zhong, "Turbo-like codes for transmission of correlated sources over noisy channels," *IEEE Signal Processing Mag.*, pp. 58–66, Sept. 2007.
- [8] F. R. Kschischang, B. J. Frey, and H. A. Loeliger, "Factor graphs and the sum-product algorithm," *IEEE Trans. Inform. Theory*, vol. 44, pp. 498–519, Feb. 2001.

Erratum to Serially-Concatenated LDGM Codes for Correlated Sources over Gaussian Broadcast Channels

M. Hernaez, P. M. Crespo, J. Del Ser and J. Garcia-Friás,
IEEE Communications Letters, Vol 14, No. 03, 235-235,
March 2010.

Erratum to “Serially-Concatenated LDGM Codes for Correlated Sources over Gaussian Broadcast Channels”

Mikel Hernaez, Pedro Crespo, *Senior Member, IEEE*,
Javier Del Ser, *Member, IEEE*, and Javier Garcia-Frias, *Senior Member, IEEE*

Due to a programming glitch in [1], the curves in Fig. 3 should be shifted 3.2 dB to the right. Thus, the gap as defined in expression (10) becomes positive. However, in terms of E_c/σ_i^2 , the proposed system still outperforms the theoretical limit assuming separation between source and channel coding. Specifically, for $BER = 10^{-4}$ the gap is -0.6 dB for $p = 0.01$ and 0 dB for $p = 0.1$. These results are obtained with a (13, 6.5) inner LDGM code instead of the (14,7) code mentioned in the letter.

REFERENCES

- [1] M. Hernaez, P. M. Crespo, J. Del Ser, J. Garcia-Frias, “Serially-concatenated LDGM codes for correlated sources over Gaussian broadcast channels,” *IEEE Commun. Lett.*, vol. 13, no. 10, pp. 788-790, Oct. 2009.

Manuscript received December 2, 2009. The associate editor coordinating the review of this letter and approving it for publication was V. Stankovic.

M. Hernaez and P. M. Crespo are with the Centro de Estudios e Investigaciones Técnicas de Gipuzkoa (CETI) and TECNUN (University of Navarra), 20009 San Sebastian, Spain (e-mail: {mhernaez, pcrespo}@ceit.es).

J. Del Ser is with TECNALIA-TELECOM, 48170 Zamudio, Spain (e-mail: jdelser@robotiker.es).

J. Garcia-Frias is with the University of Delaware, Newark, DE 19716, USA (e-mail: jgarcia@ee.udel.edu).
Digital Object Identifier 10.1109/LCOMM.2010.03.092344

Turbo Joint Source-Channel Coding of Non-Uniform Memoryless Sources in the Bandwidth-Limited Regime

I. Ochoa, P. Crespo, J. Del Ser and M. Hernaez,
IEEE Communications Letters, Vol. 14, No. 04, April
2010.

Turbo Joint Source-Channel Coding of Non-Uniform Memoryless Sources in the Bandwidth-Limited Regime

Idoia Ochoa, *Student Member, IEEE*, Pedro Crespo, *Senior Member, IEEE*,
Javier Del Ser, *Member, IEEE*, and Mikel Hernaez, *Student Member, IEEE*

Abstract—This letter proposes a novel one-layer coding/shaping scheme with single-level codes and sigma-mapping for the bandwidth-limited regime. Specifically, we consider non-uniform memoryless sources sent over AWGN channels. At the transmitter, binary data are encoded by a Turbo code composed of two identical RSC (*Recursive Systematic Convolutional*) encoders. The encoded bits are randomly interleaved and modulated before entering the sigma-mapper. The modulation employed in this system follows the unequal energy allocation scheme first introduced in [1]. The receiver consists of an iterative demapping/decoding algorithm, which incorporates the *a priori* probabilities of the source symbols. To the authors' knowledge, work in this area has only been done for the power-limited regime. In particular, the authors in [2] proposed a scheme based on a Turbo code with RSC encoders and unequal energy allocation. Therefore, it is reasonable to compare the performance – with respect to the Shannon limit – of our proposed bandwidth-limited regime scheme with this former power-limited regime scheme. Simulation results show that our performance is as good or slightly better than that of the system in [2].

Index Terms—Sigma-mapping, non-uniform memoryless sources, turbo codes, bandwidth-limited regime.

I. INTRODUCTION

We consider the transmission of the information generated by a non-uniform memoryless source with probability distribution $(p_0, p_1 = 1 - p_0)$ over the AWGN channel. Shannon's Separation Theorem states that source coding and channel coding can be carried out in isolation. Thus, the standard approach has been to separate the encoding process in two parts: first, a source encoder capable of compressing the source up to its theoretical limit (given by its entropy $H(p_0)$), and second, a capacity-achieving channel code. Consequently, the E_{so} (average energy per source symbol) lower limit is given by

$$\frac{E_{so}}{N_0} > \frac{2^\rho - 1}{R}, \quad (1)$$

where N_0 is the noise variance per two dimension (2D), ρ is the spectral efficiency in bits per 2D, and $R = \rho/H(p_0)$ is the transmission rate in source symbols per complex channel symbol (or per two real channel symbols). We will refer to joint source-channel coding schemes working at $R \geq 2$ as coding schemes operating in the bandwidth-limited regime;

Manuscript received December 22, 2009. The associate editor coordinating the review of this letter and approving it for publication was Z. Yan.

I. Ochoa, P. M. Crespo, and M. Hernaez are with the Centro de Estudios e Investigaciones Técnicas de Gipuzkoa (CEIT) and TECNUN (University of Navarra), 20009 San Sebastián, Spain (e-mail: {iochoa, pcrespo, mhernaez}@ceit.es).

J. Del Ser is with TECNALIA-TELECOM, 48170 Zamudio, Spain (e-mail: jdelser@robotiker.es).

Digital Object Identifier 10.1109/LCOMM.2010.04.092462

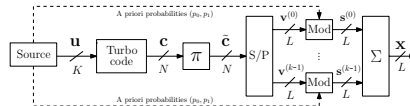


Fig. 1. Proposed Turbo encoding, modulation and sigma-mapping scheme.

otherwise it is said that they are operating in the power-limited regime.

However, when complexity is an issue, the overall performance can be improved if the tasks of source and channel coding are blended together by means of a joint source-channel encoder. In this way, the joint decoder can use some of the inherent redundancy of the source to alleviate the requirements of the channel encoder. For this reason, in the scheme proposed in this letter source and channel coding are jointly performed by a Turbo encoder operating at the bandwidth-limited regime in conjunction with a power-allocation strategy to achieve a shaping gain. To the best of our knowledge, previous work on joint source-channel coding for non-uniform memoryless sources has only been done for the power-limited regime. As to mention, in [3] they use LDPC codes, while [4], [5] employ non-systematic Turbo codes.

The remainder of the paper is organized as follows. In Section II we describe the proposed system, whereas Section III details the decoding process. Simulation results are presented in Section IV, and finally Section V concludes the paper.

II. PROPOSED SYSTEM

The proposed transmission scheme is shown in Fig. 1. The sequence \mathbf{u} of length K , which is generated by a non-uniform memoryless binary source with *a priori* probabilities p_0 and p_1 , is encoded through a Turbo code of rate¹ $R_c = 1/n$, producing the encoded sequence \mathbf{c} of length $N = nK$ which is next processed through an interleaver π . The interleaved version $\bar{\mathbf{c}}$ of \mathbf{c} is converted by a serial-to-parallel converter into k sequences $\mathbf{v}^{(i)}$ of length L , where $0 \leq i \leq k-1$. Then, the modulator assigns different amplitudes (and consequently, different energies) to the encoded symbols, yielding k non-binary sequences $\mathbf{s}^{(i)}$. Following the scheme in [2], the symbols associated to systematic bits 1 and 0 are, respectively, $+\sqrt{E_1^s} = +\sqrt{p_0/p_1}$ and $-\sqrt{E_0^s} = -\sqrt{p_1/p_0}$, where $p_1 E_1^s + p_0 E_0^s = 1$. For the parity bits, the associated symbols depend on the value of both the parity and the input bit of the underlying RSC code of the Turbo encoder. Notice

¹Notice that R_c (*code rate*) is not necessary equal to R (*transmission rate*) defined in expression (1).

that the input sequence of one RSC code corresponds to the systematic bits, while the input of the other one corresponds to the interleaved version of the source sequence. The amplitudes of parity bits 1 and 0 are given by $+\sqrt{E_i^p}$ and $-\sqrt{E_i^p}$, respectively, where the subindex i will take the value 0 or 1 depending on the value of the associated input bit. E_i^p is set to $(1 - \theta)/p_1$, and E_0^p to θ/p_0 , where $p_1 E_1^p + p_0 E_0^p = 1$. The value of θ ($0 \leq \theta \leq 1$) is chosen by simulation so as to minimize the probability of error at the receiver, which is usually achieved when $\theta = 0.5$ [2]. Thus, systematic bits can be mapped to 2 different values, while parity bits to 4 different values.

These modulated sequences enter the sigma-mapper Σ [6], which generates a single signal sequence \mathbf{x} of length L . It should be mentioned that the reason to have used a sigma-mapper instead of any other alternative mapping, is that it blends together perfectly with the unequal power allocation technique. At time t , the output of the sigma-mapper is denoted as $x_t = \phi_{\Sigma}(\mathbf{s}_t)$, where $\mathbf{s}_t = (s_t^{(0)}, \dots, s_t^{(k-1)})$ and $\phi_{\Sigma}(\mathbf{s}_t) \triangleq \sum_{i=0}^{k-1} \alpha_i s_t^{(i)}$. The sigma-mapper utilized in our scheme is known as *Type-I*², since $\alpha_i = \alpha \forall i \in \{0, \dots, k-1\}$. The value of α is chosen to satisfy $E_{x_t} = E_c$, and it can be shown that α should be set to $\sqrt{E_c/k}$. The received sequence \mathbf{y} at destination is a version of \mathbf{x} corrupted by Additive White Gaussian Noise (AWGN).

III. DECODING PROCESS

The receiver shown in Fig. 2 iterates between the sigma-demapper (labeled as Σ^{-1}) and the Turbo decoder. The sigma-demapper is based on a SISO (*Soft-Input Soft-Output*) demapping algorithm, and the Turbo decoder is implemented by the Sum-Product Algorithm (SPA) applied to the Factor Graph (FG) that describes the Turbo code. The decoding procedure allows for the successive exchange of *extrinsic* probabilities between the sigma-demapper and the Turbo decoder, which iteratively refines the *a posteriori* probabilities of the original source symbols. The sigma-demapper processes the sequence \mathbf{y} and estimates the probabilities of the k superimposed symbols contained in each channel symbol y_t ($1 \leq t \leq L$). If the symbol corresponds to a systematic bit, the sigma-demapper generates the *extrinsic* probability $P_v^{(e)}(m)$, where $m \in \{0, 1\}$. Accordingly, if the symbol represents a parity bit, the demapper calculates the probabilities $P_v^{(e)}(m|\text{input bit})$, where the input bit can take values 0 and 1.

Hereafter, the superscript (*initial*) represents the non-uniformity of the source. Thus, for the systematic bits, the probabilities $P_v^{(initial)}(m)$ will be p_0 for $m = 0$ and p_1 for $m = 1$, while for the parity bits they are always set to 0.5. The superscript (*a*) refers to the *a priori* probabilities coming from the Turbo decoder. In the first iteration they are equal to 0.5. Although the initial probabilities of the source can be estimated by both the encoder and the decoder [2], we will assume they are known in order to achieve optimum performance.

²It has been observed that the use of Type-II sigma-mapper does not improve the performance of our scheme due to the utilized unequal energy allocation.

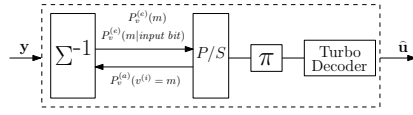


Fig. 2. Decoding scheme.

For all $V^{(i)}$ corresponding to systematic bits, the *extrinsic* probability $P_{v^{(i)}}^{(e)}(m)$ generated by the sigma-demapper is proportional to

$$P_{v^{(i)}}^{(e)}(m) \propto P_v^{(initial)}(v^{(i)} = m) \sum_{v \in \mathbb{F}_2^k} \mathbb{I}(v^{(i)} = m) P_V(v|v^{(i)}) P_{Y|V}(y|\phi(s)) \quad (2)$$

where \mathbb{F}_2^k denotes the k -extension of the binary Galois Field, and $\mathbb{I}(P)$ is the indicator function which takes the value 1 when the proposition P is true and 0 otherwise. In the above expression, $P_V(v|v^{(i)})$ is given by

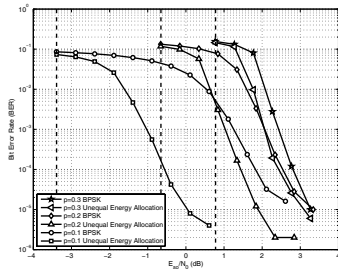
$$P_V(v|v^{(i)}) = \prod_{j \neq i} P_v^{(initial)}(v^{(j)}) P_v^{(a)}(v^{(j)}), \quad (3)$$

whereas $P_{Y|V}(y|\phi(s))$ is proportional to

$$P_{Y|V}(y|\phi(s)) \propto \sum \exp \left(-\frac{(y - \phi(s))^2}{2\sigma^2} \right), \quad (4)$$

where the number of elements in the sum varies depending on the number of parity and systematic bits that compose the vector \mathbf{v} . The reason being that for a given value of a systematic bit, there is only one possible value of its associated modulated symbol s while for a parity bit, two values of s are possible depending on the value of the associated input bit. For example, consider the case where $k = 2$ and $(V^{(1)}, V^{(2)}) = (0, 0)$. If $V^{(1)}$ and $V^{(2)}$ are both systematic, the value of $\phi(s)$ is unique and equal to $-\sqrt{p_1/p_0}$. On the contrary, if one is systematic and the other a parity bit, two values of $\phi(s)$ are possible, namely, $-\sqrt{p_1/p_0} - \sqrt{\theta/p_0}$ and $-\sqrt{p_1/p_0} + \sqrt{(1 - \theta)/p_0}$. Finally, when $V^{(1)}$ and $V^{(2)}$ are both parity bits, $\phi(s)$ may take four different values. Besides, when the vector \mathbf{v} contains parity bits, the exponential term of the righthand side of expression (4) has to be multiplied by the *a priori* probabilities of the input bits associated with such parity bits. When calculating the *extrinsic* probabilities $P_v^{(e)}(m|\text{input bit})$ of the parity bits, the only difference is that in expression (4) we do not have to multiply the exponential term by the *a priori* probability of the input bit associated with the parity bit we are considering. Furthermore notice that expression (2) is not multiplied by $P_v^{(a)}(v^{(i)} = m)$ to avoid any positive feedback to the Turbo decoder.

Once computed by the sigma-demapper, all the above *extrinsic* probabilities are passed to the Turbo decoder through a parallel-to-serial converter and the deinterleaver π^{-1} . The Turbo decoder employs these probabilities as *a priori* probabilities, and runs the SPA algorithm over the FG that describes its compounding RSC codes. However, note that a slight modification is required in such FG, since in our scheme *extrinsic* information for the parity bits is also needed to

Fig. 3. BER versus E_{so}/N_0 for $p_0 \in \{0.1, 0.2, 0.3\}$.

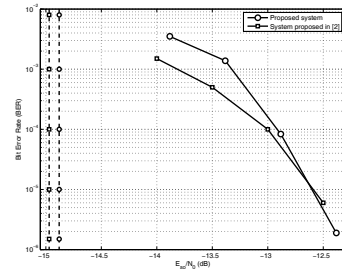
be passed to the sigma-demapper. The *extrinsic* probabilities generated by the Turbo decoder are then used as *a priori* probabilities by the sigma-demapper. The decoder stops after a fixed number of iterations.

IV. SIMULATION RESULTS

In order to verify the performance of the proposed scheme, two sets of simulations have been performed. The goal of the first set is to assess the improvement that the unequal energy allocation strategy entails in the overall performance of the proposed scheme. To that end, the proposed system is simulated with and without energy allocation. In the latter case the encoded symbols at the output of the Turbo coder are simply BPSK modulated (i.e. by using equal energy). The Turbo code from [6, Example A] with rate $R_c = 1/3$ and generator polynomial $G(D) = 1/(1+D)$ has been used. The value of k was set to $k = 3$, so the transmission rate R is 2 binary source symbol per 2D (bandwidth-limited regime).

Monte Carlo simulations have been performed for a block-length $K = 10000$ and a maximum of 50 decoding iterations. Three source symbol distributions $p_0 \in \{0.1, 0.2, 0.3\}$ have been selected, giving rise to source entropies $H(p_0) = 0.47$, 0.72 and 0.88 bits per source symbol, respectively. Figure 3 shows the BER versus E_{so}/N_0 , where the vertical lines correspond to the theoretical limit given by expression (1). Notice that for $p_0 = 0.1$, the performance improvement when utilizing, in our scheme, an unequal energy allocation modulation instead of standard BPSK is 2.37 dB at a BER = 10^{-4} . On the other hand, observe that the proposed scheme is 2.84 dB away from the Shannon limit. Further simulations included in the plot show that, for $p_0 = 0.2$ and $p_0 = 0.3$, we obtain a gain of 1.1 and 0.37 dB, respectively, and they are 2.08 and 1.66 dB away from their theoretical limit.

The above gaps to the Shannon limit can be reduced by using a more powerful Turbo code. This is shown in the second set of simulations, where the goal is also to compare our scheme operating at the bandwidth-limited regime with the Turbo coding scheme proposed in [2] (suitable for operating only at the power-limited regime). In this comparison, both systems use the same Turbo code of rate $R_c = 1/3$, generator polynomial $G(D) = (1 + D + D^2 + D^4)/(1 + D^3 + D^4)$ and $K = 16384$. Notice that although both schemes utilize the

Fig. 4. BER versus E_{so}/N_0 for $p_0 = 0.005$.

same Turbo code of rate $R_c = 1/3$, our scheme implements a transmission rate of 2 ($R = 2$), whereas the scheme in [2] one of 2/3 ($R = 2/3$). Figure 4 plots the BER versus E_{so}/N_0 for $p_0 = 0.005$, where the vertical lines represent the corresponding theoretical limits of both systems. Although both schemes need approximately the same E_{so}/N_0 to obtain a BER of 10^{-5} , our system performs slightly better, since its corresponding Shannon limit is closer. Further results show that for $p_0 = 0.01$, both schemes are 2.0 dB away of their corresponding theoretical limits.

V. CONCLUSION

We have proposed a one-layer coding/shaping system with single-level codes and sigma-mapping, for the case of non-uniform memoryless sources sent over AWGN channels. The proposed scheme has proved to have similar or slightly better BER performance, in the bandwidth-limited regime, when compared to the system in [2] for the power-limited regime.

ACKNOWLEDGMENT

This work was supported in part by the Spanish Ministry of Science and Innovation through the CONSOLIDER-INGENIO 2010 programme (CSD200800010, www.comensons.org).

REFERENCES

- [1] F. Cabarcas, R. D. Souza, and J. Garcia-Frias, "Source-controlled turbo coding of non-uniform memoryless sources based on unequal energy allocation," in *Proc. IEEE International Symposium on Information Theory*, p. 166, June 2004.
- [2] F. Cabarcas, R. D. Souza, and J. Garcia-Frias, "Turbo coding of strongly non-uniform memoryless sources with unequal energy allocation and PAM signaling," *IEEE Trans. Signal Process.*, vol. 54, no. 5, pp. 1942-1946, May 2006.
- [3] G. I. Shamir and J. J. Boutros, "Non-systematic low-density parity-check codes for nonuniform sources," in *Proc. 2005 IEEE International Symposium on Information Theory*, pp. 1898-1902, Sep. 2005.
- [4] R. D. Souza, G. I. Shamir, J. Garcia-Frias, and K. Xie, "Non-systematic turbo coding with unequal energy allocation for nonuniform memoryless sources," in *Proc. IEEE International Symposium on Information Theory*, pp. 1893-1897, Sep. 2005.
- [5] G. Zhu, F. Alajaji, J. Bajcsy, and P. Mitran, "Non-systematic turbo codes for non-uniform i.i.d. sources over AWGN channels," *Conference on Information Sciences and Systems*, Mar. 2002.
- [6] X. Ma and L. Ping, "Coded modulation using superimposed binary codes," *IEEE Trans. Inf. Theory*, vol. 50, no. 12, Dec. 2004.

LDPC Codes for Non-Uniform Memoryless Sources and Unequal Energy Allocation

I. Ochoa, P. Crespo and M. Hernaez,

IEEE Communications Letters, Vol. 14, No. 09, Sept. 2010.

LDPC Codes for Non-Uniform Memoryless Sources and Unequal Energy Allocation

Idoia Ochoa, *Student Member, IEEE*, Pedro M. Crespo, *Senior Member, IEEE*, and Mikel Hernaez, *Student Member, IEEE*

Abstract—In this paper, we design a new energy allocation strategy for non-uniform binary memoryless sources encoded by Low-Density Parity-Check (LDPC) codes and sent over Additive White Gaussian Noise (AWGN) channels. The new approach estimates the *a priori* probabilities of the encoded symbols, and uses this information to allocate more energy to the transmitted symbols that occur less likely. It can be applied to systematic and non-systematic LDPC codes, improving in both cases the performance of previous LDPC based schemes using binary signaling. The decoder introduces the source non-uniformity and estimates the source symbols by applying the SPA (Sum Product Algorithm) over the factor graph describing the code.

Index Terms—Systematic and non-systematic LDPC codes, non-uniform memoryless sources, unequal energy allocation.

I. INTRODUCTION

We consider the transmission of the information generated by a non-uniform memoryless source with probability distribution $(p_0, p_1 = 1 - p_0)$. The standard approach to tackle this problem has been to separate the encoding process in two parts: first, a source encoder capable of compressing the source up to its theoretical limit (which is given by its entropy $H(p_0)$), and second, a capacity achieving channel code. Consequently, the lower limit E_{br} , average energy per source symbol, is given by

$$\frac{E_{br}}{N_0} = \frac{2^{2R_c H(p_0)} - 1}{2R_c} \quad (1)$$

where N_0 is the one-sided noise power spectral density of the additive gaussian noise, and R_c is the code rate (source symbols per channel symbol).

The justification for this partition lies on Shannon's Separation Theorem. However, when complexity is an issue, the overall performance can be improved if the tasks of source and channel coding are blend together by means of a joint source-channel encoder. In this way, the joint decoder can employ some of the inherent redundancy of the source to alleviate the requirements of the channel encoder. For this reason, in the proposed scheme source and channel coding are jointly performed by an LDPC encoder.

Point-to-point communication schemes including non-uniform memoryless sources and joint source-channel coding have been well-studied for both Turbo and LDPC codes. As to mention, systematic Turbo codes are considered in [1] and [2], where significant improvements are obtained by using Unequal

Manuscript received April 22, 2010. The associate editor coordinating the review of this letter and approving it for publication was V. Stankovic.

The authors are with the Centro de Estudios e Investigaciones Técnicas de Gipuzkoa (CEIT) and TECNUN (University of Navarra), 20009 San Sebastian, Spain (e-mail: {iochoa, pcrespo, mhernaez}@ceit.es). Digital Object Identifier 10.1109/LCOMM.2010.09.100662

Energy Allocation (UEA) rather than binary signaling (BPSK). In [5] they extend this scheme to the case of sources with memory. In [4] they show that non-systematic Turbo codes perform better than systematic Turbo codes for non-uniform sources. In [3] they combine non-systematic Turbo codes and unequal energy allocation, improving the performance over previous schemes. In [6] and [7] they use systematic and non-systematic LDPC codes, respectively, with binary signaling. To the best of our knowledge, no schemes with LDPC codes and unequal energy allocation are found in the literature.

The remainder of the paper is organized as follows. Section II introduces the proposed system. Then, Section III and IV describe the encoding and decoding process with UEA for systematic and non-systematic LDPC codes, respectively. Simulation results are presented in Section V and some concluding remarks are given in Section VI.

II. SYSTEM DESCRIPTION

Let $\mathbf{u} \doteq (u_1, \dots, u_K) \in \{0, 1\}^K$ be a binary sequence of length K generated by an i.i.d. source with probability distribution (p_0, p_1) . The sequence \mathbf{u} is then encoded by an LDPC code of rate $R_c = K/N$ into the code sequence $\mathbf{c} \doteq (c_1, \dots, c_N)$, and then modulated by an unequal energy allocation technique, producing an amplitude signal $\mathbf{x} \doteq (x_1, \dots, x_N)$ of length N . The destination receives \mathbf{y} , which is a version of \mathbf{x} corrupted by Additive White Gaussian Noise (AWGN). The decoder estimates \mathbf{u} by applying the SPA over the factor graph describing the corresponding LDPC code, and introducing the source statistics (p_0, p_1) .

III. PROPOSED SYSTEM WITH SYSTEMATIC LDPC CODES

An LDPC code is defined by its low-density parity-check matrix \mathbf{H} of dimension $(N - K) \times N$, which can be regular or irregular. We will consider only regular codes for explanation purposes. The extension to irregular codes is straightforward. We will denote by (d_b, d_c) LDPC codes those codes in which the matrix \mathbf{H} has exactly d_b non-zero entries per column and d_c non-zero entries per row. The encoding is done by simply multiplying the source sequence \mathbf{u} by the systematic generator matrix \mathbf{G} of dimensions $K \times N$, which satisfies $\mathbf{GH}^T = \mathbf{0}$.

The new approach modulates the encoded symbols depending on their *a priori* probability p_{ci} , for $i = 1, \dots, N$. Hereafter, we will consider that the first K bits of \mathbf{c} correspond to the source symbols. Therefore, $(p_{c_i}(0), p_{c_i}(1)) = (p_0, p_1)$, for $i = 1, \dots, K$. For the remaining $N - K$ parity symbols, we estimate the *a priori* probabilities p_{ci} , for $i = (K + 1), \dots, N$. These probabilities differ from 0.5 when the next two conditions hold:

- 1) The source symbols are generated by a non-uniform source.
 - 2) The generator matrix \mathbf{G} has only a few ones per column. The *a priori* probabilities of the parity symbols can be estimated off-line, as follows. Since $\mathbf{c} = \mathbf{u}\mathbf{G}$, the value of the parity bit c_i is given by multiplying the source sequence \mathbf{u} by the column i of \mathbf{G} . Let us denote by $w(i)$ the number of non-zero elements of column i . Then, the value of the parity bit c_i is given by the sum of the $w(i)$ source symbols located at the same position as the $w(i)$ ones of column i . Therefore, c_i will be 0 when the considered source symbols have an even number of 1's, and 1, otherwise. We propose a simple algorithm based on this principle to estimate these probabilities. For $i = (K+1), \dots, N$ we perform the following pseudo program:
 - 1) Initialize the variables $p_{c_i}(0)$ and j to 0.
 - 2) Update $p_{c_i}(0)$ as $p_{c_i}(0) = p_{c_i}(0) + \binom{w(i)}{j} p_1^j p_0^{w(i)-j}$, where the binomial coefficient indicates the number of sequences of length $w(\cdot)$ with j 1's and $(w(\cdot) - j)$ 0's.
 - 3) Increment variable j by 2, so the number of ones is still even, and perform the algorithm from step 2 until $j \leq w(i)$.
 - 4) $p_{c_i}(1) = 1 - p_{c_i}(0)$
- Notice that the actual position of the $w(\cdot)$ ones is irrelevant, since the source is stationary and all the source symbols have the same a priori probability (p_0, p_1) .

Finally, the coded symbols are modulated following the UEA strategy given by

$$\begin{cases} -\sqrt{\frac{p_{c_i}(1)}{p_{c_i}(0)} E}, & \text{if } c_i = 0 \\ +\sqrt{\frac{p_{c_i}(0)}{p_{c_i}(1)} E}, & \text{if } c_i = 1 \end{cases} \quad (2)$$

which allocates more energy to the less likely symbols, as in [2]. This results in asymmetric 2-PAM constellations with the same average energy per coded symbol (i.e., $E[c_i^2] = E, \forall i$), and maximized distance between the two points. This makes the symbols with higher distance (those with probability close to 0 or/and 1) be more protected against noise than those with lower distance (those with probability close to 0.5).

At the destination, the decoder estimates \mathbf{u} by applying the SPA over the factor graph describing the LDPC code. Due to the UEA, the channel probabilities are proportional to

$$\begin{aligned} p(y_i|c_i = 0) &\propto e^{-\left(\frac{y_i + \sqrt{\frac{p_{c_i}(1)}{p_{c_i}(0)} E}}{N_0}\right)^2} \\ p(y_i|c_i = 1) &\propto e^{-\left(\frac{y_i - \sqrt{\frac{p_{c_i}(0)}{p_{c_i}(1)} E}}{N_0}\right)^2}. \end{aligned} \quad (3)$$

Furthermore, the decoder also introduces the source statistics (p_0, p_1) for the systematic symbols. However, it is not required to introduce the estimated *a priori* probabilities for the parity bits since at the first iteration, the parity bit nodes receive that information from the parity check nodes, which are connected to the systematic bit nodes.

IV. PROPOSED SYSTEM WITH NON-SYSTEMATIC LDPC CODES

We consider the scrambler-LDPC and the splitter-LDPC non-systematic codes proposed in [6] and [7] since they present good performance for channel coding of nonuniform

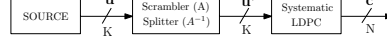


Fig. 1. General scheme of scrambler-LDPC and splitter-LDPC codes.

sources. As shown in Fig. 1, the encoders are implemented by the concatenation of a pre-coder matrix modeled either by a low density squared matrix \mathbf{A} of size K and column and row degree d_s (scrambler-LDPC), or by its inverse \mathbf{A}^{-1} (splitter-LDPC), followed by a systematic LDPC encoder.

Due to the non-systematic nature of the codes, the *a priori* probabilities p_{c_i} for $i = 1, \dots, N$ are unknown, and they have to be estimated. We distinguish between the first K symbols of \mathbf{c} , which correspond to \mathbf{u}' , and the remaining $N - K$ symbols, which will be referred to as parity symbols. For the first K symbols, we follow the steps introduced in the previous section, but referring to the pre-coder matrix instead of to the generator matrix \mathbf{G} . On the other hand, since $\mathbf{c} = \mathbf{u}'\mathbf{G}$ instead of $\mathbf{c} = \mathbf{u}\mathbf{G}$, in order to estimate the *a priori* probabilities of the remaining $N - K$ parity symbols, we have to replace the *a priori* probabilities of the source symbols, i.e., (p_0, p_1) , by the *a priori* probabilities of \mathbf{u}' , i.e., $(p_{c_i}(0), p_{c_i}(1))$ for $i = 1, \dots, K$. However, since these probabilities are in general non-stationary, i.e., $p_{c_i} \neq p_{c_j}, \forall i \neq j$, one has to modify the steps introduced in the previous section. Instead, for the sake of simplicity, we estimate the *a priori* probabilities of the parity symbols by simulation using

$$\hat{p}_{c_i}(0) = \frac{1}{M} \sum_{k=1}^M \mathbb{I}(c_i(k) = 0), \quad \text{for } i = (K+1), \dots, N, \quad (4)$$

where M is the number of sequences simulated, $\mathbb{I}(P)$ is the indicator function that takes the value 1 when the proposition P is true and 0, otherwise, and $c_i(k)$ corresponds to the coded symbol c_i of sequence k . Notice that as $M \rightarrow \infty$, $\hat{p}_{c_i} \rightarrow p_{c_i}$. Observe that due to the pre-coder matrix, the symbols of \mathbf{u}' become more uniformly distributed than those of \mathbf{u} , making the latter symbol probabilities closer to 0.5. This symbol uniformity will manifest more strongly in the case of splitter-LDPC non-systematic codes since in this case the pre-coder matrix \mathbf{A}^{-1} is not of low density. Therefore, although the encoded symbols are modulated following expression (2), the non-systematic codes are expected to perform worse than their systematic counterpart, since the UEA strategy will have less effect.

At the destination, the decoder estimates \mathbf{u} by running the SPA over the factor graph describing the non-systematic LDPC code. The decoding graphs of scrambler-LDPC and splitter-LDPC codes are detailed in [[6], Fig. 1-bottom] and [[7], Fig. 4-right], respectively. Both graphs contain K variable nodes corresponding to the source symbols, which allows to include the source non-uniformity (p_0, p_1) , and N variable nodes corresponding to the channel symbols, which introduce only the channel probabilities calculated by expression (3).

V. SIMULATION RESULTS

To assess the performance of the proposed LDPC-UEA scheme over previous LDPC based systems for non-uniform

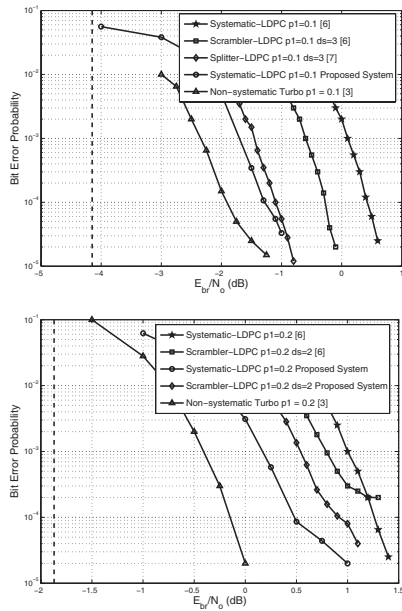


Fig. 2. Bit error probabilities vs. signal-to-noise ratio for $R = 1/2$ LDPC and Turbo codes and distributions $p_1 = 0.1$ (top) and $p_1 = 0.2$ (bottom).

memoryless sources, MonteCarlo simulations have been done. To that end, the proposed system is compared with the results shown in [6] and [7], where a regular-(3,6) LDPC systematic code of rate $R = 1/2$ and block length $K = 1000$ is used for the systematic code and for the design component of the non-systematic codes. Simulations have been performed with the same LDPC codes, 10,000 input blocks and a maximum number of decoding iterations of 100. As shown in Fig. 2 (top), for $p_1 = 0.1$ and $\text{BER} = 10^{-4}$ the proposed scheme with the systematic LDPC code is 2.87 dB away from the Shannon limit (1), denoted by a vertical line. A gain of 1.71 dB is obtained with respect to the same systematic LDPC code but now using binary signaling. Furthermore, our system performs 1 dB and 0.18 dB better than the scrambler-LDPC code and the splitter-LDPC code considered in [6] and [7], respectively, both with optimum degree $d_s = 3$. The results for $p_1 = 0.2$ are presented in Fig. 2 (bottom), where the curves of the proposed scheme (systematic and scrambler-LDPC), the systematic LDPC code from [6] and the scrambler-LDPC code with optimum degree $d_s = 2$ from [6] are shown. As suggested in the previous section, the systematic LDPC proposed scheme outperforms all the others and is 2.35 dB away from the Shannon limit. The scrambler-LDPC code has a gain of 0.28 dB with respect to the same code proposed in

[6] for equal energy allocation and does not present an error floor. The asymptotic performance of the proposed scheme can be calculated by density evolution. However, since it is not straightforward to apply it for non-uniform sources and no-symmetric constellations, we give an upperbound by simulating with $K = 20,000$. The gap to the Shannon limit is reduced to 1.93 dB ($p_1 = 0.1$) and 1.53 dB ($p_1 = 0.2$).

The proposed system has also proved to have good performance for extremely non-uniform sources. For $p_1 \in \{0.005, 0.01\}$ and a rate $R = 1/2$ irregular LDPC code with $K = 20,000$, the gap to the theoretical limit for the systematic case is 3.91 dB and 3.81 dB, respectively, for a $\text{BER} = 10^{-4}$.

Although the improvement in performance of the proposed LDPC-UEA scheme is substantial when compared to existing LDPC based schemes for non-uniform sources, this is not in general the case when compared to their counterpart, i.e., Turbo code-UEA schemes [1]-[3]. For example, as shown in Fig. 2, an optimized non-systematic Turbo code with the same rate and block length ($K = 1000$) as before, outperforms our scheme by 0.63 dB and 0.62 dB for $p_1 = 0.1$ and $p_1 = 0.2$, respectively, and a BER of 10^{-4} [3].

VI. CONCLUSION

We have proposed a source-controlled LDPC coding scheme for the transmission of non-uniform memoryless sources over AWGN channels. The novel scheme is based on the UEA strategy which allocates more energy to the less likely encoded symbols. This strategy can be applied to systematic and non-systematic LDPC codes, improving in both cases the performance of existing LDPC based schemes using binary signaling. Besides, the proposed system has proved to have good performance even for strongly non-uniform sources.

ACKNOWLEDGMENT

This work was supported in part by the Spanish Ministry of Education and Science and by the European Regional Development Fund through the MultiMIMO TEC2007-68020-C04-03 and the CONSOLIDER-INGENIO 2010 CSD200800010.

REFERENCES

- [1] F. Cabarcas, R. D. Souza, and J. Garcia-Frias, "Source-controlled turbo coding of non-uniform memoryless sources based on unequal energy allocation," in *Proc. IEEE Intern. Symp. on Inform. Theory*, p. 166, June 2004.
- [2] F. Cabarcas, R. D. Souza, and J. Garcia-Frias, "Turbo coding of strongly non-uniform memoryless sources with unequal energy allocation and PAM signaling," *IEEE Trans. Signal Process.*, vol. 54, no. 5, pp. 1942-1946, May 2006.
- [3] R. D. Souza, G. I. Shamir, J. Garcia-Frias, and K. Xie, "Non-systematic turbo coding with unequal energy allocation for nonuniform memoryless sources," in *Proc. IEEE Intern. Symp. on Inform. Theory*, pp. 1893-1897, Sep. 2005.
- [4] G. Zhu, F. Alajaji, J. Bajcsy, and P. Mitran, "Non-systematic turbo codes for non-uniform LDPC sources over AWGN channels," *Conference on Information Sciences and Systems*, Princeton University, Mar. 2002.
- [5] J. del Ser, P. Crespo, I. Esnaola, and J. Garcia-Frias, "Joint source-channel coding of sources with memory using turbo codes and the Burrows-Wheeler transform," *IEEE Trans. Commun.*, accepted.
- [6] G. I. Shamir and J. J. Boutros, "Non-systematic low-density parity-check codes for nonuniform sources," in *Proc. IEEE Intern. Symp. on Inform. Theory*, pp. 1898-1902, Sep. 2005.
- [7] A. Alouini, J. J. Boutros, G. I. Shamir, and L. Wang, "Non-systematic LDPC codes via scrambling and splitting," in *Allerton Conference on Communication and Control*, Illinois, Sep. 2005.

Turbo Joint Source-Channel Coding of Cycle-Stationary
Sources in the Bandwidth-Limited Regime
I. Ochoa, P. Crespo, J. Del Ser and M. Hernaez,
*The 2nd International Conference on Mobile Lightweight
Wireless Systems (MOBILIGHT), Barcelona (Spain),*
May 2010.

Turbo Joint Source-Channel Coding of Cycle-Stationary Sources in the Bandwidth-Limited Regime

Idoia Ochoa¹, Pedro M. Crespo¹, Javier Del Ser², and Mikel Hernaez¹

¹ CEIT and TECNUN (University of Navarra), 20009 San Sebastian, Spain
{iochoa,pcrespo,mhernaez}@ceit.es

² TECNALIA-TELECOM, 48170 Zamudio, Spain
jdelser@robotiker.es

Abstract. In this paper we propose a novel one-layer coding/shaping transmission system for the bandwidth-limited regime based on single-level codes and sigma-mapping [1]. Specifically, we focus on cycle-stationary information sources with independent symbols. High spectral efficiencies can be achieved by combining at the transmitter a Turbo code with a sigma-mapper. Furthermore, the encoded symbols are modulated by using an asymmetric energy allocation technique before entering the aforementioned sigma-mapper. The corresponding decoder iterates between the Turbo decoder and the sigma-demapper, which exchange progressively refined *extrinsic* probabilities of the encoded symbols. For the Additive White Gaussian Noise (AWGN) channel, simulation results obtained for very simple Turbo codes show that the proposed system attains low bit error rates at signal-to-noise ratios relatively close to the corresponding Shannon limit. These promising results pave the way for future investigations towards reducing the aforementioned energy gap, e.g. by utilizing more powerful Turbo codes.

Key words: Turbo codes, sigma-mapping, bandwidth-limited regime, unequal energy allocation, cycle-stationary sources

1 Introduction

We consider the transmission, over the Additive White Gaussian Noise (AWGN) channel, of binary symbols generated by cycle-stationary random processes, $\{T_k\}_{k=1}^{\infty}$, with independent symbols. This kind of processes may arise, for instance, when the output sequence generated by a binary stationary source with memory¹ is partitioned into blocks of K symbols, before being processed by the block-sorting Burrows-Wheeler Transform (BWT) [2] of length K . For large K , it can be shown [3] that the corresponding random process $\{T_k\}_{k=1}^{\infty}$ at the output of the BWT can be asymptotically approximated by a cycle-stationary random process with time period K (i.e. the length of the BWT input block),

¹ A source with memory may be modeled by either a Markov Chain (MC) or a Hidden Markov Model (HMM).

2 Cycle-Stationary Sources in the Bandwidth-Limited Regime

and independent symbols inside each output block. Under these conditions, the output process is completely specified once the probability distribution of each of the symbols inside an arbitrary block, say the first block, are known, i.e., when $P_{T_k}(t)$, for $k = 1, \dots, K$ are known. Notice that the random sequence $\{T_k\}_{k=1}^K$ is non-stationary.

The entropy rate of such a process can be computed as

$$\mathcal{H}(\mathcal{T}) = \lim_{n \rightarrow \infty} \frac{1}{nK} H(T_1, \dots, T_{nK}) = \frac{1}{K} H(T_1, \dots, T_K) = \frac{1}{K} \sum_{k=1}^K H(T_k), \quad (1)$$

where $H(T_1, \dots, T_K)$ denotes the entropy of the random vector $\{T_k\}_{k=1}^K$ with joint distribution $P_{\mathbf{T}}(t_1, \dots, t_K) = \prod_{k=1}^K P_{T_k}(t_k)$. In what follows, we will denote by $P^0(k) = P_{T_k}(t=0)$, and the set of values $\{P^0(k)\}_{k=1}^K$ inside a non-stationary block will be referred to as the *zero probability profile*. Notice that by cycle-stationarity $P^0(lK + k) = P^0(k)$, $\forall l \in \mathbb{N}$.

By the Shannon Source-Channel Coding Theorem [4], the minimum average energy per source symbol E_{so} required for reliable communication of $\{T_k\}_{k=1}^\infty$ over an AWGN channel is given by

$$\frac{E_{so}}{N_0} > \frac{2^{2R\mathcal{H}(\mathcal{T})} - 1}{2R}, \quad (2)$$

where N_0 is the one-sided noise power spectral density, R denotes the transmission rate (source symbols per channel symbol), and $2R$ is the spectral efficiency (binary source symbols per two dimensions). When the system has a spectral efficiency equal or greater than 2, it operates in the bandwidth-limited regime. Otherwise, it is said that the system works in the power-limited regime.

By the Separation Theorem, the lower limit in expression (2) can be achieved by an ideal source encoder followed by a capacity achieving channel code. However, in this paper we propose a novel scheme, suitable for the bandwidth-limited regime, which do not use a source encoder but rather uses the distribution $P^0(k) = P_{T_k}(t=0)$ (*zero probability profile*) of the source symbols T_k to modify the BPSK constellation at the output of the Turbo encoder before entering the sigma-mapper [1]. Preliminary simulation results with very simple Turbo codes show a Bit Error Rate performance relatively close to the associated Separation limit, which sets the scene for future research aimed at narrowing this performance gap.

In this context, the present paper can be viewed as an extension of the scheme proposed in [5], suitable in the power-limited regime, for the transmission of the symbols generated by a stationary source with memory over the AWGN channel.

The rest of the paper is organized as follows: Section 2 and 3 describe the encoding and decoding process, respectively. Simulation results are presented in Section 4, and finally, some concluding remarks are drawn in Section 5.

2 Encoding Process

Figure 1 shows the proposed system, which combines Turbo coding and shaping in a one-layer scheme. The cycle-stationary source \mathcal{T} of period K , generates blocks of K independent symbols $\{T_k\}_{k=1}^K$ having a *zero probability profile* $\{P^0(k)\}_{k=1}^K$. The source symbols are first encoded by a Turbo code of rate $R_c = K/N$. The encoded sequence \mathbf{c} of length N is next interleaved to form the sequence $\tilde{\mathbf{c}}$ of the same length. The interleaved block $\tilde{\mathbf{c}}$ is then transformed by a serial-to-parallel converter in \mathcal{I} sequences $\mathbf{v}^{(i)}$ of length L , where $0 \leq i \leq (\mathcal{I}-1)$ and $N = L \cdot \mathcal{I}$.

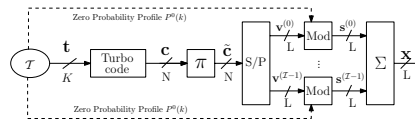


Fig. 1. Proposed transmission scheme.

Before entering the sigma-mapper, the modulator assigns different amplitudes to the encoded symbols, depending on their position and their systematic or parity nature. The proposed energy allocation scheme (further detailed in Sub-section 2.1) renders a set of \mathcal{I} non-binary sequences $\mathbf{s}^{(i)}$, which are next fed to the sigma-mapper Σ [1]. The underlying idea of the sigma-mapper hinges on imposing a gaussian distribution on the output amplitude signal \mathbf{x} of length L while satisfying, at the same time, the energy constraint² $(1/L) \cdot \sum_{l=1}^L \mathbb{E}\{|X_l|^2\} = E_c$. Finally, the destination receives a corrupted version of the amplitude sequence \mathbf{x} , denoted as $\mathbf{y} = \mathbf{x} + \mathbf{n}$, where \mathbf{n} denotes a L -length sequence of i.i.d. Gaussian random variables with zero mean and variance per dimension $N_0/2$.

2.1 Asymmetric Energy Allocation Scheme

From expression (2), the minimum average energy per channel symbol E_c for reliable communication of the data generated by the binary cycle-stationary source \mathcal{T} is given by³

$$\frac{E_c}{N_0} > \frac{2^{2R\mathcal{H}(\mathcal{T})} - 1}{2}, \quad (3)$$

with

$$\mathcal{H}(\mathcal{T}) \doteq \frac{1}{K} \sum_{k=1}^K h_b(P^0(k)), \quad (4)$$

² $\mathbb{E}\{\cdot\}$ stands for *expectation*.

³ Notice that in equation (3), R refers to the overall rate of the system, which may differ from R_c (coding rate).

4 Cycle-Stationary Sources in the Bandwidth-Limited Regime

where $h_b(p) \doteq -p \log_2 p - (1-p) \log_2(1-p)$. However, since in our case the symbols inside a block are non-stationary, each output symbol will require a different average energy $E_c(k)$ depending on its distribution $P^0(k)$. From expression (3), the corresponding lower limit will be given by

$$E_c^*(k) = (2^{2R h_b(P^0(k))} - 1) \frac{N_0}{2}, \quad (5)$$

and the minimum average energy per block as

$$E_c^* = \frac{1}{K} \sum_{k=1}^K E_c^*(k). \quad (6)$$

The energies used to modulate the encoded symbols are now given by $E(k) = \beta E_c^*(k)$, for $k = 1, \dots, K$ where $\beta > 1$ is a scaling factor. Following the scheme of [5], the amplitudes of the encoded systematic symbols depend on both their value and the associated *a priori* probability $P^0(k)$, whereas the amplitude of a given encoded parity symbol is driven by 1) its value and 2) the value and the *a priori* probability of the associated systematic bit. In particular, the amplitudes are set to:

$$\text{Systematic symbols: } \begin{cases} -\sqrt{\frac{1-P^0(k)}{P^0(k)}} E(k), & \text{if } u_k = 0, \\ +\sqrt{\frac{P^0(k)}{1-P^0(k)}} E(k), & \text{if } u_k = 1. \end{cases} \quad (7)$$

$$\text{Parity symbols: } \begin{cases} -\sqrt{\frac{\theta}{P^0(k)}} E(k), & \text{if the parity symbol is 0 and } u_k = 0, \\ -\sqrt{\frac{1-\theta}{1-P^0(k)}} E(k), & \text{if the parity symbol is 0 and } u_k = 1, \\ +\sqrt{\frac{\theta}{P^0(k)}} E(k), & \text{if the parity symbol is 1 and } u_k = 0, \\ +\sqrt{\frac{1-\theta}{1-P^0(k)}} E(k), & \text{if the parity symbol is 1 and } u_k = 1. \end{cases} \quad (8)$$

where the arbitrary parameter θ ($0 \leq \theta \leq 1$) is chosen to maximize the performance of the system, which is usually achieved when $\theta = 0.5$ [6]. In the simulations presented in this paper, θ was set to 0.5. Notice that the resulting constellation is not symmetric, since more energy is allocated to those symbols with less *a priori* probability. Also observe that for the sake of clarity, the above expressions (7) and (8) do not include the time index mappings due to the Turbo and π interleavers, which must be considered in the energy allocation procedure.

A better estimation of the energies $E_c^*(k)$ defined in equation (5) can be obtained by taking into account the loss in performance due to using a non-capacity-achieving channel code, i.e. the actual gap to the corresponding Shannon limit. This is done by introducing, into expression (5), a gap factor $\Gamma(P^0(k))$, i.e.

$$E_c^*(k) = (2^{2R h_b(P_s^0(k))} - 1) \frac{N_0}{2} \Gamma(P^0(k)). \quad (9)$$

The gap $\Gamma(p)$, $p \leq 0.5$, is a function of the *a priori* probability and depends on the particular communication scheme being used. Its value should be computed off-line by Monte Carlo simulations. Once $\Gamma(\cdot)$ is known, the amplitudes of the encoded symbols are calculated by following expressions (9), (6), (7) and (8), with $E(k) = \beta E_c^*(k)$ for a given scaling factor β .

3 Decoding Process

The decoder is depicted in Figure 2. It iterates between the sigma-demapper, which introduces the *a priori* probabilities of the source symbols, and the Turbo decoder, which is based on applying the message passing Sum-Product Algorithm (SPA) over the factor graph that describes the Turbo code [7].

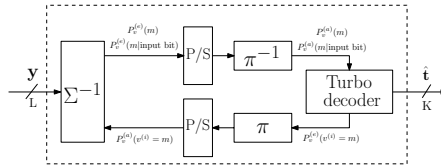


Fig. 2. Decoding scheme.

The iterative decoding process starts from the sigma-demapper Σ^{-1} , which estimates the probabilities of the symbols contained in each of the \mathcal{I} sequences $\mathbf{v}^{(i)}$ from the received sequence \mathbf{y} . These probabilities are denoted by $P_v^{(e)}(m)$ for systematic bits ($m \in \{0, 1\}$), and by $P_v^{(e)}(m|\text{input bit})$ for parity bits. Once these probabilities are computed, the Turbo decoder incorporates them (through the parallel-to-serial converter and the deinterleaver π^{-1}) as *a priori* information on the systematic and parity encoded symbols. Then, the SPA applied to the factor graph of the Turbo code produces a set of refined *a posteriori* and *extrinsic* probabilities⁴; the latter are then fed back to the sigma-demapper as *a priori* probabilities, giving rise to a new iteration. At each iteration, an estimation \hat{T}_k of T_k can be obtained for $k = 1, \dots, K$ by performing a hard-decision over the *a posteriori* probabilities generated by the Turbo decoder. The decoding process is stopped after a fixed number of iterations Ψ . It is important to observe that, in our scheme, the SPA applied to the Turbo factor graph is extended with respect to the conventional forward and backward recursions (see [7, Section IV.A]) so as to incorporate the generation of the *extrinsic* probabilities corresponding to the parity bits.

⁴ In the Turbo processing jargon, *extrinsic* refers to the fraction of the output probabilistic information that does not depend on any input *a priori* probability.

6 Cycle-Stationary Sources in the Bandwidth-Limited Regime

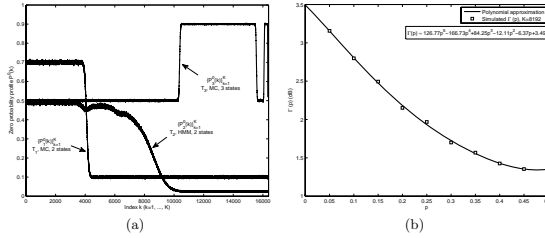


Fig. 3. (a) Zero probability profiles of the considered MC and HMM sources concatenated with the BWT, and $K = 16384$. (b) Polynomial approximation of the gap margin functions for the proposed scheme and $K = 8192$.

4 Simulation Results

In order to study the performance of the proposed system, we have considered three different cycle-stationary sources T_i with *zero probability profiles* $\{P_i^0(k)\}_{k=1}^K$, with $i \in \{1, 2, 3\}$ and $K = 16384$. They have been obtained by estimating the probability distribution at the output of the BWT for an input source with memory following a Markov Chain (MC) for $i \in \{1, 3\}$, and a Hidden Markov Model (HMM) for $i = 2$. For $i = 1$ and $i = 2$, we have utilized the MC and the HMM employed in [5], both having two states and entropy rates 0.58 and 0.62 bits per source symbol, respectively. On the other hand, for $i = 3$ we have selected a MC with 3 states and entropy rate 0.83 bits per source symbol. The corresponding *zero probability profiles* at the output of the BWT are shown in Figure 3.a, which have been estimated by using frequency of occurrence as in [8, Expression (57)]. The Turbo code from [1, Example A] with rate $R_c = 1/3$ and generator polynomial $G(D) = 1/(1+D)$ has been adopted for our simulations. The serial-to-parallel converter outputs $I = 3$ sequences $\mathbf{v}^{(i)}$, and therefore the overall transmission rate R (source symbol per dimension) is 1, i.e. we are working in the bandwidth-limited regime (spectral efficiency of 2). The corresponding Shannon limits E_{so}/N_0 when $R = 1$ are -2.13 dB (T_1), -1.69 dB (T_2) and 0.293 dB (T_3).

Figure 3.b depicts the gap factor $\Gamma(p)$, $p \leq 0.5$, used in expression (9). This gap has been calculated by simulating the proposed scheme for a stationary i.i.d. source with symbol distribution $(p, 1-p)$ and blocklength $K = 8192$ (\square markers). The figure also includes a 5th-order polynomial approximation for the simulated $\Gamma(p)$, which can be easily programmed beforehand to produce the gamma function for any arbitrary value of p . Observe that $\Gamma(p)$ is a monotonically decreasing function of p , which indicates that the performance of the proposed setup with

i.i.d. stationary sources degrades as the distribution of the source symbols is more asymmetric.

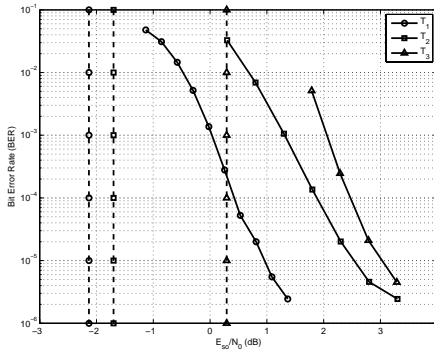


Fig. 4. BER vs E_{so}/N_0 of the proposed scheme for $\{T_i\}_{i=1}^3$.

Finally, Monte Carlo simulations have been performed for a blocklength of $K = 16384$ source symbols, $\Psi = 50$ decoding iterations and 1000 source sequences per simulated point. Figure 4 plots the Bit Error Rate (BER) versus E_{so}/N_0 for the three probability profiles and by using the energy allocation technique introduced in Section 2.1. However, we have modified the way the set of energies $E_c^*(k)$ is calculated, because simulations have empirically shown a performance improvement when R is replaced by R_c in expression (9). When the source is generated with the first probability profile $\{P_i^0(k)\}_{k=1}^K$ (T_1), the proposed system is 2.55 dB away of the theoretical limit for a BER of 10^{-4} . For the second probability profile (T_2), the system is 3.57 dB away of its corresponding Shannon limit. Finally, the system applied to the third source T_3 performs at 2.17 dB away from the corresponding Shannon limit at the same BER level. Notice that these results have been obtained by means of a very simple Turbo code. We believe that by optimizing the Turbo code better results (i.e. closer to the Shannon limit) could be obtained.

5 Concluding Remarks

We have proposed a novel scheme for the transmission of cycle-stationary sources over AWGN channels in the bandwidth-limited regime. The novel scheme is

8 Cycle-Stationary Sources in the Bandwidth-Limited Regime

based on the combination of a Turbo encoder and a sigma-mapper that jointly perform the source and channel coding task, and on the use of an asymmetric waterfilling energy allocation technique. The simulation results obtained for very simple Turbo codes state that, for a variety of cycle-stationary sources, the BER performance of our proposed scheme gets close to the corresponding Shannon separation limit. These promising results motivate further research towards narrowing the aforementioned gap, e.g. by utilizing Turbo codes with enhanced BER waterfall performance.

Acknowledgments

This work was supported in part by the Spanish Ministry of Science and Innovation through the CONSOLIDER-INGENIO 2010 programme (CSD200800010, www.comonsens.org), and through the Torres-Quevedo funding program (PTQ-09-01-00740).

References

1. Ma, X., Ping, L.: Coded Modulation Using Superimposed Binary Codes, *IEEE Transactions on Information Theory*, vol. 50, N. 12 (2004).
2. Burrows, M., Wheeler, D.: A Block Sorting Lossless Data Compression Algorithm, Digital Systems Center, Research Report 124 (1994).
3. Visweswariah, K., Kulkarni, S., Verdu, S.: Output Distribution of the Burrows-Wheeler transform. In: *IEEE International Symposium on Information Theory*. Sorrento, Italy (2000).
4. Shannon, C.E.: A Mathematical Theory of Communication. *Bell System Technical Journal*, vol. 27, pp. 379-423 and 623-656, July and October (1948).
5. Del Ser, J., Crespo, P. M., Esnaola, I., Garcia-Frias, J.: Source-Controlled Turbo Coding of Sources with Memory using the Burrows-Wheeler Transform. In: *IEEE International Symposium on Turbo Codes*. Munich, Germany (2006).
6. Cabarcas, F., Souza, R. D., Garcia-Priás, J.: Turbo Coding of Strongly Non-Uniform Memoryless Sources with Unequal Energy Allocation and PAM Signaling. *IEEE Transactions on Signal Processing*, vol. 54, N. 5, pp. 1942-1946 (2006).
7. Kschischang, F. R., Frey, B. J., Loeliger, H.-A.: Factor Graphs and the Sum-Product Algorithm. *IEEE Transactions on Information Theory*, vol. 47, N. 2, pp. 498-519 (2001).
8. Crespo, P. M., Loyo, E., Del Ser, J.: Uncoded Optimal Binary Communication for Sources with Memory. *Elsevier AEU International Journal of Electronics and Communications*, vol. 62, N. 8, pp. 597-609 (2007).

Códigos LDGM concatenados para la transmisión de fuentes
correlacionadas para canales de difusión

M. Hernaez, P. Crespo, J. Del Ser and I. Ochoa,
*XXIV National Assembly of the International Union of
Radio Science (URSI)*, Santander (Spain), September
2009.

Códigos LDGM Concatenados para la Transmisión de Fuentes Correlacionadas en Canales de Difusión

Mikel Hernaez¹, Pedro M. Crespo¹, Javier Del Ser² e Idoia Ochoa¹

⁽¹⁾ {mhernaez,pcrespo,iochoa}@ceit.es, ⁽²⁾ jdelser@robotiker.es
 (1) CEIT y TECNUN (Universidad de Navarra), 20009 Donostia-San Sebastián, Gipuzkoa.
 (2) TECNALIA-Robotiker, 48170 Zamudio, Bizkaia.

Abstract—We propose the use of serially-concatenated LDGM codes for the transmission of spatially correlated sources over 2-user gaussian broadcast channels. For this channel it is well-known that the capacity-achieving coding scheme is based on a superposition approach, where the outputs of two independent encoders are modulated with different energies and symbolwise added. This produces a channel sequence that conveys the information from both users to the distant receivers. The use of serially-concatenated LDGM codes with correlated information sources permits to keep a strong degree of correlation in the encoded symbols, which are then coherently added prior to transmission. This leads to vast Bit Error Rate improvements at both receivers, since this coherent addition not only provides a better immunity of the sent signal against noise, but also minimizes the inter-user interference in the sent signal. Thus, by properly designing the coding of the correlated sources, the obtained simulation results show that our proposal outperforms the suboptimal fundamental limit assuming separation between source and channel coding.

I. INTRODUCCIÓN

En multitud de aplicaciones tales como las redes de sensores, la coexistencia de varios transmisores y receptores ha suscitado un gran interés científico hacia el desarrollo de una teoría unificada de la información para este tipo de redes de comunicación (bautizada como la Teoría de la Información en Redes o *Network Information Theory*), así como hacia el diseño de técnicas de codificación que permitan aproximarse a los límites fundamentales dictados por dicha teoría. Centremos nuestra atención en el canal de difusión o *broadcast*, en el que los datos generados por L fuentes de información son enviados a sus correspondientes receptores empleando una única señal transmitida. Asumiendo por simplicidad $L = 2$ fuentes binarias¹, denotaremos las secuencias de información generadas por ambas fuentes como \mathbf{u}^i , con $i \in \{1, 2\}$. Por otro lado, consideraremos canales de difusión gaussianos. Así, definamos para este canal una función de codificación $f(\mathbf{u}^1, \mathbf{u}^2)$ como

$$f : 2^{NR_1} \times 2^{NR_2} \longrightarrow \mathcal{X}^N, \quad (1)$$

donde R_1 y R_2 son las tasas de información (bits por símbolo de canal) de cada una de las fuentes de información, y \mathcal{X} es el alfabeto de los símbolos de la secuencia $\mathbf{x} \triangleq \{x_1, \dots, x_N\}$ enviada a través del canal de difusión con energía media por

¹El trabajo presentado en este artículo es extrapolable a un número mayor de fuentes y/o alfabetos no binarios.

símbolo de canal E_c . La secuencia \mathbf{x} resultante es transmitida a ambos receptores a través de sendos canales de ruido aditivo gaussiano blanco, representados por las secuencias \mathbf{n}^1 y \mathbf{n}^2 de símbolos gaussianos independientes con media 0 y varianzas σ_1^2 y $\sigma_2^2 = \beta\sigma_1^2$, siendo $\beta \geq 1$. En este contexto, cuando las fuentes de datos son independientes, Cover [1] y Bergmans [2], [3] identificaron la región de capacidad para este canal, dada por

$$R_1 \leq \frac{1}{2} \log_2 \left(1 + \frac{\alpha E_c}{\sigma_1^2} \right), \quad (2)$$

$$R_2 \leq \frac{1}{2} \log_2 \left(1 + \frac{(1-\alpha)E_c}{\alpha E_c + \sigma_2^2} \right), \quad (3)$$

donde E_c es la energía media por símbolo de canal, y $\alpha \in (0, 1)$ es un parámetro que permite ajustar la energía asignada a cada una de las fuentes. Las expresiones (2) y (3) revelan cómo diseñar el esquema de codificación óptimo que alcanza, asintóticamente, la región de capacidad del canal de difusión gaussiano.

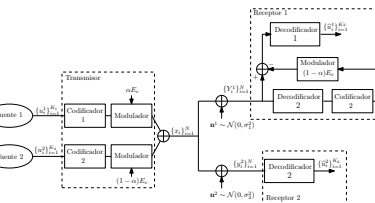


Fig. 1. Esquema de superposición para el canal de difusión gaussiano.

Dicho esquema, denominado de *superposición* (véase la Figura 1), se basa en codificar por separado las secuencias de ambas fuentes, modular cada una de las palabras código resultantes con energías medias $(1-\alpha)E_c$ y αE_c (siendo α un parámetro de diseño) y, finalmente, superponer (sumar) las señales moduladas en una única palabra código \mathbf{x} con energía media resultante E_c . Por su parte, el receptor del canal con menor varianza de ruido σ_1^2 (de aquí en adelante receptor *bueno*) debe detectar la señal interferente del usuario correspondiente al otro receptor, reconstruir su palabra código asociada y cancelarla de la secuencia recibida $\mathbf{y}^1 =$

$\mathbf{x} + \mathbf{n}^1$. Por otro lado, el receptor del canal con mayor varianza de ruido σ_2^2 (i.e. el receptor *malo*) tratará de decodificar su secuencia de interés a partir de \mathbf{y}^2 , esto es, sin ningún tipo de procesamiento adicional.

Existen diversas contribuciones (e.g. [4], [5]) en las que se presentan sistemas prácticos de superposición para fuentes independientes cuyo desempeño supera al de esquemas ortogonales (i.e. multiplexación por división en el tiempo o frecuencia). Sin embargo, en redes de comunicación con alta densidad de usuarios (e.g. las redes de sensores), la proximidad física de los nodos da lugar a cierto grado de correlación entre los datos registrados por cada uno de estos sensores. Esta correlación puede ser explotada en recepción para mejorar las prestaciones del sistema de comunicación.

Partiendo de recientes resultados sobre las propiedades preservativas de la correlación de los códigos de matrices de generación ralas (*sparse*) concatenados (*Serially Concatenated Low-Density Generation-Matrix*, SC-LDGM [6], [7]), este artículo propone el empleo de dichos códigos en el escenario de comunicación planteado en la Figura 1. El uso de códigos LDGM concatenados permite mantener la alta correlación entre las palabras código una vez realizada la superposición de señales en el transmisor. La decodificación en el receptor *malo* es llevada a cabo tratando el mensaje de la fuente 1 como ruido, sin tener en cuenta la correlación existente entre ambas fuentes. Sin embargo, debido a la naturaleza de los códigos LDGM, la suma realizada en el transmisor es coherente, por lo que la constelación de la señal transmitida es más robusta ante el ruido del canal, mejorando así el rendimiento del decodificador del receptor *malo*.

El artículo se organiza de la siguiente manera: en la Sección II se describe el sistema propuesto, mientras que la Sección III detalla el algoritmo de decodificación utilizado. Finalmente, los resultados de simulación son analizados en la Sección IV.

II. SISTEMA PROUESTO

Volviendo a la Figura 1, en este artículo se asume que las secuencias generadas por las fuentes son binarias y denotadas como $\mathbf{u}^j = \{u_k^j\}_{k=1}^K$, con $u_k^j \in \{0, 1\}$ y $j \in \{1, 2\}$. La correlación entre fuentes se modela de la siguiente forma: cada uno de los símbolos de la secuencia \mathbf{u}^1 son i.i.d. y equiprobablemente distribuidos, i.e. $P(u_k^1 = 0) = P(u_k^1 = 1) = 0.5$. Por otro lado, cada símbolo de la secuencia \mathbf{u}^2 se obtiene según $u_k^2 = u_k^1 \oplus e_k$, donde \oplus indica suma módulo 2 y e_k es una variable aleatoria binaria que toma el valor 1 con probabilidad p y el valor 0 con probabilidad $1 - p$. Así la probabilidad de que los símbolos de fuente u_k^1 y u_k^2 tomen diferentes valores es p , esto es, $P(u_k^1 \neq u_k^2) = p$.

Tal como se ha mencionado en la Sección I, la secuencia \mathbf{u}^i de la fuente i -ésima ($i \in \{1, 2\}$) es codificada – independientemente del otro codificador – mediante un código SC-LDGM, dando como resultado la correspondiente secuencia codificada \mathbf{x}^i . Estas secuencias código \mathbf{x}^1 y \mathbf{x}^2 son moduladas en BPSK (*Binary Phase Shift Keying*) con energías medias por símbolo modulado αE_c y $(1 - \alpha) E_c$, respectivamente, donde $0 \leq \alpha \leq 1$. Finalmente, ambas secuencias moduladas son

sumadas símbolo a símbolo, dando lugar a una constelación 4-PAM (*Pulse Amplitude Modulation*) con energía media por símbolo \mathbf{x} de E_c . Como se verá posteriormente, la preservación de las características estadísticas de los símbolos de fuente propia de los códigos SC-LDGM provocará la suma coherente de una gran fracción de los símbolos codificados, favoreciendo en ambos receptores el proceso de decodificación de las secuencias recibidas \mathbf{y}^1 y \mathbf{y}^2 . Estas últimas secuencias vendrán dadas por

$$\mathbf{y}^1 = \mathbf{x} + \mathbf{n}^1, \quad (4)$$

$$\mathbf{y}^2 = \mathbf{x} + \mathbf{n}^2, \quad (5)$$

donde cada uno de los símbolos de \mathbf{n}^1 y \mathbf{n}^2 son realizaciones de una variable aleatoria gaussiana i.i.d. de media cero y varianza σ_1^2 y $\sigma_2^2 = \beta \sigma_1^2$, respectivamente.

Comentaremos brevemente en qué consiste un código SC-LDGM y sus propiedades de preservación estadística.

II-A. Códigos SC-LDGM

Un código LDGM sistemático es un código lineal cuya matriz generadora es de la forma $\mathbf{G} = [\mathbf{I} \ \mathbf{P}]$, donde \mathbf{I} denota la matriz identidad de orden K y \mathbf{P} es una matriz rala o *sparse* de dimensión $K \times (N - K)$, resultando la tasa de codificación del código en K/N símbolos de fuente por símbolo codificado. Si denotamos la secuencia de información como $\mathbf{u} = [u_1, \dots, u_K]$, la secuencia de salida del codificador, calculada según $\mathbf{c} = [c_1, \dots, c_N] = u\mathbf{G}$, está compuesta por los símbolos sistemáticos (i.e. $c_n = u_n$ para $n = 1, \dots, K$) y los $N - K$ símbolos de paridad $\{c_n\}_{n=K+1}^N$. Puesto que la matriz de paridad $H = [P^T \mathbf{I}]$ es también *sparse*, los códigos LDGM pueden ser considerados como un caso particular de los códigos LDPC y, por tanto, decodificados mediante el algoritmo Suma-Producto [8] aplicado al grafo que describe el código [6], [7]. Siguiendo la notación de esta última referencia, etiquetaremos mediante (θ, ϑ) a aquellos códigos LDGM en los que la matriz de paridad \mathbf{P} de un código LDGM tiene exactamente θ componentes no nulas por fila y ϑ componentes no nulas por columna.

Siguiendo los recientes resultados [9], [10] obtenidos para los códigos LDGM distribuidos en canales de múltiple acceso (*Multiple Access Channel*), si se desea una suma coherente de las señales en la etapa de superposición de nuestro sistema, es necesario generar palabras código suficientemente alejadas unas de otras, en las cuales la correlación entre las fuentes de información se preserve lo máximo posible. Esto conllevaría un refuerzo en la mayoría de los símbolos de la señal transmitida, mejorando la robustez del sistema frente al ruido. Así, si se utiliza la misma matriz generadora \mathbf{G} para ambos codificadores, dada la baja densidad de la matriz, la correlación no es sólo preservada en los símbolos sistemáticos, sino también en los de paridad. De hecho, puede demostrarse que la probabilidad de que los símbolos de paridad en un determinado instante sean diferentes viene expresado analíticamente según

$$p_c = \frac{1 - (1 - 2p)^\theta}{2}, \quad (6)$$

la cual, para valores muy pequeños de p , puede aproximarse por $p_c \approx \theta p$. De esta forma, la correlación existente en los símbolos de paridad es significativa cuando θ es pequeño.

Sin embargo, existe una desventaja inmediata en la utilización de códigos LDGM sin concatenar en nuestro sistema. La primera de ellas radica en las prestaciones ofrecidas por este tipo de códigos en su versión no concatenada, caracterizadas por un alto suelo de error. Afortunadamente, la concatenación de dos códigos LDGM, donde el código externo (outer code) tiene una tasa de codificación cercana a la unidad, da lugar a una reducción sustancial del dicho suelo de error. Dicho esto, la Figura 2 ilustra los codificadores SC-LDGM utilizados en este artículo. Con el fin de explotar al máximo la correlación entre las fuentes de información, la misma matriz generadora es utilizada en ambos codificadores.

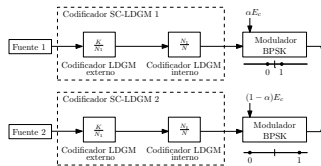


Fig. 2. Transmisor para el canal de difusión propuesto.

Previamente a la descripción del algoritmo de decodificación empleado, cabe resaltar que, para cualquier valor del parámetro de ajuste de energía α , y dadas las propiedades estadísticas de las palabras código resultantes, la energía de canal de la secuencia x es mayor que la esperada E_c . La razón de este aumento de energía es que, después de la suma coherente de señales (superposición), los símbolos exteriores de la constelación 4-PAM correspondientes a los pares $(c_k^1, c_k^2) = (0, 0)$ y $(c_k^1, c_k^2) = (1, 1)$ poseen una mayor probabilidad de ser transmitidos (este es, $(1 - p)$ para los símbolos sistemáticos y $(1 - p_c)$ para los de paridad) que los símbolos interiores. Esto es una consecuencia inevitable de la estructura de codificación empleada, que será considerada a la hora de desarrollar los límites fundamentales de la Teoría de Shannon para nuestro escenario.

III. DECODIFICACIÓN

El procedimiento de decodificación se basa en el algoritmo Suma-Producto ejecutado sobre el grafo de factores que describe la correlación entre las fuentes y el código empleado [8]. Los grafos de factores permiten representar gráficamente funciones factorizables de múltiples variables, mientras que el algoritmo SPA resuelve eficientemente la marginalización de dichas funciones mediante la transferencia de mensajes a través del grafo asociado. La aplicación de estas herramientas a funciones de probabilidad conjunta de sistemas de comunicaciones supone un método práctico de estimación de variables bajo el criterio *Máximo a Posteriori* (MAP).

Dicho esto, analicemos el proceso de decodificación para el receptor con mayor varianza de ruido (i.e. σ_2^2). Obtenremos $\hat{\mathbf{u}}^2$ (estimación de \mathbf{u}^2) mediante la ejecución del algoritmo SPA sobre el grafo de nodos del código SC-LDGM empleado (primero sobre el código interno y posteriormente sobre el externo). En este receptor no incorporaremos información sobre la correlación entre las fuentes (*información lateral*) al proceso de decodificación, sino que explotaremos dicha dependencia estadística entre los datos de ambas fuentes en el decodificador del otro receptor. Nótese que en el esquema clásico por superposición, las probabilidades del canal $p(y_k^2|c_k^2)$ suministradas al decodificador vienen dadas por

$$p(y_k^2|c_k^2) = \begin{cases} \mathcal{N}\left(-\sqrt{(1-\alpha)E_c}, \sigma_2^2 + \alpha E_c\right) & \text{si } c_k^2 = 0, \\ \mathcal{N}\left(+\sqrt{(1-\alpha)E_c}, \sigma_2^2 + \alpha E_c\right) & \text{si } c_k^2 = 1, \end{cases} \quad (7)$$

donde $\mathcal{N}(\mu, \sigma^2)$ denota una distribución gaussiana de media μ y varianza σ^2 . En el caso del decodificador SC-LDGM con fuentes correlacionadas, dicha probabilidad se computa según

$$p(y_k^2|c_k^2) = \begin{cases} (1 - p_{cor})f_{00} + p_{cor}f_{10} & \text{si } c_k^2 = 0, \\ (1 - p_{cor})f_{11} + p_{cor}f_{01} & \text{si } c_k^2 = 1, \end{cases} \quad (8)$$

donde

$$f_{00} \triangleq \mathcal{N}\left(-\sqrt{(1-\alpha)E_c} - \sqrt{\alpha E_c}, \sigma_2^2\right) \quad (9)$$

$$f_{01} \triangleq \mathcal{N}\left(+\sqrt{(1-\alpha)E_c} - \sqrt{\alpha E_c}, \sigma_2^2\right) \quad (10)$$

$$f_{10} \triangleq \mathcal{N}\left(-\sqrt{(1-\alpha)E_c} + \sqrt{\alpha E_c}, \sigma_2^2\right) \quad (11)$$

$$f_{11} \triangleq \mathcal{N}\left(+\sqrt{(1-\alpha)E_c} + \sqrt{\alpha E_c}, \sigma_2^2\right), \quad (12)$$

siendo $p_{cor} = p$ para los símbolos correspondiente a los símbolos sistemáticos y $p_{cor} = p_c$ para los correspondientes a los símbolos de paridad de la palabra código. Nótese que cuanto mayor sea la correlación entre ambas fuentes, menor será el valor de p asociado. Teniendo en cuenta la asignación de símbolos en las constelaciones BPSK utilizadas (Figura 2), la probabilidad de enviar los símbolos exteriores de la constelación 4-PAM resultante ($\sqrt{(1-\alpha)E_c} + \sqrt{\alpha E_c}$ y $-\sqrt{(1-\alpha)E_c} - \sqrt{\alpha E_c}$) aumentará, por lo que la secuencia enviada x será más robusta frente al ruido. Desafortunadamente, la energía de transmisión de x resultante también aumenta con respecto a la empleada en el caso de tener símbolos equiprobables. Específicamente, la energía total transmitida con fuentes correlacionadas está dada por $E_c^{corr} = E_c(1 + \Delta_{exc})$, donde

$$\Delta_{exc} = R_c \Delta_{sis} + (1 - R_c) \Delta_{par}, \quad (13)$$

$$\Delta_{sis} = (1 - 2p)2\sqrt{\alpha(1 - \alpha)}, \quad (14)$$

$$\Delta_{par} = (1 - 2p_c)2\sqrt{\alpha(1 - \alpha)}. \quad (15)$$

Obsérvese que los dos sumandos de la primera de estas expresiones son los asociados a los símbolos sistemáticos (párametro de correlación p) y los de paridad (p_c), siendo p_c la probabilidad asociada al código LDGM interno. Es importante destacar que se ha obviado la influencia de los símbolos de paridad introducidos por el código externo debido a su reducido número (R_{out} cercano a 1).

En lo que respecta al segundo receptor basado en superposición, adoptaremos una estrategia de decodificación basada en predetección y cancelación. Como $\sigma_2^2 \geq \sigma_1^2$, este receptor es capaz de obtener $\hat{\mathbf{u}}^2$ y generar una estimación de la palabra código $\hat{\mathbf{c}}^2$. Tras su modulación con energía media $(1 - \alpha)E_c$, cancelaremos dicha secuencia de la señal recibida \mathbf{y}^1 , dando lugar a una nueva secuencia $\tilde{\mathbf{y}}^1$. A partir de esta nueva secuencia el receptor obtendrá una estimación $\hat{\mathbf{u}}^1$ con relación señal a ruido efectiva $\alpha E_c / \sigma_1^2$. Nótese que el límite fundamental de este receptor también ha de ser reducido por Δ_{exc} dBs.

IV. RESULTADOS DE SIMULACIÓN

Con el fin de evaluar el comportamiento del sistema propuesto, se han llevado a cabo simulaciones para diferentes valores de los parámetros p y α . En todos los casos se han empleado sendos códigos SC-LDGM, compuestos por un código externo (4, 76) y un código interno (14, 7), dando lugar a una tasa de información total $R_c = 0,316$. El tamaño del bloque de información es $K = 9500$. En lo que respecta a la selección del parámetro α , uno puede suponer erróneamente que el proporcionar más energía a la señal correspondiente al receptor *malo* (i.e. disminuir α) conllevaría una mejora del rendimiento global del sistema. Es importante observar que, debido a la correlación entre las fuentes y al esquema de codificación empleado, el hecho de darle más energía a la secuencia del receptor *bueno* implica a su vez suministrar más energía al receptor *malo* en un $100 \cdot (1 - p)$ % de los símbolos de su secuencia codificada. Además, el hecho de incrementar el valor de α hace más robusto el sistema ante el ruido, ya que los símbolos exteriores de la constelación 4-PAM son desplazados aún más lejos del origen.

Desafortunadamente, si aumentamos el valor de α los símbolos interiores de la constelación 4-PAM son desplazados hacia el centro de la constelación, haciendo más difícil su detección en los casos en los que las fuentes no generen el mismo símbolo de información. Esto deriva en suelos de error elevados para valores de α cercanos a 0,5 (e.g. para $\alpha = 0,5$ el suelo de error se situaría en p). Estas observaciones conducen a una nueva formulación de la región de capacidad asumiendo separación entre codificación de fuente y de canal, dada por las desigualdades

$$R_c \leq \frac{1}{2H(p)} \log_2 \left(1 + \frac{\alpha E_c^{corr}}{\sigma_1^2} \right), \quad (16)$$

$$R_c \leq \frac{1}{2H(p)} \log_2 \left(1 + \frac{(1 - \alpha)E_c^{corr}}{\alpha E_c^{corr} + \sigma_2^2} \right), \quad (17)$$

de donde el valor de α que minimiza la relación E_c^{corr}/σ_1^2 para β y p fijados viene dado por $\alpha_{opt} \triangleq (\beta + 2^{2R_c} H(p))^{-1}$. Este valor es prácticamente constante (varía entre 0,22 y 0,25) para cualquier valor de p . Asumiendo separación, el límite de Shannon se obtiene de las desigualdades (2) y (3), y está dado por 4,3 dB para $\beta = 3$ y $R_1 = R_2 = 0,316$. Para aquellos esquemas en los que la correlación no se tiene en cuenta en el proceso de decodificación, las prestaciones se sitúan a 1,5 dB por encima del citado límite.

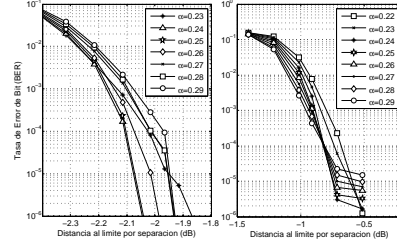


Fig. 3. Tasa de error de bit con $p = 0,1$ (izqda) y $p = 0,01$ (dcha).

Procedamos ahora a comparar este límite con el BER obtenido por el sistema propuesto cuando la correlación es de $p = 0,1$ y $0,01$. Estos resultados se muestran en la Figura 3, donde el eje de abscisas proporciona esta separación para diferentes valores de α . Obsérvese que para $p = 0,1$ nos hallamos aproximadamente 2 dB por debajo del límite de Shannon, mientras que para $p = 0,01$ éste se reduce a 0,5 dB. Este empeoramiento de prestaciones para $p = 0,01$ es el resultado de un aumento excesivo de E_c^{corr} debido a la correlación (ver expresión (13)). De esta degradación se deduce un punto de inflexión en el comportamiento del sistema a medida que p disminuye. Nótese también que, para niveles de correlación elevados (curva de la derecha), el valor de α fija un compromiso entre el suelo de error y la región de cascada.

REFERENCIAS

- [1] T. M. Cover "Broadcast Channels", *IEEE Transactions on Information Theory*, vol. 18, N. 1, pp. 2-114, Enero 1972.
- [2] P. P. Bergmans, "Random Coding Theorem for the Broadcast Channels with Degraded Components", *IEEE Transactions on Information Theory*, vol. 19, N. 2, pp. 197-207, Marzo 1973.
- [3] P. P. Bergmans, "A Simple Converse for Broadcast Channels with Additive White Gaussian Noise", *IEEE Transactions on Information Theory*, vol. 20, N. 2, pp. 279-280, Marzo 1974.
- [4] T. W. Sun, R. D. Wesel, M. R. Shane y D. Jarett, "Superposition Turbo TCM for Multi-Rate Broadcasts", *IEEE Transactions on Communications*, vol. 52, pp. 368-371, Marzo 2004.
- [5] X. Wang y M. T. Orchard, "Design of Superposition Coded Modulation for Unequal Protection", *IEEE International Conference on Communications (ICC)*, pp. 412-416, Junio 2001.
- [6] W. Zhong y J. García-Frías, "Approaching Shannon Performance by Iterative Decoding of Linear Codes With Low-Density Generator Matrix", *IEEE Communication Letters*, vol. 7, N. 6, pp. 266-268, Junio, 2003.
- [7] W. Zhong y J. García-Frías, "LDGM Codes for Channel Coding and Joint Source-Channel Coding of Correlated Sources", *EURASIP Journal on Applied Signal Processing*, vol. 44, N. 2, pp. 942-953, Mayo 2005.
- [8] F. R. Kschischang, B. J. Frey y H. A. Loeliger, "Factor Graphs and The Sum-Product Algorithm", *IEEE Transactions on Information Theory*, vol. 44, pp. 498-519, Febrero 2001.
- [9] W. Zhong y J. García-Frías, "Parallel LDGM Codes for the Transmission of Highly Correlated Senders over Rayleigh Fading Multiple Access Channels", *CISS'06*, Marzo 2006.
- [10] W. Zhong y J. García-Frías, "LDGM Codes for Transmission of Correlated Senders over MAC", *43rd Annual Allerton Conference on Communication, Control, and Computing*, Octubre 2005 (artículo invitado).